

# Formation and Characterization of Complexes of Oppositely Charged Oil-in-Water (O/W) Microemulsion Droplets and Polyelectrolytes

vorgelegt von

**M.Sc. Miriam Simon**

ORCID: 0000-0003-3065-6230

von der Fakultät II - Mathematik und Naturwissenschaften  
der Technischen Universität Berlin  
zur Erlangung des akademischen Grades

**Doktor der Naturwissenschaften**

**Dr. rer. nat.**

genehmigte Dissertation

## **Promotionsausschuss:**

Vorsitzender: Prof. Dr. Reinhard Schomäcker (TU Berlin)

Gutachter: Prof. Dr. Michael Gradzielski (TU Berlin)

Gutachter: Prof. Dr. Dominique Langevin (Université Paris Sud)

Tag der wissenschaftlichen Aussprache: 22. November 2019

Berlin, 2020



## Abstract

Oil-in-water (O/W) microemulsion droplets are thermodynamically stable liquid systems that allow to have a rather high content of hydrophobic material dispersed in aqueous solution, which otherwise could not be dissolved. Further, microemulsion droplets have a well-defined spherical structure with low polydispersity, which renders them good model colloids. In that context, mixtures of charged microemulsion droplets and oppositely charged polyelectrolytes are very interesting systems, as the polyelectrolyte is able to bridge different droplets which allows further structural control on the microemulsion.

Accordingly, we studied the interactions of positively charged O/W microemulsion droplets with negatively charged polyelectrolytes. In our experiments, we varied the size of the droplets and the type and  $M_w$  of the polyelectrolyte, as well as the mixing ratio, quantified by the charge ratio  $z = [-]/([+] + [-])$ . This was done for polyacrylate, different polysaccharides and also a number of hydrophobically modified polyacrylates. Based on a thorough determination of the phase behavior and employing different methods like light and neutron scattering, cryo-TEM, zeta potential and viscosity measurements, it was possible to obtain a detailed characterization of the formed complexes in terms of size, shape and composition. Other parameters like the concentration or the ionic strength were also investigated.

The dynamic behavior of the droplet aggregates was studied using neutron spin-echo (NSE) and dynamic light scattering. This way, it was possible to investigate the diffusional behavior of free microemulsion droplets as well as of droplets immobilized in the complexes and gain insights into the lifetimes such mixed colloidal systems.

Additional tunability of the complexation arises from the pH-value since the surfactant and the polyelectrolytes used are both pH responsive. This means the charge density on the droplet surface and on the polyelectrolyte chain can be tuned in parallel, thereby systematically modifying the electrostatic interactions in the system. The electrostatic interactions in turn strongly influence the strength of binding and complexation and thereby the structures formed.

Finally, also the reference polyelectrolyte/surfactant system was studied to deduce differences between the behavior of 'empty' and 'loaded' carriers.

In our experiments we obtained a comprehensive picture of the formed complexes and how their detailed structure depends on their molecular composition, as well as the environment (pH). These aggregates serve as a model system for complexes with a high solubilization capacity that could find potential applications in formulations which contain a large amount of hydrophobic active agents.



## Zusammenfassung

Öl-in-Wasser (O/W) Mikroemulsionströpfchen sind thermodynamisch stabile flüssige Systeme, die es ermöglichen einen sehr hohen Anteil an hydrophoben Material in Wasser zu dispergieren, der sich auf andere Weise nicht lösen würde. Mikroemulsionströpfchen haben außerdem eine wohl definierte kugelförmige Struktur mit niedriger Polydispersität, was sie zu gut geeigneten Modell-Kolloiden macht. In diesem Zusammenhang sind auch Mischungen aus geladenen Mikroemulsionströpfchen und entgegengesetzt geladenen Polyelektrolyten sehr interessante Systeme, da der Polyelektrolyt durch Verknüpfen der Tröpfchen eine weitere Strukturierung der Mikroemulsion ermöglicht.

Diese Arbeit untersucht die Wechselwirkungen von positiv geladenen O/W Mikroemulsionströpfchen mit negativ geladenen Polyelektrolyten. In verschiedenen Experimenten wurden die Größe der Tröpfchen, die Art und das Molekulargewicht des Polyelektrolyten, sowie das Mischungsverhältnis zwischen den beiden Komponenten (quantifiziert durch das Ladungsverhältnis  $z = [-]/([+] + [-])$ ) variiert. So wurden z.B. Polyacrylat, verschiedene Polysaccharide, sowie einige hydrophob modifizierte Polyacrylate eingesetzt. Anhand einer gründlichen Untersuchung des Phasenverhaltens und mittels verschiedener Methoden wie Licht- und Neutronenstreuung, cryo-TEM, Zetapotential und Viskositätsmessungen, wurden die gebildeten Komplexe detailliert charakterisiert. Dabei wurden, unter anderem, die jeweilige Größe, Form und Zusammensetzung der Komplexe bestimmt. Auch andere Parameter wie die Gesamtkonzentration oder die Ionenstärke des Systems wurden untersucht.

Das dynamische Verhalten der Tröpfchen-Komplexe wurde mittels Neutronen Spin-Echo und dynamischer Lichtstreuung untersucht. Hiermit war es möglich das diffusive Verhalten der freien Mikroemulsionströpfchen, sowie das der in Komplexen immobilisierten Tröpfchen zu untersuchen und Informationen über die Lebenszeiten in solchen gemischten Kolloidsystemen zu erhalten.

Zusätzliche Schaltbarkeit der Systeme wird auch durch den pH Wert ermöglicht, da sowohl das verwendete Tensid, als auch die Polyelektrolyte auf den pH Wert reagieren. Dadurch kann die Ladungsdichte auf der Tröpfchenoberfläche und auf der Polyelektrolytkette simultan variiert werden. Durch Änderung der Ladungsdichten verändern sich die elektrostatischen Wechselwirkungen zwischen den Komponenten systematisch, was einen starken Einfluss auf die Bindungsstärke und damit auf die gebildeten Strukturen hat.

Zum Schluss wurde auch das entsprechende Polyelektrolyt/Tensid Referenzsystem untersucht um Unterschiede zwischen 'leeren' und 'beladenen' Trägern herauszufinden.

In den hier vorgestellten Experimenten wurde ein umfassendes Bild der Polyelektrolyt/Mikroemulsions Komplexe erhalten, vor allem, wie ihre detaillierte Struktur sowohl von der genauen Zusammensetzung als auch von ihrer Umgebung (pH) abhängt. Die gebildeten Aggregate dienen hierbei als ein Modellsystem für Komplexe mit einer hohen Lösungskapazität. Sie könnten Anwendung in Formulierungen finden, in denen z.B. große Mengen an hydrophoben Wirkstoffen benötigt werden.



## Acknowledgements

Als erstes möchte ich bei meinem Doktorvater Prof. Michael Gradzielski bedanken. Vielen Dank für das schöne Thema, dessen Bearbeitung mir viel Spaß gemacht hat. Vielen Dank auch für das Vertrauen, was es mir ermöglicht hat sehr selbstständig mein Ding zu machen und auch eigene Ideen zu verfolgen. Und zum Schluss, vielen Dank für die vielen hilfreichen Gespräche und das stete Interesse an meiner Arbeit.

I would like to thank Prof. Dominique Langevin for kindly accepting to referee my thesis and for the many fundamental articles that helped me a lot in understanding my work. Bei Prof. Reinhard Schomäcker bedanke ich mich herzlich für die Übernahme des Prüfungsvorsitzes.

Ich möchte mich beim gesamten Stranski-Laboratorium für die immer gute Atmosphäre, die viele Unterstützung, wenn man mal nicht weiter kam oder auf sämtlichen Messzeiten, und die unterhaltsamen Kaffeepausen bedanken. Besonders bedanke ich mich bei Petra und Maria, ohne die ich wohl einige Dienstreisen nicht bezahlt bekommen hätte, Monika für Hilfe bei Computerproblemen und René für Hilfe bei aller Art von Problemen und dafür, dass er immer gute Laune verbreitet. Bei Michaela möchte ich mich für die Synthese des Blockcopolymers bedanken und bei Jana die vielen verschiedenen kleinen Messungen, bei denen sie mir geholfen hat.

Besonderer Dank geht an meine Bürokollegen, Anja und Sebastian, und auch an Albert und Sven und den Rest des Arbeitskreises einfach dafür das ihr da seid, es war immer schön mit euch zusammen zu arbeiten. Vielen Dank auch für das Korrekturlesen dieser Arbeit. Vielen Dank an Leo für das gute Vorbild und die viele Unterstützung. Danke auch für dein Formfaktor Modell. Ganz besonders möchte ich mich bei Ingo bedanken. Danke für die viele Unterstützung und Geduld, vor allem bei dem Dynamik-Paper, das hätte ich ohne dich nicht geschafft. Vielen Dank auch für das Asyl während diverser Grenoble-Aufenthalte und das Korrekturlesen.

Ich möchte mich auch bei meinen Bachelorstudenten und studentischen Hilfskräften bedanken. Thorsten, Henning, Patrick, Sunil und Sofia, vielen Dank für eure Hilfe, es hat Spaß gemacht mit euch zusammen zu arbeiten.

Danke an Lucas für die Begleitung während des gesamten Studiums, vom ersten bis zum letzten Tag. Danke für die vielen gemeinsamen Lern- und Arbeitsstunden und den Ansporn vor allem am Ende. Danke an Jens für viele lustige Abende und Telefonbiere.

Vielen Dank an Jonny für gemeinsames Lernen, Unterstützung als es schwierig war und schöne Kaffeepausen. Danke Francis, dass du wieder in meinem Leben bist, mich motivierst und für das 'einfach machen' Mantra.

Vielen Dank auch an meine Familie, vor allem meine Eltern, Helga und Andreas, die mich immer unterstützt haben und sich so oft Sorgen um mich gemacht haben, dass ich zu viel arbeite oder mir zu viel vorgenommen habe und trotzdem immer an mich geglaubt haben.

Zum Schluss geht der größte Dank an meinen Mann Christian. Danke für die viele Unterstützung, das Essen kochen und Wäsche waschen während ich lange gearbeitet habe, das Zuhören und Aufbauen, wenn ich von allem genervt war und den Glauben an mich, dass ich das schaffen kann.

# Contents

<b>1</b>	<b>General Introduction</b>	<b>1</b>
1.1	Microemulsions . . . . .	1
1.2	Polymer/Microemulsion Systems . . . . .	4
1.3	Polyelectrolyte/Surfactant Complexes (PESC) . . . . .	5
1.4	Motivation . . . . .	7
<b>2</b>	<b>Theoretical Background</b>	<b>9</b>
2.1	Materials . . . . .	9
2.1.1	The Microemulsion . . . . .	9
2.1.2	The Polyelectrolytes . . . . .	10
2.1.3	Sample Preparation . . . . .	11
2.1.4	List of Chemicals . . . . .	12
2.2	Methods . . . . .	13
2.2.1	Light Scattering . . . . .	13
2.2.2	Small-Angle Neutron Scattering (SANS) . . . . .	16
2.2.3	Analysis of SANS data . . . . .	17
2.2.4	Neutron Spin Echo (NSE) . . . . .	20
2.2.5	Cryo-TEM Imaging . . . . .	21
2.2.6	Nuclear Magnetic Resonance (NMR) . . . . .	22
2.2.7	Other Methods . . . . .	22
2.3	Theoretical and Geometrical Discussion of the System . . . . .	24
<b>3</b>	<b>Polyacrylate/Microemulsion Complexes</b>	<b>27</b>
3.1	Introduction . . . . .	27
3.2	Results . . . . .	27
3.2.1	Structural Control of Polyelectrolyte/Microemulsion Droplet Complexes (PEMECs) with Different Polyacrylates . . . . .	27
3.2.2	Dilution of Complexes . . . . .	30
3.2.3	Variation of Microemulsion Charge . . . . .	34
3.3	Conclusion . . . . .	36
<b>4</b>	<b>Microemulsion Complexes with Biopolyelectrolytes</b>	<b>39</b>
4.1	Introduction . . . . .	39
4.2	Results . . . . .	39
4.2.1	Effect of the Polymer Architecture on the Phase Behavior and Structure of Polyelectrolyte/Microemulsion Complexes (PEMECs) . . . . .	39
4.2.2	Investigations of the Coacervate Phase . . . . .	44
4.2.3	Comparison of NaPA and NaHA Samples in Cryo-TEM . . . . .	47
4.3	Conclusion . . . . .	50

<b>5</b>	<b>Dynamics in Polyelectrolyte/Microemulsion Complexes</b>	<b>53</b>
5.1	Introduction . . . . .	53
5.2	Results . . . . .	53
5.2.1	Dynamics in Polyelectrolyte/Microemulsion Complexes . . . . .	53
5.2.2	Effect of Other Parameters on Complex Dynamics . . . . .	56
5.3	Conclusion . . . . .	59
<b>6</b>	<b>Variation of pH in Polyelectrolyte/Microemulsion Systems</b>	<b>61</b>
6.1	Introduction . . . . .	61
6.2	Results . . . . .	61
6.2.1	Variation of pH in the ME50-NaPA60 Systems . . . . .	61
6.2.2	pH Variation, Starting with an Uncharged Microemulsion . . . . .	65
6.2.3	Variation of pH in Hyaluronate/Microemulsion Systems . . . . .	66
6.3	Conclusion . . . . .	67
<b>7</b>	<b>Formation of Larger Clusters with Hydrophobically Modified Polyelectrolytes</b>	<b>69</b>
7.1	Introduction . . . . .	69
7.2	Results . . . . .	69
7.2.1	Statistically C12-modified PAA . . . . .	69
7.2.2	Hydrocarbon-modified PAA with Longer Side Chains and Hydrophobically Modified Blockcopolymer . . . . .	72
7.2.3	PEO-PAA Diblockcopolymer . . . . .	75
7.3	Conclusion . . . . .	77
<b>8</b>	<b>The Reference Polyelectrolyte/Surfactant System</b>	<b>79</b>
8.1	Introduction . . . . .	79
8.2	Results . . . . .	79
8.2.1	Phase Behavior . . . . .	79
8.2.2	Characterization by Light Scattering . . . . .	80
8.2.3	Characterization by SANS . . . . .	81
8.3	Conclusion . . . . .	83
<b>9</b>	<b>General Conclusion and Outlook</b>	<b>85</b>
	<b>References</b>	<b>89</b>
	<b>Appendix</b>	<b>99</b>
	A. List of Abbreviations . . . . .	99
	B. SANS Models . . . . .	103
	C. Publications . . . . .	109



# 1 General Introduction

## 1.1 Microemulsions

Emulsions are dispersed systems of two immiscible liquids like water and oil that appear homogenous even though there are still two phases present at the microscopic level. Energy input is required to disperse the two liquids into domains that are typically sized a few hundred nanometers. Emulsions are only kinetically stable for rather short time until macroscopic phase separation reoccurs.<sup>[1,2]</sup> The kinetic stability can be enhanced by adding stabilizers such as surfactants.<sup>[3]</sup> Surfactants accumulate at the interface between oil and water leading to a lower interfacial tension and thus smaller domains. Emulsions with droplet sizes of 20 - 200 nm are called nanoemulsions.<sup>[4]</sup> Even though some low energy input methods (PIC, PIT) have been established recently<sup>[5,6]</sup> nanoemulsions still require energy input for formation. The small droplet sizes make nanoemulsions relatively resistant to creaming, flocculation and coalescence so the main problem for stability is Ostwald-ripening. Nanoemulsions can be kinetically stable for rather long times before macroscopic phase separation is observed.<sup>[7,8]</sup>

For very low interfacial tensions, also thermodynamically stable emulsions with domain sizes of 3 - 20 nm can be obtained, called microemulsions. Microemulsions differ from other emulsions in a number of properties, such as spontaneous formation, thermodynamic stability and optical transparency due to the very small domain sizes.<sup>[9–11]</sup> The official IUPAC definition of a microemulsion is a 'dispersion made of water, oil and surfactant(s) that is an isotropic and thermodynamically stable system with dispersed domain diameter varying approximately from 1 to 100 nm, usually 10 to 50 nm'.<sup>[12]</sup> This definition is rather limiting to the variety of possible microemulsions, since they can be formed with alternative solvents, such as ionic liquids as well and so-called 'surfactant-free' or 'ultraflexible' microemulsions formed with short chain alcohols are also possible.<sup>[13–16]</sup> An overview of the different types of emulsions is given in Tab. 1.

Microemulsions were first described in 1943 by Schulman and Hoar who called them the 'oleopathic hydro-micelle',<sup>[17]</sup> the term 'microemulsion' was only defined somewhat later.<sup>[18]</sup> In 1947

**Table 1:** Properties of different types of emulsions

	size	stabilizer	formation	stability	refs
(Macro-) Emulsion	> 200 nm	little or no surfactant	energy input shearing mixing agitation	creaming flocculation coalescence Ostwald-ripening	[1, 2]
Nanoemulsion	20 - 200 nm	little surfactant	energy input high pressure ultrasonic PIT/PIC	kinetically stable Ostwald-ripening	[4–8]
Microemulsion	3 - 50 nm	surfactant and cosurfactant	spontaneous formation no extra energy	thermodynamically stable	[9–11]

Winsor first classified microemulsions into water-in-oil (W/O), oil-in-water (O/W) and bicontinuous structures.<sup>[19]</sup> These first discoveries were followed by a thorough investigation of microemulsion systems with nonionic surfactants by several groups with special focus on their temperature dependent behavior.<sup>[20]</sup> Nonionic alkylethoxylate surfactants undergo pronounced changes of their EO headgroup polarity with temperature, which results in different solvation and therefore geometric requirements at the oil/water interface. The spontaneous curvature of the surfactant film is one key parameter to tune microemulsion structures. In this contents, also the so-called 'Kahlweit fish' was developed to describe structural properties of microemulsion systems according to the Winsor phases in dependence of their composition and temperature.<sup>[21]</sup> Similar changes in the spontaneous curvature of the interfacial surfactant film can be obtained by increasing the ionic strength (for ionic surfactants only) or addition of a cosurfactant. Three driving forces are responsible for the structural appearance of microemulsions. First, the interface between oil and water favors to be as small as possible. Second, the entropy that is gained by the dispersion of droplets should be large. The entropy gain is larger the more droplets are present, hence the smaller the droplets are. And third, the geometrical preferences of the employed surfactants, meaning the spontaneous curvature of the surfactant film, have to be satisfied. The free energy  $F$  of such a system is given by the sum of the interfacial energy  $F_t$ , a bending energy term  $F_b$  and an entropic term  $F_{ent}$ .<sup>[22,23]</sup>

$$F = F_t + F_b + F_{ent} = \gamma A + \int \left[ \frac{\kappa}{2} (c_1 + c_2 - 2c_0)^2 + \bar{\kappa} c_1 c_2 \right] dA + nk_B T \cdot f(\phi) \quad (1)$$

Here,  $\gamma$  is the interfacial tension,  $A$  is the total surface area,  $c_1$  and  $c_2$  the two principal curvatures and  $c_0$  the spontaneous curvature of the surfactant film.  $\kappa$  is the mean bending modulus,  $\bar{\kappa}$  is the Gaussian modulus and finally  $f(\phi)$  is a function of the dispersed volume fraction  $\phi$ , that accounts for the entropy of mixing.<sup>[24]</sup> Most current theories name the bending elasticity of the amphiphilic film as the key factor to describe microemulsion structure and formation.<sup>[25]</sup> The mean bending modulus  $\kappa$  should always be positive, since only in this case the spontaneous curvature is favored. The Gaussian modulus  $\bar{\kappa}$  might either be negative in which case droplet structures will be favored, or positive which will favor saddle-splay structures as in bicontinuous microemulsions.

Microemulsions are thermodynamically stable if the interfacial tension is low enough to be compensated by the dispersion entropy of the droplets, typically below  $10^{-2}$  mN/m,<sup>[9,10]</sup> so  $F_t$  can be neglected. For the case of spherical droplets of radius  $R$  as they are present in this work,  $c_1 = c_2 = c = 1/R$  and Eq. 1 can be simplified to:

$$\frac{F}{A} = 2\kappa \left( \frac{1}{R} - \frac{1}{R_0} \right)^2 + \frac{\bar{\kappa}}{R^2} + \frac{nk_B T}{A} \cdot f(\phi) \quad (2)$$

As mentioned above, one key parameter for microemulsion formation is the spontaneous curvature. This can be tuned by parameters like temperature, salt or the addition of a cosurfactant (typically medium chain length alcohols). Cosurfactants facilitate the microemulsion formation

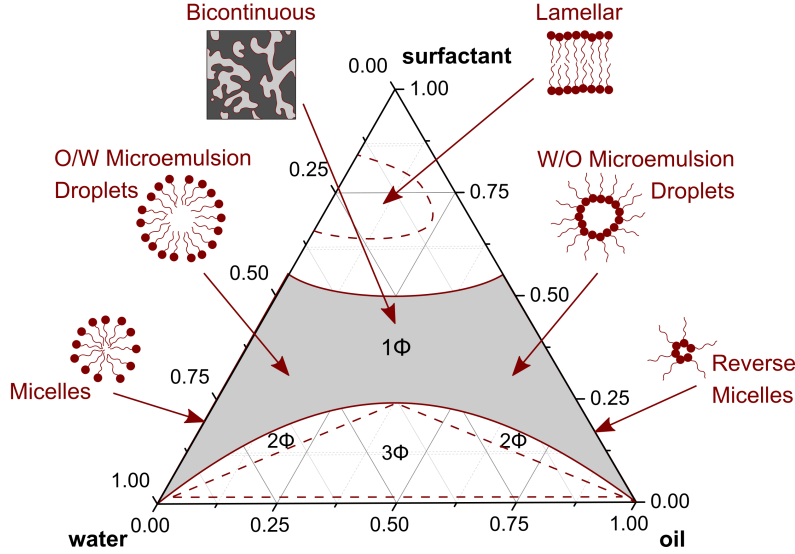


**Figure 1:** Generic phase diagram of a microemulsion forming surfactant/oil/water system indicating the structural arrangements in different regions of the single phase domain. At high concentrations a liquid crystalline lamellar phase is formed.

by decreasing the interfacial tension, but are also structurally affecting the microemulsion by contributing to the hydrophobic volume of the surfactant and thereby increasing the packing parameter  $p$ .

$$p = \frac{v_h}{a \cdot l} \quad (3)$$

where  $v_h$  is the volume of the hydrophobic chain,  $a$  is the head group area and  $l$  is the chain length. A larger packing parameter reduces the preferred curvature of the amphiphilic film, allowing larger droplets to be stable. The addition of cosurfactant can therefore be used to tune the size of the microemulsion droplets.<sup>[26,27]</sup>

Depending on the spontaneous curvature of the surfactant and the composition of the microemulsion system, different structures can be obtained. The phase behavior of a simple microemulsion system comprising oil, water and surfactant is summarized in a generic ternary phase diagram in Fig. 1. Each corner of the phase diagram represents 100 % of the respective compound. It should be noted that the structural changes, from O/W over bicontinuous to W/O microemulsions, occur continuously so no phase boundaries can be drawn here.

The formation of charged microemulsions is complicated by the fact that ionic surfactants generally induce higher interfacial tensions and higher curvatures than nonionic ones. This problem can be mitigated by adding salt to screen the charges or adding cosurfactants. By substituting only small amounts of uncharged surfactants with an ionic one it is possible to induce a charge without changing the droplet structure. This approach is limited to small amounts of ionic surfactant, but within this range the charge density of the droplets can be varied systematically.<sup>[28,29]</sup>

Applications of microemulsions are very versatile as they are widely used, whenever it is necessary to disperse hydrophobic molecules in a hydrophilic solvent or vice versa. This is the case

for example in enhanced oil recovery (EOR), where the good wetting properties and very low interfacial tensions of microemulsions are needed for optimum performance.<sup>[30]</sup> In diesel fuels, water-in-fuel microemulsions can be used to reduce nitrogen oxide and soot emissions.<sup>[31]</sup> The low interfacial tensions of microemulsions are also used in detergents and cleaning products, where the microemulsion dissolves hydrophobic soil into the oil phase and can afterwards be removed with water. This bears the advantage of water-based formulations, lowering the need of harmful and toxic solvents.<sup>[32]</sup> A large field of microemulsion application is in cosmetics and pharmaceutical formulations.<sup>[33,34]</sup> For example O/W microemulsions are employed in shower formulations, cremes and sunscreen to achieve a light, not 'oily' feeling. Sometimes two- or three-phase microemulsion systems with added dyes are used for visual attractiveness. The first pharmaceutical microemulsion on the market is Neoral<sup>®</sup>, a self-microemulsifying system that forms a drug loaded O/W microemulsion when diluted in a drink.<sup>[35]</sup> In general microemulsion formulations provide a long shelf-life due to their thermodynamic stability. Further applications are in chemical reactions,<sup>[36]</sup> food industry<sup>[37]</sup> or extraction and recovery processes<sup>[38]</sup>.

## 1.2 Polymer/Microemulsion Systems

To adapt microemulsions to the specific needs of such applications, it might be necessary to add additives. For many applications controlled rheological properties are required that can be achieved by addition of polymers to microemulsion systems. Microemulsion gels were achieved by adding gelling agents such as gelatin that increase the viscosity of the continuous phase without adsorbing on or interacting with the microemulsion droplets.<sup>[39]</sup> In a different approach microemulsion gels were prepared by physically cross-linking O/W microemulsion droplets into a connected network with telechelic polymers, where the rheological effect depends largely on the length of the hydrophobic modification and the amount of added polymer.<sup>[40–42]</sup> Pronounced viscosity increases were also obtained by amphiphilic graft copolymers or by ABA blockcopolymers (A = hydrophilic block, B = hydrophobic block), both in oil-continuous microemulsions.<sup>[43,44]</sup> Kabalnov *et al.* studied the solubility of different polymer types in bicontinuous microemulsions, it was shown that hydrophobically modified polymers are incorporated into the microemulsion, while unmodified polymers only assemble in the water domains.<sup>[45,46]</sup> For blockcopolymer/microemulsion systems a dramatically enhanced solubilization capacity of the microemulsion was found.<sup>[47]</sup>

Surprisingly little research has been done on the interactions of charged microemulsion droplets with oppositely charged polyelectrolytes, where the complexation does not rely on hydrophobic forces but is based on electrostatic interactions. The effect of polyelectrolytes on the phase behavior and structure of W/O microemulsions was studied, but mostly with the aim of forming nanoparticles in these systems.<sup>[48,49]</sup> Note *et al.* investigated the phase diagram of a negatively charged SDS/pentanol based W/O microemulsion with the cationic polyelectrolyte poly(ethyleneimine) (PEI) and found that more than 30 wt% PEI can be incorporated within the aqueous phase. The incorporation of PEI leads to a substantial shift of the microemulsion regime within

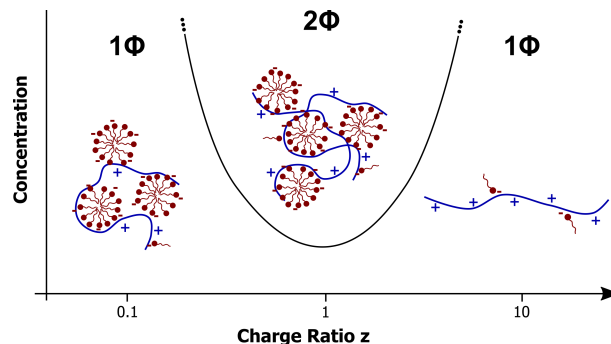


**Figure 2:** Schematic phase diagram of oppositely charged surfactant/polyelectrolyte mixtures as a function of the concentration and the charge ratio  $z = [\text{polyelectrolyte}]/[\text{surfactant}]$ . Inspired by Chiappisi *et al.*<sup>[54]</sup>

the phase diagram, leading to the formation of bicontinuous and even O/W structures.<sup>[50]</sup> One paper was published on the electrostatic and hydrophobic interactions of polyacrylic acid with O/W microemulsion droplets at different pH.<sup>[51]</sup> In most cases phase separation was observed. This paper gives an overview on different findings but little explanations and a subsequent paper was never published.

Work by Shi *et al.* addresses the electrostatic complexation of weakly charged silica nanoparticles with oppositely charged polyelectrolytes.<sup>[52,53]</sup> Even though nanoparticles instead of microemulsion droplets were used as model carriers in this work, the approach of this study is very similar to the work presented here.

### 1.3 Polyelectrolyte/Surfactant Complexes (PESC)

The interactions of charged surfactants with oppositely charged polyelectrolytes (PE) have been a subject of colloid science for more than 40 years. Surfactants and polyelectrolytes themselves already exhibit a structurally very versatile self assembly behavior thus it is not surprising that their combination offers even more possibilities. Special research interest lies in the formation of optimized smart systems that are responsive to certain stimuli.

The main driving force of complexation between oppositely charged surfactants and polyelectrolytes is the entropic gain by the release of counterions.<sup>[55]</sup> The phase behavior in dependence of the mixing ratio is typically characterized by a two-phase region (precipitated complexes or sometimes a coacervate phase with excess water) around equimolar charge mixing, where no excess charge is left for stabilization. Stable complexes with a variety of structures are observed at surfactant- and at polyelectrolyte excess, Fig. 2 depicts the situation. The formed structures depend on a number of parameters that can be tuned and adjusted to meet specific needs, such as the types of surfactants (packing parameter, head group), molecular weight, stiffness and charge density of the polyelectrolytes, the mixing ratio of both or the total concentration. External stimuli such as temperature, pH or ionic strength also play an important role, especially for smart responsive systems.

Out of the large variety of structures, only a few examples are chosen to be described in this context. Mixed aggregate formation may take place well below the cmc of the surfactant with single

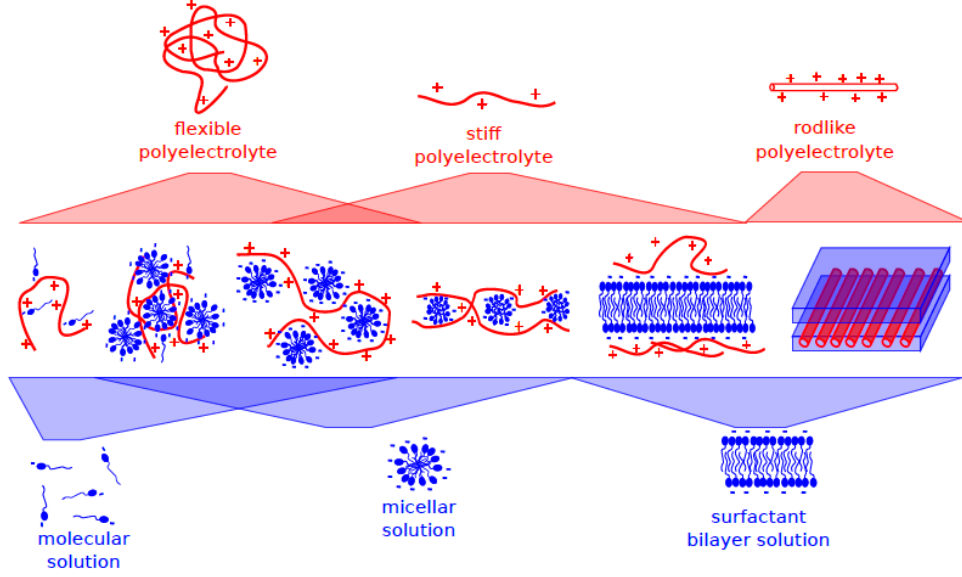


**Figure 3:** Variety of possible structures in polyelectrolyte/surfactant complexes, depending on the polyelectrolyte stiffness and the surfactant concentration and packing parameter. Reproduced from Ref. [63] with permission of L. Chiappisi.

surfactant molecules attached to a polyelectrolyte chain but also the formation of micelle-like aggregates on a polyelectrolyte chain is possible below the cmc.<sup>[56]</sup> Above the cmc, the complex structures also depend on the type of formed micelles. Spherical micelles can be arranged in dense aggregates or in pearl-necklace like structures, depending on the stiffness and charge density of the employed polyelectrolyte.<sup>[57]</sup> In some cases core-corona like structures are found, where the core is formed of densely packed micelles in an almost crystalline order, surrounded by a water soluble polymer-corona.<sup>[58,59]</sup> Cylindrical micelles can be decorated by polymer<sup>[60]</sup> and in the case of less curved surfactant aggregates, possible structures are the formation of multi-lamellar vesicles or surfactant bilayers decorated with polymer.<sup>[61]</sup> Fig. 3 summarizes different types of possible structures. In the two-phase region of the phase diagram, the phase separation can occur as precipitation of solid polyelectrolyte/surfactant complexes (PESC) or undergo a liquid-liquid phase separation to form a so-called coacervate. Coacervates are considered to be interesting materials for biomedicine and have therefore received a lot of attention.<sup>[62]</sup> In many cases solid precipitation is observed at low ionic strength, which can swell into a coacervate phase at sufficiently high amounts of added salt.

For all these different structural possibilities, one has to keep in mind, that the surfactant micelles might not retain their original shape when interacting with polyelectrolytes as the packing parameter (especially for ionic surfactants) will be influenced by the electrostatic interaction.

The formation of mixed polyelectrolyte/surfactant aggregates can lead to a pronounced increase in viscosity for specific compositions, typically close to the phase boundaries. Applications often require adjusted viscosities, it is therefore interesting to be able to modulate the viscosity of a system, simply by variation of the mixing ratio, without additional additives such as gelling agents. However, this is no general phenomenon and only observed for specific polyelectrolytes such as cationically modified cellulose (JR400), while complexes of hyaluronate (HA) show no

change in viscosity.<sup>[60,64,65]</sup> It is assumed that the viscosity increase might be correlated to the location of the charge on the polymer backbone, but the exact structural origin and especially the difference between JR400 and HA is not yet understood.

Potential applications of PESCs include medical and cosmetic applications, such as drug delivery processes or recovery and separation of pollutants or metal ions for example in wastewater treatment. Most of these applications require the loading of surfactant micelles with hydrophobic molecules or active agents, however solubilization capacities of micelles are typically rather small and very few studies address the solubilization capacity of micelles in PESCs.<sup>[66]</sup> For instance the loading and release properties of a hydrophobic model drug into a cationic hydrogel with SDS micelles was successfully studied but very small concentrations of the drug ( $< 0.2$  g/L) were used.<sup>[67]</sup> In a rare example, high loading capacities of 37.5 wt% were achieved for doxorubicin (DOX) in PESCs of the blockcopolymer PEG-*b*-PVBP with cationic surfactants.<sup>[68]</sup>

## 1.4 Motivation

As described above, a large number of PESC systems have been studied with respect to applications as drug delivery systems or model systems for carriers. It is often neglected that even though micelles contain hydrophobic cores, their solubilization capacity for hydrophobic molecules might be small and has to be studied for each surfactant system and each loading separately.

Microemulsions however, are an excellent medium for solubilization as they intrinsically combine large amounts of hydrophobic and hydrophilic material in one homogeneous mixture. Depending on the structure (O/W, bicontinuous or W/O) the dispersed phase can act as a potential reservoir for hydrophilic and/or lipophilic compounds. Due to the different domains, both polar and apolar and even amphiphilic molecules or molecules with a complex internal polarity can be solubilized. Additionally, microemulsion droplets are well-defined and monodisperse model colloids which makes them highly suited for a systematic investigation.

Regarding the large structural variety of PESCs and the high research interest in such structures, it is surprising that complexes of polyelectrolytes with microemulsions have only received very little attention so far. Nearly no research has been carried out on mixtures of charged microemulsion droplets with oppositely charged polyelectrolytes, where the complexation would be driven by electrostatic interactions and concomitant counterion release. The idea of gaining structural control of the microemulsion system on a larger length scale via polyelectrolyte addition has not been exploited yet.

The aim of this work is to develop and characterize polyelectrolyte/microemulsion systems based on weakly charged O/W microemulsion droplets interacting with different types of oppositely charged polyelectrolytes as a model hybrid system with high hydrophobic loadings. For a thorough fundamental investigation of such systems we have studied the phase behavior, the structure of the formed complexes and the dynamic properties in dependence of the mixing ratio, the droplet size and the type and molecular weight of the polyelectrolyte. Other parameters

that influence the interactions like the concentration, the ionic strength and the charge densities of microemulsion droplets and polyelectrolyte chains were also studied. In addition the corresponding polyelectrolyte/surfactant system, where the micelles are symbolizing empty carriers, was investigated. The results obtained from all these different experiments are compiled in the following chapters.

## 2 Theoretical Background

### 2.1 Materials

#### 2.1.1 The Microemulsion

As a model microemulsion the already well-studied (O/W) microemulsion system of TDMAO/decane/water was chosen.<sup>[26]</sup> TDMAO (tetradecyldimethylamine oxide, freeze dried from its 25 % aqueous solution 'Ammonyx M', received as a gift from Stepan, USA) self-assembles into rodlike micelles. It was found that upon addition of oil, a rod to sphere transition occurs and spherical microemulsion droplets are formed. Depending on the pH conditions, the behavior of the zwitterionic surfactant lies between that of a cationic and a purely nonionic surfactant.<sup>[69]</sup> At lower pH the oxygen becomes protonated, leading to  $\text{TDMAOH}^+$ , so the charge of the microemulsion could be varied by simply adjusting the pH. To vary the charge density on the microemulsion droplet surface separately from the added polyelectrolyte, a cationic surfactant was added to the system. TTAB (tetradecyltrimethylammonium bromide, 99 %, Sigma Aldrich, used without further purification) was chosen because of its structural resemblance to TDMAO. This way, small fractions of the neutral surfactant TDMAO can be substituted by the cationic TTAB without changing the microemulsion structure.<sup>[29]</sup>

If not indicated otherwise, all samples in this work were prepared between pH 7 and 8 where TDMAO behaves as a neutral surfactant and the charge can be assumed to originate from the TTAB molecules only. The charge of the microemulsion droplets can be adjusted by simply varying the amount of added TTAB. If not indicated otherwise, the microemulsions are prepared with a total surfactant concentration (TDMAO + TTAB) of 100 mM, containing 5 % of TTAB. Since  $\gamma R^2 \propto k_B T$ , bigger microemulsion droplets can be obtained by lowering the interfacial tension  $\gamma$ . This can be achieved by varying the amount of added cosurfactant (1-hexanol, >98 %, MERCK-Schuchardt OHG). Bigger microemulsion droplets are of course able to solubilize more oil (decane, >98 %, Fluka Chemika). Three different microemulsion droplet sizes were used in this work: containing 0, 50, and 75 mM of hexanol with 30, 80, 200 mM decane respectively, resulting in sizes of  $\sim 3$ , 4 and 6.5 nm. They were named according to their hexanol content: ME00, ME50 and ME75.

Fig. 4 shows the chemical structures of the components contained in the microemulsion. All microemulsions were prepared as stock solutions that consisted of 200 mM surfactant (TDMAO + TTAB). They were always prepared by first dissolving the two surfactants in water before adding the cosurfactant. The oil was always added last, after all other ingredients were mixed properly. It

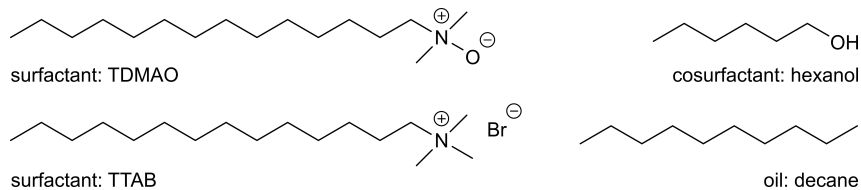


**Figure 4:** Chemical structures of all chemical components contained in the microemulsion.

was shown that the microemulsion (as well as the microemulsion/polyelectrolyte complexes) form independently of the mixing protocol, which proves their state of thermodynamic equilibrium. But other than for this test the protocol described above was followed for convenience reasons.

### 2.1.2 The Polyelectrolytes

The main polyelectrolyte used in this work is the sodium salt of polyacrylic acid (PAA), i.e., sodium polyacrylate (NaPA) which was either purchased directly or prepared by adding a stoichiometric amount of NaOH to the PAA. The molecular weights used in this work were: 5.1 kDa (DP = average degree of polymerization =  $[-]/\text{polymer} = 54$ ; sodium salt, used as received from Sigma Aldrich), 15 kDa (DP = 160; sodium salt solution from Sigma Aldrich, freeze dried before use), 60 kDa (DP = 638; sodium salt, used as received from Fluka Chemika) and 240 kDa (PAA; solution from Acros Organics, prepared by adding a stoichiometric amount of NaOH to the solution and freeze dried before use, which results in an average molecular weight of 315 kDa for NaPA, DP = 3330). These molecular weights correspond to contour lengths (lengths of the stretched polyelectrolyte) of 14, 40, 160, and 850 nm respectively. The corresponding overlap concentrations for these polymers (assuming fully stretched chains) are 32, 3.9, 0.25, and 0.007 mM (in monomer units). To distinguish between the different lengths, the polymers were named according to their molecular weight: NaPA05, NaPA15, NaPA60 and NaPA315.

More experiments were carried out with biopolyelectrolytes, namely the sodium salt of hyaluronic acid, sodium hyaluronate (NaHA) and sodium carboxymethyl cellulose (NaCMC). Sodium hyaluronate was initially used in four different molecular weights: 51 kDa, 150 kDa, 360 kDa (Lifecore, used as received without further purification) and 800 kDa (SRD, used as received). Later, new batches of NaHA were ordered with 31, 186, 572 and 2073 kDa (all Laboratory Grade from CONTIPRO, used as received). Sodium carboxymethyl cellulose was employed as 90 kDa and 250 kDa (Sigma Aldrich, used as received). The theoretical lengths of the stretched polyelectrolytes (contour lengths) are: 130, 370, 900 and 2000 nm for the NaHA51, 150, 360 and 800 respectively and 80, 460, 1400 and 5200 nm for NaHA31, 186, 572 and 2073. The contour lengths for CMC90 and CMC250 are 200 and 480 nm respectively.

The biopolyelectrolytes differ from the NaPA in their charge density and also in their persistence lengths. NaPA is a very flexible polyelectrolyte with an intrinsic persistence length of 1.3 nm<sup>[70]</sup> and a high charge density of 4 charges/nm. In contrast, NaHA has a persistence length of 9 nm<sup>[71]</sup> and a charge density of 1 charge/nm. NaCMC has a persistence lengths of 6-16 nm<sup>[72]</sup> and differs from the other polyelectrolytes in the location of the charges. The charges are located further

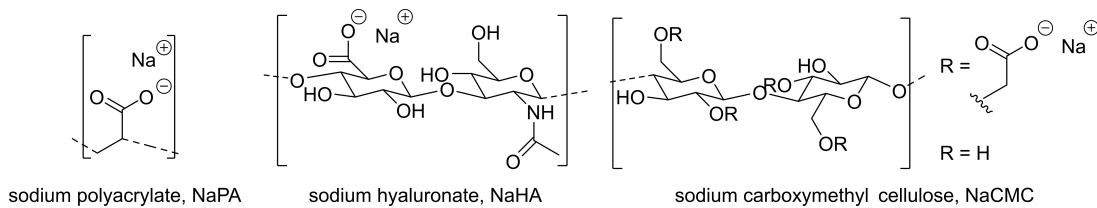


**Figure 5:** Chemical structures of all employed polyelectrolytes.

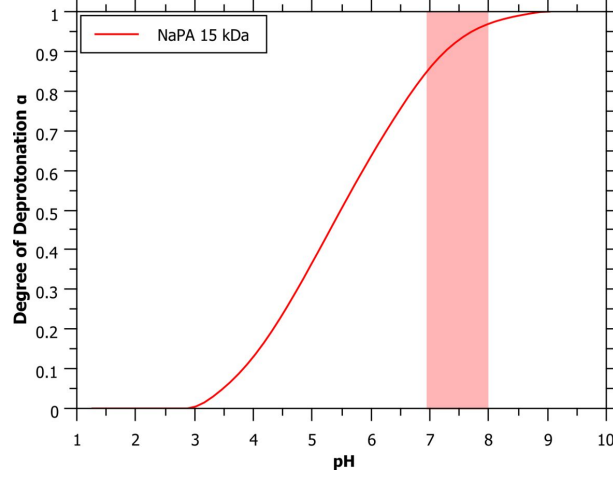


**Figure 6:** Degree of deprotonation of NaPA15, obtained from titration with HCl. All samples were prepared between pH 7 and 8, the area is shaded in red. Reproduced from Ref. [73] with permission of the Royal Society of Chemistry.

away from the polymer backbone and are therefore more easily accessible. The two sodium carboxymethyl celluloses employed do not only differ in their molecular weight but also in their charge density, which is defined by the degree of substitution (DS). The higher  $M_w$  NaCMC250 also contains the higher charge density with 1.2 charges per monomer unit while NaCMC90 only has a DS of 0.7. A monomer unit of CMC is  $\sim 1$  nm long.

Since all polyelectrolytes employed contain carboxylates as their charged groups, their charge density strongly depends on the pH. Titration curves were measured and from the titration curves the degree of deprotonation  $\alpha$  was calculated which can be seen exemplary in Fig. 6 for NaPA15. All samples were prepared at pH-values between 7 and 8 where the polyelectrolytes should be more than 85 % deprotonated.

### 2.1.3 Sample Preparation

To form microemulsion/polyelectrolyte complexes, the charged microemulsion and the polyelectrolytes were mixed in different charge ratios  $z$ . The charge ratio is defined by the amount of negative polyelectrolyte charges divided by the total amount of charge:

$$z = \frac{[-]}{[-] + [+]} \quad (4)$$

where  $[-]$  and  $[+]$  are the nominal charges of the negatively charged polyelectrolytes and the positively charged TTAB molecules in the microemulsion droplets respectively. The prepared charge ratios range from 0 to 1 where  $z$ -values  $< 0.5$  indicate a microemulsion charge excess and samples with  $z > 0.5$  contain a polyelectrolyte charge excess. A  $z$ -value of 0.5 indicates a (nominal) charge equilibrium.

All samples prepared consisted of a constant microemulsion concentration of 100 mM surfactant and varying polyelectrolyte concentrations, according to the desired  $z$ -value. It is assumed that the formed complexes are at thermodynamic equilibrium, hence the mixing procedure should

not have any influence on the complexes. Still, all samples were prepared by first diluting the 200 mM microemulsion stock solution with water and then adding the right amount of NaPA stock solution. The samples were shaken briefly to mix all ingredients properly. All samples were prepared in Milli-Q water or D<sub>2</sub>O (>99.5 %D, Eurisotop) for neutron and NMR experiments. Samples are named according to composition, the first block indicates the used microemulsion by the amount of hexanol, the second specifies type and  $M_w$  of the used polyelectrolyte and the mixing ratio is given in the end. E.g. ME50-NaPA60-70 is a sample with medium sized droplets (50 mM of hexanol) and sodium polyacrylate of 60 kDa, mixed at  $z = 0.70$ .

The macroscopic phase behavior of the samples was studied by taking photographs of the samples one hour, one day and one week after sample preparation. Samples that show phase separation in less than an hour after mixing were labelled biphasic. Metastable samples are samples which need from one hour up to one week to phase separate. Directly after mixing, the metastable samples appeared clear, but then changed color to bluish and eventually white before phase separating into a clear liquid and a solid, white precipitate. All samples that still consist of one single phase after one week were considered as thermodynamically stable single phase systems, as they did not evolve during the course of several months.

### 2.1.4 List of Chemicals

Other compounds like hydrophobically modified polymers or microemulsions with different amounts of added TTAB are described in the respective chapters.

**Table 2:** Summary of all used chemicals.

Name	$\Sigma$ formula	origin	$M_w$ g/mol	$\rho^*$ g/cm <sup>3</sup>	SLD 10 <sup>-6</sup> Å <sup>-2</sup>	$dn/dc^{**}$ cm <sup>3</sup> /g
TDMAO	C <sub>14</sub> H <sub>29</sub> N(CH <sub>3</sub> ) <sub>2</sub> O	Stepan Company	257.45	0.897	-0.197	-
TTAB	C <sub>14</sub> H <sub>29</sub> N(CH <sub>3</sub> ) <sub>3</sub> Br	Sigma Aldrich	336.41	1.026	-0.476	-
hexanol	C <sub>6</sub> H <sub>13</sub> OH	MERCK-Schuchardt	102.18	0.82	-0.323	-
decane	C <sub>10</sub> H <sub>22</sub>	Fulka Chemika	142.29	0.73	-0.489	-
d-decane	C <sub>10</sub> D <sub>22</sub>	Eurisotop	164.42	0.842	6.58	-
NaPA	(C <sub>3</sub> H <sub>3</sub> COONa) <sub>n</sub>	Sigma Aldrich, Fulka Chemika, Arcos Organics	94.05	1.22	1.87	0.1494
NaHA	(C <sub>14</sub> H <sub>19</sub> O <sub>11</sub> Na) <sub>n</sub>	Lifecore, SRD, CONTIPRO	401.3	1.8	2.57	0.1563
NaCMC	(C <sub>12</sub> H <sub>14</sub> O <sub>10</sub> R <sub>3</sub> ) <sub>n</sub> R = CH <sub>2</sub> COONa, H	Sigma Aldrich	436 - 516	1.6	2.38	0.1546
HCl	HCl	Roth	36.46	-	-	-
NaOH	NaOH	Roth	40.0	-	-	-
NaCl	NaCl	Sigma Aldrich	58.44	-	-	-
H <sub>2</sub> O	H <sub>2</sub> O	Milli-Q	18.02	1.0	-0.561	-
D <sub>2</sub> O	D <sub>2</sub> O	Eurisotop	20.03	1.1	6.34	-

\* Density  $\rho$  at 25 °C

\*\*  $dn/dc$  measured in D<sub>2</sub>O

**Table 3:** Summary of microemulsions used in this work.

Name	TDMAO/TTAB / mM	hexanol / mM	decane / mM	$R_{(SANS)}$ / nm	$\phi$	$\Delta SLD$ $10^{-4} \text{ nm}^{-2}$	$dn/dc^{**}$ $\text{cm}^3/\text{g}$
ME00	95 / 5	0	30	3.1	0.032	-6.60	0.1176
ME50	95 / 5	50	80	4.3	0.047	-6.65	-
ME75	95 / 5	75	200	6.5	0.070	-6.70	-
S00	95 / 5	0	0	ellipsoid	0.028	-6.55	-

## 2.2 Methods

### 2.2.1 Light Scattering

An often used technique for examining micro or nano structures in solution is the analysis of scattering patterns from light, x-rays or neutrons. Light is scattered due to differences in the refractive index, which are caused by a different polarizability of the medium and the particles. x-rays interact with the electron clouds of atoms and are therefore scattered by different electron densities, while neutrons interact differently with different atomic nuclei. This means, that complementary information can be obtained from experiments with the different radiation sources due to the different contrasts. Neutron scattering has the advantage that different isotopes like H and D can be distinguished, which gives more possibilities of adjusting the contrast.

As shown in Fig. 7, the setup of a scattering experiment is very simple. The radiation source is focused on the sample and the scattering intensity over time is detected in dependence of the magnitude of the scattering vector  $q$ .

$$q = |\vec{q}| = \frac{4\pi n \cdot \sin \frac{\theta}{2}}{\lambda} \quad (5)$$

The scattering vector  $q$  depends on the wavelength  $\lambda$  and the scattering angle  $\theta$ ,  $n$  is the refractive index of the sample which is  $\sim 1$  for neutrons.

**Static Light Scattering (SLS).** For static light scattering (SLS) the average intensity scattered by the sample over time is measured as a function of the scattering angle to obtain structural

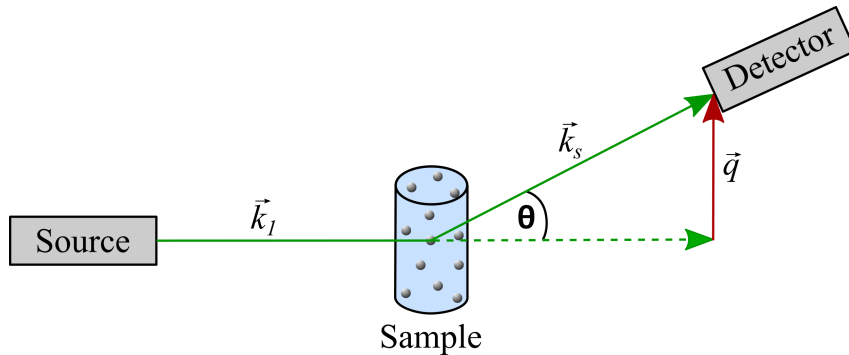


**Figure 7:** Simple set up for scattering experiments, the source can be a laser for visible light, but also x-rays or neutrons.

information. The measured intensity has to be corrected and normalized for each angle as follows:

$$I(q) = \frac{\left(\frac{CR1}{I_{mon}}\right)_{\text{sample}} - \left(\frac{CR1}{I_{mon}}\right)_{\text{solvent}}}{\left(\frac{CR1}{I_{mon}}\right)_{\text{toluene}}} \cdot R_{\theta, \text{toluene}} \quad (6)$$

$CR1$  is the mean scattered intensity of the sample, normalized by the initial laser intensity  $I_{mon}$ . The background scattering from the solvent and the cuvette has to be subtracted and a calibration with a standard (toluene in this case) has to be applied.  $R_{\theta, \text{toluene}}$  is the Rayleigh ratio of toluene.<sup>[74]</sup> Theoretically, the scattered intensity has to be corrected for the transmission of the sample as well. In this work, the transmission was neglected because UV-Vis measurements showed transmissions of  $> 99\%$  at 632.8 nm, the wavelength of the laser used for light scattering experiments, for all tested samples.

For particle sizes  $> \lambda/20$  information about the particle shape can be extracted from the angular dependence of the scattered intensity. In this case, the scattered intensity  $I(q)$  can be described with the Guinier approximation.<sup>[75]</sup>

$$\lim_{q \rightarrow 0} I(q) = I(0) \cdot \exp\left(-\frac{q^2 \cdot R_g^2}{3}\right) \quad (7)$$

To obtain the forward scattering and the radius of gyration,  $\ln I(q)$  can be plotted versus  $q^2$ .

$$\ln I(q) = \ln I(0) - \frac{R_g^2}{3} \cdot q^2 \quad (8)$$

$I(0)$  is the forward scattering which, in case of non-interacting particles, is directly proportional to the mass average molecular weight  $M_w$  and  $R_g$  is the radius of gyration around the center of mass of the particle.

$$I(0) = K_L \cdot c \cdot M_w \quad (9)$$

$$\text{with: } K_L = \frac{4\pi^2}{\lambda^4 \cdot N_A} \cdot n_0^2 \cdot \left(\frac{dn}{dc}\right)^2 \quad (10)$$

$K_L$  is the optical constant, which is calculated from the wavelength  $\lambda$ , the Avogadro constant  $N_A$ , the refractive index of the solvent  $n_0$  and the refractive index increment  $(dn/dc)$ .

**Dynamic Light Scattering (DLS).** In dynamic light scattering (DLS), the intensity fluctuations of the sample at a given angle with time are observed. Provided the fluctuations are due to Brownian motion of the scattering particles, the collective diffusion coefficient can be obtained. The intensity-auto-correlation function  $g^{(2)}(\tau)$  is calculated from the scattering intensity fluctuations as follows.<sup>[76]</sup>

$$g^{(2)}(\tau) = \frac{\langle I(t)I(t+\tau) \rangle}{\langle I(t) \rangle^2} \quad (11)$$

with  $I(t)$  and  $I(t+\tau)$  being the measured intensities at time  $t$  and  $t+\tau$  respectively. The intensity

correlation function is linked to the field-auto-correlation  $g^{(1)}(\tau)$  by the Siegert relation.<sup>[77]</sup>

$$g^{(2)}(\tau) = B + \beta \left[ g^{(1)}(\tau) \right]^2 \quad (12)$$

The field correlation function  $g^{(1)}(\tau)$  for each measured angle was fitted with a stretched exponential function to obtain the decay time  $\tau_K$ . The stretched exponential function can be interpreted as a superposition of simple exponentials with a distribution of relaxation times. Here the stretching exponent  $\alpha$ , which can attain values between 0 and 1, is a measure for the polydispersity with  $\alpha = 1$  being the case of perfectly monodisperse scatterers.

$$g^{(1)}(\tau) = A \cdot \exp \left( - \left( \frac{1}{\tau_K} \cdot \tau \right)^\alpha \right) \quad (13)$$

The  $n^{th}$  moment of the distribution can be calculated by

$$\langle \tau_K^n \rangle = \frac{\tau_K^n}{\alpha} \cdot \Gamma \left( \frac{n}{\alpha} \right) \quad (14)$$

so that the mean relaxation time is  $\langle \tau_K \rangle = \frac{\tau_K}{\alpha} \cdot \Gamma \left( \frac{1}{\alpha} \right)$  with  $\Gamma(t)$  being the gamma function  $\Gamma(t) = \int_0^\infty x^{t-1} e^{-x} dx$ . If the observed motion is a diffusive relaxation,  $\langle \tau_K \rangle$  is inversely proportional to  $q^2$  with the proportionality constant being the collective diffusion coefficient  $D_{coll}$ .

$$\frac{1}{\langle \tau_K \rangle} = D_{coll} \cdot q^2 \quad (15)$$

So finally  $D_{coll}$  can be obtained from the slope of an  $\frac{1}{\langle \tau_K \rangle}$  vs.  $q^2$  plot. Other non-diffusive motions may follow different power laws  $q^x$ , e.g.  $q^3$  was observed for polymer relaxation.<sup>[78]</sup>

DLS measures the collective diffusion coefficient  $D_{coll}$ , which is not always equal to the diffusion coefficient of non-interacting particles ( $D_0$ ). Neglecting hydrodynamic interactions and just taking into account the direct particle interactions, the structure factor  $S(q)$  modifies  $D_0$  according to de Gennes narrowing.<sup>[79]</sup>

$$D_{coll} = \frac{D_0}{S(q)} \quad (16)$$

With the Stokes Einstein equation the hydrodynamic radius  $R_h$  can be calculated from the diffusion coefficient of non-interacting particles:

$$R_h = \frac{k_B \cdot T}{6\pi \cdot \eta_0 \cdot D} \quad (17)$$

with  $k_B$  being the Boltzmann constant and  $\eta_0$  the viscosity of the solvent.

The polydispersity index (PDI) can be calculated by dividing the second moment by the square of the first moment of the distribution.<sup>[80]</sup>

$$\text{PDI} = \frac{\langle \tau_K^2 \rangle}{\langle \tau_K \rangle^2} \quad (18)$$

For some samples that showed two decays in their correlation function a bimodal size distribution was used by fitting the sum of two stretched exponentials to  $g^{(1)}(\tau)$ .

Static (SLS) and dynamic (DLS) light scattering measurements were performed simultaneously on an ALV/CGS-3 instrument, with a He-Ne laser with a wavelength of  $\lambda = 632.8$  nm. Pseudo-cross-correlation functions were recorded using an ALV 5000/E multiple- $\tau$  correlator at scattering angles  $\theta$  ranging from 40 to 130°, set with an ALV-SP 125 goniometer.

### 2.2.2 Small-Angle Neutron Scattering (SANS)

For a neutron scattering experiment, a neutron source is needed that can be a nuclear reactor or a spallation source. In general, the white neutron beam first passes a velocity selector where only the fraction of neutrons with the chosen wavelength is selected, before being focused on the sample by a collimator. Time-of-flight (TOF) instruments measure with a pulsed white beam and the wavelength of each neutron is calculated from the travel time and distance to the detector. The neutrons that are scattered in the sample are detected by a 2D detector which is set at a certain (adjustable) distance from the sample. All non-scattered neutrons are absorbed by a beamstop. The wavelength of neutrons is typically in the Å regime, which allows measuring much higher  $q$  values than in light scattering. Since a scattering experiment always gives information in reciprocal space, higher  $q$  values allow to examine smaller structures. Which, next to the contrast conditions, is one big advantage of neutron scattering. In a SANS experiment (as it was performed in this work), typically three configurations of sample-detector distance and wavelength are measured to cover a wide  $q$ -range.

Three SANS beamtimes were carried out at PAXY at the Laboratoire Léon Brillouin (LLB) in Saclay, France. Measurements in May 2015 were performed with sample-to-detector distances of 1.2, 2, and 6 m, collimation lengths of 2, 2, and 6 m and wavelengths of 4, 10, and 10 Å, respectively, to cover a  $q$  range from 0.031 to 5.05 nm<sup>-1</sup>. Measurements in May 2016 and March 2017 were performed with sample-to-detector distances of 1.2, 5, and 6.6 m, collimation lengths of 2, 5, and 6 m and wavelengths of 4, 4, and 12 Å, respectively, to cover a  $q$  range from 0.03 to 5.4 nm<sup>-1</sup>.

Two beamtimes were carried out at the Institut Laue-Langevin (ILL) in Grenoble, France. In November 2016 the samples were measured at the instrument D11<sup>[81]</sup> with a wavelength of 6 Å and sample to detector distances of 1.5, 8 and 34 m and collimation lengths of 8, 8 and 34 m, respectively. The  $q$  range covered was 0.024 to 4.1 nm<sup>-1</sup>. In June 2019 measurements were performed on D33 with sample-to-detector distances of 2(1.2), 7.8 and 12 m, collimation lengths of 2.8, 7.8, and 12 m and wavelengths of 4.6, 4.6, and 13 Å, respectively, to cover a  $q$  range from 0.013 to 6.1 nm<sup>-1</sup>. D33 has an additional detector at 1.2 m to measure the large  $q$  simultaneously to the 2 m setting.

One beamtime was granted in June 2018 at KWS-2,<sup>[82,83]</sup> operated by the Jülich Centre for

Neutron Science (JCNS) at MLZ in Munich. Here, sample to detector distances of 2, 8 and 20 m were used with collimation lengths of 8, 8 and 20 m and wavelengths of 5, 5, and 10 Å, respectively. The  $q$  range covered was 0.014 to 4.9 nm<sup>-1</sup>.

Some additional measurements were carried out at the instrument V4 at Helmholtz Zentrum Berlin (HZB)<sup>[84]</sup> in August 2015. The samples were measured at wavelengths of 4.5, 4.5 and 10 Å with sample to detector distances of 1.35, 6.75 and 15.75 m and collimation length of 2, 8 and 16 m respectively. Here, a  $q$  range of 0.025 to 5.2 nm<sup>-1</sup> was covered.

Data reduction was done using the software BerSANS<sup>[85]</sup> for LLB and HZB data, LAMP<sup>[86]</sup> for ILL data and QtiKWS<sup>[87]</sup> for MLZ data. In all cases, the raw intensity data was corrected for the scattering of the background (solvent and sample containers) and weighted by the transmission of the sample. Additionally, the background noise was subtracted using a cadmium sample, which absorbs all incoming neutrons. The normalization and absolute scaling was done by using a 1 mm reference sample of milli-Q water as an isotropic scatterer. Finally, the 2D data were radially averaged into 1D scattered intensity.

### 2.2.3 Analysis of SANS data

**Model-free Analysis.** For the model-free analysis of SANS data, only separate features of the SANS curves are analyzed and no form or structure factor is fitted. Here, it is important to remember that  $q$  has the unit of an inverse length. Therefore, large areas are probed at small  $q$  while small distances can be seen at large  $q$ .

The scattering curve at very low  $q$ , where the probed range is much larger than the particle size, can be described by the Guinier approximation just as in static light scattering (Eq. 7). The Guinier approximation is restricted to low angles where  $qR_g < 1$  and to non-interacting particles. If interparticle interaction (a structure factor) is observed, the determined radius of gyration can not be interpreted, but the Guinier approximation can still be used to obtain the forward scattering  $I(0)$ . This is possible since the  $q^2$  dependency of  $I(q)$  is maintained as it was shown by Ostanevich.<sup>[88]</sup> Just like in light scattering, the forward scattering intensity  $I(0)$  can be used to calculate the molecular weight  $M_w$  by using the density of the particles  $\rho$ , the volume fraction  $\phi$  and the contrast, meaning the difference in scattering length densities of particles and solvent  $\Delta SLD$ .

$$M_w = I(0) \cdot \frac{\rho \cdot N_A}{\phi \cdot \Delta SLD^2} \quad (19)$$

Larger particles or aggregates cause an increase of the scattered intensity at low  $q$ . This increase may follow a  $q^{-x}$  power law, where  $x = 1$  is usually interpreted as rodlike or cylindrical aggregates and  $x = 2$  as planar or lamellar structures. A power law of  $q^{-2}$  can also originate from random walk polymers or Gaussian coils. In this work, slopes between  $q^{-1}$  and  $q^{-2}$  were detected which shows the transition from rodlike aggregates starting to become more flexible and bending, until a Gaussian coil-like behavior is reached.

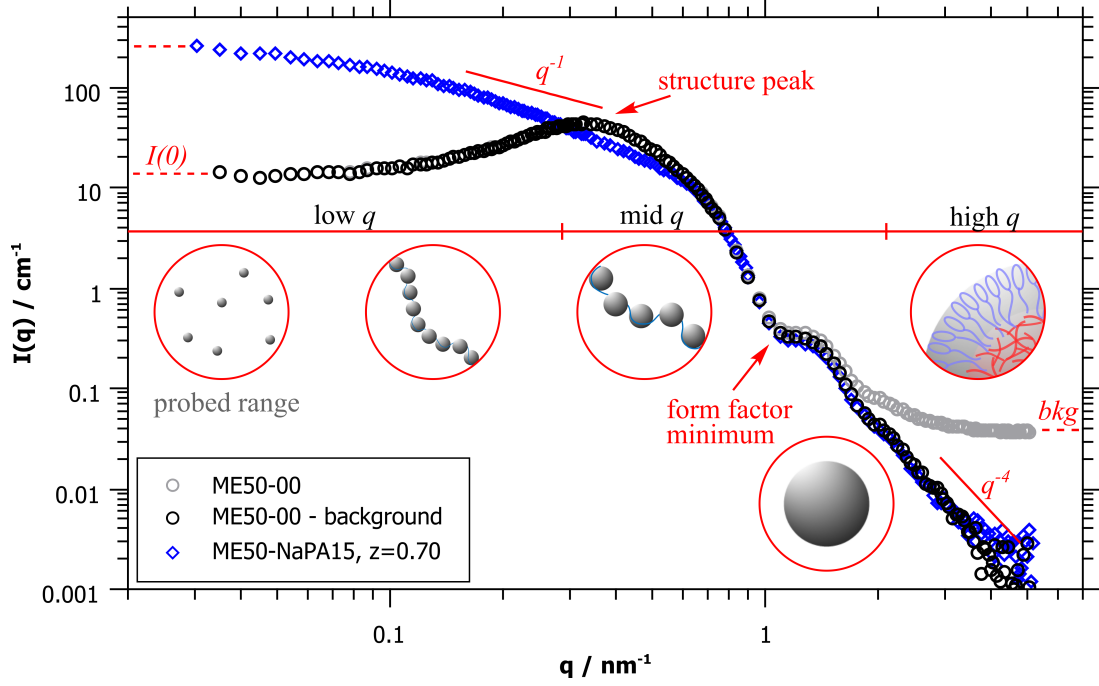


**Figure 8:** Features of SANS curves to be interpreted in model-free analysis. At low  $q$  the intercept  $I(0)$  can be extrapolated by Guinier analysis and is proportional to the  $M_w$ . The slope of the data at low to mid  $q$  gives information about the shape of complexes and a structure peak indicates the average distance between particles. The form factor minimum shows the size of one particle. At high  $q$ , after subtraction of the incoherent background, a  $q^{-4}$  power law indicates a smooth particle surface.

When relatively monodisperse particles are present at a sufficiently high concentration, a pronounced peak can appear in the mid  $q$  range. This peak belongs to the structure factor and arises from interactions of ordered particles. From its position  $q_{max}$ , the mean spacing between particles  $d$  can be obtained:

$$d = \frac{2\pi}{q_{max}} \quad (20)$$

For relatively monodisperse particles, a form factor minimum becomes visible if the probed range is approaching a size range similar to the probed objects. The depth of this minimum depends on the polydispersity of the particles. For spheres, the particle radius  $R$  can be calculated from the minimum as follows.

$$\tan(q_{min}R) = q_{min}R, \quad R \approx 4.5/q_{min} \quad (21)$$

The Porod region (at very high  $q$ ) corresponds to a probed range smaller than the scattering objects, so that the local structure is observed. Therefore, no interparticle effects and only the interface of the particles is visible. The Porod region gives information about the surface of the particles (smooth or rough) and the specific surface area ( $S/V$ ).<sup>[89]</sup> For sharp interfaces, the scattered intensity decays with the fourth power of  $q$ . A Porod fit can also be used to determine the incoherent background ( $bkg$ ) of the sample, as it was done for all SANS measurements in

this work.

$$I(q) = 2\pi(S/V)\Delta SLD^2 \cdot q^{-4} + bkg \quad (22)$$

For some analysis, it is useful to extend the  $q$  range to even smaller  $q$  values by combining light and neutron scattering data. This can be done by scaling the intensities obtained from SLS measurements, according to the differences in contrast with SANS data:

$$I(q)_{SLS} \cdot \frac{\lambda^4 \cdot \phi \cdot \Delta SLD^2}{4\pi^2 \cdot n_0^2 \cdot \left(\frac{dn}{dc}\right)^2 \cdot c \cdot \rho} = I(q)_{SANS} \quad (23)$$

**Fitting of SANS Data.** The scattering intensity as a function of the scattering vector  $q$  for homogenous, monodisperse, spherical particles can be described by the following expression:

$$I(q) = {}^1NV^2\Delta SLD^2 \cdot P(q) \cdot S(q) \quad (24)$$

where  ${}^1N$  is the number density of scattering particles,  $V$  is the volume of one particle,  $\Delta SLD$  is the contrast,  $P(q)$  is the form factor that describes the particle shape and  $S(q)$  is the structure factor, describing inter-particle interactions.

SANS fits were performed in absolute units using the software SASfit.<sup>[90]</sup> The volume fractions and  $\Delta SLD$ s were calculated under the assumption that all of the surfactant, cosurfactant, and oil are contained in the aggregates. The polyelectrolyte was considered as part of the solvent.

$$\Delta SLD = SLD_{ME} - SLD_{D_2O+PE} \quad (25)$$

A homogeneous sphere form factor was used to describe the microemulsion droplets. Depending on the scattering length density profiles, microemulsion droplets could also be regarded as spherical core-shell particles, but in this work, the simpler model was found to be sufficient. The polydispersity of the spheres was taken into account by a log-normal distribution of the radius. Microemulsions prepared with deuterated decane (Chapter 4.2.2) can be described by a spherical core-shell form factor. Decane-d<sub>22</sub> has a SLD very close to that of D<sub>2</sub>O, so only the surfactant shell of the microemulsion droplets is visible in SANS.

Most samples of PE/ME complexes close to the phase boundary showed a slope of  $q^{-1}$ . In some cases the cylindrical arrangement of droplets was described as a homogeneous cylinder with the Porod model for long cylinders. But since cylinders show slightly different intensities at medium  $q$  and also different form factor minima compared to spheres, a model which describes a cylindrical arrangement of separate droplets, developed in our group, was found to be in much better agreement with the measured data.<sup>[91]</sup> The special characteristic of this model is, that the interparticle distances between droplets within one aggregate are considered polydisperse. Thanks to this, no artificial structure peak is predicted at mid  $q$ , only a continuous increase of intensity with a slope of  $q^{-1}$ .

Since this model is designed to describe straight cylindrical arrangements of droplets but the ag-

gregates observed in this work tend to be more flexible cylinders that bend over their persistence lengths, another model was needed. In cooperation with E. Schneck, we have developed a Monte Carlo model that is able to simulate of curved droplet chains and deduce their respective persistence lengths. This model is especially interesting for the quantitative comparison of different polyelectrolytes (Chapter 4.2.1).

A somewhat simpler model to describe a bent chain is the wormlike chain model by Kholodenko, also known as 'Kholodenko worm'.<sup>[92]</sup> This model calculates a chain of homogeneous cylinders with lengths equal to the persistence length  $l_p$ , that are joined in random angles, accounting for excluded volume interactions. The model was used in Chapter 5.2.1, since the more physical model we have developed was still not available.

The reference surfactant aggregates consisting of TDMAO and TTAB, without hexanol and decane (Chapter 8) showed some deviations from the spherical model and were therefore treated as ellipsoids.

Structure factors were only rarely used to describe the SANS data in this work. In Chapter 3.2.1 we used a structure factor that accounts for the repulsive interactions of charged microemulsion droplets as well as for the attractive interactions induced by the bridging polyelectrolyte simultaneously.<sup>[93]</sup> With this model, it was only possible to describe the aggregates of small droplets and short chains because only the attractive interactions and no arrangement of particles is included. In Chapter 5.2.1 the structure factor of Baba-Ahmed *et al.* was used to account for the repulsive electrostatic interactions of free microemulsion droplets.<sup>[94]</sup>

Further details of all used models to describe the SANS data are given in the [Appendix](#).

#### 2.2.4 Neutron Spin Echo (NSE)

Neutron Spin Echo (NSE) is a high-resolution dynamic method, being able to deduce diffusion times or relaxations on the ns time scale and over a wide  $q$  range.

A NSE setup consists of a polarized neutron beam that undergoes a  $\pi/2$  spin flip. All spins are now oriented perpendicular to the beam and start Larmor precession due to the precession field along the beam axis. Due to the different velocities of all neutrons in the beam, the polarization is lost very soon. The phase angle  $\phi_p$  of a neutron with velocity  $v_1$  after a distance  $d_1$  is  $\phi_p = \gamma_N B_0 d_1 / v_1$ .  $\gamma_N$  is the gyromagnetic ratio of the neutron and  $B_0$  the strength of the guide field. The beam then passes a  $\pi$  flip which inverts the spins, effectively letting the spins rotate backwards. All spins are aligned again, i.e. the difference in phase angles is 0, after having traveled the same distance  $l_1$  again as from the  $\pi/2$  to the  $\pi$  flip.

$$\phi_{p,1} - \phi_{p,2} = \gamma_N B_0 d_1 / v - \gamma_N B_0 d_1 / v = 0 \quad (26)$$

The 'echo'-signal of the aligned spins is measured with the help of a second  $\pi/2$  flipper and an analyzer. The sample is placed at the position of the  $\pi$  flipper. If neutrons are scattered by the sample quasielastically, i.e. with a small change in their velocity, the echo amplitude is reduced, which is what is being measured in an NSE experiment.<sup>[95]</sup> The echo amplitude is also reduced

for higher magnitudes of the magnetic guide field applied parallel to the polarized beam. The Fourier time  $t_F$  is defined as follows:

$$t_F = \frac{\gamma_N J_i m_N^2}{2\pi h^2} \cdot \lambda^3 \quad (27)$$

with  $J_i$  being the field integral for a constant magnetic field,  $m_N$  is the mass of one neutron and  $h$  the Planck constant. The Fourier time scales with  $\lambda^3$ , so long wavelengths are needed to detect long times (small energy changes). During the measurement, the current of the magnetic field is increased to achieve higher Fourier times  $t_F$ .

An echo signal is measured for each Fourier time at different scattering angles and neutron wavelengths to cover a wide  $q$  range. The method then yields the intermediate scattering function  $S(q, t)$ , from which an apparent diffusion coefficient  $D_{app}$  can be deduced.

$$S(q, t)/S(q, 0) = \exp(-D_{app} \cdot q^2 t) \quad (28)$$

The dynamics of spherical microemulsion droplets can be described with the Milner-Safran Model.<sup>[96,97]</sup> This model accounts for the membrane undulation motions at high  $q$  and the translational diffusion of the free microemulsion droplets. The contributions from the membrane undulations are most pronounced at the form factor minimum.

NSE measurements were performed at the instrument IN15<sup>[98,99]</sup> at ILL (Grenoble, France) using wavelengths of 6, 10 and 14 Å reaching Fourier times of 42, 194 and 531 ns and covering a  $q$  range from 0.019 to 0.14 Å<sup>-1</sup>.

### 2.2.5 Cryo-TEM Imaging

Cryo-transmission electron microscopy (cryo-TEM) images were taken of selected samples by group members of Yeshayahu (Ishi) Talmon at the Technion in Haifa (Israel). A small droplet of the solution was placed on a perforated carbon film supported on a TEM copper grid, held by tweezers. It was then blotted by a piece of filter paper, resulting in the formation of thin films of 100 – 300 nm thickness within the micropores in the carbon film. The specimen was then plunged into a reservoir of liquid ethane, cooled by liquid nitrogen, to ensure its vitrification (fast-freezing) and to prevent ice crystal formation. The vitrified specimen was transferred under liquid nitrogen and mounted on a cryogenic sample holder, cooled to -170 °C. All samples were observed under low-dose conditions with a FEI Talos 200C TEM. Most images were recorded using novel “phase-plates”, which convert phase differences between areas of the specimen to amplitude differences, thus enhancing image contrast without resolution loss. The TEM is equipped with a Falcon III direct-imaging camera, that allows imaging at very low electron exposure, essential for electron-sensitive specimens such as soft-matter samples. About 20 images were taken from each sample, the images were taken at different sample areas to ensure statistically relevant information.

### 2.2.6 Nuclear Magnetic Resonance (NMR)

Nuclear magnetic resonance (NMR) was measured with a Bruker Avance III 500 MHz instrument. For standard  $^1\text{H}$  measurements the pulse program 'zg30' was used with  $30^\circ$  pulses and a  $D_1$  time of 30 s. All measured spectra were calibrated for the peak of the solvent ( $\text{D}_2\text{O}$  at 4.67 ppm<sup>[100]</sup>) and analyzed with the software TopSpin by Bruker.

### 2.2.7 Other Methods

**Small-Angle X-Ray Scattering (SAXS).** Small-angle x-ray scattering (SAXS) is in principle very similar to small-angle light and -neutron scattering. Since x-rays interact with the atom shell and not the nucleus like neutrons, the scattering is sensitive to different contrast conditions and therefore complementary to neutron scattering. Some SAXS measurements were carried out with Andreas Thünemann on a SAXSess instrument at Bundesagentur für Materialforschung und -prüfung (BAM), Berlin.

**Zeta Potential.** The zeta potential  $\zeta$  gives information about the surface charge of colloidal particles. Charged particles in solution are surrounded by an electrical double layer. The first layer (Stern layer) is made of ions of opposite charge to the particle. In the second, diffusive layer, ions of both charges are statistically distributed. Here, the potential decays exponentially. For zeta potential measurements, an alternating electric field is applied to the sample so that charged particles are moving correspondingly within the sample. Due to the forced movement a shearing occurs in the diffusive layer. Some ions are moved with the particle, while others are left behind. The potential at this shear plane is called the zeta potential and can be calculated from the velocity  $v$  of a moving particle in an electric field  $E$ .

$$\zeta = \frac{3\mu_E\eta}{2\varepsilon_0\varepsilon_r f(D/k_D)} \quad (29)$$

with  $\mu_E$  being the electrophoretic mobility, calculated from the velocity:  $\mu_E = v/E$ .  $\varepsilon_0$  is the permittivity of vacuum,  $\varepsilon_r$  the relative permittivity of the medium,  $\eta$  the viscosity of the medium and  $f(D/k_D)$  the Henry-function<sup>[101]</sup> which is dependent on the Debye screening length  $k_D$  and the particle diameter  $D$ . For small particles and low ionic strengths the Henry-function converges to 1 and can be neglected in Eq. 29.

Zeta potential measurements were carried out on a Litesizer 500, by Anton Paar.

**Viscosity Measurements.** The dynamic (or shear) viscosity can be measured with a calibrated capillary viscometer. The time that the liquid takes to pass through a calibrated volume of the capillary is related to its viscosity through the Hagen-Poiseuille law:

$$\frac{dV}{dt} = \frac{\pi R^4 |\Delta P|}{8L\eta} \quad (30)$$

where  $V$  is the volume of the liquid,  $t$  is the time,  $R$  is the radius of the tube,  $\Delta P$  is the pressure difference between both ends,  $\eta$  is the dynamic viscosity and  $L$  is the total length of the tube in flow direction. The solution to the differential equation gives the following expression:

$$\frac{\eta t}{\rho} = A + Bt^2 \quad (31)$$

where  $\rho$  is the density of the fluid.  $A$  and  $B$  are constants that depend on the viscometer geometry, usually,  $A$  can be neglected. The kinematic viscosity  $\nu$  is the ratio of the dynamic viscosity and the density of the fluid  $\rho$ :

$$\nu = \frac{\eta}{\rho} = Bt \quad (32)$$

Kinematic viscosities were measured in either a micro-Ubbelohde capillary or micro-Ostwald capillaries at a constant temperature of  $(25.0 \pm 0.1)^\circ\text{C}$ . The flow time  $t$  was averaged from at least three consecutive measurements.

**Density.** The densities of the employed molecules are required to calculate the scattering length densities ( $SLDs$ ) from the coherent neutron scattering lengths  $b_c$  of each atom and the molecular volume  $v_m = M_w/(N_A \cdot \rho)$ . Densities were measured using an Anton Paar DMA 4500 instrument, thermostated at  $25.0^\circ\text{C}$ . The densities of solid compounds were determined by measurements of diluted solutions with varying weight fractions of material, followed by extrapolation to 100 wt%.

**Refractive Index Increment.** The refractive index increment ( $dn/dc$ ) describes the change in refractive index with the concentration and is needed to account for the contrast conditions in light scattering experiments. ( $dn/dc$ ) measurements of polyelectrolyte solutions and microemulsions were carried out with a dn/dc Orange 19", Orange Analytics instrument by refractive index measurements of 5 concentrations of each sample. The slope of a  $n$  vs.  $c$  plot then gives the refractive index increment.

**Transmission.** The transmission ( $T$ ) of light by a sample can be described with the Beer-Lambert law.

$$T = \frac{I_1}{I_0} = \exp(-\epsilon cd) \quad (33)$$

Where  $I_0$  is the intensity of the incoming light,  $I_1$  the intensity of the transmitted light,  $\epsilon$  is the molar extinction coefficient,  $c$  the concentration and  $d$  the pathlength of the light in the sample. The transmission of a sample is needed to correct the measured intensity of static scattering experiments. Neutron transmissions were measured during each beamtime for all employed wavelengths. The scattered intensity was then corrected for the transmission in the data reduction process. The transmissions of visible light, needed for SLS analysis, was measured with a Cary 50 UV-VIS spectrometer by Varian. It was found that the transmission at 632.8 nm (laser

wavelength of the DLS setup) is higher than 99 % for all microemulsion/polyelectrolyte samples in a  $d = 1$  cm UV/Vis cuvette, hence even higher in a  $d = 0.8$  cm DLS cuvette and therefore negligible.

### 2.3 Theoretical and Geometrical Discussion of the System

For a better understanding of the system studied here, some theoretical considerations about size relations and charge ratios of microemulsion droplets and polyelectrolytes were made.

Three different sizes of microemulsion droplets were studied here. The droplet radius was varied by the amount of added hexanol and the resulting size of the droplets was determined from SANS measurements with a simple spherical form factor fit and a log-normal size distribution. This radius was used to calculate the surface area of one droplet. The average headgroup area of one surfactant is assumed to be  $0.5 \text{ nm}^2$ , together with the surface area this gives an average aggregation number. Since the ratio of charged and uncharged surfactant is known from the sample preparation, it is now possible to calculate the number of charges per droplet. Tab. 4 summarizes the microemulsion droplet properties.

In most cases weakly charged droplets were used with only 5 % of the surfactant being charged, which results in an average distance between charges of 3.6 nm (the surface area divided by the number of charges gives an average area per charge, the diameter of a circle with this area is the average distance between droplet charges). This is in contrast with the high charge density of the employed polyelectrolytes, which exhibit distances between charges of 0.25 nm for NaPA and 1 nm for NaHA and NaCMC. Due to this obvious mismatch, the polyelectrolyte charges can never be fully compensated by the microemulsion droplets. In addition, the charges on the microemulsion droplets are expected to be evenly distributed for entropic reasons. Since the polyelectrolyte chains have a limited flexibility, it is unlikely that one polyelectrolyte chain can compensate all charges on one microemulsion droplet. Fig. 9 sketches the situation.

The most interesting aggregates of microemulsion droplets and polyelectrolytes were found at a charge ratio of  $z = [-]/([+] + [-]) = 0.7$ , at polyelectrolyte excess close to the phase boundary. Here the formation of long cylindrical arrangements of droplets was observed in SANS measurements. At this charge ratio 70 % of all charges are negative polyelectrolyte charges and only 30 % belong to the microemulsion droplets. According to the number of microemulsion and polyelectrolyte charges, a number of droplets per chain can be estimated. The numbers for samples with NaPA are summarized in Tab. 5.

**Table 4:** Parameters of microemulsion droplets, the radius was determined with SANS, the number of charges are calculated from theoretical assumptions.

Name	hexanol / mM	$R_{(SANS)}$ / nm	$\sigma$	surface area / $\text{nm}^2$	charges/ droplet	distance of charges / nm
ME00	0	3.1	0.11	121	12.1	3.6
ME50	50	4.3	0.12	232	23.2	3.6
ME75	75	6.4	0.13	515	51.5	3.6

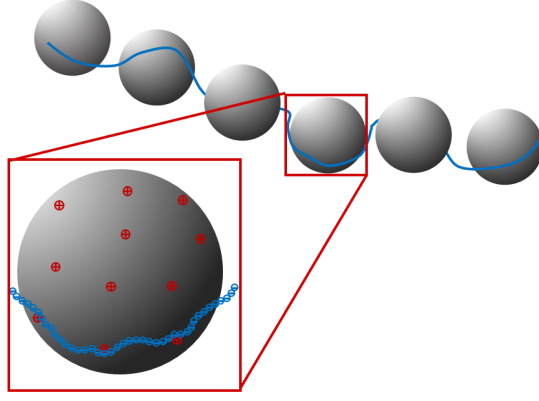


**Figure 9:** Sketch of the structural situation in the polyelectrolyte/microemulsion complexes. A single NaPA chain decorated with droplets and zoom to one droplet (drawn to scale for droplets with  $R \sim 4$  nm). Reproduced from Ref. [73] with permission of the Royal Society of Chemistry.

These numbers are calculated by taking into account all present charges and no geometrical restrictions. The numbers given are of droplets per chain, even though one chain alone would not be able to screen all charges of the droplets effectively. Since not all microemulsion charges can be compensated for geometrical reasons, the droplets are expected to still repel each other, even though the overall charge of the aggregate is negative due to polyelectrolyte charge excess. The stiffer polysaccharides (NaHA and NaCMC) will be less effective in charge compensation than the flexible NaPA. The repulsion of the remaining droplet charges might be one driving force for the formation of cylindrical aggregates, since in this geometry the charged droplets can realize the largest distances between charged droplets within one aggregate.

The interactions between charged droplets can be estimated with the generalized Bjerrum length  $l_B$ , which is the distance at which the interaction energy between two charged objects equals the thermal energy  $k_B T$ :  $l_B = (Z \cdot e)^2 / (4\pi\epsilon \cdot k_B T)$ , where  $Z$  is the number of charges,  $e$  is the elementary charge and  $\epsilon = \epsilon_r \epsilon_0$  is the permittivity. A rough estimation for medium sized droplets (ME50) where the polyelectrolyte successfully screens half the charges ( $23.2/2 = 11.6$  charges in water at 25 °C) yields a Bjerrum length of  $l_B = 100$  nm. The situation is complicated by the additional polyelectrolyte charges that provide electrostatic screening and lower the Debye screening length which would have to be included in the Bjerrum length calculation, resulting in a significantly smaller value.

In another estimation the total length of added polyelectrolyte (if all separate chains would be joined to one long chain) at  $z = 0.7$  can be calculated from the sample composition. This number

**Table 5:** Number of microemulsion droplets per polyelectrolyte chain, calculated at  $z = 0.7$  for NaPA chains of different  $M_w$  and different droplet sizes.

	ME00	ME50	ME75
NaPA05	1.92	1.00	0.45
NaPA15	5.66	2.94	1.33
NaPA60	22.64	11.77	5.31
NaPA315	118.86	61.78	27.89

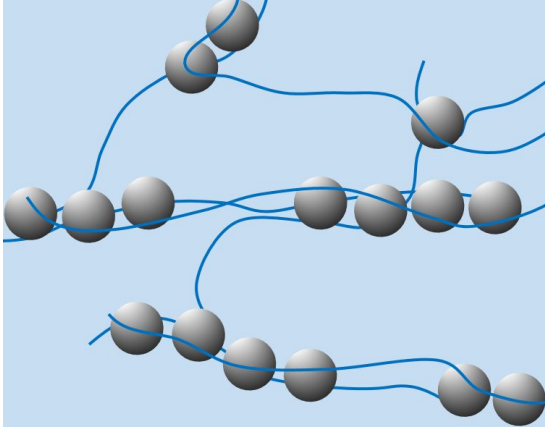


**Figure 10:** Sketch of the structural arrangement of PEMECs, network with elongated complexes. Reproduced from Ref. [73] with permission of the Royal Society of Chemistry.

**Table 6:** Overlap concentrations of different NaPA chain lengths, calculated for stretched chains.

NaPA	overlap concentration / mM	exceeded at sample
NaPA05	0.696	$z = 0.9$
NaPA15	0.024	$z = 0.5$
NaPA60	3.9E-04	$z = 0.1$
NaPA315	2.7E-06	$z = 0.1$

is the same for all different  $M_w$  of one polyelectrolyte type since the concentration of charges is kept constant. Together with the number and diameter of droplets this yields and average distance between droplets aligned on the polyelectrolyte. For medium sized droplets (ME50,  $R = 4.3$  nm) and NaPA chains one droplet would be located per 13 nm, resulting in a distance between droplets of 4.2 nm. This distance is much shorter than the Bjerrum length, even if the Debye screening length would be taken into account, showing that the aligned droplet still strongly interact with each other.

Since NaHA and NaCMC have a lower charge density, the distances between droplets will be larger here. But the stiffer polyelectrolytes should be less effective in droplet charge compensation because of the curved droplet surface and also employ a higher Debye screening length, so the general outcome will be similar.

Another parameter to be considered is the polyelectrolyte conformation. In general, single chains can be present in solution or a continuous network, depending on the overlap concentration, which depends on the chain length. The overlap concentrations for different  $M_w$  NaPAs, calculated by assuming stretched PE chains, are summarized in Tab. 6. At polyelectrolyte excess, charge ratio of  $z = 0.7$ , all NaPA chains are already above the overlap concentration, except for the shortest NaPA05. For NaHA and NaCMC samples, higher polyelectrolyte concentrations are needed to achieve the same charge ratios due to the lower charge density. Therefore all prepared samples are always above the overlap concentration.

Adding oppositely charged microemulsion droplets to these polyelectrolyte networks deforms the networks so that the droplets are arranged in one dimensional complexes. We can expect the complexes to be held together by several polyelectrolyte chains since effective charge compensation by just one single chain would be entropically unlikely, see sketch in Fig. 10.

## 3 Polyacrylate/Microemulsion Complexes

### 3.1 Introduction

Many polyelectrolyte/surfactant systems are studied with the aim to solubilize molecules, e.g. hydrophobic compounds like drugs, dye molecules or pollutants. The disadvantage of these surfactant systems is the low solubilization capacity of micelles and the lack of studies with swollen micelles, that might behave quite differently compared to their predecessors. Accordingly, an interesting alternative is to use microemulsion droplets, which are structurally well understood and already contain a large amount of solubilized hydrophobic material. Using a microemulsion instead of micelles for complexation allows to combine their high loading capacities with mesoscopic structuring opportunities via the polyelectrolyte, which are very promising properties for applications. Weakly charged microemulsion droplets can be complexed with oppositely charged polyelectrolytes, thereby offering new options for structural control, modifications and stimuli responsiveness. These easily formed hybrid systems are structurally very versatile, as many different properties in architecture and size are accessible by varying the composition. In this chapter, a polyelectrolyte/microemulsion system composed of different sodium polyacrylates (NaPA) and weakly charged O/W microemulsion droplets is studied. Part of the experiments were already performed during my master thesis<sup>[93]</sup> but some experiments and all analysis was redone for the first publication on this subject.<sup>[73]</sup>

### 3.2 Results

#### 3.2.1 "Structural Control of Polyelectrolyte/Microemulsion Droplet Complexes (PEMECs) with Different Polyacrylates" by M. Simon, P. Krause, L. Chiappisi, L. Noirez and M. Gradzielski, *Chemical Science*, 10, 2019.

In this first article we present a general overview on the complexes formed by weakly charged microemulsion droplets with polyacrylates.<sup>[73]</sup> The complete article can be found in the [Appendix](#). In this work the size of the droplets, the  $M_w$  of the NaPA and the mixing ratio of both were varied and the effects on the phase behavior and on the size, shape and composition of the formed complexes were studied. Additionally effects of the overall concentration and the ionic strength in the system were investigated.

**Phase Behavior.** In order to gain a comprehensive overview over the phase behavior, samples were prepared with different microemulsion droplet sizes and different chain lengths of NaPA. A wide range of precipitation is observed around equimolar charge mixing ( $z = 0.5$ ) and only for the microemulsion or polyelectrolyte excess single phases are found. It is interesting to note that the biphasic region of the phase diagram has a very asymmetric shape, i.e. a polyelectrolyte excess provides much higher colloidal stability to the systems. It was observed that larger droplets and increasing  $M_w$  of the NaPA both lead to larger biphasic regions in the phase diagram (see Fig. 11). Samples in the long-time stable single phase regions for larger  $z$  (polyelectrolyte charge

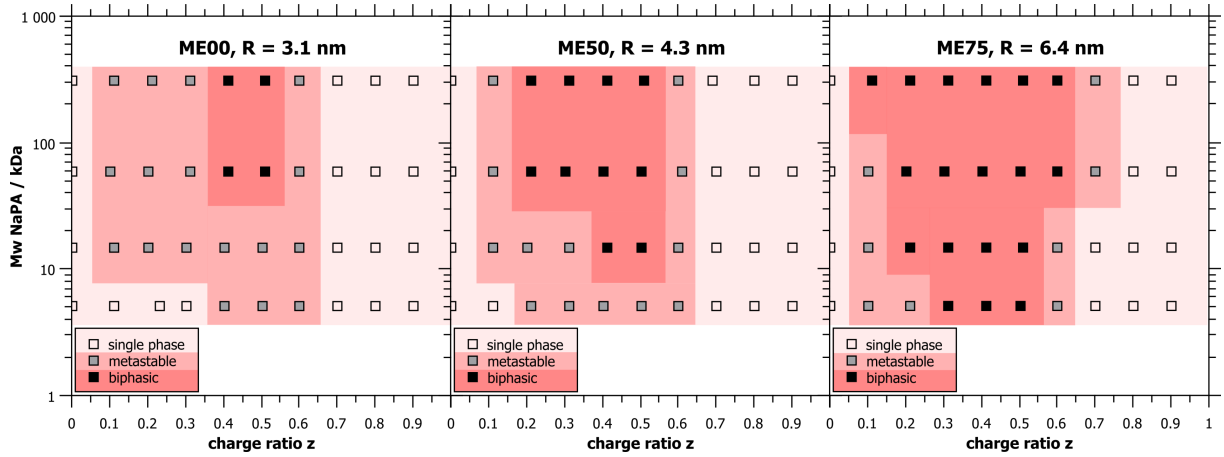


**Figure 11:** Phase diagrams showing the biphasic and meta stable regions for ME00, ME50 and ME75 at 100 mM surfactant concentration, mixed with NaPA of different  $M_w$  and at different charge ratios  $z$ . Reproduced from ref. [73] with permission of the Royal Society of Chemistry.

excess) show different optical appearances ranging from clear to bluish (when being closer to the precipitation area), indicating the formation of differently sized complexes as a function of  $z$ .

The microemulsion droplets have a low number of charges with about one charge per  $12 \text{ nm}^2$ , while the charge density along the NaPA backbone with one charge per  $0.25 \text{ nm}$  is rather high. For larger droplets the number of charges per droplets is higher, making it easier to compensate the high charge density of the NaPA. This effect is increased by a lower curvature of larger droplets, making it easier for the NaPA to bend around the droplets. The improved conditions for interactions with large droplets explain the higher tendency for precipitation in these samples.

**Structural Characterization.** Light scattering (DLS and SLS) measurements were carried out for all stable and most metastable samples. The measurements show, that the largest complexes are always formed at the polyelectrolyte rich side of the phase diagram, close to the phase boundary. The size of the complexes is also increasing with increasing  $M_w$  of the polyelectrolyte and increasing droplet size. Zeta potential measurements confirmed the formation of mixed aggregates. Additional SANS measurements (see Fig. 12A for examples) show that the scattering intensity at high  $q$  is not changing when polyelectrolyte is added to the microemulsion, the form factor minimum still retains its original shape and position. This is an important finding as it confirms that the microemulsion droplets are not altered when interacting with the polyelectrolytes, hence they would be available as carriers.

Fig. 58 in the Appendix shows the comparison of a homogeneous cylinder model and a cylindrical arrangement of separate droplets fitted to the SANS data. The cylindrical arrangement of droplets describes the data more accurately, confirming again the retention of the droplet structure in the complexes.

The rising scattering intensity at medium and low  $q$  proves that larger aggregates are formed when microemulsion droplets interact with polyacrylates. First model free analysis can deduce an aggregation number  $N_{agg}$  of microemulsion droplets contained in one aggregate by dividing

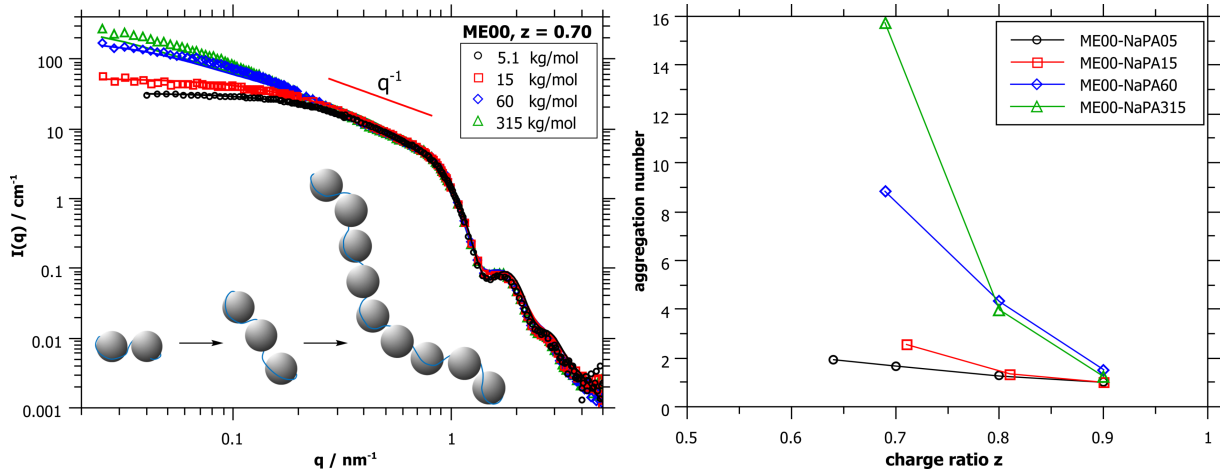


**Figure 12:** A) Comparison of Complexes formed with ME00 and NaPA of different  $M_w$  at charge ratio  $z = 0.7$ . Solid lines were calculated for a cylindrical arrangement of droplets. B) Aggregation number  $N_{agg}$  deduced from extrapolated  $I(0)$  values of SANS data. Reproduced from Ref. [73] with permission of the Royal Society of Chemistry.

the forward scattering intensity  $I(0)$  (obtained by Guinier approximation) by the theoretical  $I(0)_{th}$  value of non-interacting droplets. Some aggregation numbers for different NaPA chain lengths and different mixing ratios are shown in Fig. 12B. It can be seen, that high numbers are obtained for samples close to the phase boundary, especially for high  $M_w$  NaPA, and  $N_{agg}$  is reduced to 1 at high polyelectrolyte excess. A similar trend is observed for larger droplet sizes with even higher aggregation numbers of up to 35 droplets/aggregate.

The SANS data also show a  $q^{-1}$  power law in the mid- $q$  intensity, which is usually interpreted as elongated, rodlike structures. This  $q^{-1}$  power law is most pronounced for samples at  $z = 0.7$  i.e. large complexes close to the phase boundary on the polyelectrolyte excess side, and decreases for higher  $z$  values. This linear region is more extended for higher  $M_w$  NaPA. Since the form factor minimum indicates that the droplets remain unchanged, a cylindrical arrangement of droplets seems logical. Indeed, it was possible to simulate the scattering curves by using a model developed in our group<sup>[91]</sup> for spherical particles arranged in a straight line (see solid lines in Fig. 12A). This model was able to describe SANS data of complexes formed with lower  $M_w$  NaPA very well, but showed deviations at low  $q$  for longer NaPA chains. This is most likely due to the flexible nature of polyacrylate. Long aggregates composed of many droplets tend to bend over their persistence length, which results in a higher slope in the SANS data and thus a poorer fit of the model that is only describing a straight cylindrical arrangement.

The one-dimensional droplet complexes are held together by several NaPA chains as effective charge compensation by one single chain is entropically unlikely. The length of one complex increases with increasing length of the NaPA chain, but only to a limited extent, since the negative charge excess of the complexes increases rapidly as well, because the charge density of NaPA is much higher than that of the microemulsion droplets. For larger droplets, the local amount of positive charges increases and therefore the possibility of building larger aggregates becomes electrostatically enhanced.

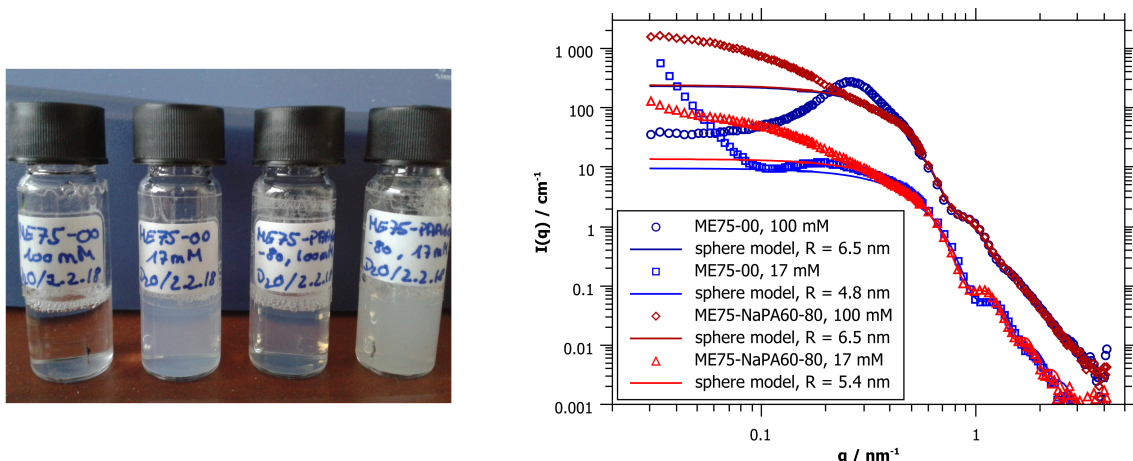


**Figure 13:** A) Photo and B) SANS data of pure ME75 (large droplets) and ME75-NaPA60-80 complex, both at the usual concentration of 100 mM surfactant and diluted by a factor of 6 (resulting concentration about 17 mM). Photo was taken one day after preparation.

**Variation of Ionic Strength.** The variation of the total concentration also studied in this paper is discussed in detail in Chapter 3.2.2. As a final point, the effect of ionic strength was investigated. Since the complex formation is based on electrostatic interactions, it is interesting to study their behavior at different ionic strengths. It could be shown, that already very small amounts of added salt (50 mM NaCl) is enough to screen the microemulsion charges sufficiently to dissolve the PEMECs that are held together by electrostatic interactions. This is in striking contrast to observations for polyelectrolyte/surfactant complexes (PESCs) or interpolyelectrolyte complexes (IPECs), where typically an ionic strength of 500 – 700 mM is required in order to dissolve them.<sup>[102–104]</sup> The PEMECs studied here possess a very high degree of responsiveness to ionic strength that can be discussed in the context of the driving force of complexation. Since the droplets are only 5 % charged, the volume available per counterion is about 20 times larger than for a fully charged surface. Therefore the entropy gain of counterion release through complexation becomes smaller and a correspondingly lower salt concentration is already effectively dissolving the complexes.

### 3.2.2 Dilution of Complexes

Only shortly included in the paper, but highly interesting is the behavior of the formed PEMECs upon dilution of the system. Questions to be addressed under this aspect would be whether the formed complexes are stable when diluted, whether the original complex shape and composition can be retained and if potentially present large networks break upon dilution and form large but separate clusters

Dilution experiments were conducted with small microemulsion droplets (ME00,  $R \sim 3 \text{ nm}$ ), which do not contain any added hexanol. Since hexanol is partly water soluble, dilution would have an effect on the amount of cosurfactant contained in the microemulsion droplets, which would automatically affect the solubilization capacity and the droplet size. This would lead to undefined and therefore not directly comparable systems. In fact, to prove this point, dilution

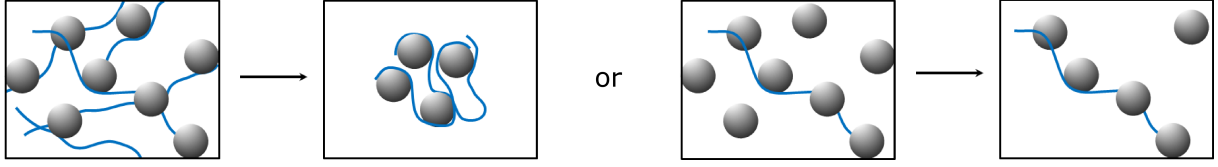


**Figure 14:** Possible processes occurring upon dilution of PEMECs. A) a space filling network is diluted to single clusters. B) Clusters are always present, but only become distinguishable below a certain concentration.

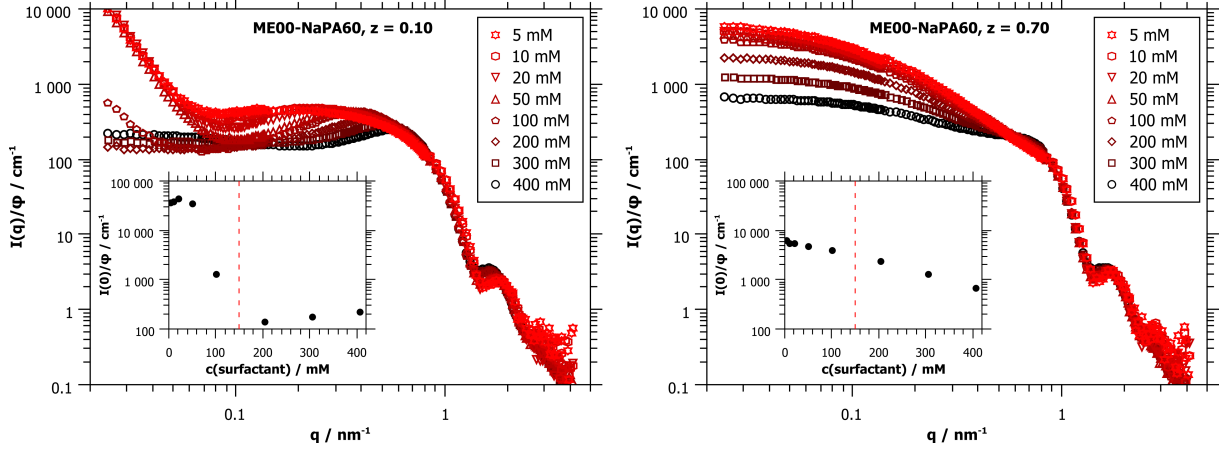


**Figure 15:** SANS data of dilution series of two ME00-NaPA60 samples at  $z = 0.1$  and  $z = 0.7$ , normalized by the respective volume fraction  $\phi$ . Extrapolated  $I(0)$  values are plotted over the concentration in the insets. Dotted lines indicate concentrations where large clusters are first observed.

experiments were carried out with larger droplets as well. Complexes of ME75 with NaPA60 were stable at 100 mM surfactant concentration but showed visible phase separation into two liquid phases when diluted. Interestingly, the phase separation did not occur instantly, but only after several hours. Fig. 13A shows a photo of the pure ME75 and the ME75-NaPA60-80 complex sample, both at the usual concentration of 100 mM surfactant and diluted by a factor of 6 to about 17 mM surfactant, taken one day after preparation. The diluted samples appear turbid. Upon resting, those turbid samples will phase separate into two liquid phases, forming smaller microemulsion droplets as can be seen from the form factor minimum shift in the SANS data (see Fig. 13B). The second liquid phase on top is most likely excess decane. It should be mentioned here, that diluted samples prepared with ME00 stayed optically clear for the whole time of observation.

In a first experiment, a dilution series of ME00-NaPA15 complexes ( $z = 0.0$ ,  $z = 0.1$  and  $z = 0.7$ ) was analyzed with SANS.<sup>[93]</sup> It was shown, that for a low charge ratio ( $z = 0.1$ ), the scattering intensity shows a steep increase at very low  $q$ , when diluting below a certain concentration (below 100 mM surfactant concentration in this case). It was assumed, that this strong increase shows the isolated clusters that are present in the sample and are now, due to the dilution, visible as individual, non-interacting aggregates. At higher charge ratio ( $z = 0.7$ ), the sample structure changes from densely packed droplets to elongated aggregates. This can be seen by the appearance of a linear part with a slope of  $q^{-1}$  in the scattering curves. Further dilution below

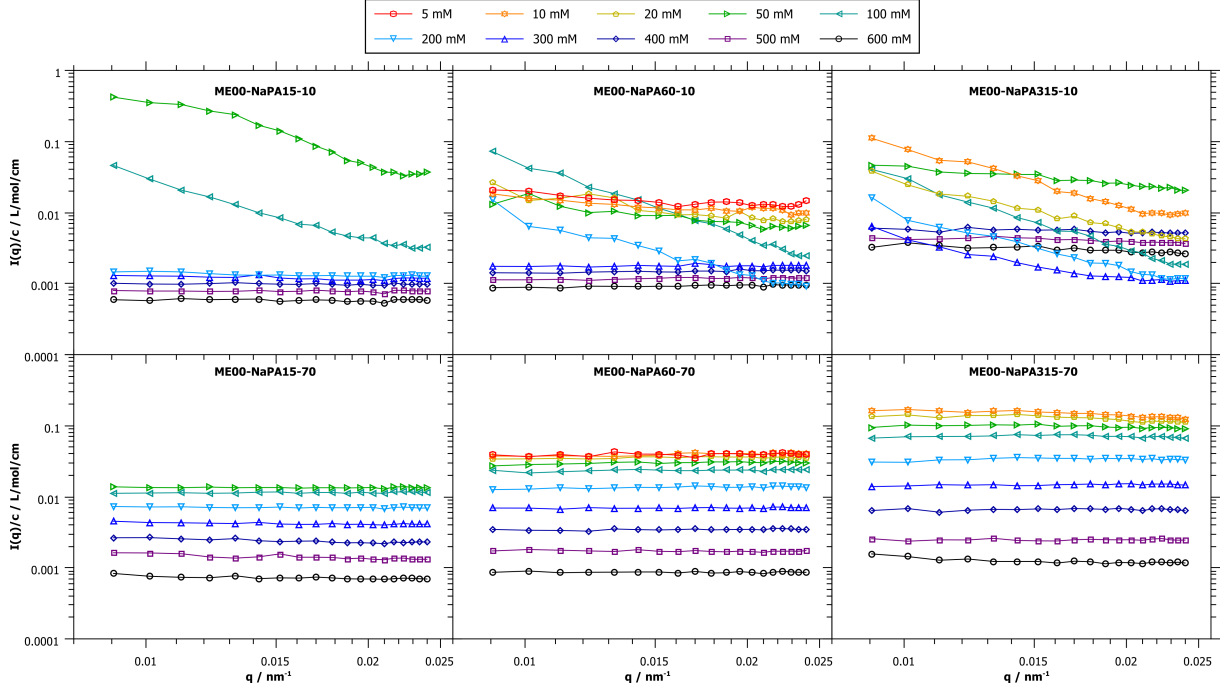


**Figure 16:** Static light scattering data of dilution series of ME00/NaPA complexes with NaPA of different  $M_w$ . Samples were prepared at  $z = 0.1$  (top) and  $z = 0.7$  (bottom). All intensities were normalized by the respective surfactant concentrations.

100 mM has no effect on the scattering curve, the formed aggregates seem to have reached a thermodynamically stable composition that is not concentration dependent.

The increase of the intensity at low  $q$  for low concentrations could be explained by two possible processes. First, if a space filling polyelectrolyte network was present at higher concentrations, this network would be diluted into single clusters (see Fig. 14A). In this case, the transition between the network and isolated clusters should depend on the overlap concentration of the polyelectrolyte and longer chains should therefore show this transition at lower concentrations. A second possible explanation would be that the clusters are always present, in diluted as well as in concentrated samples. But at high concentrations, the microemulsion droplets are simply too closely packed to distinguish between separate aggregates, these aggregates only become visible below a certain concentration (see Fig. 14B). In this case the visibility of aggregates depends on the microemulsion concentration and should therefore be independent of the polyelectrolyte chain lengths.

To check these two possible explanations, more SANS measurements were carried out of a dilution series of the same microemulsion (ME00) mixed with NaPA60, a longer polyelectrolyte chain compared to NaPA15. The SANS data normalized by the volume fraction can be seen in Fig. 15. The forward scattering intensity  $I(0)$  was extrapolated by Guinier approximation and plotted over the surfactant concentration. It can be seen that the increase in scattering intensity at small  $q$  for the  $z = 0.1$  sample is already visible at a concentration of 100 mM surfactant. This is at a slightly higher concentration than previously measured for the shorter NaPA15. In the sample at polyelectrolyte excess  $z = 0.7$ , the evolution of longer, rodlike aggregates can be seen until a

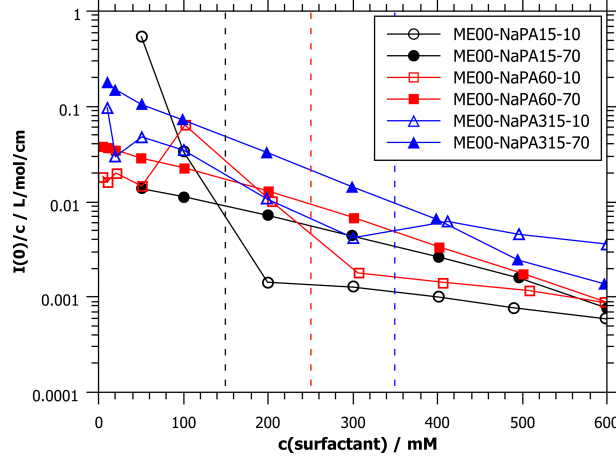


**Figure 17:** Forward scattering intensity  $I(0)$  as obtained from SLS for dilution series of ME00 with different  $M_w$  NaPA, normalized by the respective concentration. Dotted lines indicate concentrations where large clusters are first observed.

concentration of 200 mM. At lower surfactant concentrations, no further change is visible. The concentrations where larger aggregates first become visible (for  $z = 0.1$ ) or no further change can be detected (for  $z = 0.7$ ) are marked with red dotted lines in the insets of Fig. 15. It seems surprising, that aggregates formed with longer NaPA chains show their larger aggregates already at higher concentrations than samples formed with shorter chains. If this behavior is confirmed, none of the above mentioned theories would be able to explain these findings.

Additional light scattering measurements were carried out for samples with NaPA15 and NaPA60 (both previously measured in SANS) and additionally with even longer NaPA315. The static light scattering intensity, normalized by the surfactant concentration, is shown in Fig. 16. The transition from a polymer network or densely packed droplets to large isolated clusters of the  $z = 0.1$  samples is clearly visible in the SLS data by a sudden increase of the scattering intensity. The  $z = 0.7$  samples show an intensity plateau for all concentrations, but similarly to the SANS data, the value of this plateau is increasing upon first dilution and then not changing anymore below a certain concentration. For all SLS data sets, the intensity was extrapolated to the forward scattering intensity  $I(0)$  by Guinier approximation. The forward scattering intensities are summarized in Fig. 17, dotted lines represent the transition between a plateau and increasing intensities of the  $z = 0.1$  samples. It can be seen, that this transition scales with the molecular weight of the polyelectrolyte: the higher the  $M_w$ , the higher is also the concentration of this transition, meaning cluster formation occurs at higher concentrations for longer polyelectrolyte chains. This transition becomes visible in light scattering at slightly higher concentrations compared to the SANS measurements.

The observed trend with the  $M_w$  of polyelectrolyte is the exact opposite to the network dilution theory described before. We can therefore say that a polyelectrolyte network that separates into isolated clusters below the overlap concentration is most certainly not the main mechanism for this system. The second mechanism could not be proven with the scattering experiments but still seems more likely. Since the scattering intensity originates almost exclusively from the

microemulsion droplets, it seems logical that no separate clusters can be distinguished when a dense packing of droplets is present. Upon dilution, the distances between the droplets become larger and at a certain concentration clusters are separated enough to be distinguishable. It was assumed before that the aggregates should become visible at the same concentration for all different  $M_w$  of polyelectrolyte since the distances only depend on the droplet concentration. But it was found before that longer polyelectrolyte chains form larger aggregates that contain more droplets. The distances between aggregates are therefore different in different samples, depending on the number of droplets per aggregate. It is therefore possible, that higher  $M_w$  polyelectrolyte chains form larger aggregates with microemulsion droplets, that become visible in scattering experiments already at higher concentrations than smaller aggregates would.

### 3.2.3 Variation of Microemulsion Charge

Another very interesting parameter is the charge density on the microemulsion droplet surface. As described above, the driving force of complexation depends strongly on the entropic gain of counterion release. Higher charged droplets should therefore exhibit a stronger binding since the gain in free volume is larger for each released counter ion and also more counterions are available to be released. The strength of binding is expected to significantly affect the structure of the formed complexes. The charge density can be easily varied by substituting different amounts of the neutral surfactant TDMAO with the cationic TTAB.

A first important parameter to be checked, is whether the substitution of TDMAO with TTAB has an effect on the microemulsion droplets themselves. Since charged surfactants usually induce a higher interfacial tension and curvature compared to uncharged ones, this experiment bears the risk of lower solubilization capacities for higher charged droplets. To examine the solubilization capacity of microemulsion droplets with different amounts of TTAB, experiments were carried out with the largest microemulsion droplets since the effect was expected to be most pronounced here. Two stock solutions were prepared: first, a microemulsion containing 100 mM of TDMAO (no TTAB) and 75 mM hexanol, fully saturated with decane (this microemulsion is analogue to ME75 but not charged) and second, a surfactant solution containing 100 mM TTAB and 75 mM hexanol

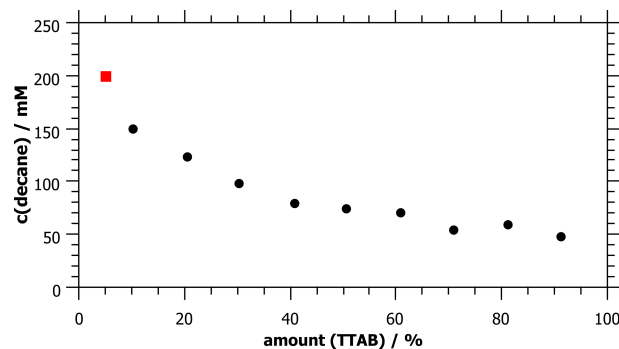


**Figure 18:** Concentrations of decane contained in microemulsions with 100 mM total surfactant concentration, 75 mM hexanol and different amounts of TTAB as obtained from NMR measurements. Red square indicates ME75 with 5 % TTAB as it was used in other parts of this work.

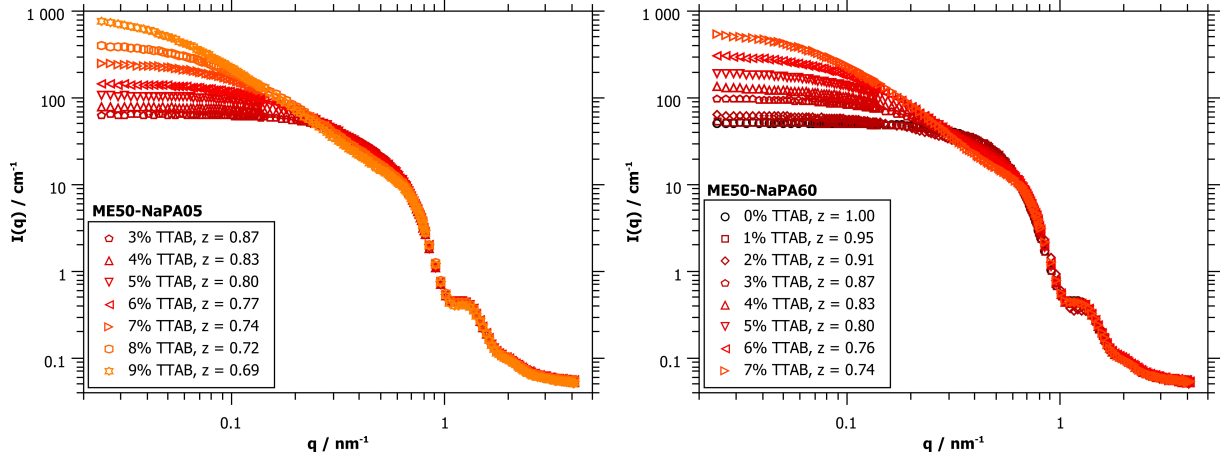


**Figure 19:** SANS data for medium sized microemulsion droplets ME50 with different charge densities mixed with NaPA of A) 5.1 kg/mol and B) 60 kg/mol. The amount of added NaPA was kept constant, therefore the charge ratio  $z$  is varying.

but no oil was added. These two stock solutions were then mixed in different ratios to result in microemulsions with 10, 20, 30, 40, 50, 60, 70, 80 and 90 % TTAB. Additional decane was added afterwards to ensure fully saturated droplets. After the excess decane accumulated on top,  $^1\text{H}$ -NMR spectra were measured of the clear microemulsions to determine the decane concentration from the relative signal integrals. Fig. 18 shows the results of the NMR measurements. It can be seen, that the amount of soluble decane depends strongly on the amount of employed TTAB but even at very high TTAB concentrations about 50 mM of decane are still soluble. The red square in Fig. 18 indicates the ME75 microemulsion with 5 % TTAB as it is usually used in other parts of this work.

The solubilization capacity varies especially strong for small TTAB contents but the effect of the charge density on the complex formation was studied nevertheless. Medium sized droplets (ME50,  $R \sim 4$  nm) were prepared with 10 mM total surfactant concentration (0 - 10 % TTAB), 50 mM hexanol and 80 mM decane for SANS measurements. The varying amount of TTAB influences the calculated charge ratio  $z$ . To obtain the same  $z$ -value with different TTAB concentrations, also different amounts of polyacrylate would be needed. In this case it was decided to keep the microemulsion and the polyacrylate concentration constant, which results in different charge ratios between  $z = 0.7$  and  $0.9$  (all in polyelectrolyte excess) for different TTAB concentrations. Samples were prepared with NaPA05 and NaPA60, the SANS data is shown in Fig. 19.

As expected the SANS data shows that the charge density of the microemulsion strongly affects the interactions between droplets and polyelectrolytes. Droplets with no or very low amounts of TTAB do not interact with the polyelectrolytes as it can be seen from the low  $q$  region where the SANS curves show a plateau with a low forward scattering intensity. The higher the amount of TTAB, the stronger become the interactions between microemulsion droplets and polyelectrolytes. The increasing scattering intensity at low  $q$  indicates that large complexes are formed at high charge densities, until at one point precipitation is observed and no further measurements were possible. The shorter polyelectrolyte (NaPA05) allows stable complexes at slightly higher

TTAB concentrations. Here complexes with a 9 % TTAB containing microemulsion were still stable, while complexes with the longer NaPA60 were only stable up to 7 % TTAB.

In this case it is hard to separate the effect of increased charge density from that of lower charge ratios  $z$  that are closer to the phase boundary, as both parameters are expected to lead to larger complexes and instable samples at one point. Further analysis is necessary to be able to give clear statements about the effect of charge density on the formation of PEMECs. In addition, it would be interesting to study the effect of ionic strength on complexes with different microemulsion charge densities. The amount of salt needed for disintegration of the complexes should strongly depend on the amount of TTAB which would prove the entropic gain of counterion release as the main driving force for polyelectrolyte/microemulsion complexes.

### 3.3 Conclusion

The first part of this chapter is already published<sup>[73]</sup> and describes the versatile structures of PEMECs in dependence of the droplet size, the  $M_w$  of the polyelectrolyte and the mixing ratio  $z$ . In polyelectrolyte excess close to the phase boundary the complexes are elongated and can be described by a cylindrical arrangement of separate droplets. The largest complexes are found for large microemulsion droplets and long NaPA chains, containing up to 35 droplets per aggregate. The microemulsion droplets retain their size and shape when interacting with polyelectrolytes and would therefore be available as carriers.

Dilution experiments of PEMECs show that large aggregates are present even at low  $z$  ratios but the visibility of these complexes depends strongly on the employed concentration. To avoid misinterpretation of the SANS data, it is therefore necessary to bring measurements at different concentrations into one consistent picture. The complex formation in the present case does not depend on the overlap concentration of polyelectrolytes as initially assumed. Instead, PEMECs are present at all concentrations but their signal in SANS might be overlaid by the strong repulsive interactions of densely packed microemulsion droplets.

The charge density of the microemulsion droplet surface can be influenced by the amount of added TTAB and has a pronounced effect on the electrostatic interactions with polyelectrolytes.

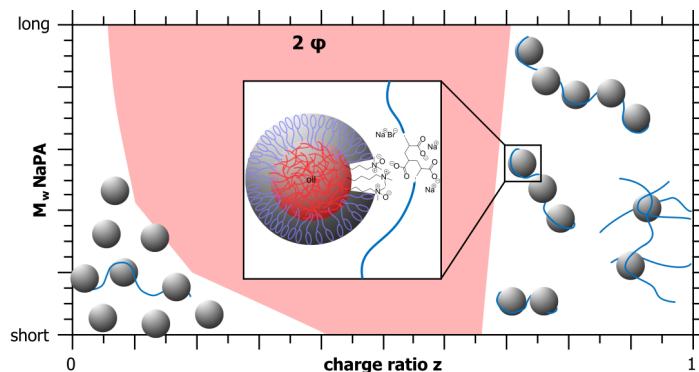


**Figure 20:** Summary of the phase behavior and different structures formed in polyacrylate/microemulsion mixtures. Reproduced from Ref. [73] with permission of the Royal Society of Chemistry.

An higher amount of TTAB increases the entropy gained through complexation, thus larger complexes are formed until the interactions become so strong that the complexes precipitate.

Some test measurements for further interesting projects were already carried out, including SANS measurements in zero-average-contrast to obtain more detailed information about the interactions between polyelectrolytes and microemulsions. Isothermal Calorimetry (ITC) measurements show pronounced differences when a polyelectrolyte solution is titrated into a microemulsion and into a surfactant solution and also measurements for different microemulsion droplet sizes show different interactions. The effects are certainly very interesting but detailed analysis is necessary to draw reliable conclusions. The interesting sensitivity to ionic strength was already presented above. Additional experiments showed that 50 mM of added NaCl can dissolve already formed solid precipitates of a  $z = 0.5$  sample, the microemulsion droplets are retained in this case. Further we were interested in the influence of the nature of the added ions. Very recent SANS measurements showed that especially the chosen anion largely influences the screening efficiency but further analysis is necessary here.

The investigations described here give, for the first time, a comprehensive overview on the complex formation of charged O/W microemulsion droplets with oppositely charged polyelectrolytes. But it also becomes clear that these investigations are not finished with this work. Many interesting questions are still open and will be studied in the future.



## 4 Microemulsion Complexes with Biopolyelectrolytes

### 4.1 Introduction

The development of biocompatible material is naturally important for many applications, such as biomedicine, food modification or wastewater treatment. On a more general note, sustainable materials derived from renewable resources are generally needed in all industry sectors to allow our raised standard of living and ensure the well-being of our planet in the future. In order to develop biofriendly formulations it is interesting to explore how a change from the fossil-based polyacrylate to a biopolyanion affects the structures of polyelectrolyte/microemulsion complexes. From a more fundamental point of view, the persistence length and the charge density of the employed polyelectrolyte is expected to play a key role in the droplet assembly. Most biopolyelectrolytes consist of sugar backbones which are more rigid than the flexible polyacrylate and contain a lower charge density and are therefore naturally suited to explore this aspect of PE-MECs.

The main biopolyelectrolyte employed here is sodium hyaluronate (NaHA), a biologically extremely relevant polyelectrolyte. E.g. Hyaluronic acid determines the viscoelastic properties of synovial fluids and many medical conditions can be attributed to HA degradation.<sup>[105,106]</sup> The sodium salt of carboxymethyl cellulose (NaCMC) was employed as a second biopolyelectrolyte for comparison. CMC is produced from cellulose by chemical modification, making this renewable resource water soluble.<sup>[107]</sup> NaHA and NaCMC exhibit intrinsic persistence lengths of 9 and 16 nm,<sup>[71,72]</sup> both significantly higher than the persistence length of NaPA with 1.3 nm.<sup>[70]</sup> The charge density of NaHA is with 1 charge/nm only 1/4 of that of NaPA. Two NaCMCs with different degrees of substitution (charge densities of 0.7 and 1.2 charges/nm) were employed. In addition the charges of NaCMC are sterically more easily accessible as they are linked to the polymer backbone by a spacer. Structural formulas of the employed polyelectrolytes are given in Fig. 5.

### 4.2 Results

#### 4.2.1 "Effect of the Polymer Architecture on the Phase Behavior and Structure of Polyelectrolyte/Microemulsion Complexes (PEMECs)" by M. Simon, E. Schneck, L. Noirez, S. Rahn, I. Davidovich, Y. Talmon and M. Gradzielski, *Macromolecules*, 2020.

This chapter is based on an article that was recently accepted in *Macromolecules*,<sup>[108]</sup> the full article can be found in the [Appendix](#). In this paper we analyzed the phase behavior of NaHA and NaCMC with differently sized microemulsion droplets in dependence of the mixing ratio  $z$  and the molecular weight of the polyelectrolyte and compared the behavior to that of NaPA. Further the shape and composition of stable complexes was analyzed in terms of an aggregation number and interpreted for different persistence lengths of the polyelectrolytes.

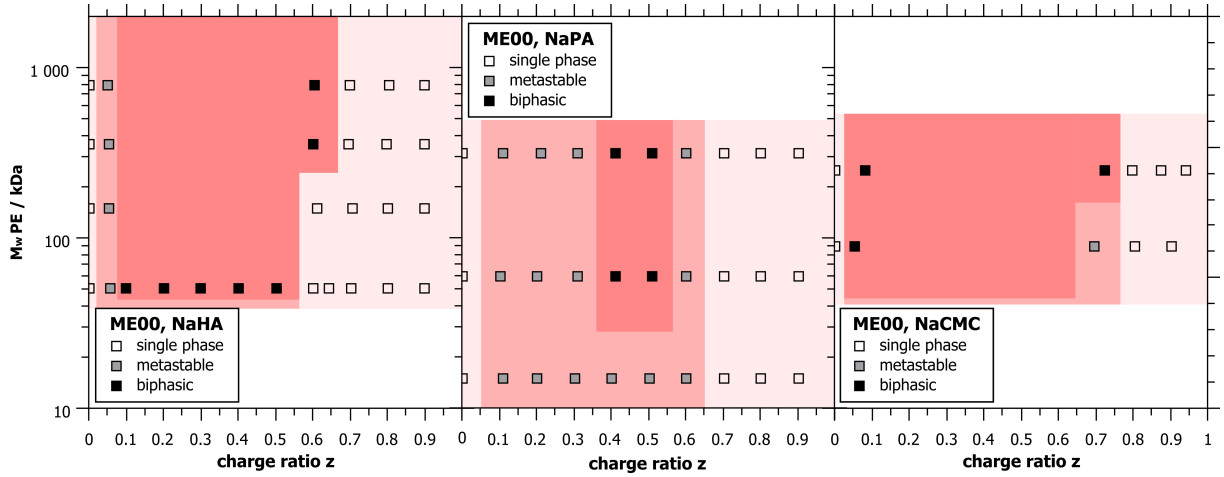


**Figure 21:** Phase diagrams for ME00 mixed with NaHA (left), NaPA (middle) and NaCMC (right) of different  $M_w$  and in different charge ratios  $z$ . Reprinted with permission from Ref. [108]. Copyright 2020 American Chemical Society.

**Phase Behavior.** In a first step the phase behavior of different mixtures of NaHA and NaCMC and microemulsion droplets was analyzed by regular visual inspection of the samples. Fig. 21 compares the phase diagrams of small microemulsion droplets (ME00,  $R \sim 3$  nm) with the different polyelectrolytes of varying  $M_w$  and in dependence of the mixing ratio  $z$ . A surprisingly similar phase behavior for all three very different polyelectrolytes is observed. In all cases the microemulsion charge excess parts of the phase diagrams are unstable, while long-time stable complexes were found at polyelectrolyte excess. It is interesting to note that the upper critical mixing ratio  $z$  for stable PEMECs is quite similar ( $\sim 0.7$ ) for all polyelectrolytes, showing that the stability is largely governed by the relative charge ratio between surfactant and polyelectrolyte. The nature of the two-phase region seems to depend strongly on the type of employed polyelectrolyte. For NaPA, a large metastable region is found where the precipitation is observed only after a couple of days while phase separation occurs much faster (within one hour) for the sugar polyelectrolytes. This might also be linked to the type of observed phase separation. While solid white particles are found in the biphasic samples of NaPA/ME complexes, a liquid-liquid phase separation is observed for NaHA and NaCMC. This second liquid phase is analyzed in detail in Chapter 4.2.2.

**Structural Characterization of NaHA Complexes.** Structural characterization of the formed complexes was mainly carried out with light scattering and SANS experiments but also some additional viscosity measurements were done. Viscosity measurements show almost no effect of the microemulsion droplets on the polyelectrolyte viscosity, indicating weak interactions that can be explained by the low charge density on the droplet surface.

Both static and dynamic light scattering results show that, just as for the NaPA system, large aggregates are formed close to the phase boundary which are decreasing in size for larger charge ratios. The aggregate size is increasing with increasing droplet size or  $M_w$  of NaHA. The static scattering intensity shows a plateau for most samples. The aggregation number of droplets per

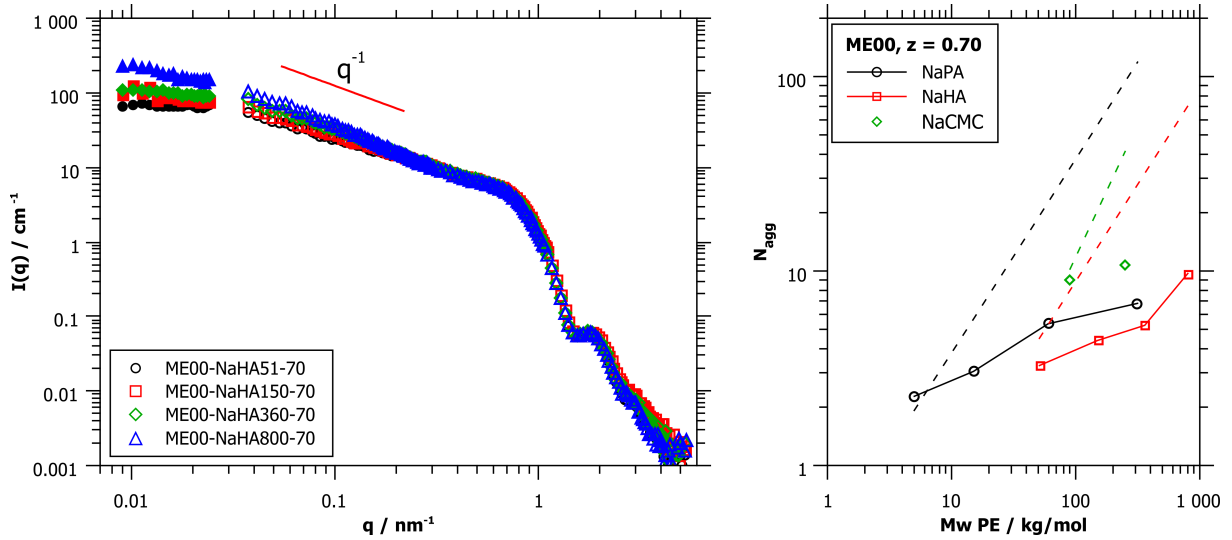


**Figure 22:** A) Scattering data of ME00 with different  $M_w$  NaHA at  $z = 0.7$ . Filled symbols are SLS data and empty symbols are SANS data. B) Aggregation numbers as obtained from SLS. Dotted lines represent theoretical number of droplets per polyelectrolyte chain according to the number of charges. Reprinted with permission from Ref. [108]. Copyright 2020 American Chemical Society.

aggregate was calculated from the molecular weight of the complexes divided by that of one microemulsion droplet (pure microemulsion measured with added salt to suppress inter-particle interactions), see Fig. 22. Aggregation numbers are ranging from 30 to 1 droplet per complex, depending on the mixing ratio  $z$ . In contrast to previously measured NaPA/ME complexes the number does not depend on the droplet size and only little on the molecular weight of the polyelectrolyte. An explanation for this might be that NaHA with the stiffer sugar backbone can not wrap around the droplet to compensate all microemulsion charges as efficiently as the flexible NaPA and therefore the amount of charges per droplet plays only a minor role.

While light scattering is a good tool to determine the overall size of the formed complexes, it is not able to yield information about the internal structuring of these complexes. This information was obtained by SANS measurements. As previously observed for the NaPA/ME complexes, the microemulsion droplets remain unchanged in size and shape when interacting with hyaluronate, as can be seen from the unchanging form factor minimum at high  $q$ . At low  $q$ , where the interactions of the droplets are probed all SANS data show an increase of intensity with a slope depending on the mixing ratio  $z$  (highest for samples close to the phase boundary and decreasing with increasing  $z$ ). At  $z = 0.7$  the slope follows a  $q^{-1}$  power law that can be interpreted as locally rodlike structures, see Fig. 22. Note here, that no plateau is visible in any of the SANS data of NaHA complexes, hence no determination of the complex length can be made. By simulations of cylinders with different lengths it can be concluded that the cylindrical structure exceeds over more than 100 nm. Static light scattering shows a plateau for most samples (Fig. 22A), so only by combining these two methods a full characterization of the PEMECs can be achieved.

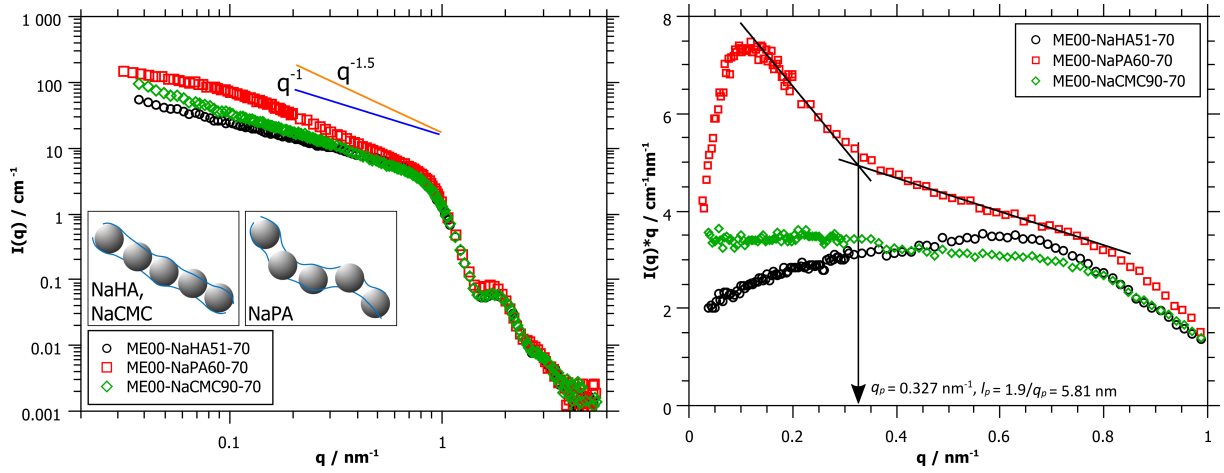


**Figure 23:** A) Comparison of SANS data for small microemulsion droplets mixed with NaHA, NaPA and NaCMC at  $z = 0.7$ , close to the phase boundary. B) Holtzer plot of SANS data of NaHA and NaPA mixed with small microemulsion droplets. Reprinted with permission from Ref. [108]. Copyright 2020 American Chemical Society.

**Comparison of PEMECs Formed with Different Polyelectrolytes.** SLS data of PEMECs with different polyelectrolytes of different  $M_w$  shows the same trend for all polyelectrolytes. The aggregation number at constant charge ratio  $z$  is increasing with increasing  $M_w$  of the polyelectrolyte. NaPA/ME complexes have higher aggregation numbers than complexes with NaHA at a given  $M_w$  of polyelectrolyte but the aggregation numbers are highest for NaCMC complexes, see Fig. 22B.

Again, SANS measurements are able to give more information about the shape and composition of the mixed complexes. The general behavior of all SANS curves looks very similar. With all polyelectrolytes, large mixed aggregates were observed close to the phase boundary that decrease in size with increasing polyelectrolyte excess. At  $z = 0.7$  (close to the phase boundary) the SANS data for all polyelectrolytes show an intensity increase with a slope close to  $q^{-1}$ . A direct comparison shows that the slopes of NaPA samples are generally higher than for NaHA or NaCMC. While the slopes of the rigid polysaccharides are very close to a  $q^{-1}$  power law, the slope of NaPA is  $\sim q^{-1.5}$  (see Fig. 23A). This can be attributed to the different flexibilities of the employed polyelectrolytes. The stiffer NaHA and NaCMC are more likely to arrange the droplets in a straight cylindrical geometry while the flexible NaPA also forms locally cylindrical arrangements of droplets but this cylinder is more flexible and starts to bend with increasing extension, causing a higher slope. It can therefore qualitatively be concluded, that all polyelectrolytes most likely form long cylindrical arrangements of separate droplets when interacting with microemulsion droplets, but the aggregates formed with NaPA show a semi-flexible behavior.

Further information can be obtained by plotting the data in the so-called 'Holtzer plot',<sup>[109]</sup>  $I(q) \cdot q$  vs.  $q$ , Fig. 23B. For flexible polymers, the Holtzer plot typically shows a maximum in the intensity at smaller  $q$  that decreases first rapidly and then with a smaller slope. The kink between the two linear parts can be interpreted as the transition between coiled and linear structure and can be used to calculate the persistence length.<sup>[110,111]</sup> When looking at the Holtzer

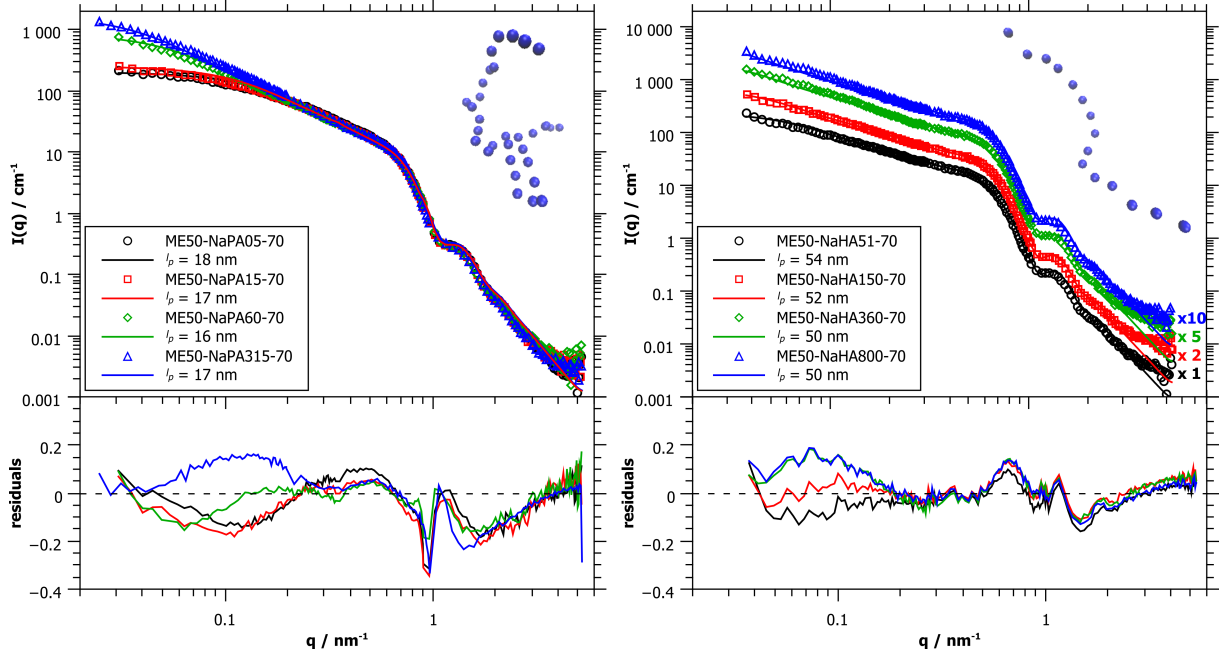


**Figure 24:** Modeled SANS data of NaPA (left) and NaHA (right) samples at  $z = 0.7$ . The insets show examples of simulated complexes for the longest chain lengths. Reprinted with permission from Ref. [108]. Copyright 2020 American Chemical Society.

plots of different polyelectrolytes with microemulsion droplets, the differences become much more visible than in the simple log-log plot. While NaPA samples follow the classical behavior of polymers, the trend of NaHA and NaCMC samples looks completely different. Interestingly the obtained persistence lengths of NaPA samples correspond almost exactly to the respective droplet diameter, which indicates that in this structure the droplets are joined together rather loosely. NaHA and NaCMC samples do not follow the classical Holtzer plot behavior so no persistence length can be determined here. This supports the previously made assumptions that here the microemulsion droplets arrange into straight cylindrical aggregates of substantial length.

Due to the lack of an appropriate model to describe SANS data of curved droplet chains quantitatively, a Monte Carlo model was developed by us for this purpose. The model describes chains of  $N$  homogeneous spheres of average radius  $R$ , which are separated by an average distance  $d$  between the sphere surfaces. The chains assume the random conformations of semiflexible polymers of a given persistence length. To obtain the scattering curves given in Fig. 24, at least 5000 conformations were randomly generated. The scattering intensities were then computed based on each set of sphere coordinates using the Debye formula,<sup>[112]</sup> and averaging over all conformations. The persistence length  $l_p$  was calculated a posteriori from the ensemble-averaged ratio between contour length  $L_C$  and end-to-end distance  $h_{ee}$ , where  $\langle h_{ee}^2 \rangle = 2L_C l_p - 2l_p^2(1 - e^{-L_C/l_p})$ .<sup>[113]</sup> With this model at hand, it was possible to quantitatively describe the full set of SANS data of samples with  $z = 0.7$  for different polyelectrolytes (Fig. 24). To this end, all microemulsion droplet parameters ( $R$ , polydispersity in  $R$ , volume fraction, contrast) were kept constant for all samples. Parameters that depend on the type of polyelectrolyte ( $d$ , polydispersity in  $d$ ,  $V_0$ ) were used as global model parameters for all samples with the same PE type. So, the only

parameter changing with the  $M_w$  of PE is the number of droplets per aggregate  $N$ . The results show that all data of samples close to the phase boundary (where elongated complexes are found) can be described accurately with the new model of cylindrically arranged droplets with a persistence length of the aggregate that depends on the type of polyelectrolyte. The obtained persistence lengths are  $l_p(\text{NaPA}) \sim 17$  nm and  $l_p(\text{NaHA}) \sim 51$  nm, confirming and quantifying the assumptions stated above. Furthermore, the distances between droplet surfaces depend on the type of polyelectrolyte, being  $\sim 2$  nm for NaPA and  $\sim 5.5$  nm for NaHA complexes, which can be explained by the different charge densities of both polyelectrolytes.

It can be discussed here, whether the straight shape of hyaluronate aggregates is not caused by a higher persistence length but instead arises from repulsive interactions of the droplets that can not be sufficiently screened by the polyelectrolyte due to the lower charge density of NaHA compared to NaPA. In this case the repulsive interactions of the droplets would be minimized by addition of salt that screens the charges, which would result in a more flexible aggregate and thus a higher slope in the SANS data. Experiments showed, that the addition of NaCl lowers the forward scattering intensity of these complexes, hence the aggregates become smaller since the interactions between polyelectrolyte and microemulsion droplets are weakened by the salt. Therefore the electrostatic repulsion as driving force for straight cylindrical arrangements can be neglected and the intrinsic persistence length of the respective polyelectrolyte is still most likely responsible for the appearance of the complex.

#### 4.2.2 Investigations of the Coacervate Phase

The phase behavior of hyaluronate/microemulsion complexes is discussed in detail in Chapter 4.2.1. While samples at polyelectrolyte excess show one clear and transparent phase, samples in the unstable region of the phase diagram contain a second optically transparent liquid phase which floats on top of the microemulsion-complex phase. When the sample is shaken, the two phases mix and the sample appears white and low-viscous. Upon resting the sample the two phases separate again, typically within a few hours. It is interesting to note that the second phase, floating on top of the other is very viscous. This is a marked difference to the previously studied polyacrylate complexes where samples phase separated into a clear liquid and a white solid precipitate. Similar phase separation into two liquid phases was already observed elsewhere,<sup>[52,114,115]</sup> this second viscous phase was therefore labeled a 'coacervate phase' and examined in more detail in this chapter.

Fig. 25A shows a photo of ME50 samples, mixed with different polyelectrolytes (NaHA of different  $M_w$ , NaPA60 and CMC90) always at charge equilibrium ( $z = 0.5$ ), where the most pronounced phase separation is expected. It can be seen, that the polysaccharides NaHA and NaCMC show a small, turbid coacervate phase on top of the liquid sample, while the NaPA sample shows a white, solid precipitate, sticking to the glass of the sample container. It is surprising that the coacervate phases of the different  $M_w$  NaHA samples appear optically quite different. In the first sample (NaHA31, shortest NaHA chain) both phases appear blueish, indicating large aggregates.

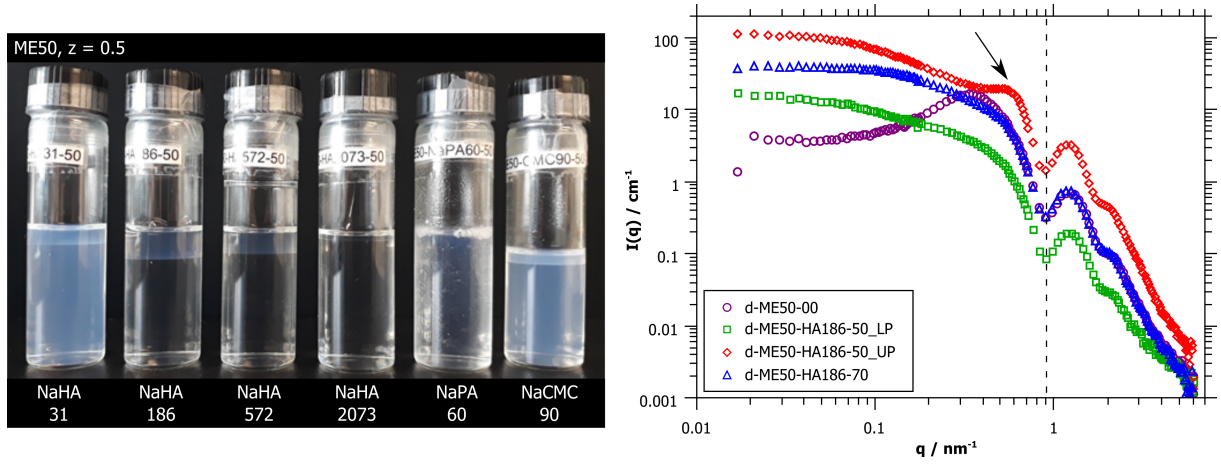


**Figure 25:** A) Photo of samples of ME50 mixed with different  $M_w$  NaHAs and NaPA60 and CMC90 as comparison at  $z = 0.5$  where the most pronounced phase separation is expected. B) SANS data of d-ME50-NaHA186 samples: UP = upper phase, LP = lower phase, both at  $z = 0.5$ ; stable reference sample at  $z = 0.7$  and pure microemulsion.

In the samples with longer NaHA chains, the coacervate phase remains blueish, but the lower liquid phase is now colorless. The volume of the coacervate is also changing for different  $M_w$ , even though the mixing ratio (and therefore the amount of NaHA) is always the same in all samples. The coacervate phase is largest for the NaHA186 sample and almost non-existent for the longest chain NaHA2073 sample.

To examine the phase behavior in more detail and especially obtain information about the composition of the two phases, SANS and NMR measurements were carried out of both phases separately. As a reference, the pure microemulsion and a stable monophasic sample at  $z = 0.7$  for each polyelectrolyte and  $M_w$  were also measured. To see possible changes of the microemulsion droplets more clearly in SANS, samples were prepared in shell contrast of the microemulsion with deuterated decane (d22-decane).

Fig. 25B shows the measured SANS data of the lower (LP) and upper phase (UP) of a d-ME50-NaHA186-50 sample, as well as the  $z = 0.7$  reference sample and the pure microemulsion. First, it can be seen from the unshifted form factor minimum, that the microemulsion droplets remain unchanged. They still have the same size and polydispersity in the phase separated samples, as in the stable sample and the pure microemulsion. This is an important information, as it proves, that no oil was excluded from the microemulsion and the droplets would still be available as potential carriers, even in the coacervate phase. The intensities shown in the plot are absolute intensities and therefore directly correlated to the microemulsion concentration. It can be seen, that the microemulsion concentration is significantly reduced in the LP sample and more concentrated in the UP (coacervate) sample, compared to the pure microemulsion and the stable sample. All samples were initially prepared at 100 mM surfactant concentration. The comparison of the intensities yields a concentration of 25 mM in the lower phase and 400 mM in the upper phase. The accumulation of droplets in the upper phase can also be seen from the correlation peak of the red curve at  $q_{max} \sim 0.6 \text{ nm}^{-1}$ ,  $d = 2\pi/q_{max} \sim 10 \text{ nm}$  originating from a close packing of droplets. The intensity increase towards low  $q$  is similar in the upper phase, lower phase and the

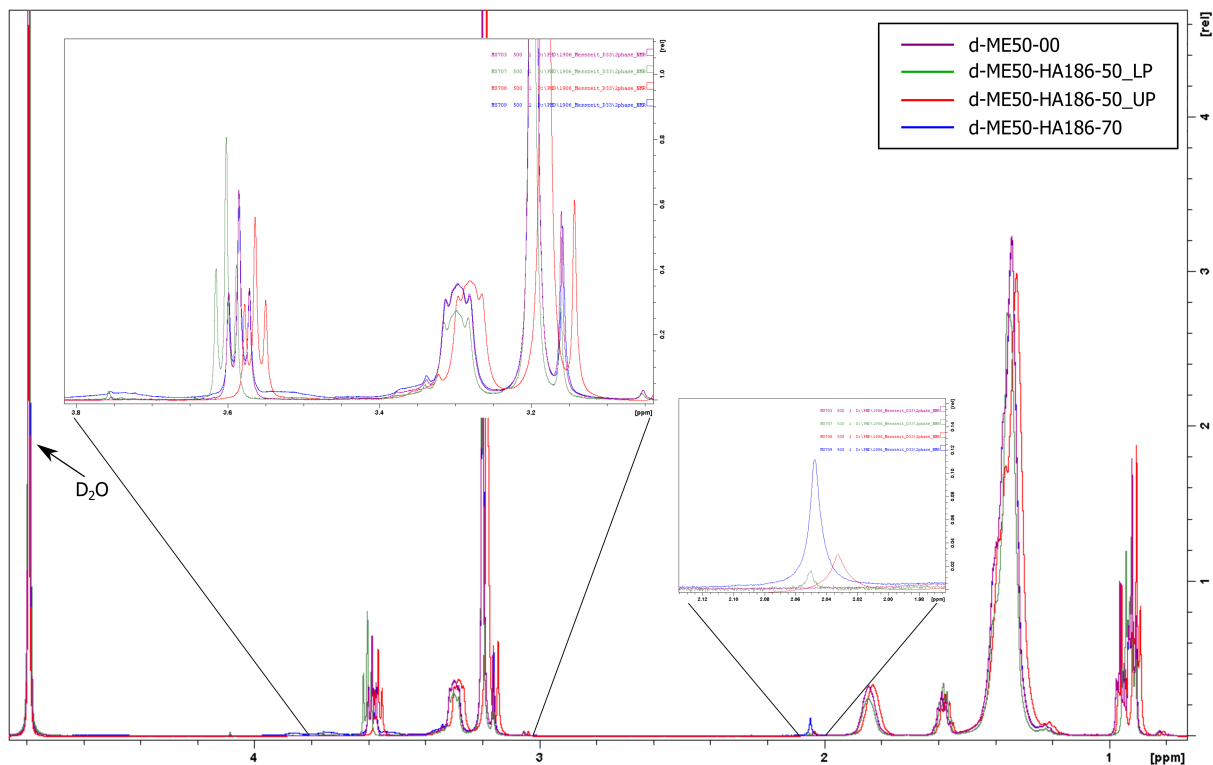


**Figure 26:**  $^1\text{H}$  NMR spectra of upper (UP) and lower (LP) phase of d-ME50-NaHA186 samples at  $z = 0.5$  with reference spectra of pure d-ME50 a stable mixture at  $z = 0.7$ .

stable sample, indicating that no significant changes occurred in the arrangement of the droplets by the NaHA. The low concentration of the lower phase and the very similar scattering pattern to the other samples suggest the assumption that the lower phase still contains traces of the upper phase. When analyzing this issue more closely, it would be interesting to see whether a better phase separation could be obtained by centrifugation.

One theory that comes to mind directly when observing the upper viscous phase, is that the hyaluronic acid is accumulating here and causing the viscosity increase, while excess free ME droplets remain in the lower phase. To examine the composition of the different phases,  $^1\text{H}$ -NMR spectra were taken of the same samples that were already measured in SANS. The spectra of the NaHA186 samples are shown in Fig. 26. On first glance, the NMR spectra all look very similar, upper and lower phase of  $z = 0.5$ , as well as the single phase sample at  $z = 0.7$  and the pure microemulsion all show the same peaks. At least from these spectra, the accumulation of one compound (e.g. NaHA or TTAB) in one of the phases is not detectable. When analyzing the spectra more closely (see zoom in Fig. 26), a small shift of the upper phase-spectra becomes visible, the peaks in this spectra all appear at slightly lower shifts (more to the right). This trend is visible in the NMR spectra measured of the different phases of other  $M_w$  samples as well. It is possible, that either different interactions in the highly concentrated coacervate or a change in the solvent (e.g. from mainly  $\text{D}_2\text{O}$  to a NaHA enriched  $\text{D}_2\text{O}$ ) induce the shift. The comparison with a spectra of the pure microemulsion shows a peak originating from the polyelectrolyte at 2.0 - 2.1 ppm. This peak appears in all mixed samples but not in the pure microemulsion. It shows

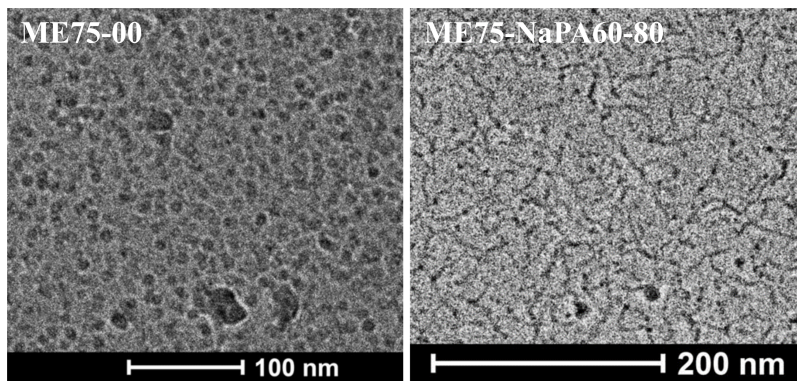


**Figure 27:** Comparison of pure microemulsion ME75 (left) and ME75/NaPA60 complexes (right) in cryo-TEM micrographs. Samples were diluted before specimen preparation, which shows a structural effect in the images.

that hyaluronate is present in all mixed samples. To indicate an enrichment of NaHA in one of the phases is hard with these NMR data, since the intensity is adjusted by the device and no internal standard was added to the samples. However, it is possible to compare the relative peak heights within one spectra (peaks of the microemulsion and of the NaPA). Since no differences in the relative peak heights are visible between the upper and the lower phase, it can be assumed that the ratio between microemulsion and NaHA is not changing here.

Summarizing the SANS and NMR results, it can be said that no difference between the lower liquid phase and the upper viscous coacervate phase can be detected, other than the total concentration.

#### 4.2.3 Comparison of NaPA and NaHA Samples in Cryo-TEM

Cryo-TEM images of PEMEC samples were taken in several attempts by members of the Talmon group at the Technion in Haifa, Israel. The goal was to confirm the linear droplet arrangements suggested by SANS measurements and to see possible differences in the linearity of complexes with the flexible NaPA and the more rigid NaHA.

Because the microemulsion droplets are in general rather small, cryo-TEM images were taken of the largest droplets, ME75, to achieve the best possible resolution. First images of ME75 samples (pure and in mixture with NaPA60, see Fig. 27) showed unrealistic size effects. The pure microemulsion sample showed much larger droplets (size comparable to results obtained by SANS) than the mixed sample, where threadlike aggregates of small diameters are visible in the images. This effect can only be caused by dilution of the sample. Most cryo-TEM samples were diluted before specimen preparation to give better (not overlapping) signals. Separate experiments showed, that the large microemulsion droplets ME75 become unstable upon dilution, due to the cosurfactant hexanol being partly soluble in water. Interestingly, it was found that these samples do not instantly become unstable, but need about one day to show a visible change. SANS measurements of concentrated and diluted samples (several days old) show a clear shift in the form factor minimum from  $q \sim 0.7$  to  $q \sim 1.0 \text{ nm}^{-1}$  for the diluted samples. See Fig. 13 in Chapter 3.2.2 for photos and SANS data of diluted samples. The exact procedure of specimen

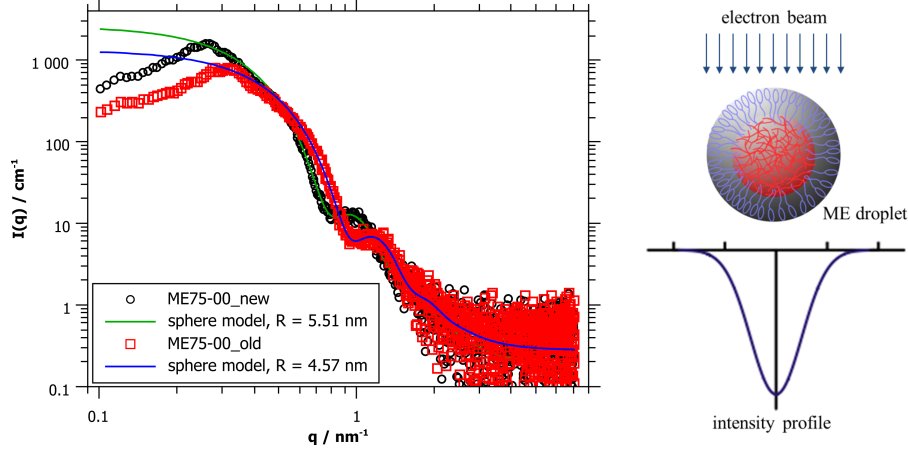


**Figure 28:** A) SAXS measurements of large microemulsion droplets ME75, measured a few days and one year after preparation, showing the aging process. B) Schematic representation of electron beam profile when passing through a microemulsion droplet.

preparation for cryo-TEM can not be reconstructed, but it is likely that both samples, the pure microemulsion and the complexed sample, were diluted in a first step. While the microemulsion sample was vitrified in liquid ethane instantly, the complexed sample was probably left on the side for later vitrification, which caused the deviations from the expected structure. This is only an assumption, but it would explain the threadlike micellar structures shown in the first cryo-TEM images that are not consistent with previous SANS results.

More cryo-TEM images were taken of samples of large microemulsion droplets (ME75) with NaPA60 and NaHA51 at charge ratios of  $z = 0.8$  and  $0.7$ , both in polyelectrolyte excess but close to the phase boundary, see Fig. 29. This time the samples were vitrified in their original concentration at 100 mM surfactant to prevent dilution effects. The mixed samples of microemulsion and polyelectrolyte both show linear arrangements of separate droplets and no threadlike micelles as before. The diameter of these droplets is with  $d \sim 7.5$  nm still much smaller than expected from SANS and this time the discrepancy can not be explained by dilution effects.

One possible explanation for different droplet sizes would be the different contrasts arising from electrons and neutrons. To check this theory, SAXS (small-angle x-ray scattering) measurements of the exact same samples as used for cryo-TEM were carried out on a SAXSess instrument at BAM, Berlin. Two conclusions could be drawn from the SAXS measurements. First, the different contrast is responsible for a slight change in the observed size. For the small droplets ME00, SANS has given a radius of  $R = 3.1$  nm while the radius obtained by SAXS was only 2.5 nm. For the large ME75 droplets the radii changed from 6.4 to 5.5 nm for SANS and SAXS respectively. Both fits were done using a simple homogeneous sphere model, but most likely a core-shell model would be better suited to describe the SAXS data, as here the contrast is coming from the surfactant headgroups and counterions. Secondly, an aging of the microemulsion droplets was observed. The microemulsion stock solution used for the last set of cryo-TEM measurements was about one year old. It was stored in a glass vial, closed with a plastic lid and sealed with parafilm. But still the droplets sizes measured in SAXS were smaller than those of freshly

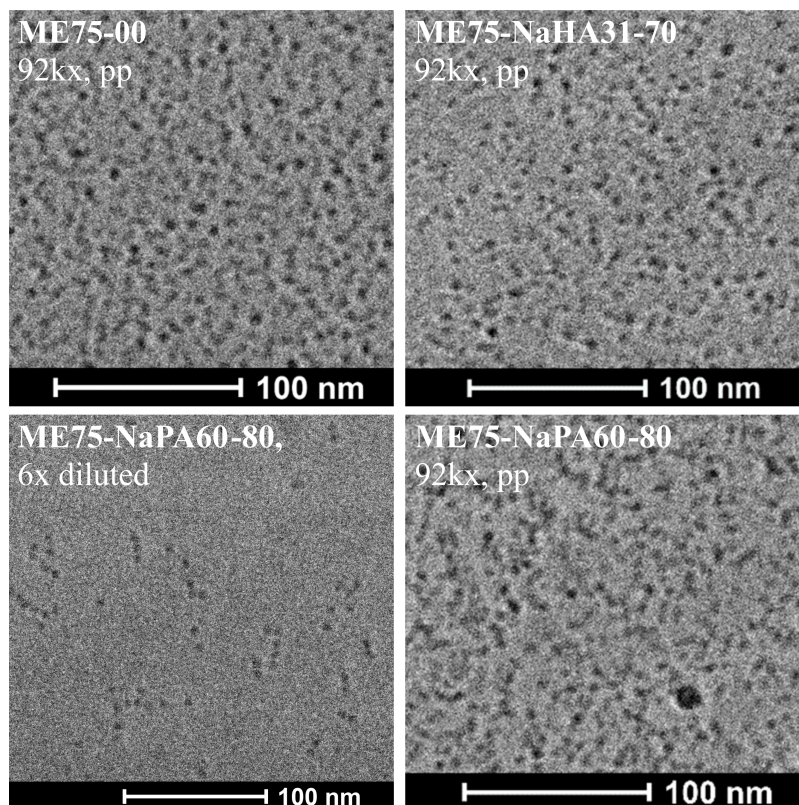


**Figure 29:** Comparison of cryo-TEM micrographs of pure microemulsion droplets (top left) with ME droplets mixed with NaPA (bottom) and NaHA (top right) at a  $z$ -value in PE excess but close to the phase boundary.

prepared microemulsions (ME00<sub>new</sub>:  $R = 2.5$  nm, ME00<sub>old</sub>:  $R = 2.3$  nm, ME75<sub>new</sub>:  $R = 5.5$  nm, ME75<sub>old</sub>:  $R = 4.6$  nm). Most likely the either the cosurfactant hexanol or the oil decane have evaporated from the sample, which decreased the stable droplet size. See Fig. 28A for SAXS data of freshly prepared and aged microemulsion.

As a general objective for cryo-TEM, it should also be mentioned, that the imaged microemulsion droplets are composed of molecules that mainly contain Carbon and Hydrogen and therefore have rather low contrast for electrons. The image is capturing the transmittance of the electron beam through the sample. Of course the way of one electron through one droplet, and therefore the probability to be absorbed is longest in the middle of the droplet and shorter towards the edges. In the image the microemulsion droplet therefore occurs black in the middle and lighter gray towards the edges, see Fig. 28B for a sketched intensity profile of an electron beam passing through a microemulsion droplet. Additionally, the imaged sample film can be several 100 nm thick, so many droplets can be superimposed in the image. All these parameters are making it very hard to distinguish the exact size of droplets in cryo-TEM micrographs. All these thoughts discussed above state, that a reliable size of microemulsion droplets is very hard to measure in cryo-TEM, whereas a qualitative analysis is straight forward.

Reverting to the initial question of comparing the elongated complexes of different polyelectrolytes, Fig. 29 shows nicely the interconnected droplet nature of the PEMECs for both, NaPA and NaHA samples. Due to the high concentrations used the images are crowded with droplets,

making it very hard to distinguish separate complexes and make statements of the elongated nature of these complexes. The strands of droplets of the NaPA sample look slightly more branched and bent than for the NaHA sample but this subjective impression might be biased by expectations. Dilution is necessary to be able to distinguish separate complexes, as is also shown in Fig. 29. This sample was prepared by diluting the original sample at 100 mM surfactant concentration 6 times with water, directly before preparing the cryo-TEM specimen. In the micrograph of this image, small but straight arrays of droplets are visible, containing 3 to 5 droplets. Extra care was taken to have a short time between dilution and vitrification of the sample but nevertheless it is not guaranteed that the original sample is retained.

In summary, it can be said that cryo-TEM images provide qualitative evidence for the structures that were previously assumed from SANS measurements of polyelectrolyte/microemulsion complexes. Arrays of separate droplets can be clearly seen in micrographs of undiluted polyelectrolyte/microemulsion samples. Small differences in the linearity and extension of NaPA and NaHA complexes can be seen in these images but are difficult to verify. Further quantitative analysis is necessary to deduce an average persistence lengths of these complexes. However, obtaining quantitative information from these images becomes very hard due to bad contrast, high concentrations and superimposed droplets or undefined diluted samples and unavailability of suitable automatic image analyzing tools.

### 4.3 Conclusion

In this chapter it was shown, that PEMECs can not only be formed with the crude oil based polyacrylate (NaPA) but also with bio-derived polyelectrolytes, such as hyaluronate (NaHA) and carboxymethyl cellulose (NaCMC). The employed polyelectrolytes do not differ only in the origin and environmental impact but also in their chemical architecture. The biopolyelectrolytes are composed of sugar backbones that are more rigid than the flexible NaPA and also exhibit a lower charge density. In addition the charges of NaCMC are not located directly on the backbone but linked by a flexible spacer.

Even though the biopolyelectrolytes and NaPA are very different in architecture, they show a surprisingly similar phase behavior when mixed with oppositely charged microemulsion droplets. In all cases long-time stable samples are found on the polyelectrolyte excess side of the phase diagram. SANS measurements show that close to the phase boundary cylindrical arrangements of droplets are found for NaHA and NaCMC as well as for NaPA. Direct comparison reveals that the stiffer polyelectrolytes form straight cylinders, while the cylindrical aggregates of the flexible NaPA tend to bend over a certain persistence length which induces a higher slope in the SANS data. Fig. 30 shows a sketch of possible droplet arrangements. A Monte Carlo model was developed in cooperation with E. Schneck to quantitatively describe the SANS data of semiflexible PEMECs with different persistence lengths. With this model, we are able to describe the SANS data very accurately and also obtain a persistence length of the complexes from the simulations. This new SANS model to describe arrayed spherical particles should not only be applicable for

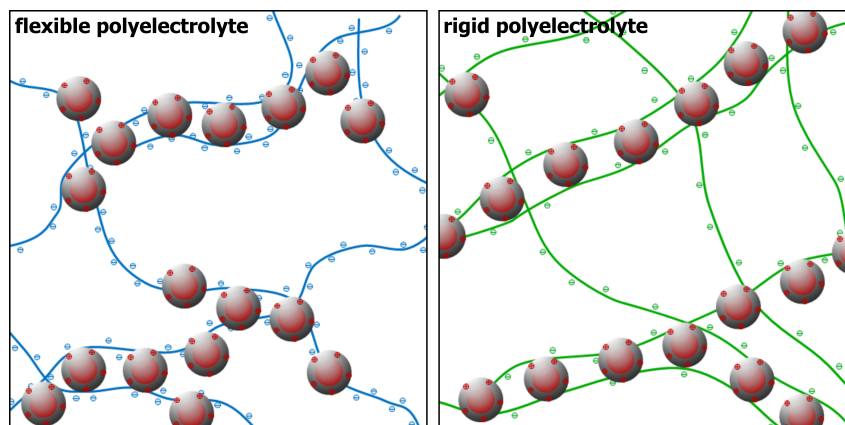


**Figure 30:** Sketch of qualitative differences of rigid and flexible polyelectrolytes in the formation of PEMECs. Reprinted with permission from Ref. [108]. Copyright 2020 American Chemical Society.

PEMECs but also be very useful for surfactant- or nanoparticle complexes.

One pronounced difference between the biopolyelectrolytes and NaPA was found in the nature of the second phase in the two-phase region. While a solid white precipitate was found for NaPA/ME complexes, a viscous coacervate phase was formed in samples with NaHA or NaCMC. This coacervate phase was analyzed with SANS and  $^1\text{H}$ -NMR measurements but no exact composition could be determined. The coacervate phase seems to be more concentrated than the lower phase but no accumulation of one specific compound could be detected. However, this coacervate phase seems very interesting and should be analyzed in more detail in the future.

The observation of PEMECs with cryo-TEM turned out to be complicated by a number of factors that make the quantitative interpretation of cryo-TEM micrographes very difficult. The formation of complexes made of separate aligned droplets as observed in SANS could be qualitatively confirmed in cryo-TEM. Images were taken of complexes of microemulsion droplets with NaPA and NaHA but until now it was not possible to deduce a persistence lengths of these complexes, so no quantitative comparison could be made. Until now we have used large droplets (ME75) for the cryo-TEM studies. In future experiments it would be better to use small droplets (ME00), even though they are more difficult to image, since the volume fraction of small droplets is smaller and dilution is also possible.

The difference in stiffness of the employed polyelectrolytes should also become apparent in electron birefringence (EDB) measurements. In this technique, the complexes are aligned by an electric field which gives a birefringence signal. When the electric field is turned off, the relaxation process can be followed by the weakening of the birefringence signal. First test showed promising signals for NaPA and NaHA complexes but the data was not yet analyzed.



## 5 Dynamics in Polyelectrolyte/Microemulsion Complexes

### 5.1 Introduction

Until now, we have mostly analyzed the static behavior of PEMECs. To further study the dynamic behavior of such systems is of great interest with respect to potential applications as delivery systems but also to gain a deeper general understanding of the interactions between microemulsion droplets and polyelectrolytes. Some questions can only be answered by the combination of static and dynamic methods together, as one method alone would give an incomplete picture.

For many applications it would be interesting to not only know the size, shape and composition of complexes but also get information about their lifetime or the exchange rates of droplets. In dynamic measurements of polyelectrolyte/microemulsion complexes, one might expect to find two dominant motions, a fast motion of freely diffusing droplets and a slower one of droplets arrested on polyelectrolyte chains. As a simple way to study the dynamic behavior, DLS was already employed in previous chapters. In a consecutive experiment, we additionally employed neutron spin echo (NSE) to study the dynamics on different time scales. NSE is a high-resolution dynamic method, allowing to resolve nanometer length scales and nanosecond time scales.

### 5.2 Results

#### 5.2.1 "Dynamics in Polyelectrolyte/Microemulsion Complexes" by M. Simon, M. Gradzielski and I. Hoffmann, *submitted to Nanoscale Advances*

SANS measurements of PEMECs showed, that in polyelectrolyte excess close to the phase boundary large rodlike aggregates, composed of many cylindrically arranged droplets are present. An increase in viscosity would be expected from the formation of long, rodlike aggregates or the incorporation of microemulsion droplets into an interconnected network. This was observed in previously studied systems of microemulsion droplets and telechelic polymers.<sup>[42]</sup> However, the PE/ME systems interacting via electrostatic interactions studied here were always low viscous and did not show this expected increase, even though the polyelectrolyte concentration is above the overlap concentration (compare Tab. 6). In order to examine this situation we employed static SANS and dynamic NSE and DLS measurements. These first results are going to be published in a short paper that was recently submitted to *Nanoscale Advances*.<sup>[116]</sup> The paper draft can be found in the [Appendix](#).

In this work we have addressed the question of droplet mobility in complexes of medium sized microemulsion droplets (ME50,  $R \sim 4$  nm) with polyacrylates of different  $M_w$ . Here, we have focused on the structurally most interesting complexes formed in polyelectrolyte excess close to the phase boundary, at  $z = 0.7$ . In a first step, the intermediate scattering functions  $S(q, t)$  measured in NSE can be fitted with a simple exponential decay to yield the apparent diffusion coefficients  $D_{app}$  as a function of  $q$ , shown in Fig. 31A. The peak at  $\sim 0.1$  1/Å is a typical feature in NSE measurements of microemulsions. It arises from undulation motions of the surfactant

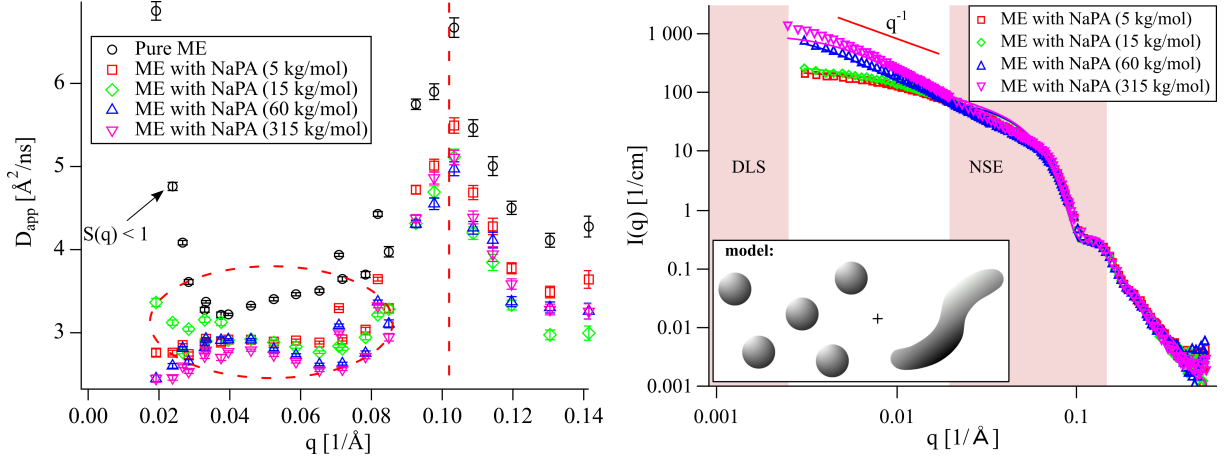


**Figure 31:** A) Apparent diffusion coefficient  $D_{app}$  obtained from NSE measurements as a function of  $q$ . B) SANS curves PEMECs fitted with a combination of wormlike chain and free spheres according to NSE results.

films, which are most pronounced at the form factor minimum. The peak position is in good agreement with previously measured SANS data of ME50 (see Fig. 31). At lower  $q$ , in a region where the aggregate diffusion is probed ( $0.04 < q / 1/\text{\AA} < 0.07$ ),  $D_{app}$  shows that the dynamics are slower for the complexes than for the pure microemulsion. At  $q$  values lower than  $0.04 \text{ 1/\AA}$ , the effect of the structure factor becomes visible and  $D_{app}$  is not easily interpreted anymore.

The values of  $D_{app}$  of the complexes are rather similar regardless of the different  $M_w$  of the NaPA and despite the different sizes of the complexes observed in SANS. In addition a diffusion coefficient of  $\sim 3 \text{ \AA}^2/\text{ns}$  as observed for mixed complexes in NSE, corresponds to a hydrodynamic radius of  $\sim 7 \text{ nm}$  via the Stokes-Einstein relation. These diffusion coefficients are too fast for complexes of about  $100 \text{ nm}$  length, as they were observed in SANS.

A closer inspection of the intermediate scattering functions  $S(q, t)$  at  $q$  values where only diffusion should be visible reveals that  $S(q, t)$  is not single exponential for the complexes as opposed to the pure microemulsion. This is in contrast to our findings from DLS where the data of the complexes as well as the microemulsions could always be described accurately with a single exponential. There are two possibilities to interpret these findings. Either free microemulsion droplets coexist with large complexes and due to the much stronger scattering of large structures at low  $q$  (light scattering) only the complexes are observed in DLS, or the complexes are highly dynamic and microemulsion droplets are exchanging with a rate longer than the nanosecond timescale of NSE but shorter than the micro- to millisecond timescale of DLS.

To address this question in more detail, the NSE data was fitted with a combination of the Milner-Safran model<sup>[96,97]</sup> to account for the membrane undulations at high  $q$  and the translational diffusion of the free droplets and a second slow diffusive mode with a  $q$  independent diffusion coefficient  $D_{slow}$  and a  $q$  dependent amplitude  $x_{slow}$ . The contribution from the free droplets was fixed according to fits to the data from the pure microemulsion.

The fit results for  $x_{slow}$  are shown in Fig. 32A in a  $q$  range where the influence from the membrane undulations is weak. The values are quite similar for all samples and do not show a very

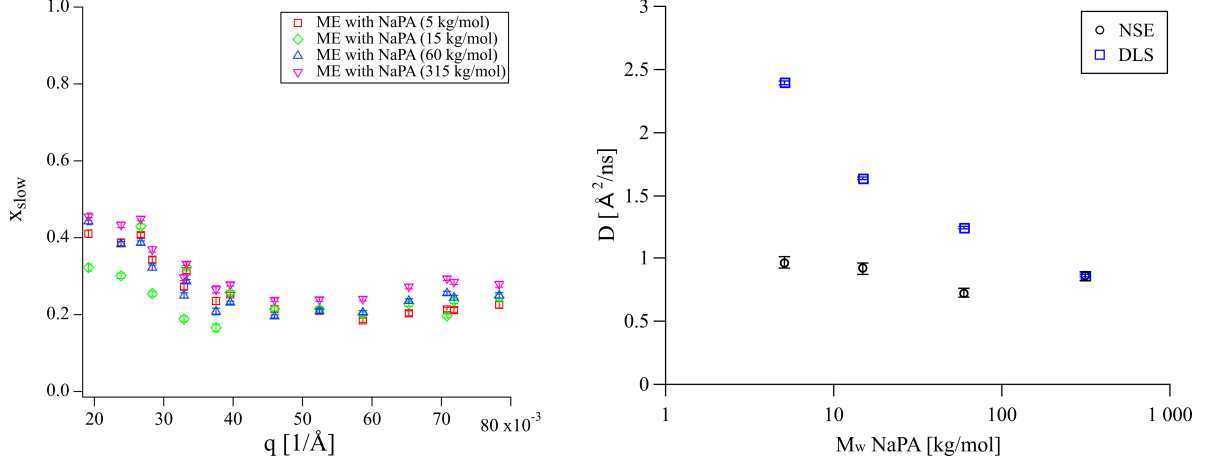


**Figure 32:** A)  $x_{slow}$  obtained from NSE as a function of  $q$  and B)  $D_{slow}$  obtained from NSE and diffusion coefficient obtained from DLS as a function of the  $M_w$  of NaPA.

pronounced trend with  $q$ .  $x_{slow}$  should be a reasonably good approximation for the fraction of droplets bound in complexes at a given time, which is about 20 to 30 % of the microemulsion droplets for all complexes with a slight increase with increasing  $M_w$  of the NaPA. The values obtained for  $D_{slow}$ , shown in Fig. 32B are  $\sim 0.7 - 1.0$  Å<sup>2</sup>/ns and do not show a strong dependence on the  $M_w$  of the NaPA, even though SANS shows significantly larger complexes for high  $M_w$  NaPA. This means that the diffusion constant  $D_{slow}$  measured here is mostly describing the diffusion of complex segments and not of the whole complex. A direct comparison (Fig. 32B) shows that the diffusion coefficients obtained by DLS are faster for short NaPA chain lengths and approach the same value as  $D_{slow}$  for high  $M_w$  NaPA. This can be explained with the lifetime of the complexes. Large complexes are coexisting with free microemulsion droplets that are exchanging fast in comparison of the millisecond time scale of a DLS experiment. For this reason only one exponential decay is present here that corresponds to a weighted relaxation of free and bound droplets. The time scale of a NSE measurement is fast compared to the exchange rate of droplets, therefore a bimodal decay represents the free droplets and the larger complexes. The diffusion coefficients measured in DLS are slower for samples with higher  $M_w$  NaPA since large complexes are scattering significantly more at the small  $q$  values of DLS (compare static scattering in Fig. 31B) and therefore contribute more to the weighted relaxation time. That both diffusion coefficients, measured with DLS and NSE approach the same value indicates that the same process of segment diffusion is measured in both methods. Another measurement at even higher  $M_w$  of NaPA would have been nice at this point to verify the trend.

It is stated above that the lifetime of complexes must be longer than the nanosecond time scale of NSE but shorter than the millisecond time scale of DLS measurements. The time scales of DLS and NSE measurements can be estimated with  $1/(D \cdot q^2)$ . Assuming a diffusion coefficient of  $3.5$  Å<sup>2</sup>/ns for the free microemulsion droplets and  $q$  values of  $0.02$  Å<sup>-1</sup> for NSE and  $0.002$  Å<sup>-1</sup> for DLS results in a lifetime of complexes between  $700$  ns and  $70$  μs.

With these results we were able to reanalyze the previously measured SANS data. Until now a model of a cylindrical arrangement of droplets was used that included all present droplets.

Now, this model is not in accordance with the NSE results anymore. Due to lack of a more sophisticated model, we used a combination of the Kholodenko worm to simulate the aggregates with a certain persistence length and free spheres that interact with a Baba-Ahmed structure factor. The ratio of aggregates and free spheres was set to 30:70 % according to the NSE results. We were able to obtain reasonably good fits with this model, see Fig. 31B, deviating only little at mid  $q$  due to the oversimplified implementation of homogeneous worms and the structure factor. In summary, these investigations show that electrostatically formed PEMECs are highly dynamic systems. Even though static SANS measurements show large complexes formed by a cylindrical arrangement of droplets, we found that on average only a relatively small fraction ( $\sim 30$  %) of the microemulsion droplets is involved in the formation of complexes at a given moment. The average life time of these complexes lies between the nanosecond time scale of NSE and the millisecond time scale of DLS. Reverting to the initial question concerning the viscosity of polymer/microemulsion complexes, we can now explain the low viscosities observed with the very dynamic situation of these complexes. Even a very high shear modulus  $G_0$ , arising from an interconnection of droplets into long rods, cannot compensate such short structural relaxation times  $\tau$ , thus no viscosity ( $\eta$ ) increase can be observed in this system, as  $\eta = \tau \cdot G_0$ .

### 5.2.2 Effect of Other Parameters on Complex Dynamics

More NSE measurements were carried out to study different effects on the droplet dynamics, such as the type of polyelectrolyte, the droplet size and the mixing ratio  $z$ . The measured intermediate scattering functions were analyzed with the combination of the Milner-Safran model and a slow diffusive contribution described above. However the results were not thoroughly evaluated yet and an complete interpretation in consistence with other methods should follow.

The diffusion coefficients  $D_{slow}$  obtained in the previous chapter are still rather high for large elongated aggregates. One possible explanation for this situation would be that due to the soft and flexible nature of the NaPA complexes, the diffusion times  $D_{slow}$  measured in NSE belong to an effective persistence length of the polyelectrolyte. The effective persistence lengths are similar for polyelectrolytes of the same nature but different  $M_w$ , consequently  $D_{slow}$  is also similar for all different  $M_w$  of NaPA measured even though the static picture shows pronounced  $M_w$  dependent differences. This explanation could be verified by employing other polyelectrolytes with significantly different persistence lengths which should have a marked effect on  $D_{slow}$ .

Consequently, more NSE measurements were performed with complexes formed with ME50 and sodium hyaluronate (NaHA) of two different  $M_w$  as polyelectrolyte. The results are shown in Fig. 33. It can be seen, that the stiffer biopolyelectrolyte exhibits a slower diffusion coefficient than the flexible NaPA (ignoring NaPA60 that deviates from the other NaPAs). Even though the effect is not very pronounced, it supports the hypothesis that segments with lengths similar to the persistence length are moving slower for stiffer polyelectrolytes than for flexible ones. Using the Stokes-Einstein relation with the  $D_{slow}$  values of NaPA, one obtains a radius of  $\sim 300$  Å. This coincides nicely with the Kuhn segments obtained with SANS fits of 330 Å for low  $M_w$ .

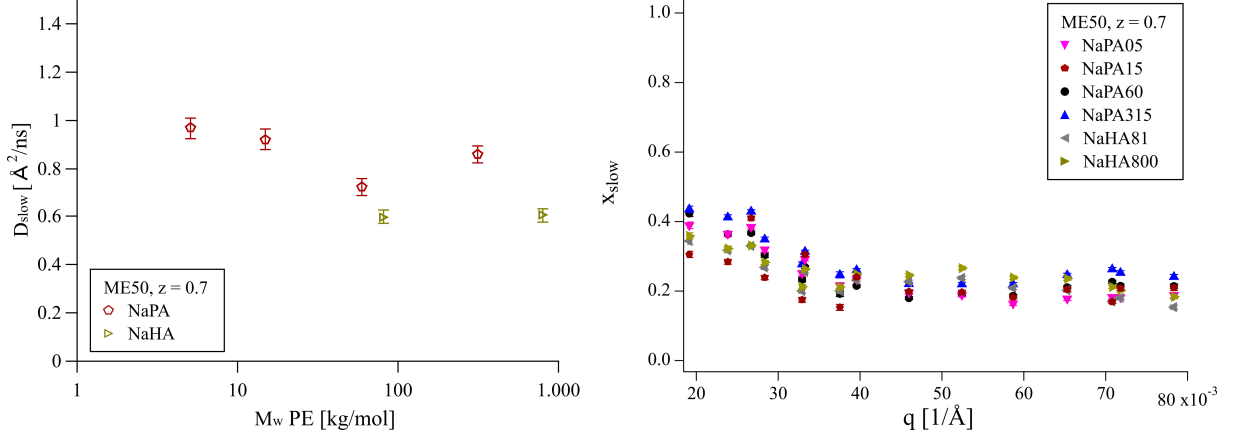


**Figure 33:** A) Diffusion coefficients  $D_{slow}$  in dependence of the  $M_w$  of polyelectrolyte and B) fraction of ME droplets  $x_{slow}$  contained in large clusters at a given time, obtained from NSE of NaPA and NaHA samples in comparison

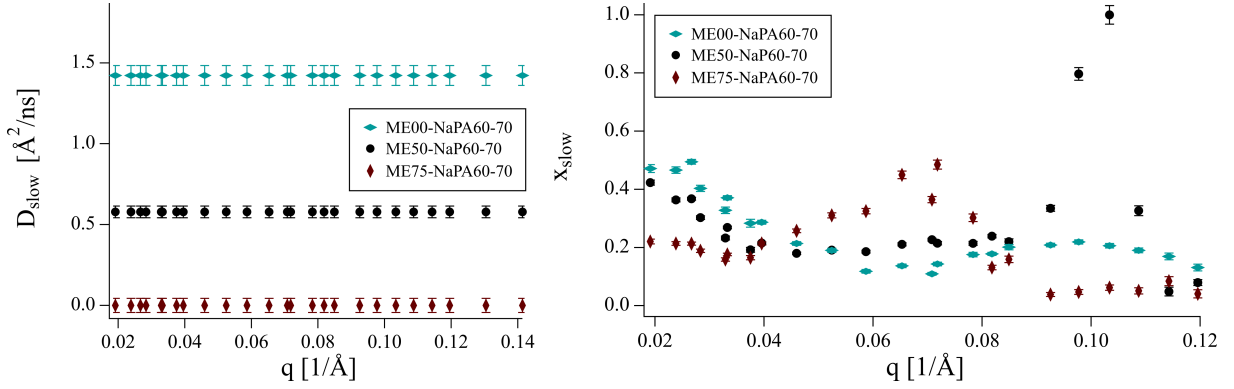


**Figure 34:** A) Diffusion coefficients  $D_{slow}$  and B) fraction of ME droplets  $x_{slow}$  contained in large clusters at a given time, obtained from NSE of different ME droplet sizes in comparison

to 130  $\text{\AA}$  for high  $M_w$  (see SI of paper draft). Samples with NaHA show a longer  $q^{-1}$  slope in SANS than the NaPA samples so longer Kuhn lengths are expected here, which fits to the smaller diffusion coefficients obtained in NSE. In Fig. 33A, it also becomes apparent that  $D_{slow}$  is very similar for the two NaHAs of very different  $M_w$ , while the range of  $D_{slow}$  for different  $M_w$  of NaPA is much larger.

Another important parameter to be varied is the droplet radius. NSE measurements were carried out with NaPA complexes of small, medium and large droplets (ME00  $R \sim 3$  nm, ME50  $R \sim 4$  nm, ME75  $R \sim 6.5$  nm), see Fig. 34. A large effect in  $D_{slow}$  is observed here with the droplet size. Complexes of small droplets ( $D_{slow} = 1.3 \text{\AA}^2/\text{ns}$ ) seem to be moving almost double as fast as medium sized droplets ( $D_{slow} = 0.7 \text{\AA}^2/\text{ns}$ ) and large droplets show a very slow diffusion coefficient of  $0.12 \text{\AA}^2/\text{ns}$ .

Of course, it was found in SANS measurements before (Chapter 3.2.1), that larger complexes are formed with larger droplets. However, if the diffusion time  $D_{slow}$  measured in NSE would correspond to the persistence length of the complexes, the values should not be as different. It is worth consideration whether the stronger electrostatic interactions of large droplets (that contain more charges per droplet) lead to slower exchange rates, which influences the results shown here.

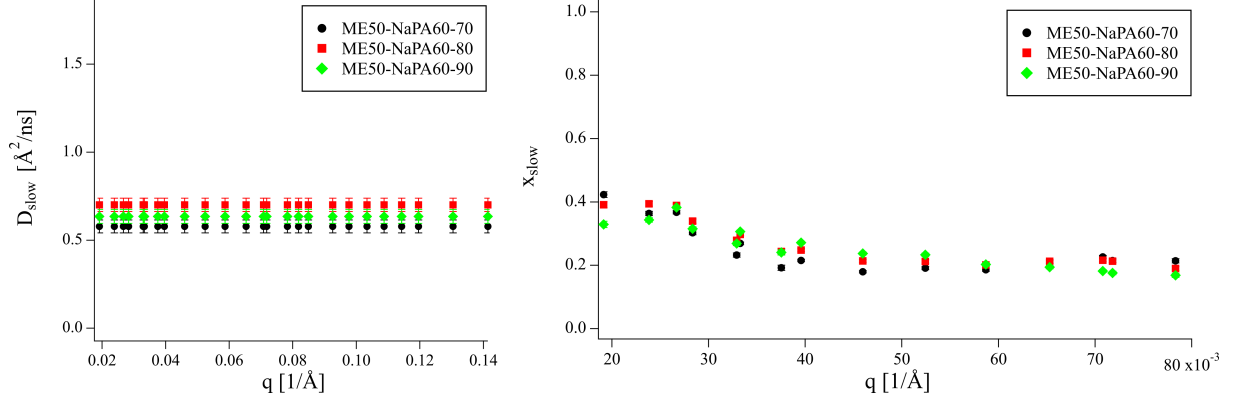


**Figure 35:** A) Diffusion coefficients  $D_{slow}$  and B) fraction of ME droplets  $x_{slow}$  contained in large clusters at a given time, obtained from NSE of ME50-NaPA60 complexes with different charge ratios  $z$  in comparison

In Fig. 34B in the respective  $q$  range for each droplet size, it can be seen that all complexes bind the same fraction of droplets, independent of the droplet size.

Finally also the effect of the charge ratio  $z$  for polyelectrolyte excess samples of ME50-NaPA60 was tested in NSE measurements, the results are presented in Fig. 35.  $D_{slow}$  is very similar for all three charge ratios. If one would expect to see the diffusion of large rodlike aggregates close to the phase boundary at  $z = 0.7$  and single droplets at larger polyelectrolyte excess as suggested from SANS measurements, these results are surprising. However, we have already learned from previous NSE measurements that not the diffusion of whole complexes but only the arrested motion of separate droplets is visible here. Since all droplets employed in this series have the same charge density and bind to the same polyelectrolyte, it is logical that the arrested diffusion coefficients  $D_{slow}$  are similar.

It is more surprising to observe also very similar fractions of microemulsion droplets bound in aggregates for all charge ratios (see Fig. 35B). For  $z = 0.9$  the amount of added polyelectrolyte has increased substantially, making it statistically much more likely to interact with microemulsion droplets. Upon close inspection of the obtained  $x_{slow}$  values, a small trend with  $z$  is visible. This effect is very small, which can only be explained by the very weak electrostatic interactions between microemulsion droplets and polyelectrolytes, due to the low charge density of the microemulsion droplets. If we consider the entropic gain of counterion release, the first released counterion is gaining a lot of entropy but this effect is weakened with increasing ion concentration with  $\ln(1/N_{counterion})$ . At one point no further electrostatic bonds are formed because the entropy gain is too small. With the assumption that the major part of counterions is located close to the polyelectrolyte chains and microemulsion droplets and are only released when new electrostatic bonds are formed, the polyelectrolyte concentration would not influence the ion concentration and therefore have no impact on the probability of bond forming. In this case the fraction of microemulsion droplets bound in aggregates would be similar for all charge ratios since it does not depend on the polyelectrolyte concentration.

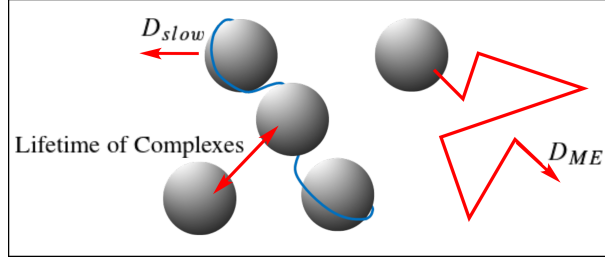


**Figure 36:** Schematic illustration of different processes occurring simultaneously in PEMECs.

### 5.3 Conclusion

In this chapter the dynamics of microemulsion droplets in mixtures with polyelectrolytes were studied thoroughly. NSE measurements elucidate even more clearly than SANS measurements the weak electrostatic interactions between the microemulsion droplets and polyelectrolyte chains. It was shown that the microemulsion system is very tolerant to polyelectrolyte addition and at least in the concentration range investigated here, the microemulsion droplets can be employed in mixed systems without alterations.

It was found that the formed complexes are very dynamic with fast exchange rates of droplets and only a very small fraction of droplets is bound to the polyelectrolytes at a given time. Fig. 36 summarizes the different dynamic motions occurring simultaneously in PEMECs. This short structural relaxation time also explains the low viscous behavior of these mixtures, which is not expected for long rodlike aggregates.

The variation of different system parameters shows, that the  $M_w$  of the employed polyelectrolyte plays a minor role in the observed diffusion times. Small differences can be seen here for polyelectrolytes with different persistence lengths, suggesting that the measured diffusion times ( $D_{slow}$ ) belong to motions of segments and not of the whole complex. In addition, also the droplet size and the mixing ratio  $z$  were varied. Those measurements showed interesting results that have to be analyzed in detail in a consecutive study.

Further, it is interesting to examine how the polyelectrolyte/microemulsion interaction affects the membrane undulations and the bending rigidity of the surfactant film of the microemulsion droplets. These properties can also be studied in NSE measurements and will be analyzed in detail in the future.



## 6 Variation of pH in Polyelectrolyte/Microemulsion Systems

### 6.1 Introduction

Modern materials need to fulfill more and more specialized demands, while still remaining versatile and compatible for different needs. Being able to tune the complexation by simple pH variation offers great new opportunities for applications such as drug delivery<sup>[117]</sup> or pollutant recovery,<sup>[118]</sup> where the switching between free carriers and large complexes is an essential property e.g. for releasing active agents.

The previous chapters illustrated the variety in structures that can be achieved in systems composed of weakly charged O/W microemulsion droplets and oppositely charged polyelectrolytes. The pH was not controlled in the previous work in order to not add any additional ions to the system, as the complexes are sensitive to ionic strength. Measurements of the pH showed, that it was usually in the neutral region, between 7 and 8 for all samples. Since the surfactant employed in this work (TDMAO), as well as all polyelectrolytes (NaPA, NaHA) are pH responsive, additional tuneability of the complexation arises via the pH value. TDMAO is uncharged at neutral to basic conditions and becomes charged at low pH, while the polyanions contain carboxylic acids as ionic groups, that are uncharged when protonated at low pH and become more and more charged at higher pH values (see Fig. 37 for titration curves). This means that it is possible to tune the charge density on the droplet surface and on the polyelectrolyte chain simultaneously, thereby systematically modifying the electrostatic interactions in the system. The electrostatic interactions strongly influence the strength of binding for complexation and thereby the structures of the formed complexes.

### 6.2 Results

#### 6.2.1 Variation of pH in the ME50-NaPA60 Systems

As a first step, titration curves were recorded for the microemulsion and for the polyelectrolytes separately. Fig. 37 shows the titration curves, converted to the percentage of charges, meaning the degree of deprotonation for the polyelectrolyte NaPA60 and the degree of protonation for the microemulsion ME50. The signal of the microemulsion originates mainly from the surfactant

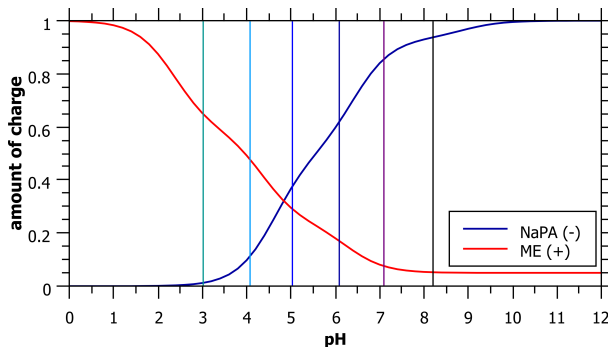


**Figure 37:** Titration curves of NaPA and a 5% TTAB containing microemulsion. The colored lines indicate the pH values of samples taken for further analysis.

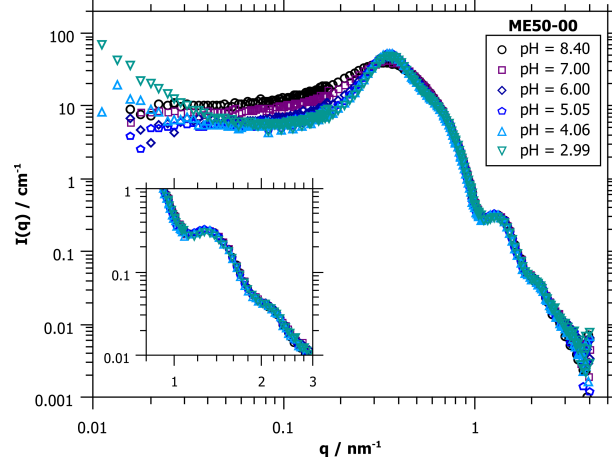


**Figure 38:** SANS data of pure ME50 at different pH values. A zoom into the  $q$ -region of the form factor minimum shows the retention of the microemulsion droplets.

TDMAO, but the used microemulsion also contained 5% TTAB, which is positively charged and not pH dependent. Therefore the microemulsion remains weakly charged, even at high pH values. To examine the pH dependent behavior of polyacrylate/microemulsion complexes, ME50-NaPA60 samples were prepared as usual at a 100 mM surfactant concentration. NaPA was added in different amounts to obtain different samples, first the pure microemulsion at  $z = 0.0$ , one sample at  $z = 0.1$  in the microemulsion excess part of the phase diagram and one at  $z = 0.7$ , at polyelectrolyte excess where large cylindrical aggregates are present. The pH of the samples was then adjusted by adding small amounts of 1 M HCl under stirring. The visual appearance of the samples was followed carefully during the HCl addition, at points where a change of the visual appearance occurred in the sample, probes of ca. 1 mL were taken from the batch for later analysis. The colored lines in Fig. 37 indicate the approximate pH values where probes were taken. This procedure bears the disadvantage that the system is more and more diluted, the lower the pH values get. To minimize this effect, a concentrated HCl solution of 1 M was used to add as little extra volume as possible. In total not more than 400  $\mu\text{L}$  were added to a sample of initially 8 mL, which results in a surfactant concentration of 95 mM so the dilution effect should be neglectable.

Fig. 38 shows the measured SANS spectra of the pure microemulsion ME50 at different pH values. As expected, the structure factor becomes more pronounced as the microemulsion droplets get more charged, due to the increased repulsion between the droplets. The charges on the droplet surface increase the interfacial tension, which reduces the stable radius of the droplets and thus the solubilization capacity. At a pH of  $\sim 3$  the microemulsion starts to become unstable. Here, at a microemulsion charge of  $\sim 60\%$ , the solubilization capacity is exceeded and excess decane is released. It is interesting to note that the transition of the microemulsion droplets is rather slow. Initially the sample appeared colorless, after 12 hours the color had changed to blueish and only after 24 hours the sample appeared turbid due to the larger decane droplets present in the sample. a kinetic light scattering study of this phenomenon would be very interesting in the future. SANS was measured one week after sample preparation. An increase of the intensity

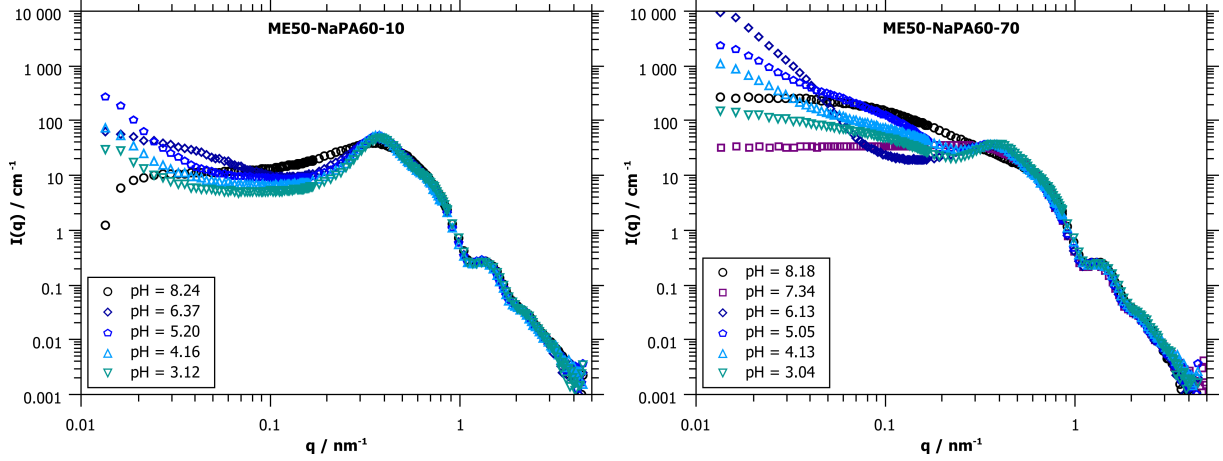


**Figure 39:** SANS data of the two ME50-NaPA60 samples, A) in microemulsion excess ( $z = 0.1$ ) and B) in polyelectrolyte excess ( $z = 0.7$ ), at different pH values.

at low  $q$  can be seen in the scattering data, indicating larger decane droplets. Since the pure microemulsion initially still appeared clear, the pH was decreased further. The experiment was stopped at  $\text{pH} = 1.98$ , even though the sample was still clear and colorless. After 12 hours the microemulsion at  $\text{pH} = 1.98$  had turned white and turbid, as bigger excess decane droplets had formed. This experiment shows, that the microemulsion remains unchanged until a  $\text{pH} > 3$ , so the pH in the system can be varied until this point without altering the carriers. Below  $\text{pH} = 3$ , the microemulsion starts to become instable but the release of decane is kinetically hindered and occurs faster the lower the pH is. To obtain a number of charges per droplet for each pH value, this SANS data should be fitted with a Baba-Ahmed structure factor in the future.

Fig. 39 shows the measured SANS spectra of the two complexed samples. The first spectra (black circles) in both graphs corresponds to the initial stock solutions without any added HCl. At this point the TDMAO is not charged so only the 5 % added TTAB is responsible for the microemulsion charge. The NaPA polyelectrolyte is about 95 % charged. The visual appearance of these samples is clear and colorless or slightly blueish for the  $z = 0.1$  and  $z = 0.7$  sample respectively. The scattering curves for these kinds of samples were analyzed before.<sup>[73]</sup> At low  $z$  ratios the amount of added polyelectrolyte is too little to have an effect on the droplet arrangement, the scattering curve looks like that of the pure microemulsion. At higher  $z$  ratios, especially at  $z = 0.7$  (polyelectrolyte excess and close to the phase boundary), elongated structures are observed as can be seen from the  $q^{-1}$  slope in the scattering data.

When decreasing the pH, the appearance of the  $z = 0.7$  sample very quickly changes from clear to turbid. Shortly after, a white precipitate is observed in the still turbid sample. The microemulsion excess sample at  $z = 0.1$  stays clear for a little longer when decreasing the pH before, also here, small white precipitates are observed in an otherwise colorless liquid. At a pH of  $\sim 6.1 - 6.4$  the droplet charge has increased a little to 10 % while the NaPA charge has decreased much more to about 60 % (see Fig. 37). A clear structure peak can be observed in the scattering data of both samples at this pH. This peak results from the increasingly charged microemulsion droplets that repel each other. In addition, both samples also show larger aggregation, which

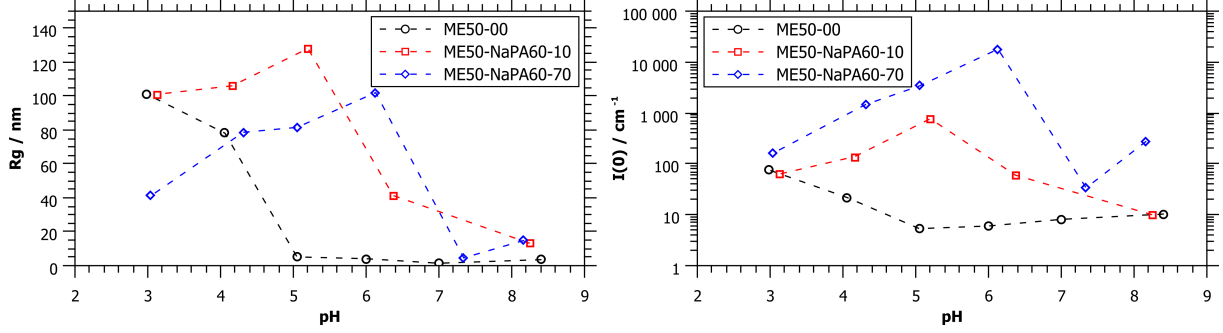


**Figure 40:** A)  $R_g$  and B)  $I(0)$  values obtained from Guinier fit to SANS data of pure microemulsion droplets and two complexes at different pH. The  $I(0)$  value is proportional to the  $M_w$  of the formed structures.

can be seen from the increase in scattering intensity at low  $q$ . The  $z = 0.1$  sample did not show any aggregation at higher pH, but now aggregates of about 40 nm ( $R_g$ , obtained by Guinier fit) are present. In contrast, the elongated complexes that were present in the  $z = 0.7$  sample at higher pH have now changed into large clusters with  $R_g \sim 100$  nm, see Fig. 40.

When the pH is decreased to about 5.1 - 5.2, the microemulsion droplet surface is about 25 % charged, while the NaPA charge has decreased to  $\sim 35$  %. Visually, both samples look similar to before but the amount of solid particles floating around has started to decrease in both samples. The increased charge density of the microemulsion can be seen in the structure factor peak appearing more pronounced, both in the microemulsion excess, as well as in the polyelectrolyte excess sample. Interestingly the size of the large clusters formed in both samples is starting to decrease again as it can be seen from the scattering intensities at low  $q$  and the  $R_g$  values.

This trend continues when the pH is decreased even further to about 4.1 - 4.2 where the droplets start to be highly charged and the remaining charge of the polyelectrolyte is decreased to only 10 %. At this pH, the  $z = 0.7$  sample has changed the color of its liquid phase back to clear and slightly blueish with little of the white precipitate still being present. The precipitates in the  $z = 0.1$  sample have been completely dissolved again. The neutron scattering curves show a pronounced structure factor peak and a further decrease in the size of the large clusters. The final probe was taken at a pH close to 3, where the polyelectrolyte is basically not charged anymore. Here, both samples appear clear and colorless with only very few solid white crumbs remaining in the  $z = 0.7$  sample. The scattering data shows, that some larger clusters are still present but they have decreased in size a lot, compared to the largest clusters found at pH values of 5 - 6.

It should be mentioned here, that all measured neutron scattering curves shown in Fig. 38 and 39 show the same scattering behavior at high  $q$ . The form factor minimum is clearly visible and appears at the same  $q$  value and of same intensity for all measured pH values. A zoom into the form factor region of the ME50 sample is exemplarily shown in Fig. 38. This shows, that the microemulsion droplets itself are not affected by the change of pH. Even though the charge on the droplet surface is changing quite significantly, the droplets remain their shape, size and, most importantly, concentration. The white precipitates observed must therefore mostly be comprised of polymer with little surfactant only, so the overall concentration is not noticeably

affected. Since the droplets retain their size, they would be available as delivery vessels. The pH dependent formation of large clusters and later release of free droplets (schematically depicted in Fig. 43) could be a very interesting starting point for stimuli responsive drug delivery systems.

### 6.2.2 pH Variation, Starting with an Uncharged Microemulsion

Another experiment was carried out with an uncharged microemulsion. The microemulsion was prepared with only TDMAO as surfactant and no added TTAB, since the charge will be induced by lowering the pH, no 'additional' permanent charge is necessary. To also avoid dilution effects on the droplets, the ME00 system without hexanol was chosen. The microemulsion was prepared at 100 mM surfactant concentration. Since the microemulsion in this case is not charged at neutral pH, no charge ratio  $z$  can be calculated. NaPA60 was added in an amount that would correspond to  $z = 0.5$  if the normal 5 % TTAB containing microemulsion was used.

Since the microemulsion is not charged, no initial interaction with the polyelectrolyte is expected. This is also confirmed by SANS measurements of the initial sample (black circles in Fig. 41), where a plateau of non-interacting (neither repelling nor attractive) spheres can be seen. Reducing the pH from  $\sim 9$  to  $\sim 8$  is slightly reducing the NaPA charge but the TDMAO remains still uncharged. It is therefore not surprising that no change in the SANS data can be observed. An interesting feature can be seen when the pH is reduced to 7, at this point the microemulsion droplets start to become slightly charged which promptly results in an increase of scattering intensity showing the formation of clusters. Upon further addition of HCl the sample quickly turns white, and starting from a pH of 6.5 big white lumps of precipitate are visible, see photo in Fig. 41. SANS was measured from the liquid phase of a precipitated sample at pH = 5.86 and the scattering data shows surprisingly, that all material in the sample has precipitated and no microemulsion droplets are left in the liquid phase (blue diamonds in Fig. 41). This behavior is very different to the previously studied system where bigger microemulsion droplets with 5 % TTAB were studied.

Nevertheless, the pH was decreased further and at a pH of  $\sim 5$  it was noticed, that the big white precipitates were dissolving again. It was also noticed, that the sample started to foam again, which indicates the resolubilization of surfactant. A SANS measurement at pH = 4.91 shows the form factor minimum of microemulsion droplets again at a very similar  $q$  value as before, only the overall intensity indicates, that not all material was dissolved again. At pH = 2.93 it can be seen from the scattering, that almost all material was redissolved. The strong increase of scattering intensity at small  $q$  indicates excess decane, which is not solubilized and therefore forms larger droplets. Finally at pH 2.63 no precipitates can be observed anymore and the scattering shows microemulsion droplets of almost identical size to pH 8 (green triangles in Fig. 41).

This experiment is particularly interesting as it shows the possibility of precipitating all material and even breaking up the microemulsion droplets in a reversible process. Once the TDMAO becomes charged, it starts interacting with the oppositely charged poly acrylate. While the microemulsion droplets are still weakly charged larger structures can be observed, similar to those

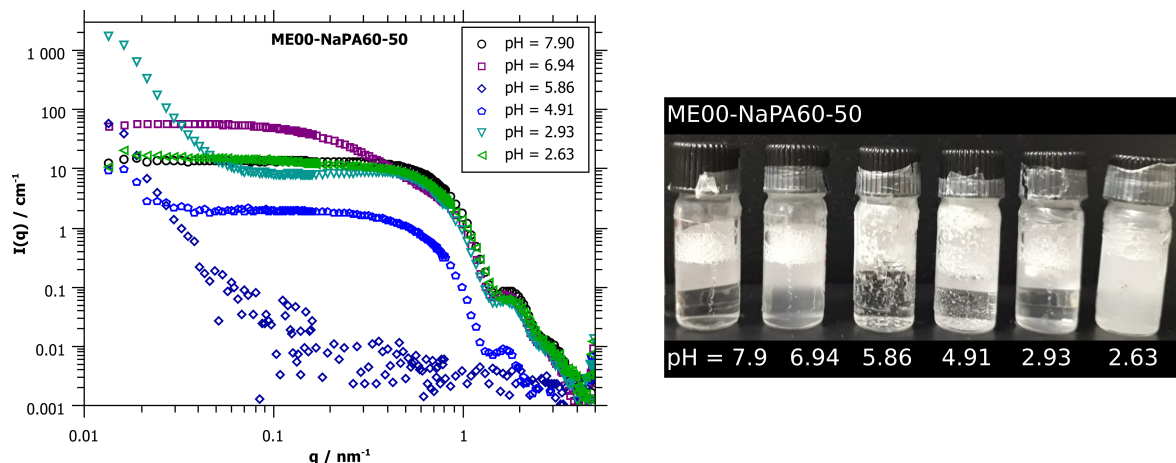


**Figure 41:** A) Neutron scattering data of an uncharged microemulsion ME00 mixed with NaPA60 at different pH. B) Photo of the samples at different pH showing the precipitation at pH = 5.86 and the clear sample at pH = 2.93.

previously found for PEMECs at polyelectrolyte excess. The precipitation at higher microemulsion surface charge densities can be explained by the formation of TDMAO/NaPA complexes that are neutral on the outside and therefore precipitating while the released decane is forming larger oil droplets that are responsible for the white appearance of the sample. At very low pH values the polyelectrolyte becomes very weakly charged and thus the interactions in the TDMAO/NaPA complexes are also weakened. Unbound TDMAO can redissolve decane and form microemulsion droplets again. At this moment it is still unclear why the pH behavior of TDMAO/TTAB/hexanol/decane/ $\text{D}_2\text{O}$  and TDMAO/decane/ $\text{D}_2\text{O}$  microemulsions is so fundamentally different. Further experiments are necessary to investigate the exact role of TTAB and hexanol and fully understand this system.

### 6.2.3 Variation of pH in Hyaluronate/Microemulsion Systems

Since the first experiments of NaPA/microemulsion complexes at different pH resulted in very promising results, it would be interesting to also apply the concept to NaHA/microemulsion complexes. First tests were carried out with this system, but a detailed study should follow in the future.

In a first experiment the NaHA/microemulsion complexes were prepared as usual and the pH was stepwise decreased by addition of 0.1 M HCl, similar to the experiments conducted with NaPA and described above. This was done for ME50-NaHA186 samples with charge ratios of  $z = 0.7$ , 0.8 and 0.9. Visual inspection of the samples showed, that already very small amounts of added HCl lead to turbid samples. The precipitates in these NaHA samples are not finely dispersed like it was found for NaPA but congregate into one big, gelly lump. This makes adjusting the pH more difficult since inside the gelly precipitate the pH will only change very slowly. For the  $z = 0.7$  sample, it was found that this gelly precipitate dissolves again at low pH-values but an optically clear sample is only recovered after 24 hours.

In order to make this experiment more reproducible, different mol equivalent of HCl to the

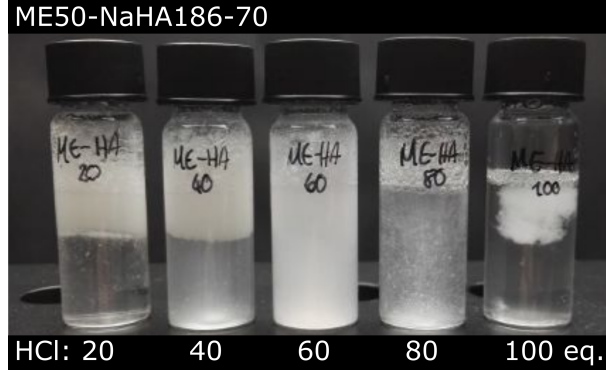


**Figure 42:** Photo of ME50-NaHA186 complexes at a charge ratio of  $z = 0.7$  with different TDMAO equivalent of HCl added.

TDMAO contained in the microemulsion (0, 20, 40, 60, 80 and 100 eq.) were added during the sample preparation. With this method, the total microemulsion concentration is kept constant at 100 mM surfactant. This was done for charge ratios of  $z = 0.0, 0.1$  and  $0.7$ . pH measurements showed, that fully protonated microemulsions (100 eq. HCl added) reach pH values of 1.9 to 2.3, depending on the NaHA186 concentration. The pure ME50 samples stayed optically clear for all eq. HCl, the microemulsion excess sample at  $z = 0.1$  showed very small precipitates at 20, 80 and 100 eq. HCl but the biggest effect was seen for the polyelectrolyte excess sample at  $z = 0.7$ , where precipitation was observed for all eq. of added HCl (see Fig. 42). Light scattering was measured for all samples (the liquid phase was measured for precipitated samples) but the interpretation is very difficult due to the highly interacting components, unknown concentration in precipitated samples and limited  $q$  range.

These first experiments show, that the interactions between NaHA and ME50 are highly pH dependent, just as the previously observed NaPA/ME complexes, but the details of the formed aggregates appear to be very different. In order to study the pH dependent behavior comprehensively, it is necessary to first choose a uniform protocol for sample preparation to ensure reproducibility. SANS measurements of the liquid phases at different pH are necessary to obtain information about whether the microemulsion droplets are retained in solution or precipitated in the gelly aggregates, as light scattering is not able to yield this kind of information.

### 6.3 Conclusion

By decreasing the pH, the TDMAO of the microemulsion and the carboxylate groups of the polyelectrolytes (NaPA and NaHA) become protonated. The zwitterionic TDMAO becomes charged by the protonation, while the charges of the polyelectrolytes are reduced. The simultaneous variation of both components allows to influence the strength of binding and with this the structures of the formed complexes significantly.

Three different systems were investigated that react very differently to changes in pH. First, the standard system used in this work consisting of medium sized microemulsion droplets (ME50,  $R \sim 4$  nm, containing 50 mM hexanol and 5 % TTAB) with NaPA60 was employed. Two

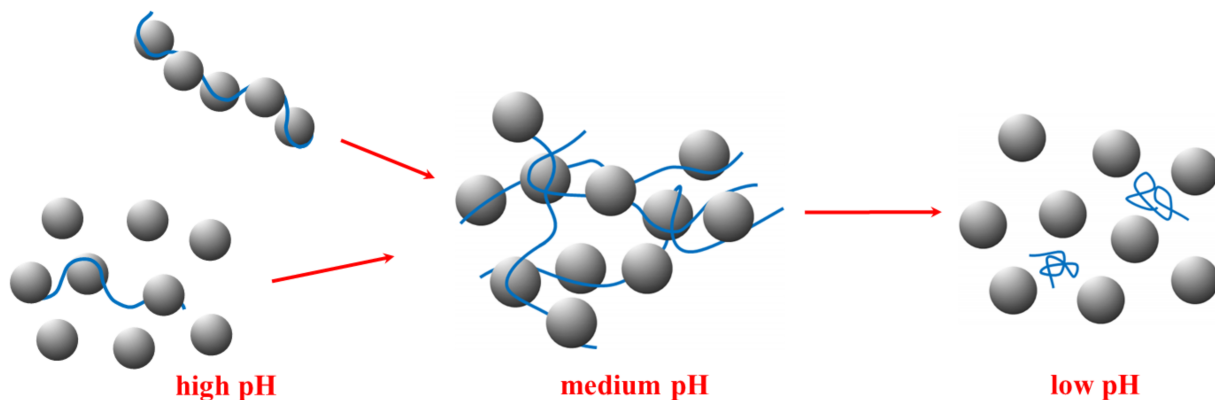


**Figure 43:** Sketch of assumed droplet complexation in polyelectrolyte/microemulsion samples at different pH values.

samples at different  $z$  ratios were prepared and the effect of pH was followed by visual inspection and SANS measurements. In this system it is possible to first bind microemulsion droplets into large clusters and later release them again as a function of pH (Fig. 43). The droplets retain their size and shape and would therefore be available as delivery vessels. This principle is highly interesting for potential drug delivery purposes. The microemulsion droplets are stable above a pH of 3.

The second system investigated consisted of uncharged small microemulsion droplets (ME00,  $R \sim 3$  nm, no hexanol, no TTAB) mixed with NaPA60. This microemulsion only becomes charged at lower pH values when the TDMAO becomes protonated. No hexanol was added to avoid dilution effects. Even though the changes to the previous system were thought to be small, a surprisingly different behavior was observed. At a pH close to 6 all material in the sample was precipitated but surprisingly, new microemulsion droplets were formed again when the pH was lowered further. Here, further experiments are necessary to investigate the exact role of TTAB and hexanol and to fully understand this system.

Finally, in a third experiment NaHA was employed as polyelectrolyte instead of NaPA. The microemulsion used was the standard ME50 microemulsion with 5 % TTAB and 50 mM hexanol. Surprisingly the two polyelectrolytes were found to behave quite differently. NaHA/ME complexes form a gelly phase when the pH is decreased, that is not dissolving again, even at very low pH values. This behavior is not suitable for delivery systems but might find potential interest in decontamination applications where pollutants can be trapped in the microemulsion droplets, which are then gelled and easily removed from the liquid phase.

## 7 Formation of Larger Clusters with Hydrophobically Modified Polyelectrolytes

### 7.1 Introduction

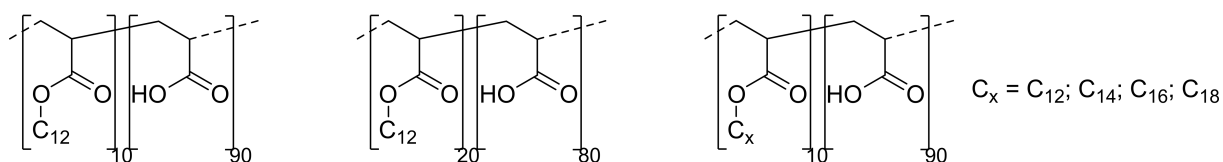
For drug delivery purposes high loading capacities within one aggregate are desirable. Among other approaches, this could be realized by a close packing of many microemulsion droplets within the core of a large core-shell structure, where the shell is formed by a hydrophilic polymer that stabilizes the core. Similar aggregates were already found in several polyelectrolyte/surfactant systems<sup>[119,120]</sup> and seem very promising for applications as delivery systems. If a dense packing of micelles is possible, this concept should also be applicable to microemulsion droplets, which are larger than micelles but otherwise very similar and would provide even higher loading capacities. Since the complex formation in the PEMEC system studied here was, until now, limited to electrostatic interactions, we now want to explore further possibilities for structural control, arising from introducing additional hydrophobic interactions. Since microemulsions naturally combine hydrophobic and hydrophilic domains, it was assumed, that hydrophobically modified polyelectrolytes (HM-PE) are a good way to induce the formation of large clusters with densely packed droplets. The hydrophobic side chains of these polymers would be located in the oily cores of the microemulsion droplets while the charged hydrophilic parts would be used for stabilization. A number of different polymers, all synthesized in our lab, were employed to achieve this kind of complexation. All structures are depicted in Fig. 44.

### 7.2 Results

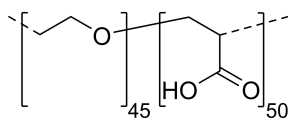
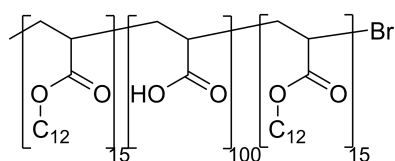
#### 7.2.1 Statistically C12-modified PAA

First experiments were conducted with hydrophobically modified polyacrylic acid (HM-PAA). Those polymers were synthesized by Sven Riemer in our lab<sup>[121]</sup> and consist of an acrylic acid backbone ( $\sim 100$  monomer units) where 10 or 20 mol% were substituted by n-dodecyl ( $C_{12}$ ) chains. The polymers were synthesized via controlled radical polymerization with statistically

Monomers statistically distributed:



Block-Copolymers:



Reference: NaPA15

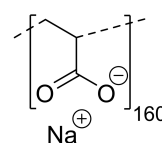


**Figure 44:** Structures of all different modified polyacrylates used in this chapter.

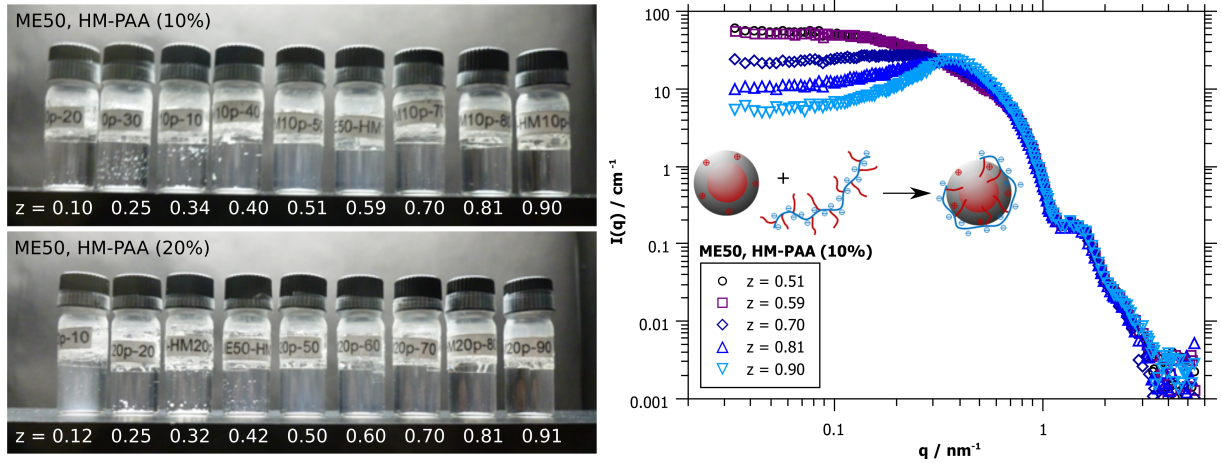


**Figure 45:** A) Photos of samples prepared with 10 and 20 % HM-PAA at different  $z$  ratios and B) SANS data of HM-PAA/ME complexes formed with 10 %  $C_{12}$ -modified PAA.

incorporated  $C_{12}$  side chains. To obtain the sodium salt of the polyacrylate, a stoichiometric amount of NaOH was added to the  $C_{12}$ -PAA stock solutions. Since this HM-PAA shows a pronounced aggregation behavior in aqueous solution by itself, it was expected to also strongly interact with microemulsion droplets, and, for appropriate conditions induce a dense packing of droplets within a complex aggregate. The microemulsion used in this experiments was ME50, containing medium sized droplets of ca. 4 nm radius and 5 % of the total surfactant was substituted by the charged surfactant TTAB. Just like in the previous chapters, samples were prepared at a constant microemulsion concentration of 100 mM surfactant with different amounts of added polyelectrolyte. The mixing ratio  $z$  was characterized as before by the number of charges, without taking into account the hydrophobic modification.

The formed complexes were analyzed by visual inspection, light scattering (DLS and SLS) as well as small-angle neutron scattering (SANS) measurements. Fig. 45A shows photos of medium sized microemulsion droplets with 5 % TTAB (ME50) mixed with 10 and 20 %  $C_{12}$ -modified HM-PAA in different charge ratios. In the photos, it can be seen, that not all mixed samples are stable. Samples at small  $z$ -values (e.g. at microemulsion charge excess) show a macroscopic phase separation into a clear liquid phase and a white solid powder. Monophasic samples close to the phase boundary show a slightly blueish color. SANS measurements were taken of stable monophasic samples only. The SANS data in Fig. 45B shows that the slightly blueish samples close to the phase boundary contain PE/ME aggregates but the size is not very large (compare  $I(0)$  of  $\sim 60 \text{ cm}^{-1}$  in both cases shown here to  $I(0)$  values of up to  $100 \text{ cm}^{-1}$  for ME50-NaPA15 samples). Surprisingly, higher mixing ratios show a decrease in the scattering intensity at low  $q$  until the scattering curve resembles very much the scattering of the pure repulsive microemulsion droplets. This is different to the previously analyzed NaPA/ME complexes where higher charge ratios  $z$  always lead to screened (non-interacting) droplets. The pure microemulsion droplets are positively charged. When HM-PAA is added the hydrophobic side chains arrange in the microemulsion core, leaving the negatively charged backbone wrapped around the droplet. Due to the short length of the HM-PAA (100 units  $\sim 25 \text{ nm}$ ) one chain can only wrap around one

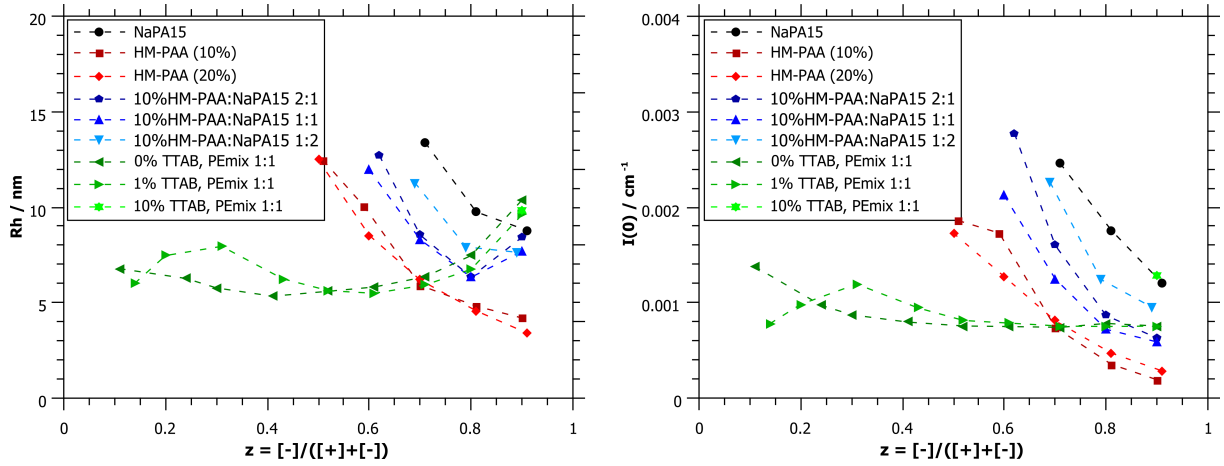


**Figure 46:** A) Hydrodynamic radii obtained from DLS measurements and B) extrapolated forward scattering intensity  $I(0)$  obtained from SLS measurements of PEMECs with differently modified HM-PAA, NaPA15 as a reference and different mixtures of 10 % HM-PAA and NaPA15. If not indicated otherwise, the microemulsion contained 5 % of TTAB.

droplets leading to a high overcompensation of the droplet charge. The structure factor at higher charge ratios is reappearing due to the repulsion of separate now negatively charged droplets, see sketch in Fig. 45B. To confirm this charge reversal, zeta potential measurements would be very useful.

The SANS data of samples with 20 % modified HM-PAA looks very similar to the data shown in Fig. 45B and is therefore not shown here. Apparently the degree of modification does not have an influence on the formed structures. The light scattering data (shown in Fig. 46) is confirming these results.

More experiments were carried out with mixtures of 10 % C<sub>12</sub>-HM-PAA and the slightly longer NaPA15, which was added in order to retain the colloidal stability of the complexes by providing electrostatic repulsion. Three mixtures of HM-PAA:NaPA15 in ratios of 1:1, 1:2 and 2:1 were employed that did not show a significantly different effect in mixtures with microemulsion droplets, see Fig. 46 for light scattering results. Not surprisingly, it can be concluded, that the higher the amount of added NaPA15, the closer is the sample behavior to that of samples with pure NaPA15, hence the larger are the formed aggregates. In these series it seems like the HM-PAA is not interacting with the microemulsion droplets at all.

Finally, also the effect of microemulsion charge was examined by varying the amount of TTAB in the microemulsion and thereby the charge density of the droplet surface. Additionally to the 5 % TTAB microemulsion that was already employed above, three more microemulsions, all medium sized with 50 mM hexanol, with 0, 1 and 10 % TTAB were prepared and mixed with the 1:1 HM-PAA:NaPA15 mixture in different charge ratios. Already from the visual inspection, it becomes clear, that the lower the amount of TTAB, the more stable samples are formed. For the series with the uncharged microemulsion (0 % TTAB), no phase separation is observed at all. This is most likely due to no interaction between microemulsion droplets and polyelectrolytes, as can be seen by the unchanged forward scattering intensity of the light scattering data (see Fig. 46B). While it seems obvious that no interaction can be observed of uncharged droplets in

mixtures with charged polyacrylic acid, it is surprising that the HM-PAA is apparently also not interacting with the hydrophobic cores of the microemulsion droplets. Mixtures with 1, 5 and 10 % microemulsion charge show increasingly more interaction, that can be seen both, in the instability of the samples (phase separation) and the change of scattering intensity in the SLS data. For the 10 % charged microemulsion, only one sample at  $z = 0.9$  is still stable.

Comparing again the scattering curves of samples formed with microemulsion droplets with different charge densities mixed with a HM-PAA:NaPA15 mixture, it becomes obvious, that the droplets and polyelectrolytes seem to only interact via electrostatic interaction. The higher the charge of the microemulsion, the more complexation is observed. Or, in other words, if the microemulsion is not charged, no interaction can be observed at all. The driving force of the complexation is not depending on the amount of added hydrophobically modified polyelectrolyte but only on the charges present in the system. The lack of hydrophobic interaction could be due to two reasons. First, the employed polyelectrolytes were rather short, only about 100 monomers, which would result in a lengths of the stretched polyelectrolyte of only  $\sim 30$  nm. Considering the droplet diameter of  $\sim 8$  nm, there might simply not be enough space to link many droplets. And second, the hydrophobic side chain is also rather short. It contains 12 C atoms and is therefore still quite hydrophilic. Apparently the driving force of the hydrophobic effect is not strong enough here to induce aggregation. Since it is technically quite difficult to synthesize well-defined longer polyelectrolyte chains by radical polymerization, we employed longer side chains with up to 18 C atoms in the next step.

### **7.2.2 Hydrocarbon-modified PAA with Longer Side Chains and Hydrophobically Modified Blockcopolymer**

Since the experiments with  $C_{12}$  HM-PAA did not yield the expected outcome, we also employed HM-PAA with longer side chains. In a second experiment we used polymers with dodecyl to octadecyl side chains where the PAA backbone was always 10 % modified and the modification statistically distributed. All HM-PAAs were synthesized in our lab by Sven Riemer.<sup>[122]</sup> It was expected that the longer hydrocarbon side chains are more hydrophobic than the previously used  $C_{12}$  chains and therefore show a stronger tendency to be incorporated into the hydrophobic cores of the microemulsion droplets, which would lead to a stronger aggregation behavior. Additionally, a triblock-HM-PAA with one PAA block in the middle (100 monomer units) and two  $C_{12}$  modified blocks on both sides (15 monomer units each) was synthesized by Michaela Dzionara and also employed in mixtures with microemulsion droplets. Because of the two hydrophobically modified blocks within one polymer we hoped to be able to link more droplets and thereby form larger aggregates. Like in the experiments described above, stoichiometric amounts of NaOH were added to the polymer stock solutions before they were mixed with the microemulsion to ensure fully charged polymer backbones. The microemulsion concentration was kept constant at 100 mM surfactant in all mixtures and the charge ratio  $z$  was calculated as before from positive microemulsion charges and negative polyelectrolyte charges without taking the hydrophobic side

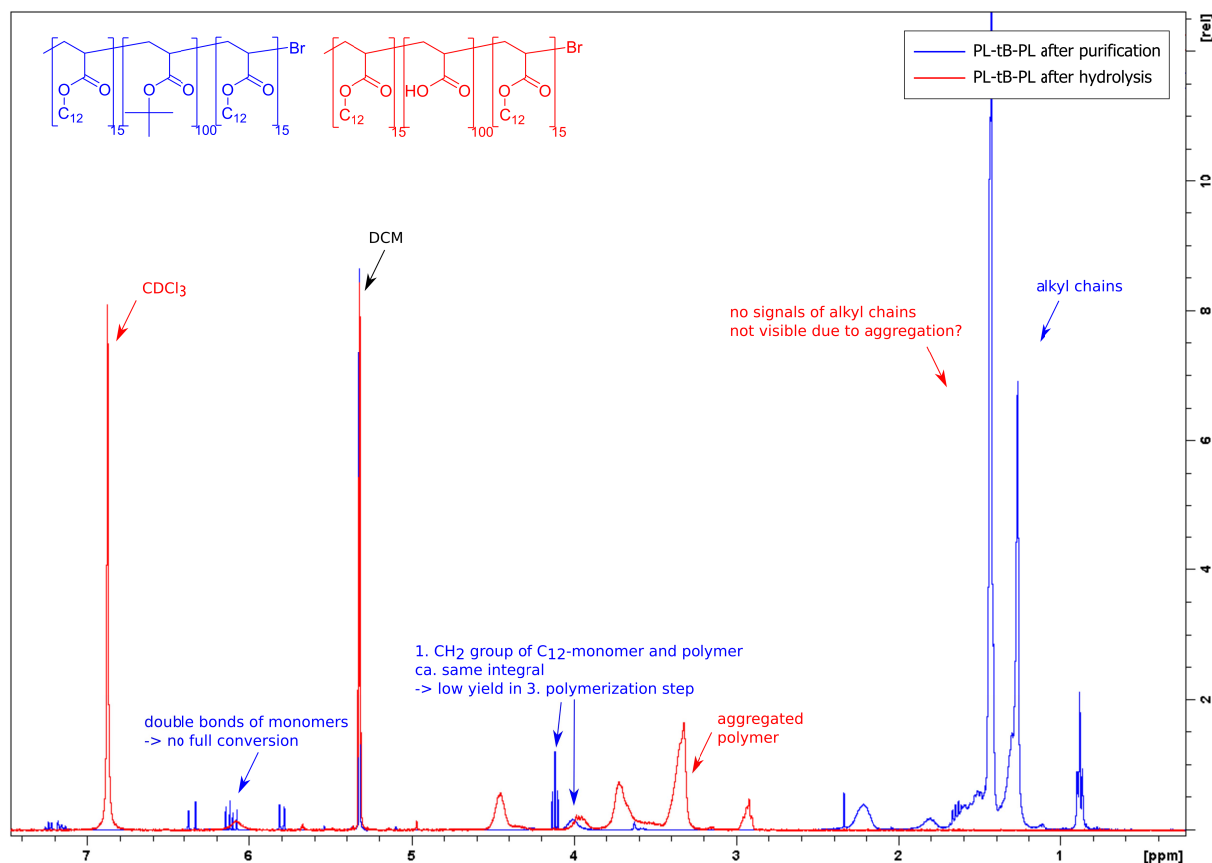


**Figure 47:**  $^1\text{H}$ -NMR spectra of triblockcopolymer after purification (blue) and after hydrolysis to remove the tert-butyl protective groups (red) in DCM as solvent.

chains into account.

While the the HM-PAA with different side chain modifications were already studied in detail,<sup>[122]</sup> the block-HM-PAA is a new type of polymer with no preceding characterization that was synthesized especially for this work. Fig. 47 shows two  $^1\text{H}$ -NMR spectra of the synthesized block-copolymer. The blue spectrum was taken after the three polymerization steps (for the three blocks) were completed. From the aryl-signals appearing at shifts between 5.5 and 6.5 ppm it can be seen, that the polymerization was not complete and double-bound containing monomer is still present in the reaction mixture. At a shift of  $\sim 4$  ppm, the signal of the first  $\text{CH}_2$  group of the  $\text{C}_{12}$  chain can be seen. This signal appears as a clear triplet for the monomer and a broader bump for the polymer. The integrals of these two signal have almost the same value, suggesting that the third polymerization step, the radical polymerization of the second  $\text{C}_{12}$ -modified block did not work or at least only with a very low yield. If this assumption was true, a diblockcopolymer would be present here instead of a triblock. The second NMR spectrum (in red) was taken after hydrolysis to remove the tert-butyl protection groups form the acrylic acid. This spectra shows many broad bands that can not be assigned to specific H atoms of the polymer. Due to interactions and coupling within the polymer, it is not surprising to find broadened peaks here. However the large shifts of peaks to 3 - 4.5 ppm and the absence of the classical alkyl signals at lower shifts are unexpected. This can only be explained by the pronounced aggregation

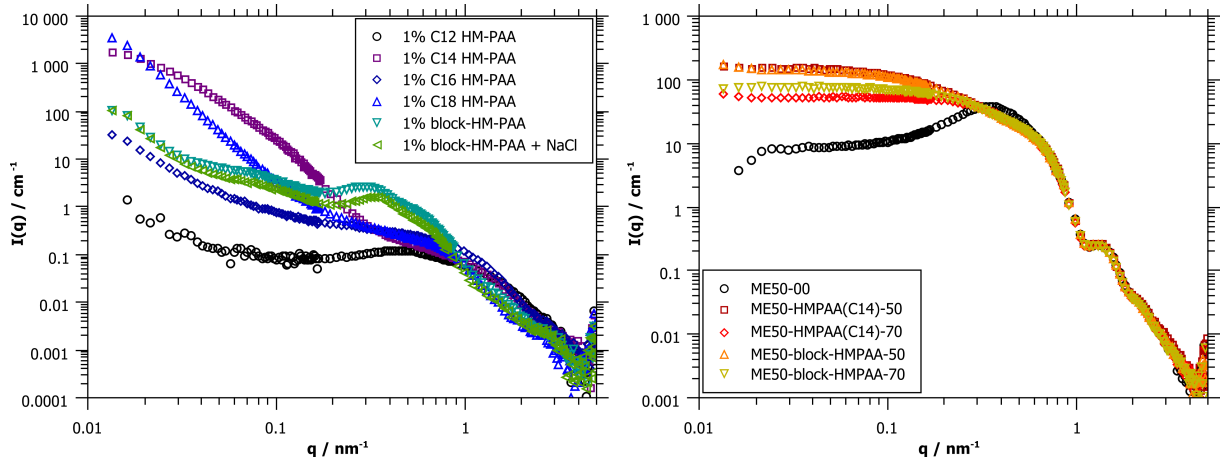


**Figure 48:** A) Measured SANS data of 1 wt% HM-PAA solutions. B) Measured SANS data of microemulsion droplets mixed with different HM-PAA in different mixing ratios  $z$ .

behavior of this polymer, resulting in a different chemical surrounding and potentially even a loss in rotational freedom of the side chains. It can therefore be concluded that most likely a diblockcopolymer was synthesized instead of a triblock and the NMR signals of the alkyl chains are shifted due to a pronounced self-aggregation behavior.

Fig. 48 shows selected SANS data of the HM-PAA and the mixed HM-PAA/microemulsion samples. In Fig. 48A the scattering of the pure polyelectrolytes is shown. It can be seen, that already the pure polymers show a pronounced aggregation behavior that depends on the length of the hydrophobic side chain. The study of inter-polymer aggregation is not the focus of this work and was already done thoroughly for the statistical  $C_x$  HM-PAA.<sup>[122]</sup> But also the block-HM-PAA shows a very interesting self-aggregation behavior, judging from these first scattering curves this would be interesting enough for a separate study. For example, it would be interesting to study the aggregation dependence on the relative block lengths, the chain lengths of the hydrophobic modification, the total concentration and, since PAA is pH dependent, the dependence on the degree of protonation.

Fig. 48B shows selected spectra of HM-PAA/microemulsion complexes in comparison with the pure microemulsion sample. It can be seen that the addition of HM-PAA (both, statistical and block type) induces the formation of larger structures, while retaining the original droplet shape (no change in the form factor minimum can be observed). For a mixing ratio of  $z = 0.5$  a small linear part can be seen at mid  $q$ , whose slope follows a  $q^{-1}$  behavior. This indicates locally rodlike structures as was shown before for NaPA/microemulsion complexes but the extension of the complexes found here is rather short. Simple simulations of a cylinder model show that a cylinder of 30 nm lengths would describe the data best. This is almost the exact length of a stretched PAA chain with a degree of polymerization of 100, which means that droplets interact with HM-PAA chains but only with one single chain at a time. The aggregation number can be obtained by dividing the  $I(0)$  value of the complex by that of one theoretical microemulsion droplet without interactions, namely the form factor fit of a sphere to the form factor minimum,  $N_{agg} = I(0)/I(0)_{th}$ . For both samples depicted here at a mixing ratio of  $z = 0.5$ , the calcu-

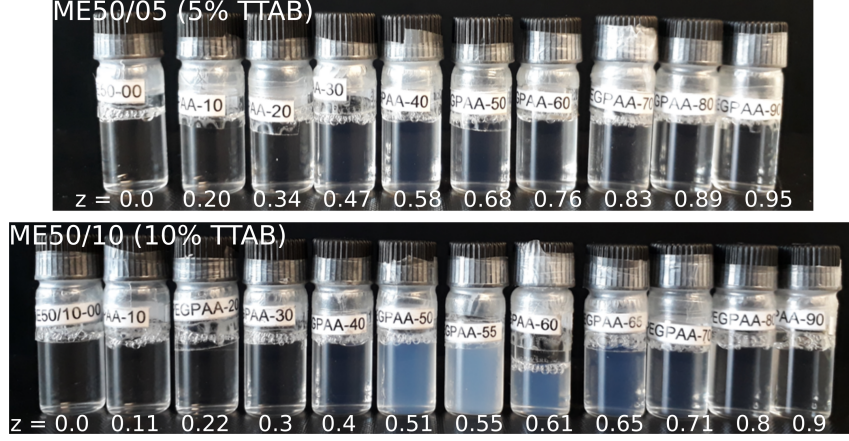


**Figure 49:** Photos of PEG-PAA/ME samples; top) ME50/05, containing 5 % TTAB; bottom) ME50/10, containing 10 % TTAB. According to the color of the samples, large complexes are formed at  $z$  values of 0.50 - 0.65 in the 10 % TTAB containing microemulsion.

lated aggregation number is  $N_{agg} = 3$ , a very small number, when compared to the previously studied NaPA/microemulsion complexes. All samples miss the correlation peak at medium  $q$  that would arise from densely packed droplets, as it was observed in literature before for polyelectrolyte/surfactant complexes with a dense packing of micelles. Additionally, it has to be mentioned that the  $C_{14}$  modified HM-PAA and the  $C_{12}$  modified block-HM-PAA look identical in the scattering data when mixed with microemulsion droplets. This is surprising since the two polymers show a very different aggregation behavior when they are dissolved by themselves. The conclusion drawn from this experiment is similar to that of the previous section. The hydrophobic side chains do apparently not have any influence on the aggregation behavior. They are responsible for the aggregation of the pure polyelectrolyte, but when mixed with microemulsion droplets this driving force for complexation is lost. Since the side chains are quite hydrophobic, their contact area with water should be minimized. It is therefore likely, that the chains do go inside the oily cores of the microemulsion droplets. Most likely, many chains assemble into the core of the same droplet, which explains the absence of large clusters. The charged microemulsion droplets can still interact with the oppositely charged backbone of the PAA by electrostatic interactions but since the PAA chains are rather short, also the formed complexes are small.

### 7.2.3 PEO-PAA Diblockcopolymer

Since the approaches described above did not yield very promising results for the complexation of microemulsion droplets into large clusters with a core of densely packed droplets, a new type of polymer was employed. In a third experiment, we used a diblockcopolymer made of a PEO (45 monomer units) and a PAA (50 monomer units) block. In contrast to the other employed polymers, this polymer is made of two hydrophilic blocks (the PAA block becomes charged and therefore hydrophilic by addition of a stoichiometric amount of NaOH). The charged PAA block can interact with the microemulsion droplets while the PEO block is still water soluble and can stabilize the formed complex. Like the other polymers, also this one was synthesized in our lab

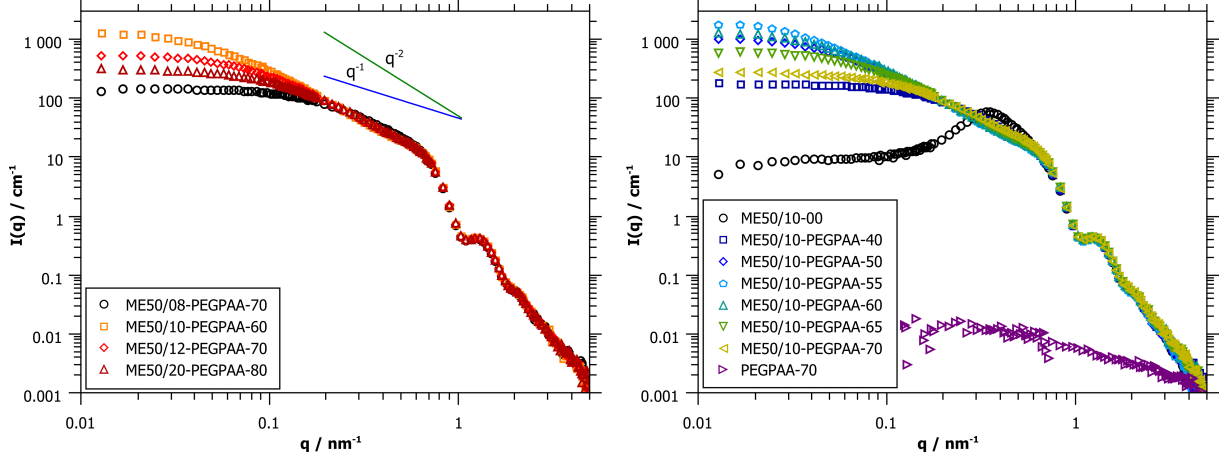


**Figure 50:** A) SANS data of complexes formed with microemulsion droplets with different amounts of added TTAB mixed with PEO-PAA diblockcopolymer and B) microemulsion droplets with 10 % TTAB mixed with PEO-PAA in different charge ratios  $z$ .

by Carolin Ganas.

In a first attempt, the diblockcopolymer was mixed with the standard reference microemulsion droplets (ME50) that contained 5 % TTAB in different charge ratios  $z$ . All of the prepared samples over the whole  $z$  range appeared clear and colorless by visual inspection and also light scattering did not show an indication for larger structures. These findings changed when a microemulsion with 10 % of TTAB was employed. Now samples prepared at medium  $z$  values (from  $z = 0.50$  to  $0.65$ ) clearly showed a blue color, an indication for larger structures (see Fig. 49 for photos). More samples were prepared with 8, 12, 15 and 20 % TTAB in the microemulsion and it quickly became clear that 10 % TTAB seems to be the optimum condition for this system. Samples with higher amounts of TTAB (already at 12 %) quickly turned turbid and phase separated, while samples with lower amounts did not show the typical blueish color.

Light scattering was measured for all stable samples and SANS measurements were carried out for those samples, where large clusters were expected. The SANS data in Fig. 50A shows, that the largest aggregates are formed with the 10 % TTAB containing microemulsion. Fig. 50B compares different charge ratios of the 10 % TTAB microemulsion/PEGPAA mixtures. Here, the largest aggregates are found at a charge ratio of  $z = 0.55$ . The calculation of the aggregation number ( $N_{agg} = I(0)/I(0)_{th}$ ) gives a value of 23 droplets per aggregate. This number is still smaller than values achieved with high  $M_w$  NaPA, but is the highest obtained for blockcopolymers so far. The slope of the scattering intensity at low  $q$  follows a  $q^{-2}$ -law, which can be interpreted as Gaussian clusters of droplets. A correlation peak at mid  $q$  that would indicate the repeat distance of the droplets in a densely packed structure is not visible in this data. However, a small correlation peak becomes visible, when looking at the effective structure factor by dividing the scattering intensity by the form factor of a single microemulsion droplet, see Fig. 51. The peak is small but clearly visible, with a maximum at  $q_{max} \sim 0.77 \text{ nm}^{-1}$ . According to  $d = 2\pi/q_{max}$  this peak corresponds to a distance of 8.16 nm, almost exactly one droplet diameter.

Employing PEO-PAA diblockcopolymers together with the appropriate charge density of the

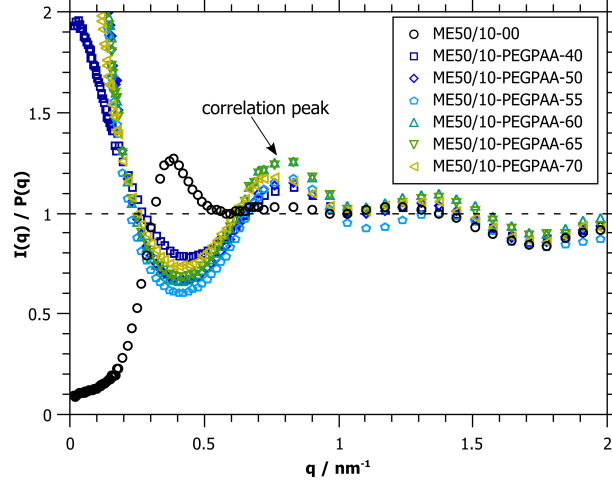


**Figure 51:** Effective structure factor  $S(q) = I(q)/P(q)$  of microemulsion droplets with 10 % TTAB mixed with PEO-PAA in different charge ratios  $z$ , showing a small structure factor peak.

microemulsion droplets can induce the aggregation into clusters with densely packed droplets. More experiments would be needed in order to indicate the right conditions for larger structures, e.g. with a variation of different PEO-PAA blockcopolymers. The PEO-PAA blockcopolymer employed here has rather short degrees of polymerization in both blocks (45 and 50). It can be assumed, that larger PAA blocks would lead to a higher aggregation number of droplets. Additionally, it would be interesting to explore the stabilizing effect of the PEO block that should scale with its length.

### 7.3 Conclusion

Initially it was assumed that hydrophobically modified PAAs would be an ideal polymer to form large clusters with charged microemulsion droplets due to the strong hydrophobic interactions that can be estimated with  $\sim 12$  kT per  $C_{12}$  chain. While the hydrophobic side chains would be located in the oily cores of the microemulsion droplets, thereby linking many droplets together, the charged PAA backbones of the polymers would still provide enough electrostatic repulsion for stabilization. Many differently modified PAAs were employed where the lengths of the hydrophobic modification was varied from  $C_{12}$  to  $C_{18}$ , as well as the amount of modification (10 or 12 %). From the data obtained in this chapter with many different HM-PAAs, it can be concluded that HM-PAAs are not suited to achieve large clusters of densely packed microemulsion droplets. It seems that the hydrophobic interaction is too weak to have an influence on the aggregation behavior and the aggregation is still largely governed by electrostatic interactions. A more promising approach was found in a successive experiment where PEO-PAA diblock-copolymers were employed in mixtures with weakly charged microemulsion droplets. Here, we refrain from hydrophobic interactions to induce complexation but rely again on the electrostatic interactions between PAA and oppositely charged microemulsion droplets, that were proven to show the desired effect before. In addition, a water-soluble PEO block is present in this experi-

ment to provide stabilization. The neutron scattering data showed that rather large complexes with closely packed droplets can be formed here. These diblockcopolymer/microemulsion complexes seem very interesting and promising for further investigations in the future.

## 8 The Reference Polyelectrolyte/Surfactant System

### 8.1 Introduction

In all previous chapters, the interactions of weakly charged microemulsion droplets with oppositely charged polyelectrolytes were studied. To gain more information about the actual role of the microemulsion droplets in such systems it is interesting to also examine a reference system, which is composed of normal surfactant micelles that are not swollen with oil but otherwise identical.

Oppositely charged polyelectrolyte/surfactant complexes (PESC) are already interesting themselves and studied in many publications.<sup>[54,65,114]</sup> Special interest arises from responsiveness to external stimuli such as temperature or pH. In the case present here the charge density of the micelles can be varied by substituting different amounts of the neutral surfactant TDMAO with the cationic TTAB. In combination with the previously studied microemulsion system, the main interest of this chapter lies in the differences of macroscopic phase behavior and formed structures of these two systems. This information can shed light onto the processes taking place when surfactant solutions dissolve pollutants, crude oil or similar hydrophobic substances during complex applications, thereby turning into microemulsions. This is for instance the case in enhanced oil recovery (EOR).<sup>[36]</sup>

### 8.2 Results

#### 8.2.1 Phase Behavior

In a first step, the macroscopic phase behavior of the reference polyelectrolyte/surfactant system was studied. To make the systems comparable, samples were prepared in the same way as the previously studied microemulsion complexes. The surfactant concentration was kept constant at 100 mM while different amounts of NaPA were added to obtain different charge ratios  $z$ . This was done for the 5 mol% TTAB/95 mol% TDMAO mixture without added hexanol (named S00, corresponding to ME00) and different  $M_w$  of NaPA. The phase behavior of the samples was studied and summarized in Fig. 52A. To evaluate the stability of the samples, photos were taken one hour, one day and one week after sample preparation. Just as defined for the microemulsion systems before, samples were labeled instable if phase separation occurred within the first hour after preparation, metastable if the phase separation took place within the first day and stable if the samples were still monophasic after one week. These stable samples did not change their visual appearance for the course of several months. Fig. 52B shows photos of surfactant-complex samples with NaPA60 taken one hour (top) and one week (bottom) after sample preparation. Those pictures show nicely the turbid color of metastable samples after one hour and the formation of solid white precipitates after one week. It can also be seen, that the stable samples did not change their appearance during that time.

On first glance, the phase diagram obtained for NaPA/surfactant mixtures looks similar to those recorded for PEMECs. In both cases phase separation is observed at the microemulsion- (here

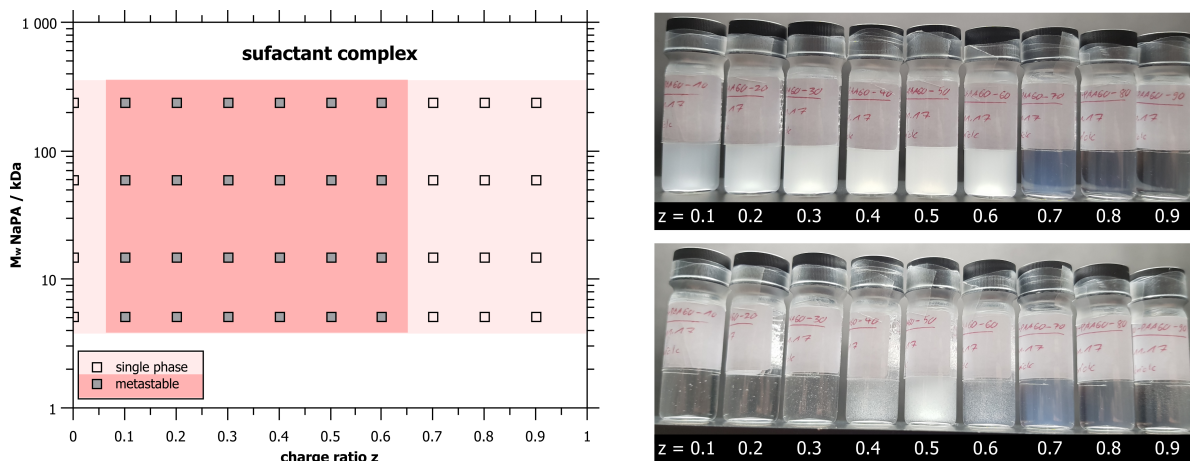


**Figure 52:** A) Phase diagram of TDMAO/TTAB/NaPA complexes. The surfactant mixture contains 95 % TDMAO, 5 % TTAB and no hexanol. B) Photos of sample series with NaPA60 after one hour (top) and after one week (bottom).

surfactant-) excess part of the phase diagram, while long-time stable complexes are formed at polyelectrolyte excess. One pronounced difference is, that the phase behavior of the surfactant system seems to be independent of the  $M_w$  of the polyelectrolyte. Further, the non-stable polyelectrolyte/surfactant complexes are not phase separating right away. After one hour samples at  $z$  ratios of 0.1 - 0.6 showed a turbid-white color but were still monophasic. After one day, a solid white precipitate was visible, that became even more apparent after one week. Samples at  $z = 0.7 - 0.9$  looked completely colorless to slightly blueish for all  $M_w$  directly after sample preparation and did not change their visual appearance over time.

### 8.2.2 Characterization by Light Scattering

DLS and SLS was measured of all stable polyelectrolyte/surfactant samples, the results are shown in Fig 53. These measurements show similar results to the previously observed PEMECs. In general, the formed complexes are largest close to the phase boundary and decrease in size with increasing polyelectrolyte excess. Additionally, they become larger with increasing  $M_w$  of the polyelectrolyte. One surprising result is that the surfactant complexes appear to be significantly larger than the microemulsion complexes, even though the micelles themselves are smaller than microemulsion droplets. In fact, the PEMECs formed with the long NaPA315 that were considered relatively large in previous chapters, show the same scattering intensity as the PESCs formed with the shortest polyacrylate NaPA05, as can be seen from the forward scattering intensities  $I(0)$  shown in Fig. 53A.

DLS measurements were complicated by the fact that bimodal distributions were found for samples with high  $M_w$  polyelectrolytes and at high charge ratios  $z$  (see Fig. 53B). This finding differs from previous DLS results of PEMECs with NaPA that were always monomodal and resembles more the behavior found for NaHA complexes. For microemulsion/NaHA complexes, a bimodal size distribution was found in DLS measurements for high polyelectrolyte excess, but in this case the second, slower mode was attributed to polymer relaxation that becomes visible

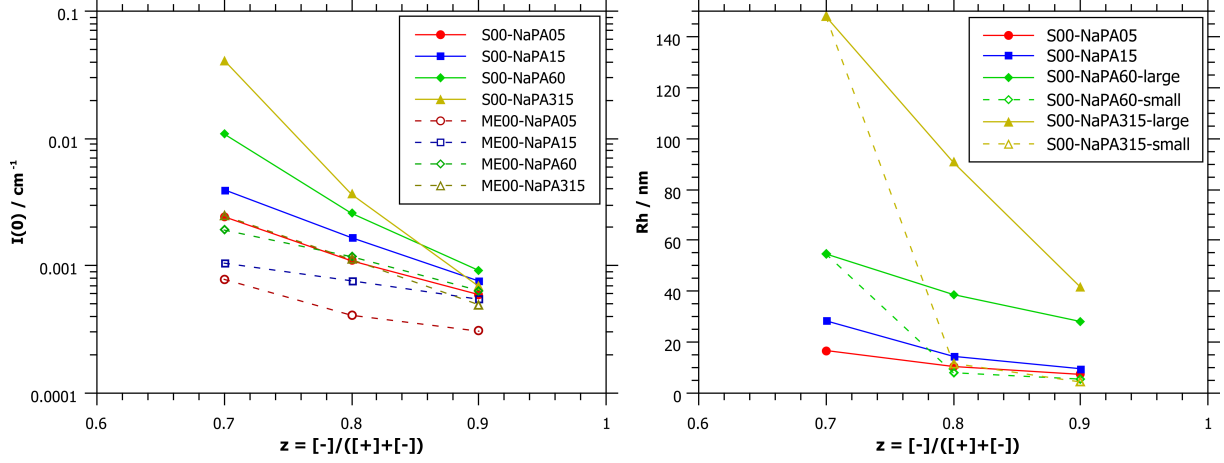


**Figure 53:** A)  $I(0)$  obtained from SLS, filled symbols represent data from polyelectrolyte/surfactant complexes while empty symbols show the corresponding polyelectrolyte/microemulsion complexes. B)  $R_h$  obtained from DLS, for some samples a bimodal distribution was found (dotted lines).

due to the increased amount of NaHA needed to reach the same charge ratio  $z$ , compared to NaPA.<sup>[108]</sup> The increased amount of polymer is no suitable argument in this case as only NaPA was employed in the same amount as for PEMEC samples before. It is possible that the smaller micelles scatter light weaker than the microemulsion droplets and therefore the also weakly scattering polymer modes become visible. This theory can be ruled out by looking at the  $1/\langle\tau\rangle$  vs.  $q^x$  behavior, which does not follow a  $x = 3$  law as observed for NaHA complexes. In this case the normal  $q^2$  dependency of translational diffusion is observed also for the slow mode.

Another theory that the slower mode corresponds to large complexes while the faster one represents free micelles seems unlikely when comparing the bimodal distribution of these PESCes with those observed for NaHA/ME complexes. One notices that the slower mode is rather fast here. In other words, both sizes are so close together that the DLS correlation function can also be mistaken for a very polydisperse monomodal distribution. E.g. the NaPA315 sample at  $z = 0.8$  can be fitted with a monomodal distribution of  $R_h = 39.6$  nm and a PDI of 1.5 or a bimodal distribution of  $R_{h,large} = 90.7$  nm (PDI = 1.2) and  $R_{h,small} = 11.7$  nm (PDI = 1.1), see Fig. 53B. Considering the absolute values of both sizes, the slower mode corresponds to large complexes but the faster one is still too large to represent free micelles. A final statement can not be given at this moment since more dynamic measurements are necessary to evaluate the structural origins of the bimodal distribution.

### 8.2.3 Characterization by SANS

Additionally, SANS was measured for polyelectrolyte/surfactant complexes for different  $z$  ratios with NaPA60 (constant  $M_w$ ) and at different  $M_w$  of NaPA for a constant charge ratio  $z = 0.7$ , the data is shown in Fig. 54A and 55A. Qualitatively the SANS data confirms what was already seen in static light scattering, that the intrinsic behavior of the surfactant complexes is similar to that of the previously studied microemulsion complexes. From the high intensities at low  $q$ ,

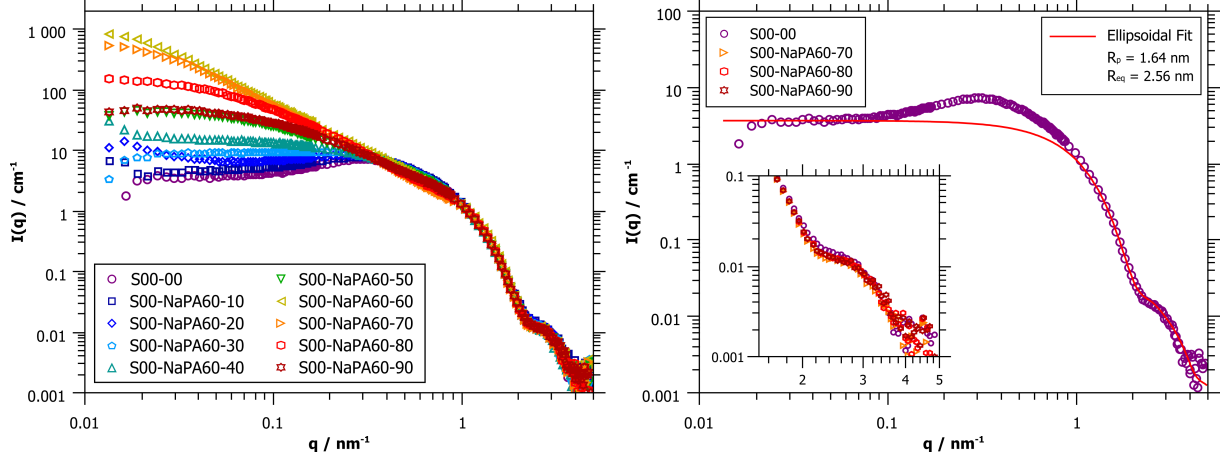


**Figure 54:** A) SANS data of NaPA60/surfactant complexes for different  $z$  ratios. Only the liquid phase was measured for precipitated samples. B) Best fit of ellipsoid model (oblate) to pure surfactant solution S00 and comparison of form factor minimum of pure surfactant and stable complexes.

it can be seen, that very large complexes are formed here. Also here, the largest complexes are found in polyelectrolyte excess close to the phase boundary and for high  $M_w$  of NaPA. The pure micelles can be fitted with an ellipsoidal form factor model as shown in Fig. 54B and it seems that the micelles retain their shape and size when interacting with the polyelectrolyte, just as found for microemulsion droplets. This can be seen from the scattering intensity and the form factor minimum at high  $q$ . The zoom into the form factor minimum (Fig. 54B) shows that the minimum is slightly more pronounced for the complexes than for the pure micelles, but this effect is very small.

The scattering data for the surfactant complex sample prepared at surfactant excess, at  $z = 0.1$ , looks very similar to the scattering of the pure surfactant solution. This finding is also analogous to the microemulsion complexes. Apparently the amount of added polyelectrolyte is simply too little here, to have a visible influence. The scattering of all polyelectrolyte excess samples shows a pronounced increase of intensity at medium to low  $q$ . The linear part in the scattering data is most pronounced for samples at  $z = 0.6$  and  $0.7$  and decreases for higher charge ratios. The effect of the molecular weight (shown in Fig. 55A) is not as marked as it was found for the microemulsion complexes, but also here the linear part is slightly more distinct for higher  $M_w$ . The slope of the scattering intensity at mid  $q$  seems to depend more on the charge ratio than on the  $M_w$ . The highest values found for  $z = 0.7$  samples are close to  $q^{-1.5}$ , so about as high as for the largest microemulsion complexes.

The plateau at low  $q$  can be extrapolated to  $I(0)$  with a Guinier fit to calculate the molecular weight. The aggregation numbers of micelles per complex can be calculated by dividing the molecular weight of one complex by the theoretical molecular weight obtained for non-interacting micelles (from  $I(0)$  of the form factor fit without interactions). The calculated aggregation numbers are shown in Fig. 55B, it can be seen that the numbers obtained are much larger than for PEMECs (compare Fig. 12).

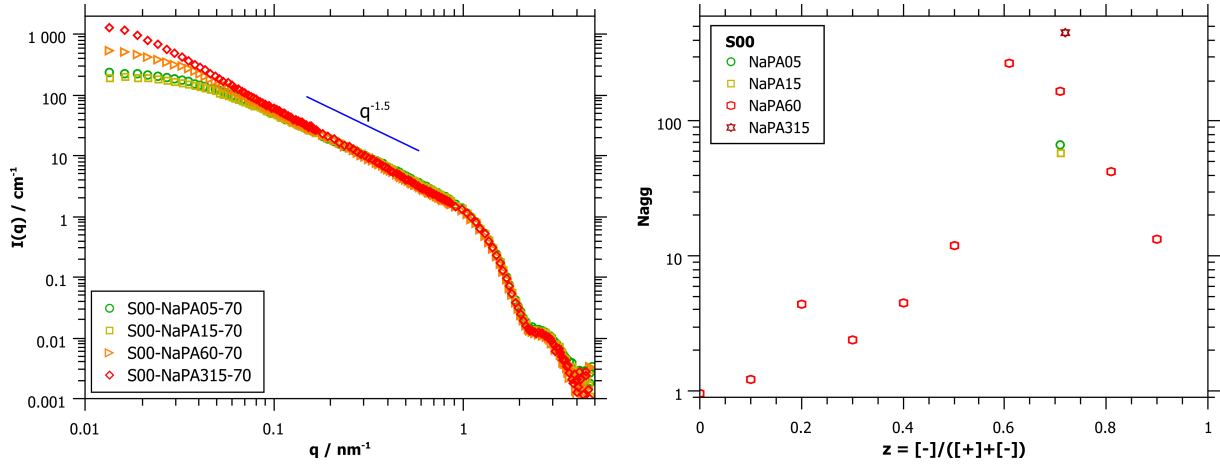


**Figure 55:** A) SANS data of NaPA/surfactant complexes for different  $M_w$  of NaPA at a charge ratio of  $z = 0.7$ . B) Aggregation numbers for PESCs of different charge ratio and  $M_w$  of NaPA. Numbers are much larger than those found for PEMECs.

### 8.3 Conclusion

In this chapter the previously studied polyelectrolyte/microemulsion droplet system was compared to a polyelectrolyte/surfactant reference system. No hexanol or decane were added to the reference system, but otherwise the composition of samples was identical.

The surfactant reference system was studied by visual inspection, static and dynamic light scattering and SANS and it was found that the general behavior is very similar to PEMECs. Both systems exhibit a two-phase region for low and medium  $z$ -values while long-time stable samples are formed in the polyelectrolyte excess part of the phase diagram. The largest complexes are always formed at polyelectrolyte excess close to the phase boundary and larger complexes are formed when higher  $M_w$  NaPA is employed.

When analyzing the behavior in more detail, pronounced differences between the two systems become apparent. E.g. the phase separation for all instable PESC sample does not occur instantly but only after a couple of days as opposed to some PEMEC. Further, the  $M_w$  of polyelectrolyte does not have an effect on the phase boundary of surfactant complexes. A surprising result is that the surfactant complexes are much larger than the complexes with microemulsion droplets even though the microemulsion droplets itself are bigger than micelles. Therefore more micelles are aggregated in one polyelectrolyte/surfactant complex than microemulsion droplets in one complex as can also be seen from the aggregation numbers.

The micelles are of ellipsoidal shape and retain that shape also when interacting with polyelectrolytes as can be seen from the form factor minimum of the SANS data.

In this surfactant system, it would be especially interesting to vary parameters analogue to the microemulsion system. For example, cosurfactant could be added to the surfactant mixture to induce different structuring of the micelles. Unlike to the microemulsion droplets, adding hexanol to the TDMAO/TTAB mixture would not only enlarge the size of the micelles but also change the packing parameter and thus form different aggregates, whose interactions with polyacrylates would be interesting. Further, of course also biopolyelectrolytes like NaHA or

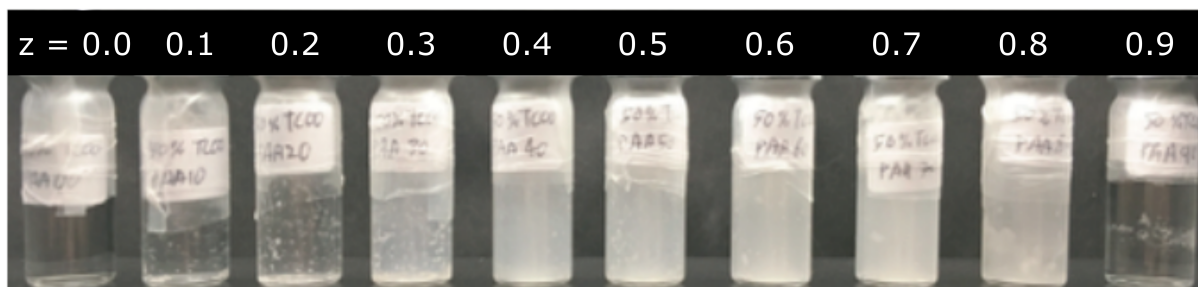


**Figure 56:** Photo of samples prepared of a 50 % TTAB/50 % TDMAO surfactant solution mixed with NaPA60 at different charge ratios.

CMC could be employed to see, if the more rigid sugar backbone has the same tendency to form straight cylindrical aggregates with micelles, as it was found with microemulsion droplets. It was seen before in the work of L. Chiappisi<sup>[58]</sup> that the charge density of the micelles can have a very pronounced effect on PESCs. In our studies on PEMECs we found that complexes quickly become instable when the charge density of the microemulsion droplets is increased (by increasing the amount of TTAB) but very interesting results were obtained by variation of the charge density of the microemulsion droplets and the polyelectrolyte in parallel by lowering the pH. We started to explore the effect of the charge density of TDMAO/TTAB micelles in complexes with NaPA by increasing the amount of TTAB.

The phase behavior of a 5 mol% TTAB/95 mol% TDMAO mixture was already studied. In a first test experiment to study the effect of charge, the amount of TTAB was increased by a factor of 10 to 50 mol%. Fig. 56 shows a photo of a sample series prepared with a 50 % TTAB containing surfactant mixture and NaPA60 at different charge ratios. It can be seen, that all samples have phase separated. The  $z = 0.9$  sample looks clear in the photo but white precipitates were sticking to the glass. It was found, that an increase in charge density of the micelles very quickly leads to instable samples. This is, again, similar to what was observed previously for polyelectrolyte/microemulsion complexes. In retrospect it was a little too optimistic to raise the TTAB content to 50 % in one step. In the future more experiments should be carried out with TTAB amounts between 5 and 10 %.

## 9 General Conclusion and Outlook

In this work, the interactions of positively charged O/W microemulsion droplets with negatively charged polyelectrolytes were studied. To study the interactions in such systems is of great importance for many applications where oppositely charged polyelectrolyte/surfactant complexes are supposed to be loaded with a hydrophobic compound.

This work gives a broad overview on how a number of different parameters affect the interactions and the complex formation in polyelectrolyte/microemulsion systems. The results are divided into six sections. In the first part the interactions of microemulsion droplets with different polyacrylates were studied. In the second part biopolyelectrolytes, such as hyaluronate and carboxymethyl cellulose were employed and compared with the results obtained for the more flexible NaPA. The dynamics of polyelectrolyte/microemulsion systems were analyzed in the third part of this work. Here, NSE measurements were employed to obtain information about the exchange rates of droplets within the complexes and the average lifetime of complexes. Further, the employed polyelectrolytes as well as the microemulsion droplets are pH responsive. So the variation of pH was examined in the fourth part. The fifth part deals with hydrophobically modified polyelectrolytes or blockcopolymers that were employed with the goal to achieve a dense packing of droplets in large aggregates. And finally, in the last part, the study of the corresponding polyelectrolyte/surfactant reference system is presented.

In all studies described here, the microemulsion droplets retain their size and shape when interacting with the polyelectrolyte. This is an important finding, as it shows that the droplets would be available as carriers for potential delivery applications. The polyelectrolyte induced structuring is especially pronounced at polyelectrolyte excess close to the phase boundary, where long cylindrical arrangements of droplets were found with up to 35 droplets per aggregate. These elongated aggregates are of straight cylindrical shape when stiff biopolyelectrolytes are employed and bend over a certain persistence length, when flexible polymers like NaPA are employed. With a Monte Carlo model developed by us, it was possible to deduce the respective persistence lengths of microemulsion complexes from the SANS data. All formed aggregates are highly dynamic. DLS and NSE measurements showed, that the average lifetime of complexes lies between 700 ns and 70  $\mu$ s and only 30 % of all droplets are contained in complexes at a given time. The systems are, among others, responsive to changes in pH. By lowering the pH, it is possible to first bind droplets into large aggregates which are then resolved and the droplets are released. A highly interesting process for drug delivery applications. Further, it could be shown that close packings of microemulsion droplets could be achieved by employing PEG-PAA blockcopolymers. A comparison with the surfactant reference system shows that microemulsion droplets behave differently to empty micelles and it is therefore important to study both systems.

In summary it can be stated that the examined complexes of O/W microemulsion droplets with oppositely charged polyelectrolytes (PEMECs) are structurally very versatile hybrid systems. Many different properties in architecture and size are accessible by systematically tuning the composition, the droplet size or the type and  $M_w$  of the polyelectrolyte. In addition, the system

is responsive to concentration, ionic strength and pH.

In this context one may rise the question for the driving force that allows particles of same charge to assemble close together in one aggregate. In Chapter 2.3 it is described that effective screening of all microemulsion droplet charges is entropically unlikely, therefore the droplets are still charged and repel each other when bound in one aggregate. This repulsion could be overcome by structural transformation of the charged aggregates as it is the case in some polyelectrolyte/surfactant systems.<sup>[60,64]</sup> But this is clearly not the case here, the microemulsions retain their droplet shape when interacting with polyelectrolytes as was shown on several occasions in this work. In this work it was also shown that the droplets of polyelectrolyte/microemulsion complexes are exchanging very quickly and only a small fraction of droplets is bound in complexes at a given time. This dynamic situation allows droplets of same charge to come close together in one aggregate as an result of statistical fluctuations and for rather short times only. This dynamic situation is also the reason for the low viscous behavior observed for these complexes, even though a viscosity increase would normally be expected from elongated structures. The high sheer modulus of long rods is compensated by a very short structural relaxation time, resulting in a low viscosity. Other polyelectrolyte/surfactant systems that exhibit structural deformation of the micellar aggregates show longer relaxation rates, which multiplies with the high sheer modulus of elongated structures and results in drastic viscosity increases.

Using a microemulsion instead of micelles makes PEMECs markedly superior to conventional PESCs as loaded colloidal carrier systems. This allows combining the high loading capacity of a microemulsion with mesoscopic structuring via polyelectrolyte complexation, thereby having the functionality of both components within a self-assembled hybrid system. Such systems are highly promising for future fundamental investigations and applications in which a high payload is to be formulated within a complex colloidal system, thereby advancing the field of colloid science into the area of controlling microemulsion properties by ionic assembly.

Other works dealing with microemulsion complexation mostly include polymers, where the polymer/microemulsion binding is based on hydrophobic interactions. Here, studies include telechelic polymers, graft copolymers and blockcopolymers.<sup>[40–47]</sup> In most examples a gelling of the sample was observed. In the case studied and presented here, the complexation between microemulsion droplets and polyelectrolytes do not rely on hydrophobic but on electrostatic interactions. Among others, this offers the possibility of modifying the strength of interaction by variation of the charge density e.g. by tuning the pH. The group of J. Koetz studied the influence of polyelectrolytes on microemulsion systems but was more interested in modifications of the phase behavior of the microemulsion than in the type and structure of the formed mixed aggregates.<sup>[48–50]</sup> To our knowledge, this makes the present study the first comprehensive work on mixed polyelectrolyte/microemulsion droplet complexes (PEMECs), analyzing not only the phase behavior but also the structure and composition of the formed aggregates as well as the responsiveness to external stimuli.

The complex behavior of polyelectrolyte/microemulsion mixtures is far from being understood. At this stage a number of parameters were investigated and some explanations are suggested but many questions remain open.

In a couple of cases the amount of TTAB (i.e. the charge density) of the microemulsion droplets was varied which mostly led to instable complexes. Since the charge density influences the strength of interaction, this parameter is highly interesting for the formation of different structures. The system is very sensitive to this parameter so careful and thorough further investigations are needed here. In that context, also the ionic strength of the system is relevant. We found that already small amounts of added salt effectively dissolve the formed complexes. For higher charge densities, also the amount of salt needed for disassembly should increase. ITC measurements should yield more information about the thermodynamic properties of this system and the binding strengths between polyelectrolytes and microemulsion droplets. Very recent SANS measurements showed that the nature of the added ions has a marked influence on the screening efficiency, an effect that would certainly be interesting to explore further.

Chapter 5 shows that the dynamic observation can change the interpretation of findings from previous static measurements. With the help of dynamic measurements, we were able to deduce an average lifetime of PEMECs with which the low viscous behavior and the objection of assembling particles with the same charge close together can be explained. More NSE measurements were only partially analyzed in this work but it is expected to gain further fundamental knowledge of PE/ME interactions from a comprehensive interpretation of these data.

A very interesting parameter with respect to applications is the variation of pH. First studies showed the incorporation of microemulsion droplets in large clusters and release of droplets, depending on the pH value but further detailed studies are necessary here, especially for systems with hyaluronate.

The experiments with hydrophobically modified polyacrylic acid showed that polyelectrolytes composed of only 100 monomer units are too short to effectively link many droplets. Since long hydrophobically modified polyelectrolytes are difficult to synthesize one should concentrate on the cluster formation with blockcopolymers in the future. Here, first test experiments with PEG-PAA blockcopolymers showed promising results but a more detailed study is necessary to find the right conditions for large densely packed microemulsion droplet aggregates.

Finally, the TDMAO/TTAB surfactant system was studied as a reference for microemulsion complexes. Here, it would be interesting to expand this study to the many other parameters that were already analyzed for the microemulsion complexes, e.g. employing biopolyelectrolytes, investigating the dynamics or the influence of pH.



## References

- [1] P. Taylor, “Ostwald ripening in emulsions”, *Advances in Colloid and Interface Science* **1998**, *75*, 107–163.
- [2] E. R. Garrett, “Prediction of stability in pharmaceutical preparations VIII. Oil-in-water emulsion stability and the analytical ultracentrifuge”, *Journal of Pharmaceutical Sciences* **1962**, *51*, 35–42.
- [3] H. Kunieda, K. Shinoda, “Conditions to Produce So-called Microemulsions: Factors to Increase the Mutual Solubility of Oil and Water by Solubilizer”, *Journal of Colloid and Interface Science* **1973**, *42*, 381–387.
- [4] C. Solans, P. Iizquierdo, J. Nolla, N. Azemar, M. Garciacelma, “Nano-emulsions”, *Current Opinion in Colloid and Interface Science* **2005**, *10*, 102–110.
- [5] P. Fernandez, V. André, J. Rieger, A. Kühnle, “Nano-emulsion formation by emulsion phase inversion”, *Colloids and Surfaces A* **2004**, *251*, 53–58.
- [6] P. Izquierdo, J. Feng, J. Esquena, T. F. Tadros, J. C. Dederen, M. J. Garcia, N. Azemar, C. Solans, “The influence of surfactant mixing ratio on nano-emulsion formation by the pit method.”, *Journal of Colloid and Interface Science* **2005**, *285*, 388–94.
- [7] T. J. Wooster, M. Golding, P. Sanguansri, “Impact of Oil Type on Nanoemulsion Formation and Ostwald Ripening Stability”, *Langmuir* **2008**, *24*, 12758–12765.
- [8] T. Tadros, P. Izquierdo, J. Esquena, C. Solans, “Formation and stability of nano-emulsions”, *Advances in Colloid and Interface Science* **2004**, *108-109*, 303–318.
- [9] E. Ruckenstein, “The Origin of Thermodynamic Stability of Microemulsions”, *Chemical Physical Letters* **1978**, *57*, 517–521.
- [10] D. Langevin, “Micelles and Microemulsions”, *Annual Review of Physical Chemistry* **1992**, *43*, 341–369.
- [11] R. Strey, “Microemulsion microstructure and interfacial curvature”, *Colloid and Polymer Science* **1994**, *272*, 1005–1019.
- [12] S. Slomkowski, J. V. Alemán, R. G. Gilbert, M. Hess, K. Horie, R. G. Jones, P. Kubisa, I. Meisel, W. Mormann, S. Penczek, R. F. Stepto, “Terminology of polymers and polymerization processes in dispersed systems (IUPAC recommendations 2011)”, *Pure and Applied Chemistry* **2011**, *83*, 2229–2259.
- [13] M. Moniruzzaman, N. Kamiya, K. Nakashima, M. Goto, “Water-in-ionic liquid microemulsions as a new medium for enzymatic reactions”, *Green Chemistry* **2008**, *10*, 497–500.
- [14] A. Martino, E. W. Kaler, “Phase Behavior and Microstructure of Nonaqueous Microemulsions”, *Journal of Physical Chemistry* **1990**, *94*, 1627–1631.

- [15] J. Marcus, D. Touraud, S. Prévost, O. Diat, T. Zemb, W. Kunz, “Influence of additives on the structure of surfactant-free microemulsions”, *Physical Chemistry Chemical Physics* **2015**, *17*, 32528–32538.
- [16] S. Schöttl, D. Horinek, “Salt effects in surfactant-free microemulsions”, *The Journal of Chemical Physics* **2018**, *148*, 222818–1–5.
- [17] T. P. Hoar, J. H. Schulman, “Transparent Water-in-Oil Dispersions: the Oleopathic Hydro-Micelle”, *Nature* **1943**, *152*, 102–103.
- [18] J. H. Schulman, W. Stoeckenius, L. M. Prince, “Mechanism of formation and structure of micro emulsions by electron microscopy”, *Journal of Physical Chemistry* **1959**, *63*, 1677–1680.
- [19] P. A. Winsor, “Hydrotropy, Solubilization and Related Emulsification Processes. Part I”, *Transactions of the Faraday Society* **1948**, *44*, 376–398.
- [20] K. Shinoda, H. Saito, “The Effect of Temperature on the Phase Equilibria and the Types of Dispersions of the Ternary System Composed of Water, Cyclohexane, and Nonionic Surfactant”, *Journal of Colloid and Interface Science* **1968**, *26*, 70–74.
- [21] M. Kahlweit, R. Strey, “Phase Behavior of Ternary Systems of the Type H<sub>2</sub>O-Oil-Nonionic Amphiphile (Microemulsions)”, *Angewandte Chemie International Edition in English* **1985**, *24*, 654–668.
- [22] D. Langevin, “Microemulsions - interfacial aspects”, *Advances in Colloid and Interface Science* **1991**, *34*, 583–595.
- [23] M. Gradzielski, D. Langevin, B. Farago, “Experimental investigation of the structure of nonionic microemulsions and their relation to the bending elasticity of the amphiphilic film”, *Physical Review E* **1996**, *53*, 3900–3919.
- [24] J. T. G. Overbeek, G. J. Verhoeckx, P. L. de Bruyn, H. N. W. Lekkerkerker, “On understanding microemulsions II”, *Journal of Colloid and Interface Science* **1987**, *119*, 422–441.
- [25] P. G. De Gennes, C. Taupin, “Microemulsions and the flexibility of oil/water interfaces”, *Journal of Physical Chemistry* **1982**, *86*, 2294–2304.
- [26] M. Gradzielski, H. Hoffmann, D. Langevin, “Solubilization of Decane into the Ternary System TDMAO/1-HexanoVWater”, *Journal of Physical Chemistry* **1995**, *99*, 12612–12623.
- [27] M. Gradzielski, “Effect of the cosurfactant structure on the bending elasticity in nonionic oil-in-water microemulsions”, *Langmuir* **1998**, *14*, 6037–6044.
- [28] M. Gradzielski, H. Hoffmann, “Structural investigations of charged O/W microemulsion droplets”, *Advances in Colloid and Interface Science* **1992**, *42*, 149–173.

- [29] M. Gradzielski, H. Hoffmann, "Influence of Charges on Structure and Dynamics of an O/W Microemulsion. Effect of Admixing Ionic Surfactants", *Journal of Physical Chemistry* **1994**, *98*, 2613–2623.
- [30] M. F. Nazar, S. S. Shah, M. A. Khosa, "Microemulsions in enhanced oil recovery: A review", *Petroleum Science and Technology* **2011**, *29*, 1353–1365.
- [31] L. Bemert, S. Engelskirchen, C. Simon, R. Strey, "Low Emissions With Microemulsion-Fuels", *Preprints of Papers- American Chemical Society Division of Fuel Chemistry* **2009**, *54*, 290–291.
- [32] C. Solans, J. García Domínguez, S. E. Friberg, "Evaluation of Textile Detergent Efficiency of Microemulsions in Systems of Water Nonionic Surfactant and Hydrocarbon at Low Temperature", *Journal of Dispersion Science and Technology* **1985**, *6*, 523–537.
- [33] E. E. Linn, R. C. Pohland, T. K. Byrd, "Microemulsion for intradermal delivery of cetyl alcohol and octyl dimethyl PABA", *Drug Development and Industrial Pharmacy* **1990**, *16*, 899–920.
- [34] M. J. Lawrence, G. D. Rees, "Microemulsion-based media as novel drug delivery systems", *Advanced Drug Delivery Reviews* **2012**, *64*, 175–193.
- [35] D. W. Holt, E. A. Mueller, J. M. Kovarik, J. B. van Bree, K. Kutz, "The pharmacokinetics of Sandimmun Neoral: a new oral formulation of cyclosporine", *Transplantation Proceedings* **1994**, *26*, 2935–2939.
- [36] M. J. Schwuger, K. Stickdorn, R. Schomaecker, "Microemulsions in Technical Processes", *Chemical Reviews* **1995**, *95*, 849–864.
- [37] E. Mitsou, G. Tavantzis, G. Sotiroidis, D. Ladikos, A. Xenakis, V. Papadimitriou, "Food grade water-in-oil microemulsions as replacement of oil phase to help process and stabilization of whipped cream", *Colloids and Surfaces A* **2016**, *510*, 69–76.
- [38] T. Zemb, M. Duvail, J. F. Dufrêche, "Reverse aggregates as adaptive self-assembled systems for selective liquid-liquid cation extraction", *Israel Journal of Chemistry* **2013**, *53*, 108–112.
- [39] S. Kantaria, G. D. Rees, M. J. Lawrence, "Gelatin-stabilised microemulsion-based organogels: Rheology and application in iontophoretic transdermal drug delivery", *Journal of Controlled Release* **1999**, *60*, 355–365.
- [40] P. Malo de Molina, C. Herfurth, A. Laschewsky, M. Gradzielski, "Structure and Dynamics of Networks in Mixtures of Hydrophobically Modified Telechelic Multiarm Polymers and Oil in Water Microemulsions", *Langmuir* **2012**, *28*, 15994–16006.
- [41] P. Malo de Molina, M. S. Appavou, M. Gradzielski, "Oil-in-water microemulsion droplets of TDMAO/decane interconnected by the telechelic C18-EO150-C18: Clustering and network formation", *Soft Matter* **2014**, *10*, 5072–5084.

- [42] P. Malo de Molina, F. S. Ihlefeldt, S. Prévost, C. Herfurth, M.-S. Appavou, A. Laschewsky, M. Gradzielski, “Phase Behavior of Nonionic Microemulsions with Multi-end-capped Polymers and Its Relation to the Mesoscopic Structure”, *Langmuir* **2015**, *31*, 5198–5209.
- [43] A. Holmberg, P. Hansson, L. Piculell, P. Linse, “Effects of an Amphiphilic Graft Copolymer on an Oil Continuous Microemulsion. Viscosity, Droplet Size, and Phase Behavior”, *Journal of Physical Chemistry B* **1999**, *103*, 10807–10815.
- [44] C. Quellet, H. F. Eicke, G. Xu, Y. Hauger, “Transient networks in ABA block copolymer-microemulsion systems”, *Macromolecules* **1990**, *23*, 3347–3352.
- [45] A. Kabalnov, U. Olsson, H. Wennerström, “Polymer Effects on the Phase Equilibrium of a Balanced Microemulsion”, *Langmuir* **1994**, *10*, 2159–2169.
- [46] A. Kabalnov, U. Olsson, K. Thuresson, H. Wennerström, “Polymer Effects on the Phase Equilibrium of a Balanced Microemulsion: Adsorbing versus Nonadsorbing Polymers”, *Langmuir* **1994**, *10*, 4509–4513.
- [47] B. Jakobs, T. Sottmann, R. Strey, J. Allgaier, L. Willner, D. Richter, “Amphiphilic block copolymers as efficiency boosters for microemulsions”, *Langmuir* **1999**, *15*, 6707–6711.
- [48] J. Baier, J. Koetz, S. Kosmella, B. Tiersch, H. Rehage, “Polyelectrolyte-modified inverse microemulsions and their use as templates for the formation of magnetite nanoparticles”, *Journal of Physical Chemistry B* **2007**, *111*, 8612–8618.
- [49] J. Koetz, J. Bahnemann, G. Lucas, B. Tiersch, S. Kosmella, “Polyelectrolyte-modified microemulsions as new templates for the formation of nanoparticles”, *Colloids and Surfaces A* **2004**, *250*, 423–430.
- [50] C. Note, J. Koetz, S. Kosmella, “Structural changes in poly(ethyleneimine) modified microemulsion”, *Journal of Colloid and Interface Science* **2006**, *302*, 662–668.
- [51] E. Buhler, J. Appell, G. Porte, “Loose complexation of weakly charged microemulsion droplets and a polyelectrolyte”, *Journal of Physical Chemistry B* **2006**, *110*, 6415–6422.
- [52] L. Shi, F. Carn, F. Boué, G. Mosser, E. Buhler, “Control over the electrostatic self-assembly of nanoparticle semiflexible biopolyelectrolyte complexes”, *Soft Matter* **2013**, *9*, 5004–5015.
- [53] L. Shi, F. Carn, F. Boué, E. Buhler, “Role of the ratio of biopolyelectrolyte persistence length to nanoparticle size in the structural tuning of electrostatic complexes”, *Physical Review E* **2016**, *94*, 1–12.
- [54] L. Chiappisi, I. Hoffmann, M. Gradzielski, “Complexes of oppositely charged polyelectrolytes and surfactants - recent developments in the field of biologically derived polyelectrolytes”, *Soft Matter* **2013**, *9*, 3896–3909.
- [55] J. Gummel, F. Cousin, F. Boué, “Counterions release from electrostatic complexes of polyelectrolytes and proteins of opposite charge: A direct measurement”, *Journal of the American Chemical Society* **2007**, *129*, 5806–5807.

- [56] J. Zhang, R. K. Thomas, J. Penfold, “Interaction of oppositely charged polyelectrolyte-ionic surfactant mixtures: Adsorption of sodium poly(acrylic acid)-dodecyl trimethyl ammonium bromide mixtures at the air-water interface”, *Soft Matter* **2005**, *1*, 310–318.
- [57] T. Wallin, P. Linse, “Monte Carlo simulations of polyelectrolytes at charged micelles. 2. Effects of linear charge density”, *Langmuir* **1996**, *12*, 305–314.
- [58] L. Chiappisi, S. Prévost, I. Grillo, M. Gradzielski, “Chitosan/Alkylethoxy carboxylates: a surprising variety of structures.”, *Langmuir* **2014**, *30*, 1778–87.
- [59] J. F. Berret, P. Hervé, O. Aguerre-Chariol, J. Oberdisse, “Colloidal complexes obtained from charged block copolymers and surfactants: A comparison between small-angle neutron scattering, cryo-TEM, and simulations”, *Journal of Physical Chemistry B* **2003**, *107*, 8111–8118.
- [60] I. Hoffmann, P. Heunemann, S. Prévost, R. Schweins, N. J. Wagner, M. Gradzielski, “Self-aggregation of mixtures of oppositely charged polyelectrolytes and surfactants studied by rheology, dynamic light scattering and small-angle neutron scattering.”, *Langmuir* **2011**, *27*, 4386–96.
- [61] L. Chiappisi, S. Prévost, I. Grillo, M. Gradzielski, “From crab shells to smart systems: Chitosan-alkylethoxy carboxylate complexes”, *Langmuir* **2014**, *30*, 10615–10616.
- [62] W. C. Blocher, S. L. Perry, “Complex coacervate-based materials for biomedicine”, *Wiley Interdisciplinary Reviews: Nanomedicine and Nanobiotechnology* **2017**, *9*, 76–78.
- [63] L. Chiappisi, “Ionic co-assembly in mixtures of polysaccharides and surfactants”, *Phd Thesis TU Berlin* **2015**.
- [64] I. Hoffmann, M. Simon, B. Farago, R. Schweins, P. Falus, O. Holderer, M. Gradzielski, “Structure and dynamics of polyelectrolyte surfactant mixtures under conditions of surfactant excess”, *The Journal of Chemical Physics* **2016**, *145*.
- [65] P. Buchold, R. Schweins, Z. Di, M. Gradzielski, “Structural behaviour of sodium hyaluronate in concentrated oppositely charged surfactant solutions”, *Soft Matter* **2017**, *13*, 2253–2263.
- [66] K. Hayakawa, S. Shinohara, S.-I. Sasawaki, I. Satake, J. C. T. Kwak, “Solubilization of Water-Insoluble Dyes by Polyion/Surfactant Complexes”, *Bulletin of the Chemical Society of Japan* **1995**, *68*, 2179–2185.
- [67] W. Wang, S. A. Sande, “Kinetics of Re-equilibrium of oppositely charged hydrogel-surfactant system and its application in controlled release”, *Langmuir* **2013**, *29*, 6697–6705.
- [68] M. Kamimura, J. O. Kim, A. V. Kabanov, T. K. Bronich, Y. Nagasaki, “Block ionomer complexes of PEG-block-poly(4-vinylbenzylphosphonate) and cationic surfactants as highly stable, pH responsive drug delivery system”, *Journal of Controlled Release* **2012**, *160*, 486–494.

- [69] H. Hoffmann, G. Oetter, B. Schwandner, “The aggregation behaviour of tetradecyldimethylaminoxide”, *Progress in Colloid and Polymer Science* **1987**, *73*, 95–106.
- [70] J. Dong, Y. Ozaki, K. Nakashima, “FTIR studies of conformational energies of poly (acrylic acid) in cast films”, *Journal of Polymer Science B* **1997**, *35*, 507–515.
- [71] I. Morfin, E. Buhler, F. Cousin, I. Grillo, F. Boué, “Rodlike complexes of a polyelectrolyte (hyaluronan) and a protein (lysozyme) observed by SANS”, *Biomacromolecules* **2011**, *12*, 859–870.
- [72] C. W. Hoogendam, A. De Keizer, M. A. C. Stuart, B. H. Bijsterbosch, J. A. M. Smit, J. A. P. P. Van Dijk, P. M. Van Der Horst, J. G. Batelaan, “Persistence length of carboxymethyl cellulose as evaluated from size exclusion chromatography and potentiometric titrations”, *Macromolecules* **1998**, *31*, 6297–6309.
- [73] M. Simon, P. Krause, L. Chiappisi, L. Noirez, M. Gradzielski, “Structural control of polyelectrolyte/microemulsion droplet complexes (PEMECs) with different polyacrylates”, *Chemical Science* **2019**, *10*, 385–397.
- [74] M. Itakura, K. Shimada, S. Matsuyama, T. Saito, S. Kinugasa, “A convenient method to determine the Rayleigh ratio with uniform polystyrene oligomers”, *Journal of Applied Polymer Science* **2006**, *99*, 1953–1959.
- [75] A. Guinier, G. Fournet, *Small-angle Scattering of X-rays*, John Wiley & Sons, New York, **1955**.
- [76] B. J. Frisken, “Revisiting the method of cumulants for the analysis of dynamic light-scattering data”, *Applied Optics* **2001**, *40*, 4087–4091.
- [77] A. J. F. Siegert, “On the fluctuations in signals returned by many independently moving scatterers”, *MIT Radiation Laboratory Report* **1943**.
- [78] E. T. Hanson, R. Borsali, R. Pecora, “Dynamic light scattering and small-angle neutron scattering studies of ternary rod/coil/solvent systems”, *Macromolecules* **2001**, *34*, 2208–2219.
- [79] P. G. De Gennes, “Liquid dynamics and inelastic scattering of neutrons”, *Antiviral Research* **1959**, *25*, 825–839.
- [80] D. E. Koppel, “Analysis of Macromolecular Polydispersity in Intensity Correlation Spectroscopy: The Method of Cumulants”, *Journal of Chemical Physics* **1972**, *57*, 4814–4820.
- [81] K. Lieutenant, P. Lindner, R. Gähler, “A new design for the standard pinhole small-angle neutron scattering instrument D11”, *Journal of Applied Crystallography* **2007**, *40*, 1056–1063.
- [82] A. Radulescu, V. Pipich, H. Frielinghaus, M.-S. Appavou, “KWS-2, the high intensity / wide Q-range small-angle neutron diffractometer for soft-matter and biology at FRM II”, *Journal of Physics* **2012**, *351*.

- [83] A. Radulescu, N. K. Szekely, M.-S. Appavou, “KWS-2: Small angle scattering diffractometer”, *Journal of Large-scale Research Facilities* **2015**, *1*, 1–5.
- [84] U. Keiderling, A. Wiedenmann, “New SANS instrument at the BER II reactor in Berlin, Germany”, *Physica B* **1995**, *213-214*, 895–897.
- [85] U. Keiderling, “The new ‘BerSANS-PC’ software for reduction and treatment of small angle neutron scattering data”, *Applied Physics A* **2002**, *1457*, 1455–1457.
- [86] D. Richard, M. Ferrand, G. J. Kearley, “Analysis and Visualisation of Neutron- Scattering Data”, *Journal of Neutron Research* **1996**, *4*, 33–39.
- [87] V. Pipich, “QtiKWS: user-friendly program for reduction, visualization, analysis and fit of SA(N)S data.”, **2012**.
- [88] V. Y. Bezzabotnov, L. Cser, T. Grósz, G. Jancsó, Y. M. Ostanevich, “Small-Angle Neutron Scattering in Aqueous Solutions of Tetramethylurea”, *Journal of Physical Chemistry* **1992**, *96*, 976–982.
- [89] G. Porod, “Die Roentgenkleinwinkelstreuung von dichtgepackten kolloidalen Systemen.”, *Colloid and Polymer Science* **1951**, *124*, 83–114.
- [90] I. Breßler, J. Kohlbrecher, A. F. Thünemann, “SASfit: a tool for small-angle scattering data analysis using a library of analytical expressions”, *Journal of Applied Crystallography* **2015**, *48*, 1587–1598.
- [91] L. Chiappisi, S. Prévost, M. Gradzielski, “Form factor of cylindrical superstructures composed of globular particles”, *Journal of Applied Crystallography* **2014**, *47*, 827–834.
- [92] A. L. Kholodenko, “Analytical Calculation of the Scattering Function for Polymers of Arbitrary Flexibility Using the Dirac Propagator”, *Macromolecules* **1993**, *26*, 4179–4183.
- [93] M. Simon, “Investigations of the Interactions of Polyelectrolytes with Oppositely Charged Microemulsion Droplets”, *M.Sc. Thesis TU Berlin* **2016**.
- [94] L. Baba-Ahmed, M. Benmouna, M. J. Grimson, “Elastic Scattering from Charged Colloidal Dispersions”, *Physics and Chemistry of Liquids* **1987**, *16*, 235–238.
- [95] I. Hoffmann, “Neutrons for the study of dynamics in soft matter systems”, *Colloid and Polymer Science* **2014**, *292*, 2053–2069.
- [96] S. A. Safran, “Fluctuations of spherical microemulsions”, *The Journal of Chemical Physics* **1983**, *78*, 2073–2076.
- [97] S. T. Milner, S. A. Safran, “Dynamical fluctuatuions of droplet microemulsions and vesicles”, *Physical Review A* **1987**, *36*, 4371–4379.
- [98] P. Schleger, B. Alefeld, J. F. Barthelemy, G. Ehlers, B. Farago, P. Giraud, C. Hayes, A. Kollmar, C. Lartigue, F. Mezei, D. Richter, “The long-wavelength neutron spin-echo spectrometer IN15 at the Institut Laue-Langevin”, *Physica B* **1997**, *241-243*, 164–165.

- [99] B. Farago, P. Falus, I. Hoffmann, M. Gradzielski, F. Thomas, C. Gomez, “The IN15 upgrade”, *Neutron News* **2015**, *26*, 15–17.
- [100] G. R. Fulmer, A. J. M. Miller, N. H. Sherden, H. E. Gottlieb, A. Nudelman, B. M. Stoltz, J. E. Bercaw, K. I. Goldberg, “NMR chemical shifts of trace impurities: Common laboratory solvents, organics, and gases in deuterated solvents relevant to the organometallic chemist”, *Organometallics* **2010**, *29*, 2176–2179.
- [101] D. C. Henry, “The Cataphoresis of Suspended Particles. I. The Equation of Cataphoresis”, *Proceedings of the Royal Society of London A* **1931**, *133*, 106–129.
- [102] M. Skepö, P. Linse, “Dissolution of a polyelectrolyte-macroion complex by addition of salt”, *Physical Review E* **2002**, *66*, 7.
- [103] M. Burkhardt, M. Ruppel, S. Tea, M. Drechsler, R. Schweins, D. V. Pergushov, M. Gradzielski, A. B. Zezin, A. H. Müller, “Water-soluble interpolyelectrolyte complexes of polyisobutylene-block- poly(methacrylic acid) micelles: Formation and properties”, *Langmuir* **2008**, *24*, 1769–1777.
- [104] K. Pojżak, E. Bertalanits, R. Meższażros, “Effect of salt on the equilibrium and nonequilibrium features of polyelectrolyte/surfactant association”, *Langmuir* **2011**, *27*, 9139–9147.
- [105] H. Fam, J. T. Bryant, M. Kontopoulou, “Rheological properties of synovial fluids”, *Biorheology* **2007**, *44*, 59–74.
- [106] K. T. Dicker, L. A. Gurski, S. Pradhan-Bhatt, R. L. Witt, M. C. Farach-Carson, X. Jia, “Hyaluronan: A simple polysaccharide with diverse biological functions”, *Acta Biomaterialia* **2014**, *10*, 1558–1570.
- [107] C. B. Hollabaugh, L. H. Burt, A. P. Walsh, “Carboxymethylcellulose... Uses and Applications”, *Industrial and Engineering Chemistry* **1945**, *37*, 943–947.
- [108] M. Simon, E. Schneck, L. Noirez, S. Rahn, I. Davidovich, Y. Talmon, M. Gradzielski, “Effect of the Polymer Architecture on the Phase Behavior and Structure of Polyelectrolyte/Microemulsion Complexes (PEMECs)”, *Macromolecules* **2020**.
- [109] A. Holtzer, “Interpretation of the angular distribution of the light scattered by a polydisperse system of rods”, *Journal of Polymer Science* **1955**, *17*, 432–434.
- [110] L. J. Magid, “The Surfactant-Polyelectrolyte Analogy”, *Journal of Physical Chemistry B* **1998**, *102*, 4064–4074.
- [111] C. A. Dreiss, “Wormlike micelles: Where do we stand? Recent developments, linear rheology and scattering techniques”, *Soft Matter* **2007**, *3*, 956–970.
- [112] B. E. Warren, *X-ray Diffraction*, Courier Corporation, **1990**.
- [113] P. C. Hiemenz, T. P. Lodge, *Polymer Chemistry*, CRC Press, **2007**.

- [114] M. Gradzielski, I. Hoffmann, “Polyelectrolyte-surfactant complexes (PESCs) composed of oppositely charged components”, *Current Opinion in Colloid and Interface Science* **2018**, *35*, 124–141.
- [115] N. Khan, B. Brettmann, “Intermolecular interactions in polyelectrolyte and surfactant complexes in solution”, *Polymers* **2019**, *11*, 51.
- [116] M. Simon, M. Gradzielski, I. Hoffmann, “Dynamics in Polyelectrolyte/Microemulsion Complexes”, *submitted to Nanoscale Advances*.
- [117] D. Schmaljohann, “Thermo- and pH-responsive polymers in drug delivery”, *Advanced Drug Delivery Reviews* **2006**, *58*, 1655–1670.
- [118] L. Chiappisi, M. Simon, M. Gradzielski, “Toward bioderived intelligent nanocarriers for controlled pollutant recovery and pH-sensitive binding”, *ACS Applied Materials and Interfaces* **2015**, *7*, 6139–6145.
- [119] M. Uchman, J. Hajduová, E. Vlassi, S. Pispas, M.-S. Appavou, M. Štěpánek, “Self- and co-assembly of amphiphilic gradient polyelectrolyte in aqueous solution: Interaction with oppositely charged ionic surfactant”, *European Polymer Journal* **2015**, *73*, 212–221.
- [120] J. F. Berret, B. Vigolo, R. Eng, P. Hervé, I. Grillo, L. Yang, “Electrostatic self-assembly of oppositely charged copolymers and surfactants: A light, neutron, and X-ray scattering study”, *Macromolecules* **2004**, *37*, 4922–4930.
- [121] S. Riemer, S. Prévost, M. Dzionara, M.-S. Appavou, R. Schweins, M. Gradzielski, “Aggregation behaviour of hydrophobically modified polyacrylate - Variation of alkyl chain length”, *Polymer* **2015**, *70*, 194–206.
- [122] S. Riemer, S. Prévost, M. Dzionara, U. Gasser, M. Gradzielski, “Hydrophobically modified polyacrylates (hmPAAs) with long alkyl chains – Self-assembly in aqueous solution”, *Polymer* **2017**, *128*, 78–86.
- [123] N. Metropolis, A. W. Rosenbluth, M. N. Rosenbluth, A. H. Teller, E. Teller, “Equation of State calculations by Fast Computing Machines”, *The Journal of Chemical Physics* **1953**, *21*, 1087–1092.
- [124] D. Frenkel, B. Smit, *Understanding Molecular Simulation – from Algorithms to Applications, Vol. 1*, Academic Press, **2002**, p. 658.
- [125] M. J. Grimson, “Small-angle scattering from colloidal dispersions”, *Journal of the Chemical Society Faraday Transactions 2* **1983**, *79*, 817.



# Appendix

## A. List of Abbreviations

### Microemulsion and Polyelectrolytes

CMC	carboxymethyl cellulose
NaCMC	sodium salt of carboxymethyl cellulose
NaCMCxx	xx indicates $M_w$ in kDa
HA	hyaluronate
NaHA	sodium hyaluronate
NaHAxx	sodium hyaluronate, xx indicates $M_w$ in kDa
HM-PAA	hydrophobically modified polyacrylic acid
HM-PE	hydrophobically modified polyelectrolyte
ME	microemulsion
MExx	microemulsion, xx indicates hexanol content in mM
ME00	small microemulsion droplets, $R \sim 3$ nm
ME50	medium sized microemulsion droplets, $R \sim 4$ nm
ME75	large microemulsion droplets, $R \sim 6.5$ nm
O/W	oil-in-water
PAA	polyacrylic acid
NaPA	sodium polyacrylate
NaPAxx	sodium polyacrylate, xx indicates $M_w$ in kDa
PE	polyelectrolyte
PEG	polyethylene glycol
PEMEC	polyelectrolyte/microemulsion complex
PESC	polyelectrolyte/surfactant complex
TDMAO	tetradecyldimethylamine oxide
TTAB	tetradecyltrimethylammonium bromide
W/O	water-in-oil
S00	surfactant mixture

### Symbols

$A$	surface area
$a$	head group area
$\alpha$	stretching exponent
$b$	Kuhn length
$B_0$	strength of guide field
$b_c$	coherent neutron scattering length
$bkg$	incoherent background
$c$	concentration
$c_0$	spontaneous curvature
$c_1, c_2$	principal curvature
$cmc$	critical micellar concentration
$d$	distance
$D, D_0$	diffusion coefficient
$D_{app}$	apparent diffusion coefficient
$D_{coll}$	collective diffusion coefficient

$D_{slow}$	slow diffusion coefficient
DP	average degree of polymerization
DS	degree of substitution
$\eta$	dynamic viscosity
$\varepsilon_0$	permittivity of vacuum
$\varepsilon_r$	relative permittivity
$\epsilon$	molar extinction coefficient
$F$	free energy
$F_b$	bending energy
$F_{ent}$	entropic energy
$F_t$	interfacial energy
$\gamma$	interfacial tension
$\gamma_N$	gyromagnetic ratio of neutron
$G_0$	shear modulus
$g^{(1)}(\tau)$	field-auto-correlation
$g^{(2)}(\tau)$	intensity-auto-correlation
$h$	Planck constant
$h_{ee}$	end-to-end distance
$I(q)$	scattered intensity
$I(0)$	forward scattering intensity
$I_0$	intensity of incoming light
$I_1$	Intensity of transmitted light
$J_i$	field integral for constant magnetic field
$\kappa$	mean bending modulus
$\bar{\kappa}$	Gaussian modulus
$k_B$	Boltzman constant
$k_D$	Debye screening length
$K_L$	optical constant
$l$	length (chain length)
$l_B$	Bjerrum length
$L_C$	contour length
$l_p$	persistence length
$\lambda$	wavelength
$\mu_E$	electrophoretic mobility
$m_N$	mass of neutron
$M_w$	molecular weight
$n$	refractive index
$(dn/dc)$	refractive index increment
$N_A$	Avogadro constant
$N_{agg}$	aggregation number of droplets per complex
$^1N$	number density
$\nu$	kinematic viscosity
$P$	pressure
$p$	packing parameter
$PDI$	polydispersity index
$\phi$	volume fraction
$\phi_p$	phase angle
$q$	magnitude of the scattering vector
$R$	radius

$R_g$	radius of gyration
$R_h$	hydrodynamic radius
$R_\theta$	Rayleigh ratio
$\rho$	density
$SLD$	scattering length density
$\Delta SLD$	contrast
$S(q)$	structure factor
$S(q, t)$	intermediate scattering function
$T$	temperature
$\theta$	scattering angle
$t$	time
$t_F$	Fourier time
$\tau$	structural relaxation time
$\tau_K$	decay time
$T$	transmission
$v$	velocity
$V$	volume
$V_0$	harmonic constraint potential
$v_h$	hydrophobic volume
$v_m$	molecular volume
$x_{slow}$	amplitude of low compound
$z$	charge ratio, $z = [-]/([+] + [-])$
$Z$	number of charges
$\zeta$	zeta potential

## Other Abbreviations

cryo-TEM	cryogenic transmission electron microscope
DCM	dichlormethane
DLS	dynamic light scattering
DOX	doxorubicin
EO	ethylene oxide
EOR	enhanced oil recovery
IUPAC	International Union of Pure and Applied Chemistry
JR400	cationically modified cellulose
NMR	nuclear magnetic resonance
NSE	neutron spin echo
PEI	Poly(ethyleneimine)
PIC	phase inversion concentration
PIT	phase inversion temperature
PVBP	poly(4-vinylbenzylphosphonate)
SANS	small-angle neutron scattering
SAXS	small-angle x-ray scattering
SLS	static light scattering
TOF	time-of-flight
SDS	sodium dodecyl sulfate



## B. SANS Models

**Homogeneous Sphere Form Factor.** A simple homogeneous sphere model with radius  $R$  was assumed for the microemulsion droplets.

$$P(q)_{\text{sphere}} = \left( 3 \cdot \frac{\sin(qR) - qR \cdot \cos(qR)}{(qR)^3} \right)^2 \quad (34)$$

**Log-Normal Distribution.** For polydisperse particles, a size distribution has to be considered. One example is the log-normal size distribution that was used in this work.

$$L_N = \frac{1}{\mu\sigma\sqrt{2\pi}} \cdot \exp\left(-\frac{(\ln \mu - \sigma)^2}{2\sigma^2}\right) \quad (35)$$

$\mu$  and  $\sigma$  are the mean and standard deviation of the log-normally distributed radius  $R$ .

$$R = \exp(\mu - \sigma^2) \quad (36)$$

**Spherical Shell.** SANS data of microemulsion droplets prepared with decane-d22 can be described with a spherical shell model with an inner radius  $R$  and a shell thickness  $\Delta R$ .  $\Delta SLD_1$  is the scattering contrast relative to the matrix of the core and  $\Delta SLD_2$  the one of the shell.

$$I(q)_{\text{shell}} = [K(q, R + \Delta R, \Delta SLD_2) - K(q, R, \Delta SLD_2 - \Delta SLD_1)]^2 \quad (37)$$

$$K(q, R, \Delta SLD) = \frac{4}{3}\pi R^3 \Delta SLD \cdot 3 \cdot \frac{\sin(qR) - qR \cdot \cos(qR)}{(qR)^3} \quad (38)$$

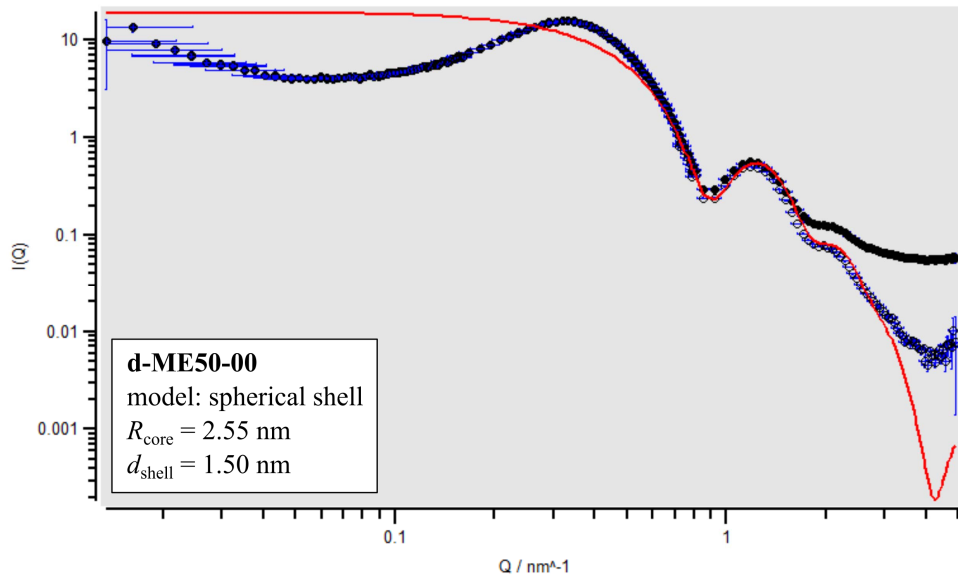


**Figure 57:** SANS data of pure microemulsion d-ME50 in shell contrast with spherical shell fit.

**Porod Model for Long Cylinders.** As a simple approximation of cylindrically arranged microemulsion droplets a homogeneous cylinder model can be applied. Here, the Porod approximation for a long cylinder was used.

$$P(q)_{\text{cylinder}} = \frac{2}{qL} \cdot \left\{ (\text{Si}_{\pi/2}(qL) \cdot \Lambda_1^2(qR) - \frac{\omega(2qR)}{qL} - \frac{\sin(qL)}{(qL)^2}) \right\} \quad (39)$$

$$\text{with: } \text{Si}_{\pi/2}(x) = \left( \text{Si}(x) + \frac{\cos x}{x} + \frac{\sin x}{x^2} \right) \xrightarrow{x \rightarrow \infty} \frac{\pi}{2} \quad (40)$$

$$\text{Si}(x) = \int_0^x \frac{\sin t}{t} dt \quad (41)$$

$$\Lambda_1(x) = \frac{2}{x} \cdot J_1(x) \quad (42)$$

$$\omega(x) = \frac{8}{x^2} \cdot (3J_2(x) + J_0(x) - 1) \quad (43)$$

$J_n(x)$  are the regular cylindrical Bessel functions of order  $n$ .

$$L_N(R) = \frac{1}{R\sigma\sqrt{2\pi}} \cdot \exp\left(-\frac{(\ln R - \mu)^2}{2\sigma^2}\right) \quad (44)$$

$$\text{with: } R = \mu - \sigma^2 \quad (45)$$

**Cylindrical Arrangement of Droplets.** The scattering form factor arising from  $N$  linearly aligned particles was developed by L. Chiappisi in our group.<sup>[91]</sup> It was used to model the scattering curves of linearly arranged microemulsion droplets at polyelectrolyte excess close to the phase boundary.

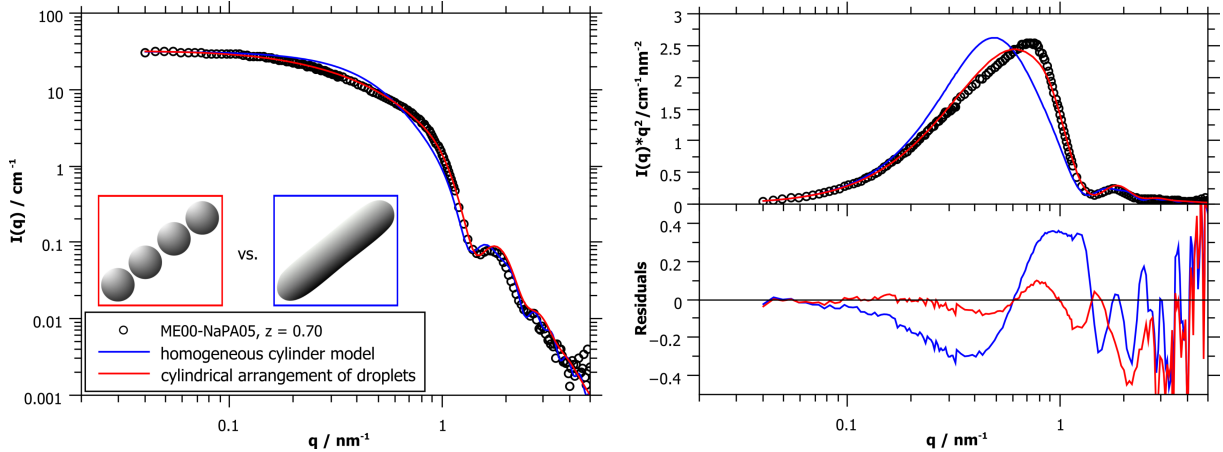


**Figure 58:** The direct comparison of the cylindrical arrangement of droplets with the homogeneous cylinder model described above shows that the cylinder model is only a rough estimation and the cylindrical arrangement of droplets describes the SANS data much better. Reproduced from Ref. [73] with permission of the Royal Society of Chemistry.

**New Model of Curved Droplet Chains.** The Monte Carlo model describes chains of  $N$  homogeneous spheres of average radius  $R$ , which are separated by an average distance  $d$  between the sphere surfaces. Both  $R$  and  $d$  are polydisperse and randomly picked from normal

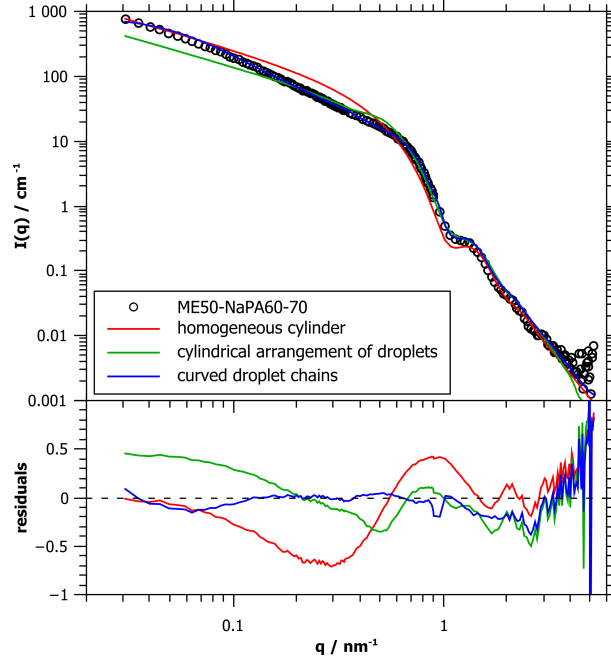


**Figure 59:** Comparison of different models to describe the SANS data of polyelectrolyte/microemulsion complexes exemplarily for ME50-NaPA60-70 sample. It can be seen, that the newly developed Monte Carlo simulation of curved droplet chains describes the scattering data best. Reprinted with permission from Ref. [108]. Copyright 2020 American Chemical Society.

distributions with standard deviations ( $\sigma$ ) corresponding to the polydispersity parameters. The chains assume the random conformations of semi-flexible polymers of a given persistence length  $l_p$ . In practice, this is achieved by sampling random conformations while penalizing high angles  $\theta$  between the vectors between each sphere and its two neighbors with a harmonic constraint potential of adjustable strength  $V_0$ :  $V(\theta) = V_0\theta^2$ .

The chains are grown stepwise, i.e., sphere by sphere. According the Metropolis algorithm,<sup>[123]</sup> the probability of accepting the addition of the next sphere is given by the associated Boltzmann factor  $p(\theta) = e^{-V(\theta)/(k_B T)}$ . Non-physical conformations with overlapping spheres are excluded. To obtain the scattering curves, at least 5000 conformations are randomly generated in this way. For longer chains (with larger  $N$ ) comparatively fewer configurations yield the same sampling as comparatively more configurations for shorter chains. The scattering intensities are then computed by calculating the form factor amplitudes of each sphere, subsequent phase-correct summation based on each set of sphere coordinates using the Debye-formula,<sup>[112]</sup> and averaging over all conformations.

The stepwise growth of non-overlapping chains employed here is computationally highly efficient but represents the thermodynamic ensemble associated with the angular potential  $V(\theta)$  only approximately.<sup>[124]</sup> The apparent persistence length resulting from  $V_0$  and was calculated a-posteriori from the ensemble-averaged ratio between contour length  $L_C$  and end-to-end distance  $h_{ee}$ , where  $\langle h_{ee}^2 \rangle = 2L_C l_p - 2l_p^2(1 - e^{-L_C/l_p})$ .<sup>[113]</sup>

**Kholodenko Worm.** The shape of the scattering curves of elongated complexes can be modeled as a combination of free, spherical microemulsion droplets and wormlike chains with contour length  $L_C$  and Kuhn length  $b$ . For the wormlike chain we use Kholodenko's formula.<sup>[92]</sup>

**Form Factor of an Ellipsoid.** The surfactant micelles of the TDMAO/TTAB reference system can be described as ellipsoidal objects. To model the SANS data of these micelles an oblate spheroid ( $R_p < R_e$ ) model was used.

$$I_{spheroid} = V^2 \Delta SLD^2 \cdot \int_0^1 K^2 \left( q \sqrt{R_p^2 y^2 + R_e^2 (1-y)^2} \right) dy \quad (46)$$

$$\text{with: } V = \frac{4}{3} \pi R_e^2 R_p \quad (47)$$

$$K = 3 \cdot \frac{\sin x - x \cos x}{x^3} \quad (48)$$

**Repulsive and Attractive Structure Factor.** To describe the repulsive interactions of charged microemulsion droplets in combination with the attractive forces induced by the polyelectrolyte a structure factor based on the random phase approximation (RPA) was developed. The structure factor  $S(q)$  is related to the direct correlation function  $C(q)$ .

$$S(q) = \frac{1}{1 - {}^1NC(q)} \quad (49)$$

When the random phase approximation (RPA) is applied, the direct correlation function can be written as the sum of the different, independent contributions to the interaction potential.

$${}^1NC(q) = {}^1NC_0(q) - \frac{1}{k_B T} {}^1NU_{eff}(q) \quad (50)$$

Here,  $C_0(q)$  is the reference system correlation function and  $U_{eff}(q)$  is the Fourier transformed perturbation potential.

The potential in the sticky hard sphere model is described by Eq. 51

$$\frac{U(r)}{k_B T} = \begin{cases} \infty & \text{for } 0 < r < \sigma \\ \ln \frac{12\tau\Delta}{\sigma+\Delta} & \text{for } \sigma < r < \sigma + \Delta \\ 0 & \text{for } r > \sigma + \Delta \end{cases} \quad (51)$$

where  $\sigma$  is the hard sphere diameter ( $\sigma = 2R_{HS}$ ),  $\Delta$  is the width of the potential and  $\tau$  is the so-called stickiness parameter that characterizes the adhesive strength.

This potential was solved by Baxter analytically with the Percus-Yevick approximation:

$$\begin{aligned} C_0(q) = & \frac{2\eta\lambda}{\kappa} \sin(\kappa) - \frac{2\eta^2\lambda^2}{\kappa^2} (1 - \cos(\kappa)) \\ & - [\alpha\kappa^3 (\sin(\kappa) - \kappa \cos(\kappa)) + \beta\kappa^2 (2\kappa \sin(\kappa) - (\kappa^2 - 2) \cos(\kappa) - 2) \\ & + \frac{\eta\alpha}{2} ((4\kappa^3 - 24\kappa) \sin(\kappa) - (\kappa^4 - 12\kappa^2 + 24) \cos(\kappa) + 24) ] \end{aligned} \quad (52)$$

$$\begin{aligned}
\text{with: } \quad \kappa &= q \cdot \sigma \\
\eta &= \phi_{HS} \left( \frac{\sigma + \Delta}{\sigma} \right)^3 \\
\epsilon &= \tau + \frac{\eta}{1 - \eta} \\
\delta &= \phi_{HS} \frac{1 + \eta/2}{3(1 - \eta)^2} \\
\lambda &= \frac{6}{\eta} \left( \epsilon - \sqrt{\epsilon^2 - \delta} \right) \\
\mu &= \lambda \eta (1 - \eta) \\
\beta &= - \frac{3\eta(2 + \eta)^2 - 2\mu(1 + 7\eta + \eta^2) + \mu^2(2 + \eta)}{2(1 - \eta)^4} \\
\alpha &= \frac{(1 + 2\eta - \mu)^2}{(1 - \eta)^4}
\end{aligned}$$

when applied, the limit  $\Delta \rightarrow 0$  is taken, so that  $\eta = \phi_{HS}$ . In this case only the stickiness parameter  $\tau$  is left to characterize the adhesive strength. The stickiness parameter can be converted to the stickiness  $1/\tau$ .

The perturbation potential  $U_{eff}(q)$  is assumed to arise from the classical DLVO potential<sup>[125]</sup>:

$$U_{DLVO}(r) = \pi \varepsilon D_{eff}^2 \psi_{0,eff}^2 \frac{\exp(-(r - D_{eff})/k_D)}{r} \quad (53)$$

which is valid for  $r > D_{eff}$ . Here,  $D_{eff}$  is the effective diameter ( $D_{eff} = 2R_{HS}$ ). When the DLVO potential is applied together with the sticky hard sphere model, the same hard sphere radius should be used:  $2R_{HS} = D_{eff} = \sigma$ .  $k_D$  is the Debye screening length,  $\psi_{0,eff}$  in an effective surface potential and  $\varepsilon$  is the dielectric constant of the medium, which is calculated from the relative permittivity of vacuum and of the medium ( $\varepsilon = \varepsilon_0 \cdot \varepsilon_r$ ).

$$\psi_{0,eff} = \frac{Z \cdot e_0}{\pi \varepsilon D_{eff} (2 + D_{eff}/k_D)} \quad (54)$$

$$k_D = \left( \frac{\varepsilon \cdot k_B T}{2N_A \cdot e_0^2 \cdot I} \right)^{1/2} \quad (55)$$

With  $Z$  being the number of charges of the particle and  $e_0$  the elementary electric charge,  $N_A$  is the Avogadro constant and  $I$  the ionic strength. The Fourier transformation of Eq. 53 yields the expression needed for Eq. 50:

$$\frac{1}{k_B T} N \cdot U_{eff}(q) = 24 \phi_{HS} \cdot \gamma \cdot \exp(-s) \cdot \frac{\kappa \cdot \cos(\kappa) + s \cdot \sin(\kappa)}{\kappa(\kappa^2 + s^2)} \quad (56)$$

$$\text{with: } \quad s = D_{eff}/k_D \quad \gamma = \frac{1}{k_B T} \pi \varepsilon D_{eff} \psi_{0,eff}^2 \cdot \exp(s)$$



## C. Publications

Parts of this thesis are already published:

**M. Simon**, P. Krause, L. Chiappisi, L. Noirez, M. Gradzielski, "Structural control of polyelectrolyte/microemulsion droplet complexes (PEMECs) with different polyacrylates", *Chemical Science* **2019**, *10*, 385-397. DOI: [10.1039/c8sc04013c](https://doi.org/10.1039/c8sc04013c)

Reproduced from [73] with permission of the Royal Society of Chemistry.

**M. Simon**, E. Schneck, L. Noirez, S. Rahn, I. Davidovich, Y. Talmon, M. Gradzielski, "Effect of the Polymer Architecture on the Phase Behavior and Structure of Polyelectrolyte/Microemulsion Complexes (PEMECs)", *Macromolecules* **2020**, DOI: [10.1021/acs.macromol.0c00236](https://doi.org/10.1021/acs.macromol.0c00236)

Reproduced with permission from [108]. Copyright 2020, American Chemical Society.

Parts of this thesis are going to be published in the near future:

**M. Simon**, M. Gradzielski, I. Hoffmann, "Dynamics in Polyelectrolyte/Microemulsion Complexes", *submitted to Nanoscale Advances*.







## EDGE ARTICLE

Cite this: *Chem. Sci.*, 2019, 10, 385

All publication charges for this article have been paid for by the Royal Society of Chemistry

## Structural control of polyelectrolyte/microemulsion droplet complexes (PEMECs) with different polyacrylates†

Miriam Simon, <sup>\*a</sup> Patrick Krause,<sup>a</sup> Leonardo Chiappisi, <sup>ab</sup> Laurence Noirez <sup>c</sup> and Michael Gradzielski <sup>\*a</sup>

The ionic assembly of oppositely charged polyelectrolyte–surfactant complexes (PESCs) is often done with the aim of constructing more functional colloids, for instance as advanced delivery systems. However, PESCs are often not easily loaded with a solubilise due to intrinsic restrictions of such complexes. This question was addressed from a different starting point: by employing microemulsion droplets as heavily loaded surfactant systems and thereby avoiding potential solubilisation limitations from the beginning. We investigated mixtures of cationic oil-in-water (O/W) microemulsion droplets and oppositely charged sodium polyacrylate (NaPA) and determined structure and phase behaviour as a function of the mixing ratio for different droplet sizes and different  $M_w$  (NaPA). Around an equimolar charge ratio an extended precipitate region is present, which becomes wider for larger droplets and with increasing  $M_w$  of the NaPA. Static and dynamic light scattering (SLS and DLS) and small-angle neutron scattering (SANS) show the formation of one-dimensional arrangements of microemulsion droplets for polyelectrolyte excess, which become more elongated with increasing  $M_w$  (NaPA) and less so with increasing NaPA excess. What is interesting is a marked sensitivity to ionic strength, where already a modest increase to ~20 mM leads to a dissolution of the complexes. This work shows that polyelectrolyte/microemulsion complexes (PEMECs) are structurally very versatile hybrid systems, combining the high solubilise loading of microemulsions with the larger-scale structuring induced by the polymer, thereby markedly extending the concept of conventional PESCs. This type of system has not been described before and is highly promising for future applications where high payloads are to be formulated.

Received 10th September 2018

Accepted 15th October 2018

DOI: 10.1039/c8sc04013c

rsc.li/chemical-science

## Introduction

Microemulsions are thermodynamically stable liquid systems of water, oil and an amphiphile which are single-phase and optically isotropic<sup>1</sup> with structural properties that can be explained by the bending elasticity of their amphiphilic monolayers.<sup>2,3</sup> Frequent structural types are oil-in-water (O/W) droplets which naturally allow having a rather high content of hydrophobic material dispersed in aqueous solution, which otherwise could not be dissolved. From a fundamental point of view, O/W microemulsion droplets are interesting as they have a well-defined spherical structure and possess a low polydispersity when prepared close to the emulsification boundary.<sup>4</sup>

From a more practical point of view, microemulsions are an excellent medium for solubilizing active agents, as often needed for formulations in cosmetics, pharmacy, *etc.*<sup>5–8</sup> However, in order to make them more versatile for such applications one may have to add additives like polymers to microemulsions which allow modulating their properties.

In a similar direction, polyelectrolyte/surfactant complexes (PESCs) have been studied comprehensively in the past few years. Because of their large structural variety,<sup>9–11</sup> that arises from the local structuring by the surfactant and the larger scale structuring by the polymer, they are considered to be very attractive for the purposes of solubilisation and drug delivery.<sup>12,13</sup> They have for instance been explored for the case of cationic hydrogels and sodium dodecyl sulfate (SDS), where controlled release of a hydrophobic drug was achieved and the loading capacity depended markedly on the charge density of the polymer.<sup>14</sup> Work regarding the solubilisation in PESCs was done for the case of SDS/TX-100 micelles complexed with poly(dimethyldiallylammonium chloride) (PDADMAC). This system showed an unchanged solubilisation power in the complexes compared to the initially present micelles.<sup>15</sup> Other studies regarding the solubilisation of hydrophobic compounds

<sup>a</sup>Stranski-Laboratorium für Physikalische und Theoretische Chemie, Institut für Chemie, Technische Universität Berlin, D-10623 Berlin, Germany. E-mail: miriam.simon@tu-berlin.de; michael.gradzielski@tu-berlin.de

<sup>b</sup>Institut Laue-Langevin, 38042 Grenoble, France

<sup>c</sup>Laboratoire Léon Brillouin (CEA-CNRS), Uni. Paris-Saclay, CEA-Saclay, 91191 Gif-sur-Yvette, France

† Electronic supplementary information (ESI) available. See DOI: 10.1039/c8sc04013c

within PESCs were concerned with the contaminant oil trichloroethylene (TCE). They confirmed such a solubilisation behaviour of PESCs and their use allowed for enhanced separation by using colloid-enhanced ultrafiltration processes.<sup>16</sup> Apart from that, PESCs of oppositely charged surfactant micelles and double hydrophilic polyelectrolytes have been investigated with respect to their ability to solubilize drug molecules, as for instance done for the case of the cationic copolymer poly(ethylene oxide)-*g*-polyethyleneimine (PEO-*g*-PEI) and sodium oleate.<sup>17</sup> Central for a successful application here is a high drug loading as was seen for doxorubicin (DOX) in PESCs obtained from combining poly(ethylene glycol)-*block*-poly(4-vinylbenzylphosphonate) (PEG-*b*-PVBP) with cationic surfactants.<sup>18</sup> In general it is important to optimise the ability to solubilise hydrophobic compounds, but typically the solubilisation capacity for drugs or dye molecules in PESCs is rather limited since only certain surfactants show high solubilisation capacities.<sup>19</sup>

Accordingly an interesting alternative is to use microemulsion droplets, which are structurally well understood and already contain a large amount of solubilised hydrophobic compounds,<sup>20</sup> and to complex them with oppositely charged polyelectrolytes, thereby forming polyelectrolyte/microemulsion complexes (PEMECs). This approach avoids the need for optimising the solubilisation properties as it is intrinsically controlled by the microemulsions. It is interesting to note that such mixtures so far have only been investigated very scarcely. In contrast, for instance the modification of microemulsion viscosity by polymeric additives has been studied in some detail and can be enhanced largely by adding hydrophobically modified telechelic water-soluble polymers, where the effect depends largely on the length of the hydrophobic modification and the amount of the added polymer.<sup>21–26</sup> Similarly complexes between neutral amphiphilic polymers and water-in-oil (W/O) microemulsions have been studied<sup>27</sup> and they can also be transformed into a transient network by ABA copolymers where the A blocks are hydrophilic.<sup>28</sup> The effect of polyelectrolytes on the phase behaviour and structure of W/O microemulsions was also studied, but mostly with the aim of forming nanoparticles in these systems.<sup>29,30</sup> Note *et al.* investigated the phase diagram of a negatively charged SDS/pentanol based W/O microemulsion with the cationic polyelectrolyte PEI<sup>31</sup> and found that more than 30 wt% PEI can be incorporated within the aqueous phase. The incorporation of PEI leads to a substantial shift of the microemulsion regime within the phase diagram, leading to the formation of bicontinuous and even O/W structures. In one of the few investigations on cationic surfactant–polyanion complexes, it was found that the solubilisation capacity of the micelles increases in the presence of the polymer, due to the additional ionic strength.<sup>32</sup> If charged droplets bind to polymers through electrostatic interactions, bridging and/or compactions of the droplets would be expected as well as a decoration of the polyelectrolyte chains with microemulsion droplets.<sup>33</sup> In general, the same structural richness is expected here, as seen for PESCs, while guaranteeing a high hydrophobic loading of the surfactant aggregates.

However, nearly no research has been carried out on mixtures of charged microemulsion droplets with oppositely charged polyelectrolytes, where the complexation would be driven by electrostatic interactions and concomitant counterion release and the idea of gaining structural control of the microemulsion system on a larger length scale *via* polyelectrolyte addition has not been exploited yet.

In order to fill this scientific gap, we investigated oil-in-water (O/W) microemulsion droplets based on tetradecyldimethylamine oxide (TMDAO), which is known to form such microemulsions with different alkanes.<sup>34</sup> The droplet size can be increased in a systematic fashion by addition of a cosurfactant, as has been demonstrated in detail in the case of 1-hexanol.<sup>35</sup> In addition, these microemulsion droplets can become variably charged without modifying their structure by substituting small amounts of TMDAO with the equivalent cationic surfactant tetradecyltrimethylammonium bromide (TTAB).<sup>36–38</sup> Accordingly, these microemulsions are highly suited for a systematic investigation as they are at the same time a well-defined and monodisperse model colloid and attractive for potential applications. It might be noted that we stayed in the range of having small amounts of ionic surfactant as the microemulsion itself is in principle a nonionic one and we just introduced some charges to allow for ionic assembly. As a simple oppositely charged polyelectrolyte we chose the sodium salt of the flexible polyacrylic acid (PAA), sodium polyacrylate (NaPA).

In the present experiments we varied the mixing ratio of microemulsion and NaPA, the radius of the droplets and the molecular weight of the NaPA, with the aim to deduce systematic correlations between these parameters, the phase behaviour and the formed structures. We also studied the effect of the total concentration on the formed structures, as well as a variation of ionic strengths in order to modify the electrostatic interactions in these systems. For the structural characterisation, we employed static and dynamic light scattering, measurements of the  $\zeta$ -potential, and small-angle neutron scattering (SANS). With the systematic variation of all relevant system parameters, we were able to gain a comprehensive insight into the structural arrangements at the mesoscopic scale as a function of these parameters (since access to the structure and dynamics of self-assembled systems is the key for their understanding<sup>39</sup>). The combination of these experimental methods shows that the formed polyelectrolyte/microemulsion complexes (PEMECs) are rich in their morphology and controlled by their composition and the details of the polyelectrolyte and microemulsion droplet employed.

## Results and discussion

### Sample preparation

Unless stated otherwise, the oil-in-water (O/W) microemulsion droplets were prepared from a 100 mM stock solution of surfactant where always 5 mol% of zwitterionic TMDAO was substituted by cationic TTAB to obtain weakly charged droplets while keeping the total surfactant concentration constant. Different droplet sizes were achieved by adding different amounts of the cosurfactant hexanol (0, 50 and 75 mM)<sup>35</sup> and

saturating the mixture with decane (30, 80 and 200 mM, respectively), which resulted in droplet radii of 3.1, 4.3, and 6.4 nm (named ME00, ME50 and ME75, respectively).

Different amounts of sodium polyacrylate (NaPA) were added to the microemulsion in order to vary the charge ratio  $z = [-]/[+] + [-]$  of the polyelectrolyte/microemulsion complexes (PEMECs) (it might be noted that here we refer to nominal charges, *i.e.* ionised or ionisable groups ( $-\text{NMe}_3$  and  $-\text{COOH}$ ), and not actual charges, which for the NaPA and TDMAO depends on the pH and chemical surrounding). The pH was checked after preparation but not further modified in order not to add additional ions to the sample. All samples had pH-values between 7 and 8, where the polyacrylate is about 90% ionised (see Fig. S1†) and TDMAO is only little protonated.

Most samples were prepared from microemulsion and polyacrylate stock solutions, which were then mixed in the desired ratios. However, the same results (complex size and shape) were obtained by mixing all 'dry' compounds (TDMAO, TTAB, hexanol, decane, and NaPA) first and adding water afterwards (see Fig. S2† for SANS curves of such an example), so we can safely assume that the observed structures are in thermodynamic equilibrium as they don't depend on the sample history.

### Phase behaviour

The determination of the macroscopic phase behaviour is very important since systems of oppositely charged colloids and polyelectrolytes have a tendency to phase separate at the vicinity of charge neutralisation.<sup>9,10</sup> This situation is complicated by the fact that this phase separation often occurs very slowly and careful investigation over a period of many days or weeks may be required in order to determine the equilibrium phase diagram.

Mixtures of cationic O/W TDMAO/TTAB/decane microemulsion droplets with negatively charged polyacrylate (NaPA) were studied at a fixed surfactant concentration of 100 mM (5 mM cationic TTAB + 95 mM uncharged TDMAO) and different amounts of NaPA to obtain different mixing ratios. In order to gain a comprehensive overview over the phase

behaviour, samples were prepared with different microemulsion droplet sizes and different chain lengths of the NaPA. A wide range of precipitation is observed around equimolar charge mixing ( $z \sim 0.5$ ) and only for the microemulsion or polyelectrolyte excess single phases are found. It is interesting to note that the biphasic region of the phase diagram has a very asymmetric shape, *i.e.* a polyelectrolyte excess provides much higher colloidal stability to the systems.

Samples close to the charge equilibrium ( $z = 0.5$ ) phase separate directly after mixing while samples away from  $z = 0.5$ , especially at microemulsion excess, appear turbid at first and need hours or even days for macroscopic phase separation, see Fig. 1. Samples that show phase separation in less than an hour after mixing were labelled biphasic. Metastable samples are samples which need from one hour up to one week to phase separate. Directly after mixing, the metastable samples appeared clear, but then changed colour to bluish and eventually white, before phase separating into a clear liquid and a solid, white precipitate. All samples that still consist of one single phase after one week were considered as thermodynamically stable single phase systems, as they did not evolve during the course of several months (examples of such samples can be seen in Fig. S3†).

It was observed that larger droplets and increasing  $M_w$  of the NaPA both lead to a larger biphasic region in the phase diagram. This increase is mostly visible at small  $z$ -values (microemulsion excess), where the phase boundary is strongly affected, inducing a much more pronounced precipitation with increasing  $M_w$  of NaPA and microemulsion droplet size. In contrast, the behaviour of the phase boundary for large  $z$  (polyelectrolyte excess) is basically independent of the  $M_w$  of the NaPA (Fig. 1). Immediate phase separation was observed to take place much more likely for the case of large droplets, which indicates a substantially lower kinetic stability of their complexes. It occurs already for the shortest NaPA (for which the small 3.1 nm droplets show rather slow precipitation and the metastability allowed investigating the structures over the whole  $z$ -range by light and neutron scattering experiments). This means that the phase behaviour depends strongly on the precise composition of the PEMEC systems.

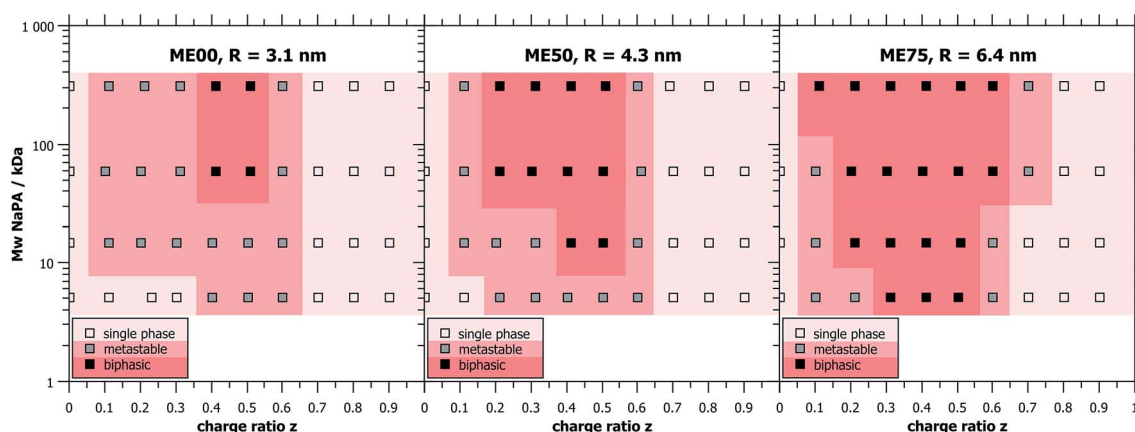


Fig. 1 Phase diagrams showing the biphasic and the metastable regions for ME00 ( $R = 3.1$  nm), ME50 ( $R = 4.3$  nm) and ME75 ( $R = 6.4$  nm) at  $c$  (surfactant) = 100 mM, mixed with NaPA of different molecular weights and at different charge ratios  $z$ .

For long time stable single phase regions for smaller or larger  $z$ , the samples show different optical appearances ranging from clear to bluish (when being closer to the precipitation area), which indicates the formation of differently sized complexes as a function of  $z$  (see Fig. S3†). The formation of mixed aggregates was confirmed by the values of the  $\zeta$ -potential that reverses sign upon the addition of the NaPA (Fig. 2). What is also interesting to note here is that the  $\zeta$ -potential is reduced very abruptly upon the addition of NaPA.

### Structural characterisation of stable polyelectrolyte/microemulsion complexes (PEMECs)

The study of the phase diagrams has enabled the identification of single-phase regions of the NaPA/ME mixtures, which are either stable or at least long-time metastable. We were now interested to determine how the colloidal structure of these PEMECs depends on their molecular composition.

The optical appearance of the samples and the  $\zeta$ -potential values suggest that differently sized mixed aggregates are formed, which was confirmed by static and dynamic light scattering (SLS and DLS). Since light scattering (both static and dynamic) does not allow deducing mesoscopic structural information, small-angle neutron scattering (SANS) was used to access a refined mesoscopic structural picture. In all these

experiments, we systematically varied the mixing ratio of NaPA to ME charges, the molecular weight  $M_w$  of the NaPA and the size of the droplets, thereby gaining an insight into how the structure of the PEMECs can be controlled by their composition.

**Variation of the mixing ratio.** SLS and DLS studies were carried out with a series where at least metastable homogeneous samples are obtained for all mixing ratios, *i.e.* small microemulsion droplets ( $R = 3.1$  nm, Fig. 1 left) with a degree of charging of 5 mol% and increasing amounts of added NaPA with  $M_w = 5.1$  kg mol<sup>-1</sup>, while the concentration of the surfactant (and therefore that of O/W microemulsion droplets) was kept constant at 100 mM. The molecular weight of the formed complexes obtained from SLS (Fig. 3A) and also the hydrodynamic radii deduced from DLS (Fig. 3B) show that the size of the aggregates increases upon addition of the polyelectrolyte until a maximum is reached close to the charge equilibrium. With increasing polyelectrolyte excess, the aggregates become smaller again. It should be noted here that for this series the hydrodynamic radii obtained by DLS are relatively small about 1–7 nm (these aggregates become much bigger for longer NaPA as discussed in the ‘Variation of the NaPA Chain Length’ and see *e.g.* Fig. S4†). For small  $z$ -ratios, at microemulsion excess, the given DLS values are actually smaller than the real size, as DLS measures the collective diffusion coefficient, which is largely influenced by the repulsive interactions within the sample. For obtaining a correct  $R_h$  value the collective diffusion coefficient would have to be corrected with the structure factor (for instance obtained from the SANS measurements) according to:  $D_{\text{coll}}(q) = D_0/S(q)$ . For example, for pure ME00 the measured diffusion coefficient is 143  $\mu\text{m}^2 \text{s}^{-1}$  and  $S(0) = 0.3$  (deduced from SANS) thereby leading to a  $D_0$  value of 43  $\mu\text{m}^2 \text{s}^{-1}$  and a hydrodynamic radius of 5.6 nm. For polyelectrolyte excess, where aggregation occurs, the measured  $R_h$  has to be reinterpreted as well, since, according to the SANS data (Fig. 4A), the formed aggregates are not spherical but elongated. The measured  $R_h$  can be converted into the length of a rod  $L$  (with fixed diameter  $d$ ):  $\frac{kT}{6\pi\eta R_h} = D_t = \frac{kT(\ln p + C_t)}{3\pi\eta L}$  with  $p = L/d$  and  $C_t = 0.312 + 0.565/p - 0.100/p^2$ .<sup>40</sup> For example a measured diffusion coefficient of 34.2  $\mu\text{m}^2 \text{s}^{-1}$  (ME00–NaPA05,  $z = 0.7$ ) equals an  $R_h$  of 7 nm and corresponds to a rod

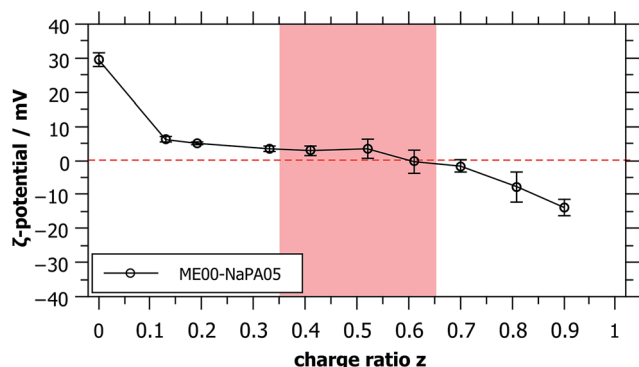


Fig. 2  $\zeta$ -Potential of microemulsion–polyelectrolyte complexes at different charge ratios, showing the transition from positively charged microemulsion droplets to negatively charged complexes. The metastable region is shaded in red.

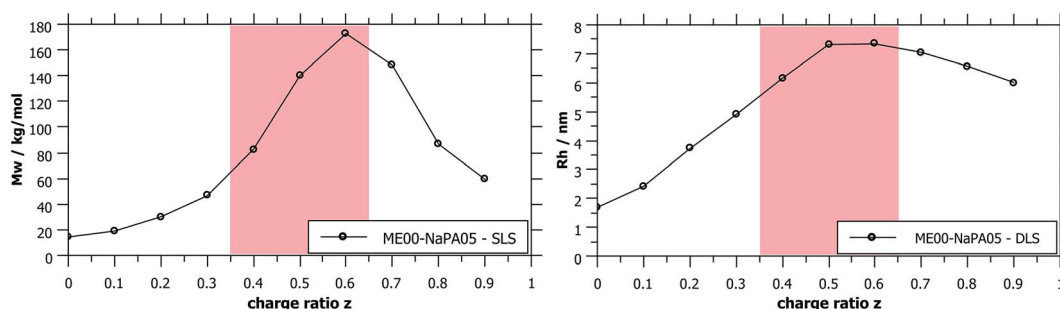


Fig. 3 Apparent  $M_w$  and  $R_h$  obtained from static and dynamic light scattering show the presence of differently sized aggregates of ME and PE depending on the charge ratio  $z$ . Metastable samples (shaded in red) were measured while still being homogeneous, typically being 3–5 days old. Measured values for longer NaPAs are given in Fig. S4†.

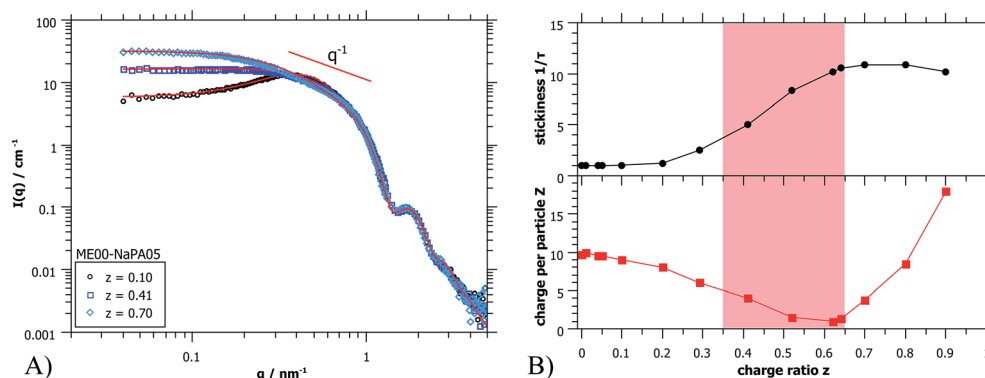


Fig. 4 (A) Fitted SANS spectra (PAXY at LLB) of three ME00–NaPA05 samples, showing the good agreement of the chosen structure factor model with the measured data points (fit curves as solid red lines). (B) Fit parameters ‘stickiness’  $1/\tau$  and ‘charge per particle’  $Z$  obtained from fitting the structure factor in dependence of the charge ratio  $z$ . The metastable region is shaded in red.

of 3 nm radius (one ME droplet) and 27 nm length (4.3 densely arranged droplets).

To complete the structural information gained from light scattering, additional SANS data were obtained. In Fig. 4A some selected SANS spectra for the same sample series are shown. The whole series is displayed in Fig. S5†. A very important finding is that the scattering curves for different charge ratios do not change at high  $q$  ( $q > 0.8 \text{ nm}^{-1}$ ), thereby indicating that in this size range ( $d < 8 \text{ nm}$ ), that characterizes the microemulsion droplets, the structure remains unchanged. It might be noted that this finding is valid in general for all systems investigated here, so the size, shape and polydispersity of the initially present microemulsion droplets are not affected by the addition of an oppositely charged polyelectrolyte. This is very important as it means that the microemulsion droplets remain structurally intact and would for instance be available as carriers in delivery systems.

The main difference in scattering intensity is seen at low  $q$  ( $q < 0.3 \text{ nm}^{-1}$ ), where the structure factor describes the interactions between the particles. This indicates that at small amounts of NaPA the charge of the ME droplets is screened and one observes a continuous increase of intensity with increasing content of NaPA ( $z = 0.0 - 0.5$ ). Once all ME charges are screened, the PE starts to introduce attractive interactions, which increases the intensity even further. For high NaPA excess ( $z > 0.6$ ) the intensity starts to decrease somewhat with increasing  $z$ , indicating a collapse of the structures, probably due to the large excess of negative charge and the resulting strong electrostatic repulsion between aggregates contained.

For quantitative analysis of the SANS curves the intensity  $I(q)$  was approximated as:

$$I(q) = {}^1NV^2\Delta\text{SLD}^2P(q)S(q) \quad (1)$$

where  ${}^1N$  is the number density of scattering particles,  $V$  the volume of the particles,  $\Delta\text{SLD}$  the contrast between aggregates and solvent (Table S1†),  $P(q)$  the hard sphere form factor (with a LogNormal size distribution) and  $S(q)$  the structure factor (experimental smearing was accounted for as described in (ref. 41) and the ESI†). The chosen model for  $S(q)$  for this series was

that of sticky hard spheres in Percus–Yevick approximation (Baxter model<sup>42</sup>) into which an electrostatic repulsion<sup>43</sup> was incorporated *via* random phase approximation (RPA) as previously done for ideal hard spheres.<sup>44</sup> In this fashion the structure factor accounts at the same time for the electrostatic repulsion between the equally charged microemulsion droplets and for the effective attractive interaction between the droplets that become bridged by the NaPA eqn (S4)–(S7) (ESI†). This model allows determining an effective charge per particle and the stickiness parameter  $1/\tau$ . The values are summarized in Fig. 4B and Table S2.† It can be seen that the deduced charge per particle decreases with increasing complexation by the NaPA within the surfactant excess region, but then increases again in the NaPA excess region. This may be explained partly by an overcharging due to the binding of the NaPA. It may also be explained by the increasing amount of NaPA chains that introduce steric and electrostatic repulsion. In our model (where the steric part arising from the excluded volume of the droplets is kept constant) the increase of charge can only be compensated by a larger charge, as it is the effective repulsive parameter. The stickiness parameter  $1/\tau$  is small but increases in the surfactant excess region and then becomes much larger in the NaPA excess regime, which indicates that here the droplet bridging is most effective.

This model works very well for small droplets and short PE chains. But only attractive and repulsive forces are not enough to describe the more elongated complexes as they are formed by higher  $M_w$  polyacrylates (see the ‘Variation of the NaPA Chain Length’).

**Variation of the microemulsion droplet size.** The previous measurements were done with small droplets of 3.1 nm hydrodynamic radius but complexes can also be formed with larger droplets of 4.3 and 6.4 nm, as already shown in the phase diagrams. The droplet size has no effect on their structural integrity during the complexation with NaPA, as seen in SANS (see Fig. S6†). However, the average number of charged surfactants in them varies substantially being 12.1, 23.2 and 51.5 respectively, with increasing size.

SLS measurements of samples with differently sized droplets but mixed with the same NaPA at the same charge ratio

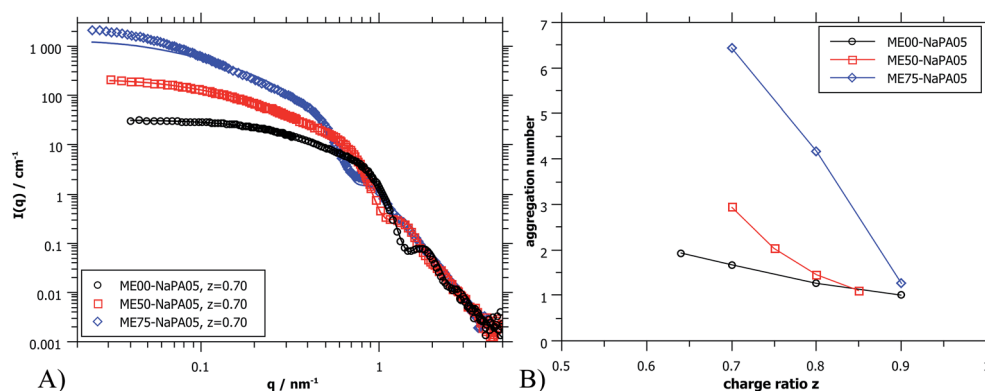


Fig. 5 (A) SANS scattering curves (ME00 and ME50 from PAXY at LLB and ME75 from D11 at ILL) of complexes formed with differently sized microemulsion droplets and NaPA05. Solid lines were calculated for a cylindrical arrangement of the droplets.<sup>45</sup> (B) Aggregation number  $N_{\text{agg}}$  of ME droplets contained in the aggregates as deduced from extrapolated  $I(0)$  values of SANS curves (for details see the ESI†).

naturally show a much higher intensity for bigger droplets, *i.e.* higher  $M_w$  complexes are formed, reaching values of  $10^6 \text{ g mol}^{-1}$  (it might also be noted that the hydrodynamic radius, measured with DLS, increases by a factor of 2.5, reaching values of 25 nm, see Fig. 6).

Again, further insight can be obtained from SANS measurements carried out at different mixing ratios  $z$  with all droplet sizes; the curves are shown in Fig. S6.† All series show the same general behaviour regardless of the droplet size, but the intensity extrapolated to  $q = 0$ ,  $I(0)$  (or equivalently the  $M_w$  of the complexes) increases strongly with increasing droplet size (see Fig. 5A, S7 and S8†). The number of microemulsion droplets contained in one complex was obtained from the scattering at zero angle,  $I(0)$  (obtained by extrapolation with Guinier approximation), compared to the forward scattering of a single non-interacting microemulsion droplet. This analysis is described in detail in the ESI† and results are shown in Fig. 5B. Here it was assumed that the contribution of the polyelectrolyte to the scattering intensity can be neglected in comparison to the scattering of the microemulsion droplets. This approach is only meaningful for polyelectrolyte excess as for microemulsion excess one just sees a modification of the interaction potential from which no aggregation number can be deduced. At polyelectrolyte excess, the highest aggregation numbers are found close to the phase boundary. Only 2 of the small droplets seem

to be effectively linked in one aggregate but this number increases to 3 and even 6 of the medium and large droplets. The corresponding number of NaPA chains per complex can be calculated as follows:

$$\frac{N_{\text{chains}}}{\text{complex}} = \frac{[\text{NaPA}]}{[\text{ME}]} N_{\text{agg}} = \frac{N_{\text{TTAB}}}{\text{DP}} \frac{z}{1-z} N_{\text{agg}} \quad (2)$$

where  $N_{\text{TTAB}}$  is the average number of TTAB molecules per droplet (see Table 1), DP is the average degree of polymerization and  $N_{\text{agg}}$  is the number of ME droplets per complex as obtained from Guinier approximation. The results are summarised in Table 2.

At first glance the results look counterintuitive, as for the small droplets this corresponds to a situation where only one NaPA is involved in the complex. This number then increases to  $\sim 14$  NaPA chains in one complex for the largest droplets (ME75). This increase can be explained by the higher number of

Table 1 Structural parameters of pure microemulsion droplets

Name	$c/\text{mM}$ (TDMAO/TTAB)	$c/\text{mM}$ (hexanol)	$c/\text{mM}$ (decane)	$R/\text{nm}$ (SANS)	[+]/droplet
ME00	95/5	0	30	3.1	12.1
ME50	95/5	50	80	4.3	23.2
ME75	95/5	75	200	6.4	51.5

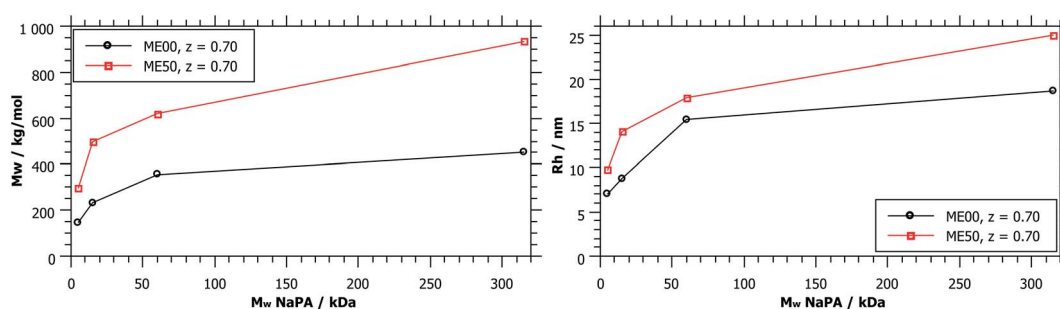


Fig. 6  $M_w$  and  $R_h$  obtained from static and dynamic light scattering as a function of  $M_w$  (NaPA), comparing different droplet sizes for a charge ratio  $z = 0.7$ .  $M_w$  (ME00) =  $52 \text{ kg mol}^{-1}$  and  $M_w$  (ME50) =  $110 \text{ kg mol}^{-1}$ .

Table 2 Structural parameters of different PEMECs from Guinier analysis

ME	NaPA	$z$	$N_{\text{droplets/complex}}$	$N_{\text{chains/complex}}$	Comment
ME00	5.1	0.7	1.7	1	Stiff rod
	15	0.7	2.6	0.5	Stiff rod
	60	0.7	8.8	0.4	Rod starts to bend
	315	0.7	15.7	0.2	Exact number of droplets not detectable
ME50	5.1	0.7	2.9	3	Stiff rod
	15	0.7	3.5	1.2	Rod starts to bend
	60	0.7	12.6	1	Exact number of droplets not detectable
	315	0.7	22.9	0.5	Exact number of droplets not detectable
ME75	5.1	0.7	6.4	14	Rod starts to bend

charges per droplet, which increases with increasing droplet size, and allows for a much more effective electrostatic polyelectrolyte/droplet interaction. At higher mixing ratios ( $z = 0.9$ ), the NaPA excess is high enough to stabilize each droplet separately, regardless of the size, so the value of  $N_{\text{agg}}$  drops to 1. In general, this is a relatively low number of aggregated microemulsion droplets compared to the typical aggregation number observed in PESCs, but it must also be noted that  $N_{\text{agg}}$  increases largely with increasing  $M_w$  of the NaPA (see the 'Variation of the NaPA Chain Length').

The most elongated complexes are present close to the phase boundary. SANS curves at  $z = 0.7$  (Fig. 5A and further curves are shown in S6†) were described by a model of spheres arranged in a cylindrical domain as described in (ref. 45) (for further details also see the ESI†). This model describes more correctly the low  $q$ -range of the curves as the sticky hard sphere model since it accounts more correctly for the local shape of the aggregates. Here the elongation becomes clearly more pronounced with increasing size of the microemulsion droplets.

**Variation of the NaPA chain length.** As illustrated in Fig. 4, SANS curves show a pronounced  $q^{-1}$  behaviour in the low  $q$ -range. This is observed mainly for samples close to the phase boundary, indicating locally rod-like structures. The experiments discussed so far were all done with the shortest NaPA of  $M_w = 5.1 \text{ kg mol}^{-1}$ . The stretched chain of this polyelectrolyte is about 14 nm long, so effectively only two microemulsion

droplets can be linked by one polyelectrolyte chain. As a next parameter variation, we increased the length of the NaPA chain to induce the formation of more elongated structures.

As shown in Fig. 1, complexes formed with longer NaPA chains have a larger two-phase region. For the stable samples in the range of NaPA excess SLS shows a significant increase of the molecular weight of the formed aggregates with increasing  $M_w$  of the NaPA (Fig. 6). Simultaneously the hydrodynamic radius determined by DLS substantially increases, for instance for the ME00 system rising from about 7 to almost 20 nm when increasing the  $M_w$  of the NaPA from 5.1 to 315  $\text{kg mol}^{-1}$ . The growth of PEMECs is confirmed by  $I(0)$  from SANS (Fig. S7 and S8†). It is also shown that this is a generic observation, which is valid for all droplet sizes.

The static light scattering at  $I(0)$  shows the formation of complexes of higher  $M_w$  but does not give further information regarding their structure. If a rod with a diameter of the droplet size was assumed, a measured diffusion coefficient of  $15.6 \mu\text{m}^2 \text{ s}^{-1}$  (ME00–NaPA60,  $z = 0.7$ ) would equal a length of 95 nm (15 densely arranged droplets). More information about the exact shape of the formed aggregates can be obtained from SANS measurements. A direct comparison of the SANS curves at a given mixing ratio  $z$  ( $z = 0.7$ ) and for identically sized microemulsion droplets (Fig. 7A) shows that with increasing  $M_w$  of the NaPA the SANS intensity at low  $q$  increases and shows a more pronounced linear part, which follows a  $q^{-1}$  law, thereby

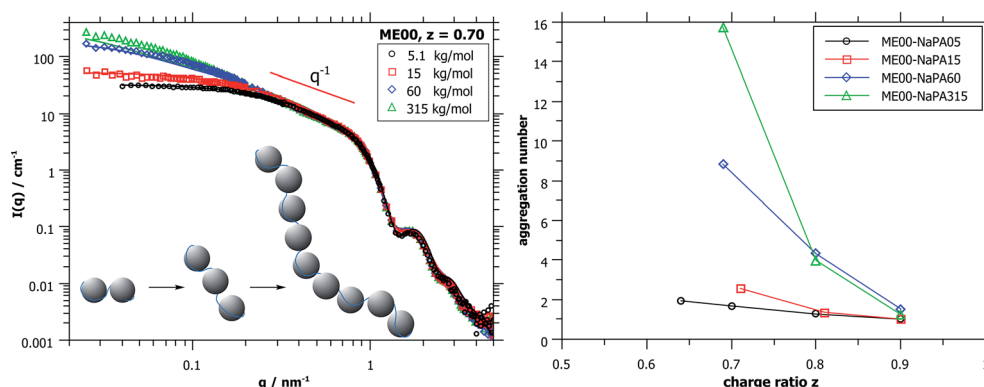


Fig. 7 (A) Comparison of complexes formed with ME00 and NaPA of different  $M_w$  at a charge ratio  $z = 0.7$  in the polyelectrolyte excess, where the biggest complexes are formed (NaPA05 and 15 from PAXY at LLB and NaPA60 and 315 from V4 at HZB). Solid lines were calculated for a cylindrical arrangement of the droplets. (B) Aggregation number  $N_{\text{agg}}$  deduced from extrapolated  $I(0)$  values of SANS data, compared for different NaPA chain lengths.

indicating the formation of increasingly more elongated complexes. The elongation of these complexes close to the phase boundary becomes more pronounced when a longer NaPA chain is employed.

One possible explanation for forming elongated complexes would be the transformation of many droplets into a cylinder with a diameter of one droplet. However, as mentioned before, the form factor minimum does not change, so the size and shape of the microemulsion droplets remain the same. Another way to form elongated complexes is by linking several droplets with polyelectrolyte chains in a cylindrical geometry. A comparison of the two models is given in Fig. S9,<sup>†</sup> showing the significantly better agreement of the second model with the measured data. Accordingly, this model was used to describe the SANS data and to quantify the elongation. The structural parameters for single microemulsion droplets were fixed to be those of the pure microemulsion sample. Additional parameters for the linear arrangement of the droplets are the number  $N$  of droplets per aggregate, the mean distance  $D$  between droplets in one aggregate and the polydispersity of this distance.

It has to be mentioned here that this model describes the measured data for short chains but the agreement becomes poorer with longer polyacrylate chains. This can be explained by the flexible nature of the polyacrylate backbone. In the model the droplets arrange to form a straight, stiff rod, which gives a slope of  $q^{-1}$  in the SANS data. In practice, however, longer aggregates composed of many droplets will tend to be less straight, which finally would lead to a slope of  $q^{-2}$  for Gaussian coils. The longest polyacrylate chain employed in this work has an  $M_w$  of 315 kDa with a stretched chain length of about 850 nm. This polyelectrolyte does not form straight rod-like complexes over the whole length scale but bends over its persistence length, and therefore the SANS data show a slope of  $q^{-1.5}$ .

The curves shown in Fig. 7A were described with cylindrical arrangements of 1.5, 3, 11 and 17 droplets per aggregate for  $M_w$ s of the NaPA of 5.1, 15, 60 and 315 kDa, respectively.<sup>45</sup> The model results for the longest NaPA (315 kDa) are not reliable anymore but here a number of 16 droplets per aggregate can be obtained from the  $I(0)$  value of the scattering data. More results obtained from the fits, also for larger droplets, are given in

Table S3,<sup>†</sup> while the aggregation numbers obtained from the forward scattering  $I(0)$  are given in Fig. 7B and Table 2.

**Concentration of the complexes.** Another parameter of interest is the total concentration. In order to address this point we investigated a concentration series of complexes of ME00 (smallest droplets with no added hexanol, because hexanol is partly water soluble, thereby complicating the dilution procedure) and 15 kg mol<sup>-1</sup> NaPA, prepared at 600 mM surfactant concentration and diluted down to 10 mM. It was observed that the colloidal stability mainly depends on the mixing ratio  $z$  and the  $M_w$  of the NaPA but not on the overall concentration. The samples stayed visually clear when diluted and no phase separation was observed. Selected SANS patterns for the microemulsion excess region ( $z = 0.1$ ) are shown in Fig. 8 (full set of data in Fig. S10<sup>†</sup>). They are normalized for the concentration (divided by the volume fraction of droplets,  $\phi$ ) and show nicely that upon dilution of the system the microemulsion correlation peak moves as expected to lower  $q$  (larger spacing). It is important to note here that the form factor minimum, which shows the droplet size, is at the same position for all concentrations. We can therefore assume that the spherical microemulsion droplets are still present down to surfactant concentrations of 10 mM and no bigger emulsion droplets have formed. However, at low concentration (below 100 mM of surfactant) one also observes a pronounced increase of the scattering intensity at low  $q$ . This can be attributed to the fact that at higher concentration the NaPA is able to bridge the microemulsion droplets yielding a space-filling network. However, once diluted too much this is no longer possible and now this network dissolves, thereby forming relatively large clusters that are scattering more strongly at low  $q$ .

The forward scattering intensities were obtained by Guinier approximation. The results are shown in Fig. 8B and it can be seen that this increase is much more marked on the side of microemulsion excess. Here one may argue that one observes a transition from a space-filling polyelectrolyte/microemulsion network at higher concentration to increasingly isolated clusters due to diluting below the effective overlap concentration. For  $z = 0.7$  a gradual increase of  $I(0)$  is observed. Because of the much higher starting concentration of NaPA no concentrations below

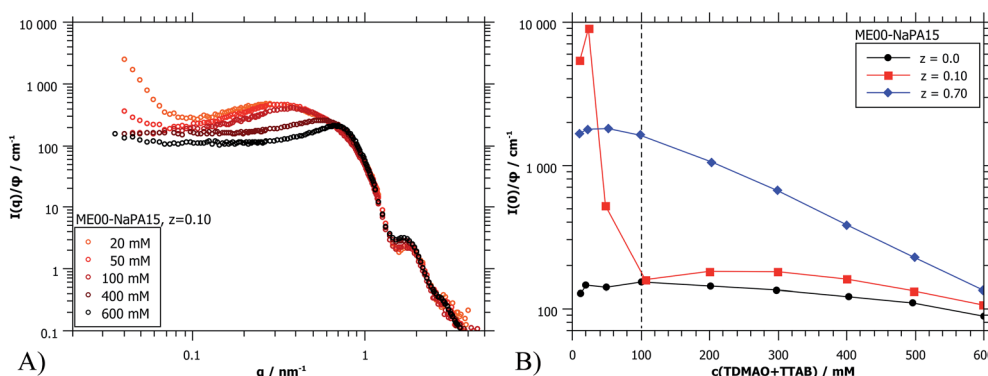


Fig. 8 (A) Selected SANS curves (PAXY at LLB) of the dilution series of ME00–NaPA15 complexes, normalized by volume fraction  $\phi$ . (B)  $I(0)/\phi$  for three different charge ratios; the charge ratios were chosen to be below and above the two phase region of the phase diagram. The dotted line shows the concentration of all other samples presented in this work.

the effective overlap concentration are reached. But below 100 mM no further changes of the scattering curves are seen upon still diluting further (Fig. 8B and S10†). Apparently here the system is diluted enough that individual complexes are visible.

**Effect of ionic strength – addition of salt.** Since the complexes examined in this study are always based on electrostatic interactions, it is interesting to investigate their behaviour at different ionic strengths. This was done by adding different amounts of sodium chloride to already formed complexes. Fig. 9A shows SANS curves at two different charge ratios of  $z = 0.1$  and  $0.7$  with added salt (50 mM) compared to the same samples without salt. The scattering curves show clearly that the repulsive interaction of the charged microemulsion droplets is strongly reduced (almost extinguished) as well as the attractive interaction of the complexes. This can be seen in the increased or decreased scattering at low  $q$  for the repulsive and attractive interaction, respectively. Complementary SANS curves for different amounts of added salt are given in Fig. S11.†

Fig. 9B shows  $I(0)$  as a function of ionic strength which modifies the interactions between the droplets. For the case of  $z = 0.1$  (microemulsion excess) the added salt apparently screens the charges of the microemulsion droplets already effectively for less than 20 mM NaCl. This is the expected behaviour for such systems as here the spacing between the droplets becomes much larger than the Debye screening length  $\delta$  (for 20 mM ionic strength:  $\delta = 2.3$  nm).<sup>36</sup> However, the behaviour of polyelectrolyte excess is surprising since a concentration of 50 mM seems to be sufficient to dissolve the PEMECs that are held together by electrostatic interactions. This is in striking contrast to observations for polyelectrolyte/surfactant complexes (PESCs) or interpolyelectrolyte complexes (IPECs), where typically an ionic strength of 500–700 mM is required in order to dissolve them.<sup>46–48</sup> Apparently the PEMECs studied here possess a very high degree of responsiveness to ionic strength.

## Discussion

These experimental observations can be interpreted in terms of molecular build-up of the studied PEMECs. The main parameters to be considered are:

- The length of the polyelectrolyte and its charge density.
- The size of the microemulsion droplets (controlled by the amount of 1-hexanol contained) and the number of charges (TTAB content) on them.
- Their mixing ratio as defined by  $z = [-]/([+] + [-])$ .
- The ionic strength of the solution.

When looking at the present PEMECs it is clear that especially the overlap concentration of the different NaPAs employed varies largely and therefore also their ability to build a space-filling polyelectrolyte network. On the other hand the microemulsion droplets have a rather low number of charges, with about one charge per 12 nm<sup>2</sup>, while the charge density along the NaPA backbone is rather high, with one charged unit per 0.25 nm (this situation is depicted in Fig. 10A). This makes their interaction delicate explaining why the larger droplets have a higher tendency for precipitating as here simply the number of charges per droplet is higher and therefore it allows more easily compensating for the high charge density of the NaPA (this even more so as they are curved less, thereby making it easier for the NaPA to bend around the microemulsion droplets).

Complexes with longer NaPAs (60 and 315 kg mol<sup>-1</sup>) prepared at polyelectrolyte excess ( $z > 0.5$ ) are already above the overlap concentration of the polyelectrolyte (calculated for a stretched chain). So, a network of polyelectrolyte chains is formed in the solution if no microemulsion droplets are present. Adding the oppositely charged microemulsion droplets deforms the network so that the droplets are arranged in one-dimensional complexes, which are held together by several NaPA chains (see Fig. 10B). Effective charge compensation by just one single NaPA chain is entropically unlikely. The extension of this cylindrical structure becomes larger with increasing  $M_w$  of the NaPA, as one may expect for longer chains. Therefore the length of one complex increases with increasing length of the NaPA chain, but only to a limited extent as the negative charge density of the complexes rapidly increases due to the fact that the charge density of the NaPA is much higher than that of the microemulsion droplets. This effect is influenced by the size of the droplets as with increasing size the local amount of positive charges increases and therefore the possibility of building larger aggregates becomes electrostatically enhanced.

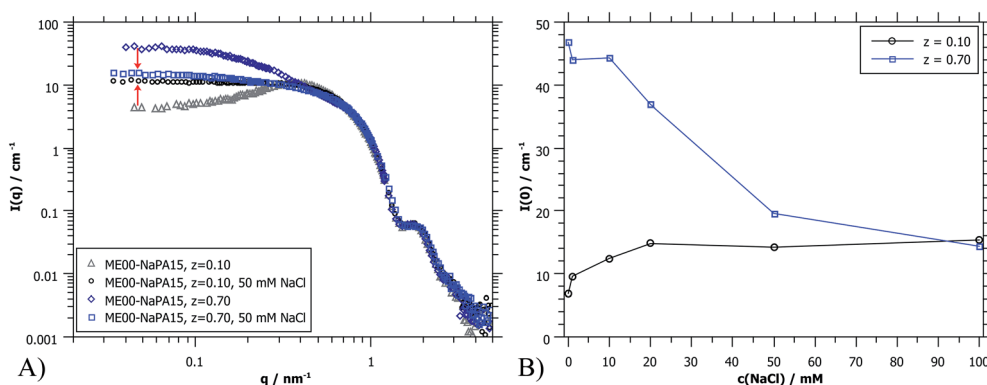


Fig. 9 (A) SANS curves (PAXY at LLB) of ME00–NaPA15 samples at two  $z$ -ratios (just below and just above the two phase region) before and after addition of 50 mM NaCl. (B)  $I(0)$  as obtained from SANS for the same samples with different amounts of NaCl added.

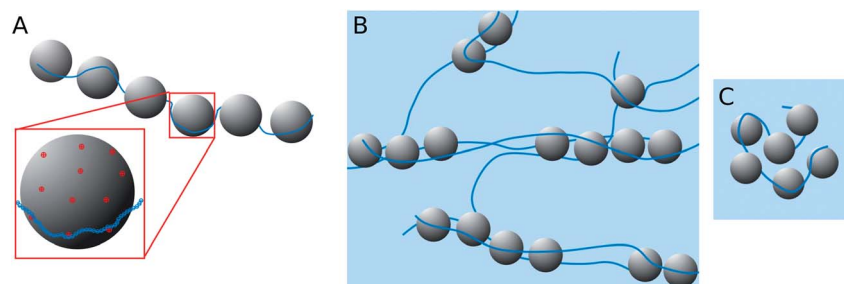


Fig. 10 Sketch of the structural arrangement in the TDMAO/TTAB/decane – NaPA polyelectrolyte/microemulsion complexes (PEMECs). (A) Single chain decorated NaPA chains (situation of ME excess) and zoom to the decoration of a droplet (drawn to scale for droplets with  $R = 3.1$  nm); (B) network with elongated complexes (situation with polyelectrolyte excess); (C) cluster with compacted ME droplets (situation with polyelectrolyte excess and high dilution).

This then explains the experimentally observed elongation of the complexes with increasing droplet size.

The behaviour is also interesting as a function of concentration. By dilution one will reach a critical concentration below the overlap concentration and therefore a network is no longer formed. For the case of polyelectrolyte excess, in the simplest case this then leads to a situation where a single NaPA chain will form a cluster which then contains the number of microemulsion droplets ( $[ME]/[PA]$ ) according to the stoichiometric composition (see Fig. 10C), which is given as:

$$\frac{[ME]}{[PA]} = \frac{DP}{N_{TTAB}} \frac{1-z}{z} \quad (3)$$

where DP is the average degree of polymerization and  $N_{TTAB}$  the average number of TTAB molecules per droplet (see Table 1). With this simple model we can calculate the expected number of microemulsion droplets per PE chain, which for the ME00 ( $R = 3.1$  nm,  $N_{TTAB} = 12.1$ ) droplet series just across the phase boundary ( $z = 0.70$ ) yields values of 1.9, 5.5, 22 and 115 for the 5.1, 15, 60 and 315 kDa NaPA, respectively. These values compare well with the data displayed in Fig. 9. For the longest NaPA chains the experimental values are still lower at the lowest experimental concentration, but they also still increase upon dilution in the light scattering experiment, as for the very long chains it is getting increasingly difficult to reach the dilute regime, where only single ME-decorated chains are still visible. Accordingly, under dilute conditions one really forms complexes that are based on a single PE chain as depicted in Fig. 10C.

Finally, the rather pronounced sensitivity of the complexes to the addition of salt can be discussed in the context of the driving force of complexation. For the case of counterion release by electrostatic binding of negative polyelectrolyte charges to the positive charges of the microemulsion droplets the driving force can be estimated by  $\Delta G_{com} = NkT \ln(V_2/V_1)$ .  $V_2$  is the volume available per counterion after complexation and  $V_1$  before complexation. However, the value of  $V_1$  for the droplets should be much larger than for an ionic surfactant micelle due to the much lower charge density on the droplet surface, in our case this charge density is only 5% (the droplets contain only 5 mol% of ionic surfactant). Accordingly, the volume ( $V_1$ ) available per ion should be about 20 times more than for a pure

micelle (the volume per ion will be given by the surface area times a layer thickness, which should be about the same for both cases and be less than the Bjerrum length).  $V_2$  is the volume in solution per free ion, which is inversely proportional to the total ion concentration in solution. Therefore in order that  $\Delta G_{com}$  becomes zero (and the driving force for complexation vanishes) if  $V_1$  is by a factor of 20 larger one may estimate that a correspondingly lower salt concentration is already effective in dissolving the complexes. This was observed experimentally in this work, as 20–50 mM of salt were enough to dissolve the PEMECs while for typical PESCs 500–700 mM of salt are needed.<sup>46–48</sup>

## Conclusions

In this work, for the first time, the complex formation between oppositely charged oil-in-water (O/W) microemulsion droplets and polyelectrolytes was systematically studied. The charge on the droplets was kept relatively low by only having 5% of the surfactant head groups charged. This allows forming hybrid systems (polyelectrolyte/microemulsion complexes: PEMECs) with highly loaded surfactant carriers in a simple way. To obtain a broad overview of the behaviour of this system, the charge ratio  $z$  between the microemulsion and polyelectrolyte (sodium polyacrylate, NaPA), the size of the microemulsion droplets, the NaPA chain length and the overall concentration were varied.

Phase diagrams showed that the region of stable complexes becomes smaller with increasing  $M_w$  of the NaPA and with increasing size of the microemulsion droplets, as the larger droplets can interact more effectively with the polyelectrolyte. Depending on the charge ratio  $z$  between the microemulsion and polyelectrolyte, differently sized and shaped complexes are formed as examined in detail with SANS measurements. In the microemulsion excess region and at high enough concentration the added NaPA simply interconnects microemulsion droplets and reduces their repulsive interactions. The binding to the droplets can be seen in the decreasing number of charges per droplet that was obtained from the structure factor and when diluting the sample below a critical concentration. As  $z$  increases further, the complexes quickly become unstable. The closer the charge ratio is to the charge equilibrium, the more

easily the samples precipitate as there is less excess charge for stabilisation.

In the polyelectrolyte excess region the complexes are negatively charged on the outside and therefore electrostatically stabilised. The biggest complexes were found close to the phase boundary and they become smaller with increasing polyelectrolyte excess (larger  $z$ ). In this region structural changes of the complexes were found. Close to the phase boundary, the complexes have a cylindrical shape and are more elongated with longer polyelectrolyte chains. At very high  $z$ -values, the NaPA excess is high enough to stabilize each droplet separately. The dependence of the complexes on  $z$  was similar for all tested droplet sizes and NaPA chain lengths. The effect was more pronounced for larger droplets, which lead to bigger complexes, as well as for longer NaPA chains. With longer NaPA chains it is possible to link more droplets, so more elongated aggregates are formed.

Upon dilution, one forms complexes of single PE chains decorated with a stoichiometric number of ME droplets, which means that the aggregation number of the effectively observed complexes increases upon dilution. What is also interesting is the high sensitivity of the complexes to salt addition. This can be explained by the rather low charge density of the ME droplets and the correspondingly reduced entropy gain by counterion release in the complexation process.

In summary it can be stated that the examined complexes of O/W microemulsion droplets with oppositely charged polyelectrolytes (PEMECs) are structurally very versatile hybrid systems, responsive to concentration and ionic strength. Many different properties in architecture and size are accessible by systematically tuning the composition. For instance the complex size increases by having longer NaPA chains and bigger ME droplets. Using a microemulsion instead of micelles makes PEMECs markedly superior to conventional PESCAs as loaded colloidal carrier systems. This allows combining the high loading capacity of a microemulsion with mesoscopic structuring *via* polyelectrolyte complexation, thereby having the functionality of both components within a self-assembled hybrid system. Such systems are highly promising for future fundamental investigations and applications in which a high payload is to be formulated within a complex colloidal system, thereby advancing the field of colloid science into the area of controlling microemulsion properties by ionic assembly.

## Experimental section

### Materials

The surfactants used in the experiments were tetradecyldimethylamine oxide (TDMAO, received as a gift from Stepan company, USA, as a 25% TDMAO solution in water named Ammonyx M. The solution was freeze dried before use) and tetradecyldimethylammonium bromide (TTAB, 99%, Sigma Aldrich, used without further purification). 1-Hexanol (>98%, MERCK-Schuchardt OHG) was used as a cosurfactant and decane (>98%, Fluka Chemika) as oil to form the microemulsions.

The employed polyelectrolyte is the sodium salt of polyacrylic acid (PAA), *i.e.*, sodium polyacrylate (NaPA) which was either purchased directly or prepared by adding a stoichiometric amount of NaOH to the PAA. The molecular weights used in this work were: 5.1 kg mol<sup>-1</sup> (DP = average degree of polymerization  $[-]/\text{polymer} = 54$ ; sodium salt, used as obtained from Sigma Aldrich), 15 kg mol<sup>-1</sup> (DP = 160; sodium salt solution from Sigma Aldrich, freeze dried before use), 60 kg mol<sup>-1</sup> (DP = 638; sodium salt, used as obtained from Fluka Chemika) and 240 kg mol<sup>-1</sup> (PAA; solution from Acros Organics, prepared by adding a stoichiometric amount of NaOH to the solution and freeze dried before use, which results in an average molecular weight of 315 kg mol<sup>-1</sup> for NaPA, DP = 3330). These molecular weights correspond to the lengths of the stretched polyelectrolyte of 14, 40, 160, and 850 nm respectively. The corresponding overlap concentrations for these polymers (assuming fully stretched chains) are 32, 3.9, 0.25, and 0.007 mM (in monomer units).

All samples were prepared in Milli-Q water or D<sub>2</sub>O (>99.5% D, Eurisotop) for the SANS experiments.

### Methods

Static (SLS) and dynamic (DLS) light scattering measurements were performed simultaneously on an ALV/CGS-3 instrument, with a He-Ne laser with a wavelength of  $\lambda = 632.8$  nm. Pseudo-cross-correlation functions were recorded using an ALV 5000/E multiple- $\tau$  correlator at scattering angles  $\theta$  ranging from 40 to 130° set with an ALV-SP 125 goniometer. The SLS curves were recorded in the same range of the magnitude of the scattering vector ( $q$ ), with

$$q = \frac{4\pi n_0 \sin(\theta/2)}{\lambda} \quad (4)$$

where  $n_0$  is the refractive index of the solution and  $\theta$  the scattering angle. All measurements were carried out at  $25.0 \pm 0.1$  °C in a thermostated toluene bath.

Small angle neutron scattering (SANS) experiments were carried out on the PAXY instrument of the Laboratoire Léon Brillouin (LLB) in Saclay. Measurements were performed in three configurations with sample-to-detector distances of 1.2, 2, and 6 m, collimation lengths of 2, 2, and 6 m and wavelengths of 4, 10, and 10 Å, respectively, to cover a  $q$  range from 0.031 to 5.05 nm<sup>-1</sup>.

Some additional SANS measurements were performed on the V4 instrument at the Helmholtz Zentrum Berlin (HZB).<sup>49</sup> The samples were measured at wavelengths of 4.5, 4.5 and 10 Å with sample to detector distances of 1.35, 6.75 and 15.75 m and collimation length of 2, 8 and 16 m respectively.

Further measurements were performed on the D11 instrument at the Institut Laue-Langevin (ILL) in Grenoble.<sup>50,51</sup> The samples were measured at a wavelength of 6 Å with sample to detector distances of 1.5, 8 and 34 m and collimation lengths of 8, 8 and 34 m, respectively.

Data reduction for PAXY and V4 data was done using Ber-SANS software.<sup>52</sup> For the D11 data, LAMP software was used.<sup>53</sup> The raw intensity data were corrected for the scattering of the

background (solvent and sample containers) and weighted by the transmission of the sample. Additionally, the (electronic) background noise was subtracted using a cadmium sample, which absorbs all incoming neutrons. The normalization and absolute scaling were done by using a 1 mm reference sample of distilled water, as an isotropic scatterer. Finally, the 2D data were radially averaged in 1D scattered intensity.

The wavelength smearing of the PAXY and V4 data described by the corresponding resolution parameters was incorporated into the analysis using SASfit software.<sup>54</sup> The wavelength spread (FWHM) was 10% and the detector pixels were  $5 \times 5$  mm for both instruments. For D11 measurements the wavelength smearing was included in the x-error. More details are given in the ESI.†

SANS fits were performed in absolute units and it was assumed that all of the surfactant, cosurfactant, and oil are contained in the aggregates. Due to the low concentration and its rather homogeneous distribution in the sample, the polyelectrolyte was not considered explicitly for modelling of the data. More information on the models used to describe the SANS data is given in the ESI.†

ζ-Potential measurements were performed using a Litesizer 500 (Anton Paar) at 25 °C and a wavelength of  $\lambda = 658$  nm and with a laser power of 40 mW.

## Conflicts of interest

There are no conflicts to declare.

## Acknowledgements

We thank the Laboratoire Léon Brillouin (LLB), the Helmholtz-Zentrum Berlin (HZB) and the Institut Laue-Langevin (ILL) for allocated beamtimes. We also thank Sylvain Prévost for his support during the SANS beamtime at LLB and Uwe Keiderling for his support during the beamtime at HZB. M. Simon thanks the TU Berlin for funding her PhD project.

## Notes and references

- 1 I. Danielsson and B. Lindman, *Colloids Surf.*, 1981, **3**, 391–392.
- 2 P. G. De Gennes and C. Taupin, *J. Phys. Chem.*, 1982, **86**, 2294–2304.
- 3 M. Gradzielski, D. Langevin and B. Farago, *Phys. Rev. E*, 1996, **53**, 3900–3919.
- 4 S. H. Chen, *Annu. Rev. Phys. Chem.*, 1986, **37**, 351–399.
- 5 P. P. Constantinides, *Pharm. Res.*, 1995, **12**, 1561–1571.
- 6 J. Lu, P. J. Liyanage, S. Solairaj, S. Adkins, G. P. Arachchilage, D. H. Kim, C. Britton, U. Weerasooriya and G. A. Pope, *J. Pet. Sci. Eng.*, 2014, **120**, 94–101.
- 7 J. Henle, P. Simon, A. Frenzel, S. Scholz and S. Kaskel, *Chem. Mater.*, 2007, **19**, 366–373.
- 8 P. Boonme, *J. Cosmet. Dermatol.*, 2007, **6**, 223–228.
- 9 L. Chiappisi, I. Hoffmann and M. Gradzielski, *Soft Matter*, 2013, **9**, 3896–3909.
- 10 D. Langevin, *Adv. Colloid Interface Sci.*, 2009, **147–148**, 170–177.
- 11 M. Rinaudo, N. R. Kil'deeva and V. G. Babak, *Russ. J. Gen. Chem.*, 2008, **78**, 2239–2246.
- 12 L. Chiappisi, M. Simon and M. Gradzielski, *ACS Appl. Mater. Interfaces*, 2015, **7**, 6139–6145.
- 13 K. Petrak, *J. Bioact. Compat. Polym.*, 1986, **1**, 202–219.
- 14 W. Wang and S. A. Sande, *Langmuir*, 2013, **29**, 6697–6705.
- 15 E. A. Sudbeck, P. L. Dubin, M. E. Curran and J. Skelton, *J. Colloid Interface Sci.*, 1991, **142**, 512–517.
- 16 H. Uchiyama, S. D. Christian, E. E. Tucker and J. F. Scamehorn, *AIChE J.*, 1994, **40**, 1969–1975.
- 17 T. K. Bronich, A. Nehls, A. Eisenberg and A. V. Kabanov, *Colloids Surf., B*, 1999, **16**, 243–251.
- 18 M. Kamimura, J. O. Kim, A. V. Kabanov, T. K. Bronich and Y. Nagasaki, *J. Controlled Release*, 2012, **160**, 486–494.
- 19 H. Katumitu, S. Satoshi, S. Shin-ichiro, S. Iwao and J. C. T. Kwak, *Bull. Chem. Soc. Jpn.*, 1995, **68**, 2179–2185.
- 20 M. Gradzielski, S. Prévost and T. Zemb, *Adv. Colloid Interface Sci.*, 2017, **247**, 374–396.
- 21 M. Gradzielski, A. Rauscher and H. Hoffmann, *J. Phys. IV*, 1993, **3**, C1-65–C1-79.
- 22 M. Odenwald, H.-F. Eicke and W. Meier, *Macromolecules*, 1995, **28**, 5069–5074.
- 23 E. Michel, M. Filiali, R. Aznar, G. Porte and J. Appell, *Langmuir*, 2000, **16**, 8702–8711.
- 24 P. Malo de Molina, C. Herfurth, A. Laschewsky and M. Gradzielski, *Langmuir*, 2012, **28**, 15994–16006.
- 25 M. Schwab and B. Stühn, *J. Chem. Phys.*, 2000, **112**, 6461–6471.
- 26 P. Malo de Molina, M. S. Appavou and M. Gradzielski, *Soft Matter*, 2014, **10**, 5072–5084.
- 27 A. Holmberg, P. Hansson, L. Piculell and P. Linse, *J. Phys. Chem. B*, 1999, **103**, 10807–10815.
- 28 C. Quellet, H. F. Eicke, G. Xu and Y. Hauger, *Macromolecules*, 1990, **23**, 3347–3352.
- 29 J. Koetz, J. Bahnemann, G. Lucas, B. Tiersch and S. Kosmella, *Colloids Surf., A*, 2004, **250**, 423–430.
- 30 J. Baier, J. Koetz, S. Kosmella, B. Tiersch and H. Rehage, *J. Phys. Chem. B*, 2007, **111**, 8612–8618.
- 31 C. Note, J. Koetz and S. Kosmella, *J. Colloid Interface Sci.*, 2006, **302**, 662–668.
- 32 H. Zhang, L. Deng, P. Sun, F. Que and J. Weiss, *J. Colloid Interface Sci.*, 2016, **461**, 88–95.
- 33 E. Buhler, J. Appell and G. Porte, *J. Phys. Chem. B*, 2006, **110**, 6415–6422.
- 34 G. Oetter and H. Hoffmann, *Colloids Surf.*, 1989, **38**, 225–250.
- 35 M. Gradzielski, H. Hoffmann and D. Langevin, *J. Phys. Chem.*, 1995, **99**, 12612–12623.
- 36 M. Gradzielski and H. Hoffmann, *Adv. Colloid Interface Sci.*, 1992, **42**, 149–173.
- 37 M. Gradzielski and H. Hoffmann, *J. Phys. Chem.*, 1994, **98**, 2613–2623.
- 38 B. Farago and M. Gradzielski, *J. Chem. Phys.*, 2001, **114**, 10105–10122.
- 39 M. Gradzielski, *Curr. Opin. Colloid Interface Sci.*, 2004, **9**, 256–263.

- 40 A. Ortega and J. García de la Torre, *J. Chem. Phys.*, 2003, **119**, 9914–9919.
- 41 J. S. Pedersen, D. Posselt and K. Mortensen, *J. Appl. Crystallogr.*, 1990, **23**, 321–333.
- 42 R. J. Baxter, *J. Chem. Phys.*, 1968, **49**, 2770–2774.
- 43 M. J. Grimson, *J. Chem. Soc., Faraday Trans. 2*, 1983, **79**, 817–832.
- 44 L. Baba-Ahmed, M. Benmouna and M. J. Grimson, *Phys. Chem. Liq.*, 1987, **16**, 235–238.
- 45 L. Chiappisi, S. Prévost and M. Gradzielski, *J. Appl. Crystallogr.*, 2014, **47**, 827–834.
- 46 M. Skepo and P. Linse, *Phys. Rev. E*, 2002, **66**, 051807.
- 47 M. Burkhardt, M. Ruppel, S. Tea, M. Drechsler, R. Schweins, D. V. Pergushov, M. Gradzielski, A. B. Zevin and A. H. E. Müller, *Langmuir*, 2008, **24**, 1769–1777.
- 48 K. Pojyak, E. Bertalanits and R. Meszaros, *Langmuir*, 2011, **27**, 9139–9147.
- 49 U. Keiderling and A. Wiedenmann, *Phys. B*, 1995, **213&214**, 895–897.
- 50 K. Lieutenant, P. Lindner and R. Gahler, *J. Appl. Crystallogr.*, 2007, **40**, 1056–1063.
- 51 L. Chiappisi, M. Gradzielski, I. Hoffmann, R. Schweins, M. Simon and H. Yalcinkaya, *Interconnecting charged microemulsion droplets via oppositely charged polyelectrolyte – effect of polyelectrolyte structure*, Institut Laue-Langevin (ILL), 2016, DOI: 10.5291/ILL-DATA.9-12-421.
- 52 U. Keiderling, *Appl. Phys. A*, 2002, **74**, 1455–1457.
- 53 D. Richard, M. Ferrand and G. J. Kearley, *J. Neutron Res.*, 1996, **4**, 33–39.
- 54 I. Breßler, J. Kohlbrecher and A. Thünemann, *J. Appl. Crystallogr.*, 2015, **48**, 1587–1598.



## Effect of Polymer Architecture on the Phase Behavior and Structure of Polyelectrolyte/Microemulsion Complexes (PEMECs)

Miriam Simon,<sup>\*</sup> Emanuel Schneck, Laurence Noirez, Sofia Rahn, Irina Davidovich, Yeshayahu Talmon, and Michael Gradzielski<sup>\*</sup>



Cite This: *Macromolecules* 2020, 53, 4055–4067



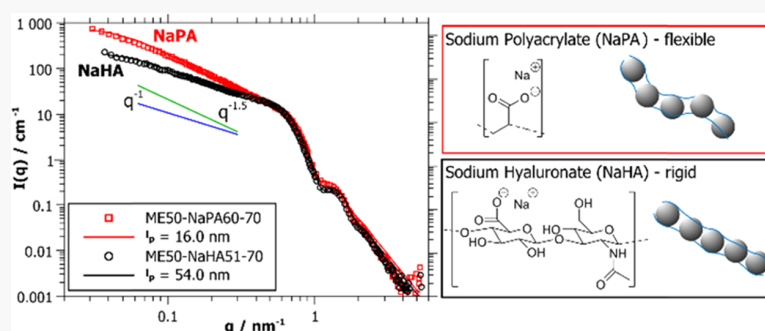
Read Online

ACCESS |

Metrics & More

Article Recommendations

Supporting Information



**ABSTRACT:** We studied polyelectrolyte/microemulsion complexes (PEMECs) formed by the biopolymer sodium hyaluronate (NaHA) and cationic oil-in-water (O/W) microemulsion droplets. Around equimolar charge conditions, a two-phase region with a liquid–liquid phase separation (coacervate formation) is observed, while mixed complexes are formed at polyelectrolyte excess. The largest complexes are found close to the phase boundary. The detailed structure of these complexes was determined by a combination of static and dynamic light scattering (SLS and DLS), small-angle neutron scattering (SANS), and cryo-transmission electron cryomicroscopy (cryo-TEM). Interestingly, these complexes formed with NaHA are much more elongated compared to previously studied complexes formed with sodium polyacrylate (NaPA). Similar observations were made for another polysaccharide, sodium carboxymethyl cellulose (NaCMC). Apparently, the persistence length of the complexes is largely proportional to the persistence length of the polyelectrolyte, which was determined by analyzing the SANS data with a specifically developed model. Accordingly, the size of the complexes formed with stiffer biopolyelectrolytes becomes much larger, increasing with the molecular weight ( $M_w$ ) of the polyelectrolyte. In summary, we conclude that the size and structure of the PEMECs can be controlled by the type of polyelectrolyte, mixing ratio, size of the microemulsion droplets, and  $M_w$  of the polyelectrolyte. This means that the polyelectrolyte addition can be used as a key structuring element for the size and shape of such complexes.

### INTRODUCTION

Microemulsions classically come in the structural form of oil-in-water (O/W), or water-in-oil (W/O) droplets, or as bicontinuous structures.<sup>1,2</sup> These structures are stabilized by the presence of a surfactant (and often also a cosurfactant<sup>3,4</sup>). Their structural units are typically in the size range of 2–20 nm, which explains their optical transparency. O/W microemulsion systems are particularly promising because of the high solubilization capacity for hydrophobic molecules in aqueous solution, which plays a key role in delivery systems, detergency, decontamination, etc.<sup>5–7</sup>

Microemulsion droplet systems have been studied to some extent. However, for some applications, one might be interested in modifying their properties and/or superstructures for further purposes. A classical case is the viscosity control, as microemulsions are generally low-viscous liquids, but for many applications, higher viscosities are required. This question is

usually addressed by either enhancing the viscosity of the continuous phase<sup>8</sup> or cross-linking individual droplets by a polymer with a number of hydrophobic linkers.<sup>9,10</sup>

Another interesting colloidal system constitutes polyelectrolyte/surfactant complexes (PESCs), which are formed by the ionic assembly of oppositely charged surfactant and polyelectrolyte.<sup>11</sup> It has been shown that the electrostatic interactions of charged surfactants with oppositely charged polyelectrolytes can induce a pronounced viscosity increase for certain compositions.<sup>12</sup> Often PESCs are studied in the context

**Received:** January 30, 2020

**Revised:** April 10, 2020

**Published:** May 6, 2020



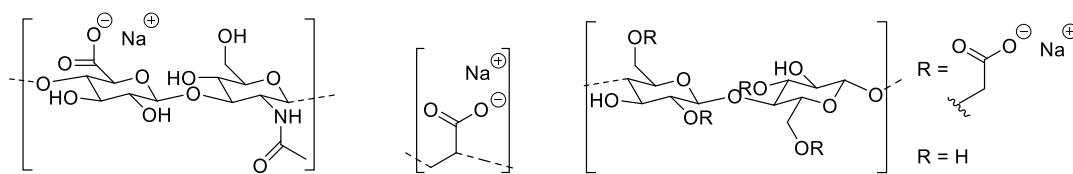


**Figure 1.** Chemical structures of sodium hyaluronate (NaHA, left), sodium polyacrylate (NaPA, middle), and sodium carboxymethyl cellulose (NaCMC, right).

of drug delivery<sup>13,14</sup> or cosmetical and detergency formulations.<sup>15</sup> However, such formulations and applications require good solubilization properties, and that is often a major difficulty in PESCs<sup>16</sup> and accordingly has hampered their further development in this direction. Yet, this problem can become circumvented by starting with ionic O/W microemulsion droplets to be complexed with an oppositely charged polyelectrolyte. Such a system combines the high solubilization capacity of the microemulsion with the mesoscopic structuring effect of the polyelectrolyte.

Recently, a detailed study of the phase behavior and structure of complexes of O/W microemulsion droplets with polyacrylate (NaPA) has been carried out by some of us.<sup>17</sup> It was observed that such mixtures form self-assembled complexes with elongated structures, where the detailed structure depends markedly on the weight average molecular weight,  $M_w$ , of the polyelectrolyte, as well as on the size of the microemulsion droplets. These interesting findings can serve as a basis for further fundamental understanding of the assembly conditions. To develop more biofriendly formulations, it is important to explore how a change from the petrol-based and non-biodegradable polyacrylate to a biopolyanion affects the structures formed in polyelectrolyte/microemulsion complexes (PEMECs). In particular, the type of polyelectrolyte (persistence length, charge density, strength of interaction) can be expected to play a key role in the structures formed in these complexes since it is also an important factor in PESCs.<sup>18</sup> The development of biofriendly materials is naturally important for applications in biomedicine, food modification, or wastewater treatment, where biocompatibility is of crucial importance.<sup>19–23</sup> However, on a more general note, sustainable materials derived from renewable resources are generally needed in all industry sectors to ensure our high standard of living and the well-being of our planet in the future.

To elucidate this question, we studied complexes of the previously investigated O/W microemulsion droplets<sup>3,24</sup> composed of tetradecyldimethylamine oxide (TDMAO), tetradecyl-trimethyl-ammonium bromide (TTAB), 1-hexanol as cosurfactant, and decane as oil, where the formerly employed sodium polyacrylate (NaPA) was substituted by the biopolyanion sodium hyaluronate (NaHA). Both polyelectrolytes differ markedly with respect to their molecular architecture (see Figure 1). Hyaluronic acid is a biopolyelectrolyte with a sugar backbone, i.e., a polymer of disaccharides of D-glucuronic acid and N-acetyl-D-glucosamine, which leads to a much higher persistence length of the NaHA (9 nm) at an ionic strength of 30 mM<sup>25</sup> and about twice the value for low ionic strength<sup>26</sup> compared to NaPA (1.3 nm).<sup>27</sup> In both cases, the charge is located close to the backbone, but the charge density of the hyaluronic acid is rather low (~1 charge/nm) compared to NaPA (~4 charges/nm). At the same time, the charged carboxylate group of the NaHA is less accessible to interact strongly with macroions due to its more restricted

molecular mobility by being fixed on the polymer backbone. Therefore additional experiments were carried out with the sodium salt of carboxymethyl cellulose (NaCMC), a biopolyelectrolyte with a rigid polysaccharide backbone (6–16 nm persistence length<sup>28</sup>), but sterically more easily accessible charges (see Figure 1).

In our investigation, we focused on the phase behavior and the mesoscopic structure of the PEMECs formed with hyaluronate at neutral pH (7–8). The main parameters were the mixing ratio of microemulsion droplets and polyelectrolyte, the  $M_w$  of the hyaluronate, and the size of the charged microemulsion droplets. The aim has been to deduce systematic correlations between the PEMEC properties and their composition, as well as the comparison to the behavior with NaCMC and with NaPA as polyanions.

## MATERIALS AND METHODS

**Materials.** The surfactants used in the experiments were tetradecyldimethylamine oxide (TDMAO), received as a gift from Stepan Company, as a 25% TDMAO solution in water, named Ammonyx M (the solution was freeze-dried before use), and tetradecyltrimethylammonium bromide (TTAB, 99%, Sigma-Aldrich), which was used without further purification. 1-Hexanol (>98%, Merck Schuchardt OHG) was employed as cosurfactant and decane (>98%, Fluka Chemika) as oil to form the microemulsions. The microemulsion droplets were prepared at a constant total surfactant concentration of 100 mM (95 mM TDMAO + 5 mM TTAB). 0, 50, or 75 mM of the cosurfactant hexanol were added, and the droplets were saturated with decane (which means 30, 80, and 200 mM decane, respectively, leading to dispersed microemulsion volume fractions of 3.0, 4.4, and 6.5%). This means that the size of the microemulsion droplets was controlled by the concentration of the cosurfactant.

In this work, we primarily employed biopolyelectrolytes, in particular, the sodium salt of hyaluronic acid (NaHA), which was used in different molecular weights: 51, 150, 360 (all Lifecore), and 800 kDa (SRD). The sodium salts of poly-acrylic acid (NaPA, 60 kDa, Sigma-Aldrich) and carboxymethyl cellulose (NaCMC, 90 and 250 kDa, Sigma-Aldrich) were employed for a generalizing comparison of polyelectrolytes (the  $M_w$  values always include the  $\text{Na}^+$  counterion). All polyelectrolytes were used as received without further purification. The contour lengths (theoretical lengths of the stretched polyelectrolyte chains) are 130, 370, 900, and 2000 nm for the NaHA51, 150, 360, and 800, respectively, 160 nm for NaPA60, and 200 and 480 nm for NaCMC90 and NaCMC250, respectively. Additional viscosity measurements were performed with NaHAs of 31, 186, 572, and 2073 kDa (all laboratory grade from Contipro, used as received).

Microemulsion droplets and polyelectrolytes were mixed in different charge ratios  $z = [-]/([+] + [-])$  (where  $[+]$  is given by the TTAB units and  $[-]$  is given by the carboxylate units) while maintaining a constant microemulsion concentration of 100 mM. Samples are named according to composition: the first block indicates the used microemulsion by giving the amount of hexanol, the second specifies the type and  $M_w$  of used polyelectrolyte, and the mixing ratio is given in the end. For example, MES0-NaHA150-0.70 is a sample with medium-sized droplets (50 mM of hexanol) and sodium hyaluronate of 150 kDa, mixed at a charge ratio of  $z = 0.70$ . The

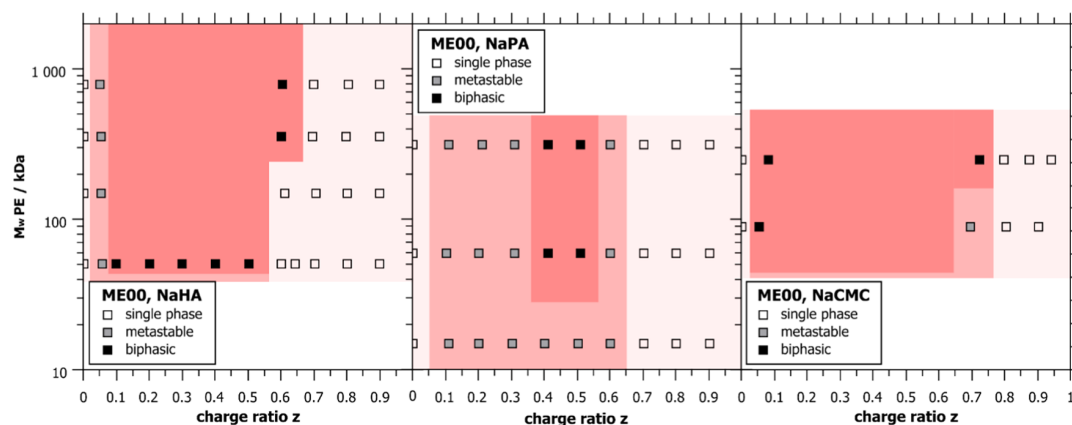


**Figure 2.** Phase diagrams for ME00 ( $R = 3.1$  nm) mixed with sodium hyaluronate (NaHA, left), sodium polyacrylate (NaPA, middle), and sodium carboxymethyl cellulose (NaCMC, right) of different  $M_w$  values and in different charge ratios  $z$ .

employed polyelectrolyte concentrations are above the overlap concentration (calculated for fully extended polymer chains) for all biopolyelectrolyte samples and most NaPA samples. The only exceptions are samples with short NaPA chains and small  $z$  ratios (the overlap concentration for NaPA05 is reached at  $z = 0.9$ , and for NaPA15 at  $z = 0.5$ ).

All samples were prepared in Milli-Q water or  $D_2O$  (>99.5% D, Eurisotop) for the SANS experiments.

## METHODS

**Static (SLS) and Dynamic (DLS) Light Scattering.** SLS and DLS measurements were performed at TU Berlin simultaneously on an ALV/CGS-3 instrument, with a He–Ne laser with a wavelength of  $\lambda = 632.8$  nm. Pseudo-cross-correlation functions for DLS were recorded using an ALV 5000/E multiple- $\tau$  correlator at 19 scattering angles,  $\theta$ , ranging from 40 to 130°, set with an ALV-SP 125 goniometer. Diffusion coefficients  $D$  were obtained by plotting the relaxation rates  $\Gamma$  of all measured angles according to  $D = \Gamma/q^2$ . The SLS data were recorded in the same range of magnitude of the scattering vector ( $q$ ), with

$$q = \frac{4\pi n_0 \sin(\theta/2)}{\lambda} \quad (1)$$

where  $n_0$  is the refractive index of the solution and  $\theta$  is the scattering angle. All measurements were carried out at  $25.0 \pm 0.1$  °C in a thermostated toluene bath.

For SLS, the mean scattered intensity of the sample at each angle was normalized by the initial laser intensity, the background scattering from the solvent and the cuvette was subtracted, and the intensity was calibrated to absolute scale with a reference measurement of toluene.<sup>29</sup>

**Small-Angle Neutron Scattering (SANS).** SANS experiments were carried out on the PAXY instrument of the Laboratoire Léon Brillouin (LLB) in Saclay, France. Measurements were performed at 25 °C at three different configurations with sample-to-detector distances of 1.2, 5, and 6.6 m; collimation lengths of 2, 5, and 6 m; and wavelengths of 4, 4, and 12 Å, respectively, to cover a  $q$ -range of  $0.03$ – $5.4$  nm<sup>−1</sup>.

Data reduction was done using the BerSANS software,<sup>30</sup> according to the standard procedure.<sup>31</sup> The raw intensity data were corrected for the scattering of the background (solvent and sample container), weighted by the respective transmissions. Additionally, the (electronic) background noise was subtracted using a cadmium sample, which absorbs incoming neutrons. The normalization and absolute scaling were done using a 1 mm reference sample of deionized water as an incoherent scatterer. Finally, the two-dimensional (2D) data were radially averaged and converted to one-dimensional (1D) scattering intensities.

Some additional measurements (ME75–NaPA samples in Figure 11) were carried out at D33 at Institut Laue-Langevin (ILL) in Grenoble, France, at sample-to-detector distances of 2(1.2), 7.8, and 12 m; collimation lengths of 2.8, 7.8, and 12 m; and wavelengths of 4.6, 4.6, and 13 Å, respectively, to cover a  $q$ -range of  $0.013$ – $6.1$  nm<sup>−1</sup>. D33 has an additional detector at 1.2 m to measure the large  $q$  simultaneously to the 2 m setting. Data reduction for these data was carried out with LAMP.<sup>32</sup>

The wavelength smearing was described by the corresponding resolution parameters and was incorporated into the analysis using SASfit software.<sup>33</sup> The wavelength spread (full width at half-maximum—FWHM) was 10%, and the size of the detector pixels was  $5 \times 5$  mm<sup>2</sup> for both instruments.

Fits were performed in absolute units, and it was assumed that all of the surfactant, cosurfactant, and oil are contained in the aggregates. The polyelectrolyte was considered as part of the solvent. More detailed information on the models used to describe the SANS data is given in the Supporting Information (SI).

**Kinematic Viscosities.** Kinematic viscosities were measured at TU Berlin with micro-Ostwald capillaries in a thermostated bath at  $25.0 \pm 0.1$  °C, where the flow time,  $t$ , is proportional to the kinematic viscosity  $\nu$ :  $\nu = \eta/\rho = Bt$ . The kinematic viscosity is the ratio of the dynamic viscosity  $\eta$  to the density of the fluid  $\rho$ , and  $B$  is a capillary constant. The flow time was averaged from at least three consecutive measurements.

**Cryo-TEM.** Cryo-TEM images of selected samples were taken at Technion, Haifa. A small droplet of the solution was placed on a perforated carbon film supported on a TEM copper grid, held by tweezers in a controlled environment vitrification system at 100% relative humidity and 25 °C. It was then blotted by a piece of filter paper, resulting in the formation of 100–300 nm thin films of spanning the holes of a perforated carbon film.<sup>34</sup> The specimen was then plunged into a reservoir of freezing liquid ethane, cooled by liquid nitrogen, to ensure its vitrification. The vitrified specimen was transferred under liquid nitrogen, mounted onto a Gatan 626 cryogenic sample holder, and cooled to  $-170$  °C. All samples were observed under low-dose conditions with an FEI Talos 200C TEM. Images were recorded using novel “phase plates,” which convert phase differences between areas of the specimen to amplitude differences, thus enhancing the image contrast without resolution loss.<sup>35</sup> The TEM is equipped with a Falcon III direct-imaging camera that allows imaging at very low electron exposure, essential for electron-sensitive specimens such as soft-matter samples. About 20 images were taken from each sample; the images were taken at different sample areas to ensure statistically relevant information.

## RESULTS AND DISCUSSION

**Phase Behavior of ME/NaHA Complexes.** As a first step, the macroscopic phase behavior of the formed complexes was

studied as a function of the nominal charge ratio  $z = [-]/([+] + [-])$  (nominal means that  $[+]$  is given by the TTAB units and  $[-]$  is given by the carboxylate units) for different molecular weights,  $M_w$ , of NaHA at room temperature. The pH was checked to be always between 7 and 8, but not controlled by adding acid or base, to avoid adding ions to the mixture. Within this pH range, the acids are largely deprotonated and  $z$  should correspond to the actual charge ratio. The phase behavior of the samples was followed by visual inspection at regular time intervals, and documented by photographs, where the most instructive ones are given in Figure S1, nicely showing the phase separation occurring around equimolarity. Samples that phase-separated within an hour were marked as biphasic, and samples that were stable for more than an hour, but not for a week, were called metastable. All samples that still consist of one single phase after 1 week were considered thermodynamically stable, as they also did not change visually during the course of several months.

Figure 2 (left) shows the phase diagram for small microemulsion droplets (ME00,  $R = 3.1$  nm) mixed with sodium hyaluronate (NaHA) of different  $M_w$  values and for different charge ratios. In this phase diagram, a very asymmetric two-phase region can be observed around the charge equilibrium ( $z = 0.5$ ). While samples at polyelectrolyte excess show one clear and transparent phase, samples in the two-phase region contain a second optically transparent liquid phase that floats on top of a low-viscous water-rich phase, i.e., a coacervate phase of lower density is formed. When the sample is shaken, the two phases mix and the sample appears white. Upon resting the sample, the two phases phase-separate again, typically within a few hours (see Figure S1 for photos of such samples). It is interesting to note that the coacervate phase, floating on top of the other, is very viscous. This is quite different from the previously studied PEMECs with NaPA,<sup>17</sup> where a powdery precipitate was formed, and no viscous coacervate phase was observed. The phase diagrams for larger microemulsion droplets (ME50,  $R = 4.1$ ; ME75,  $R = 6.6$  nm) mixed with NaHA are given in Figure S2, which generally show the same features. The single-phase regions at polyelectrolyte excess become somewhat smaller with increasing droplet size, as previously observed for NaPA.<sup>17</sup>

For a direct comparison, the phase diagrams of NaPA and NaCMC with small ME droplets are shown in Figure 2. Even though hyaluronate and polyacrylate are very different polyelectrolytes, a surprisingly similar phase behavior of mixtures with O/W microemulsion droplets is observed (phase diagrams of NaPA with larger droplets are given in Figure S3 for comparison). In both cases, aggregates in the microemulsion charge excess part of the phase diagram are very unstable (precipitation or liquid–liquid phase separation takes place), while long-time stable samples are found at polyelectrolyte excess. It is interesting to note that the upper critical mixing ratio,  $z$ , for forming stable PEMECs is quite similar,  $\sim 0.7$ , for NaPA and NaHA, which means that the colloidal stability here is largely governed by the relative charge ratio of surfactant and polyelectrolyte. For both polyelectrolytes, the phase boundary between unstable and long-time stable samples does not depend much on the  $M_w$  value of the polyelectrolyte, but for NaHA, the range of metastable phases within the unstable region is much smaller, i.e., the macroscopic phase separation occurs much faster here.

To further generalize our findings, we also employed NaCMC as polyelectrolyte, where the polymer structure and

stiffness are similar to those of NaHA, but the charge is attached to the backbone by a flexible spacer (see Figure 1), and the charge density can easily be altered by the degree of substitution (DS). Here, the higher- $M_w$  NaCMC250 has a higher charge density with DS = 1.2, while DS = 0.7 for the shorter NaCMC90. When comparing their phase behavior (see Figure 2, right), it is striking that the NaCMC phase diagram for the small droplets is somewhat different by showing a two-phase region more extended to higher  $z$ . But the more pronounced effect is seen on the droplet size when mixed with NaCMC (see Figure S4). For samples prepared with NaCMC and medium-large droplets, the monophasic range is much smaller than that with the two other polyelectrolytes, and it almost vanishes for the largest droplets. As mentioned before, the NaCMC charge is not located directly on the PE backbone, but linked with a rather flexible spacer. This spacer makes the charge more accessible for the ME droplets, so droplets can be bound more easily, which increases the strength of interaction, and the complexes then have an increased tendency for phase separation. Apparently, the accessibility of the charge via the flexibility provided by a spacer is very important here.

Interestingly, the nature of the two-phase region depends strongly on the type of PE. For NaPA, a solid powdery phase precipitates, while for NaHA and NaCMC, the second phase is a very viscous gel, i.e., a coacervate phase. Apparently, the extent of hydration in the complex is much higher for the polysaccharides, which is not surprising, given the large number of OH groups on their backbone, which enable stronger hydration. It should be noted that this behavior is quite similar to that observed for complexes of NaHA with TTAB, where a viscous second phase was observed, the difference just being that there the viscous phase precipitated to the bottom.<sup>36</sup> The difference in our case can be explained by the lower density of the microemulsion droplets.

#### Structural Characterization of ME/NaHA Complexes.

**Static and Dynamic Light Scattering (SLS/DLS).** A first structural characterization of the stable single-phase samples at NaHA excess was done by static and dynamic light scattering. DLS measurements show an interesting feature different from the previously studied NaPA samples: Some of the NaHA samples show a bimodal decay (see Figure S5). The tendency for a bimodal distribution function depends on the droplet size and the  $M_w$  value of NaHA. The smallest droplets most markedly show a bimodal distribution. For ME00, a bimodal relaxation is found for all mixing ratios and all  $M_w$ , except the shortest NaHA51, which exhibits a monomodal relaxation. For the medium droplet size ME50, only samples with higher- $M_w$  NaHA show a bimodal decay, and only for higher mixing ratios. Finally, for the largest droplets ME75, a bimodal relaxation is no longer found and all measured samples show a simple decay of the correlation function (Figure S6). The slower relaxation mode in the bimodal distribution is nondiffusive (the relaxation rate,  $\Gamma$ , follows a power law of  $\sim q^3$ ; see Figure S7) and also appears in samples of pure NaHA. It can be attributed to the generally observed “slow mode” of polyelectrolytes, seen in particular at a low ionic strength,<sup>37</sup> which has been attributed to the presence of supramolecular structures or hindered motions of interacting chains.<sup>38,39</sup> Such a slow mode with  $q^3$  scaling has been reported also for hyaluronate before.<sup>40</sup> Because of the lower charge density, NaHA has to be employed in higher weight fractions than NaPA to achieve the same mixing ratios. NaHA also scatters light more strongly than NaPA due to higher  $M_w$  per unit

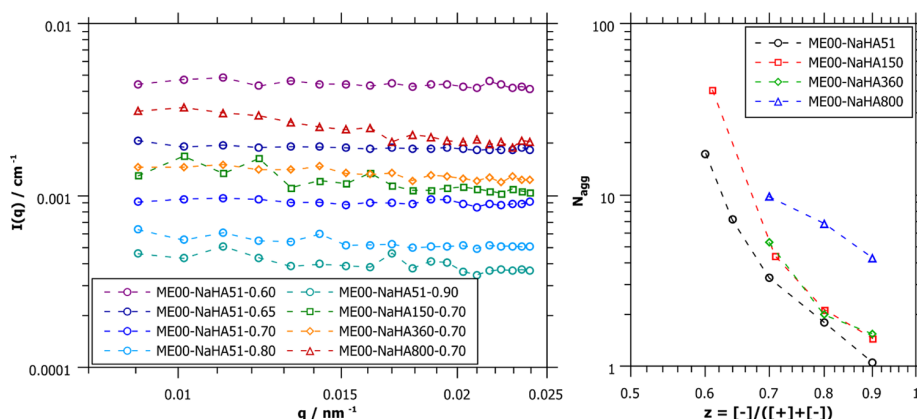


**Figure 3.** Left: SLS intensity vs  $q$  shows a plateau for most samples (small droplets,  $R = 3.1$  nm). Right: Aggregation numbers  $N_{\text{agg}}$  (number of droplets per complex) as obtained from static light scattering (small droplets,  $R = 3.1$  nm). For data on bigger droplets, see Figures S8 and S9. The last number of the sample name indicates the charge ratio  $z$  of the sample.

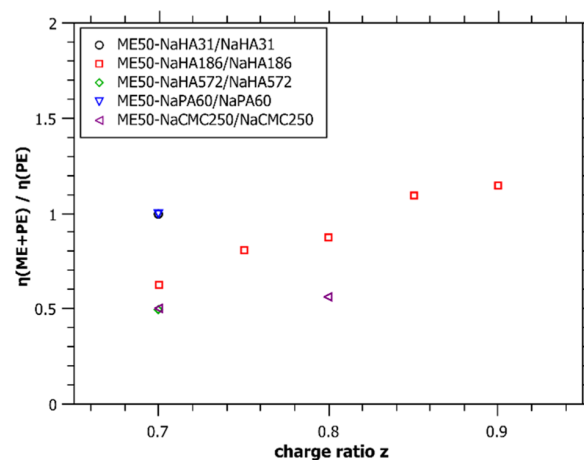
length, so it becomes visible in the measurements at higher concentrations. Even though NaHA is scattering more strongly, it is still a weak scatterer and can be easily concealed by more strongly scattering objects like larger microemulsion droplets. The faster mode observed in DLS belongs to the complexes formed by PE and ME droplets, which are of interest in this study, and thus, only this signal was further analyzed and the slower relaxation mode was neglected.

Both methods, SLS and DLS, show large aggregates close to the phase boundary, which are decreasing in size for larger charge ratios  $z$ . As expected, the higher  $M_w$  of the polyelectrolytes and larger ME droplets lead to an increase in complex size. These findings are very similar to the results previously found for ME/NaPA complexes,<sup>17</sup> indicating a generic trend for such systems, independent of the nature of the polyelectrolyte. All light scattering results summarized in Figure S8 show hydrodynamic radii of 25–50 nm close to the phase boundary for the smallest droplets, which increase with the  $M_w$  of the NaHA. Interestingly, the largest values of almost 100 nm are found for medium-size ME droplets ( $R = 4.1$  nm) and slightly smaller for the largest droplets ( $R = 6.6$  nm), where the largest complexes of  $R_h \sim 80$ –100 nm are observed for  $M_w$  values of 360 and 800 kDa for NaHA.

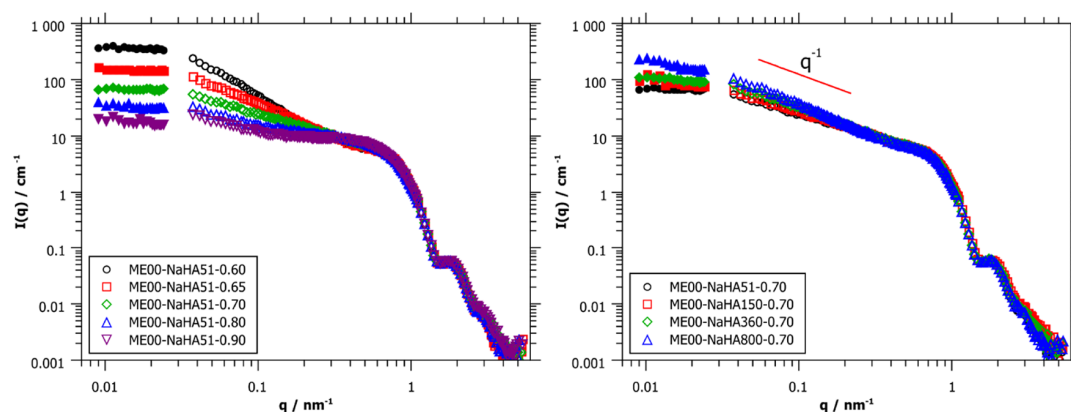
The static scattering intensity shows a plateau over the whole  $q$ -range for most samples. Only some samples with high- $M_w$  NaHA and mixing ratios close to the phase boundary ( $z = 0.7$ ) show an increase in intensity to lower  $q$  (see Figure 3, left, and Figure S9). A plateau in the SLS data means that  $R_g \cdot q \ll 1$ , which would be valid for aggregates with  $R_g < 40$  nm (with  $q_{\text{max}}$  being  $0.025 \text{ nm}^{-1}$ ), in agreement with the DLS data (one should keep in mind here that for a cylinder of length  $L$  and radius  $R$ , it holds:  $R_g^2 = L^2/12 + R^2/2$ ; accordingly, this is still valid for cylinders of a length of up to 140 nm). The molecular weight of the complexes can be obtained from the intercept  $I(0)$  of the SLS data (obtained by a Guinier approximation); it shows that close to the phase boundary, values of several million Da are achieved (Table S2). By comparing the molecular weight of the mixed complexes to that of one single ME droplet without interactions (pure microemulsion measured with added salt to suppress interparticle interactions), and neglecting the weak scattering contribution of the polyelectrolyte, an aggregation number  $N_{\text{agg}}$  of droplets per complex aggregate can be obtained. This shows that up to 40 droplets may be contained in one complex (Figure 3, right, and

Figure S8). The static light scattering results for all NaHA samples are summarized in Table S2. In general, the number of droplets contained in a complex increases with increasing  $M_w$  of the NaHA chain. However, it should be noted here that neglecting the scattering contribution of the NaHA leads to an upper estimate. Similarly, we are not claiming to find finite sized structures in the solution, but at the length scale probed here, we see structures that contain approximately the given numbers of ME droplets.

**Viscosity.** For additional information, the viscosities of a  $z$ -series of medium-sized microemulsion droplets (ME50) and NaHA186 were measured. The viscosity is very low at ME excess and increases strongly once the PE excess regime of the phase diagram is reached. This is simply due to the increased concentrations of NaHA in this regime, which already for the pure NaHA solution leads to a marked viscosity increase (see Figure S10). Figure 4 shows the viscosity ratios of ME/NaHA samples and pure NaHA solutions with the same NaHA concentration, for different charge ratios at PE excess. The viscosity ratios of NaPA and NaCMC samples of  $z = 0.7$  are also plotted for comparison. As a first statement, it can be pointed out that the added microemulsion does not have a



**Figure 4.** Viscosity ratios of pure polyelectrolytes and PEMECs for different charge ratios  $z$  for medium-sized microemulsion droplets ( $R = 4.3$  nm).



**Figure 5.** Scattering curves of PEMECs with small microemulsion droplets ( $R = 3.1$  nm). Left: different mixing ratios,  $z$ , on the polyelectrolyte-rich side of the phase diagram of NaHA51. Right: mixing ratio  $z = 0.70$  with different  $M_w$ 's of NaHA. Filled symbols are SLS data, and empty symbols are SANS data; the scaling of the SLS data is described in SI F.

strong impact on the viscosity of the polyelectrolyte solution. For NaHA186, the largest effect is obtained at  $z = 0.7$ , close to the phase boundary, where the microemulsion decreases the viscosity compared to the original PE viscosity by a factor of almost 2. This effect becomes much weaker for higher mixing ratios. The viscosity effect is markedly depending on  $M_w$  and is about 2 for NaHA572, while it almost vanishes for NaHA31. For NaCMC250, a similar value to that for NaHA572 is observed, which may be partly attributed to the similar  $M_w$ , but may also reflect a stronger attractive interaction due to the more accessible charges of NaCMC.

These results are interpreted by the rather weak electrostatic interactions of the microemulsion droplets with the polyelectrolytes, which is most likely due to the low charge density on the droplet surface. This should result in rather transient aggregates with a short structural relaxation time, thereby not affecting the viscosity significantly. The lower relative viscosity at low  $z$  can be explained such that the complexation is most pronounced here, which also leads to a condensation of NaHA chains and thereby to a relatively weaker polyelectrolyte network and correspondingly lowered viscosity. Close to the phase boundary, where large aggregates were observed by DLS and SLS, those weak interactions still have a compacting effect on the hyaluronate, the more so for longer chains (higher  $M_w$ ). When the hyaluronate is bound in aggregates, the charges are screened, and the separate strands can slide next to each other without entanglement. At larger polyelectrolyte excess, the hydrodynamic radii obtained from DLS become smaller, actually approaching those of the free droplets (see Figures 6 and S8). Together with the viscosity measurements, this can be interpreted as a continuous but transient polyelectrolyte network (no change in viscosity), which is decorated with separate ME droplets. Apparently, the transient nature of the interconnection by ME droplets results in a short structural relaxation time and the corresponding low viscosity. In general, it can be concluded that the addition of the ME droplets has a rather small effect on the viscosity of the NaHA network, as previously seen for the addition of pure cationic surfactant at surfactant excess conditions.<sup>41</sup> For a comparison, the viscosity effect on NaCMC is more strongly pronounced, confirming a stronger interaction (as seen before in the phase behavior) and a resulting more pronounced compaction of the aggregates.

**Small-Angle Neutron Scattering (SANS) and Dynamic Light Scattering (DLS).** Although light scattering is a useful

tool to determine the overall size of the formed complexes, it is not able to yield detailed information about the shape and internal structure of these complexes because of the limited  $q$ -range probed and the small size of the microemulsion droplets. For this reason, small-angle neutron scattering (SANS) was employed to characterize the different PEMEC systems with respect to their mesoscopic structure. This was done comprehensively for different  $M_w$  values of NaHA and for different size microemulsion droplets, always as a function of the mixing ratio,  $z$ . Selected SANS data are shown in Figure 5. The full set of scattering curves is shown in Figure S12.

As previously observed for the polyacrylate PEMEC,<sup>17</sup> the SANS measurements show that the droplets remain unchanged in shape and size when interacting with the hyaluronate. This is confirmed by the unchanged scattering curves at high  $q$ , especially the form factor minimum (see Figure S13 for zoom into the minimum). The complexing effect of the hyaluronate is seen at low  $q$ , where the interactions of the droplets are probed. All SANS data show an increase in intensity toward low  $q$  that continues up to  $q = 0.03$  nm<sup>-1</sup>. Note that no plateau is visible in any of the SANS data of NaHA complexes. In comparison, NaPA samples with small  $M_w$ 's showed a plateau; however, the shortest NaHA chains used in this work are still much longer than the shorter NaPA chains used previously.<sup>17</sup>

As the differences in the size of the formed complexes become clearer in static light scattering, where the observed  $q$ -range is at lower  $q$  values, the SLS data were scaled according to the contrast differences of SANS and SLS (for details of the calculation and refractive index increments, see SI F) and plotted with the SANS data in Figure 5 for a complete picture. A plateau is observed for most samples in SLS. Unfortunately, the onset of the plateau seems to be exactly in the middle between the two observable length scales of SLS and SANS, and due to the experimental constraints, no overlapping data are available, but by combining these two methods, a good characterization of the PEMECs can still be achieved.

The slope of the intensity increase in the SANS data depends on the mixing ratio,  $z$ . As previously seen for NaPA, the slope is highest for samples close to the phase boundary (low  $z$ ) and decreases with increasing polyelectrolyte excess, i.e., with increasing electrostatic screening. As an example, this is shown for the smallest microemulsion droplets (ME00,  $R = 3.1$  nm) for the shortest ( $M_w = 51$  kDa) NaHA in Figure 5 (left) (others are shown in Figure S12). The largest aggregates

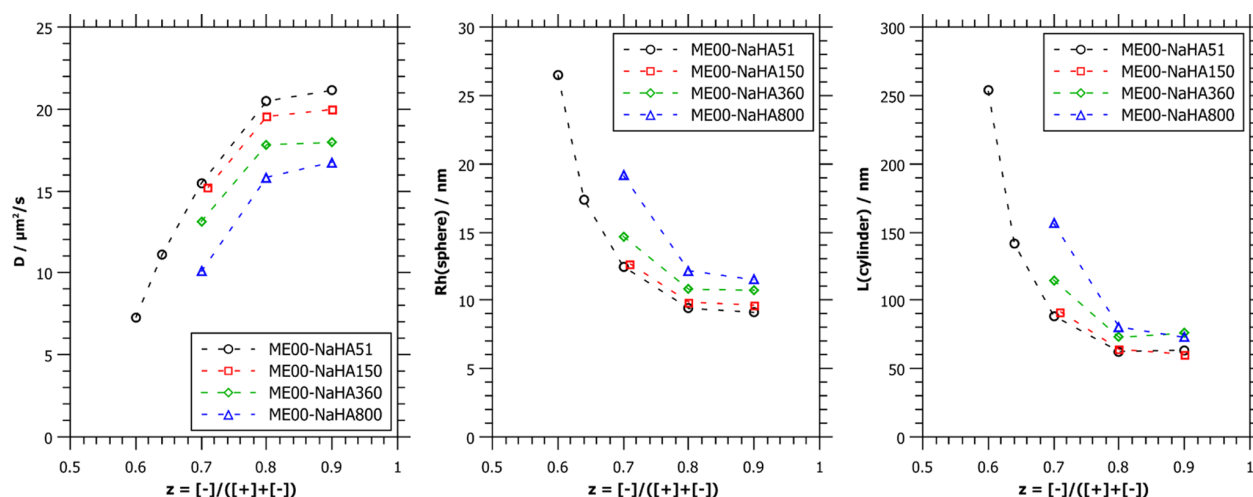


**Figure 6.** Diffusion coefficient,  $D$ , hydrodynamic radius,  $R_h$ , and lengths of cylinders,  $L$ , as deduced from DLS measurements for complexes formed by ME00 (small droplets,  $R = 3.1$  nm), with NaHA of different  $M_w$ 's at different mixing ratios,  $z$ .

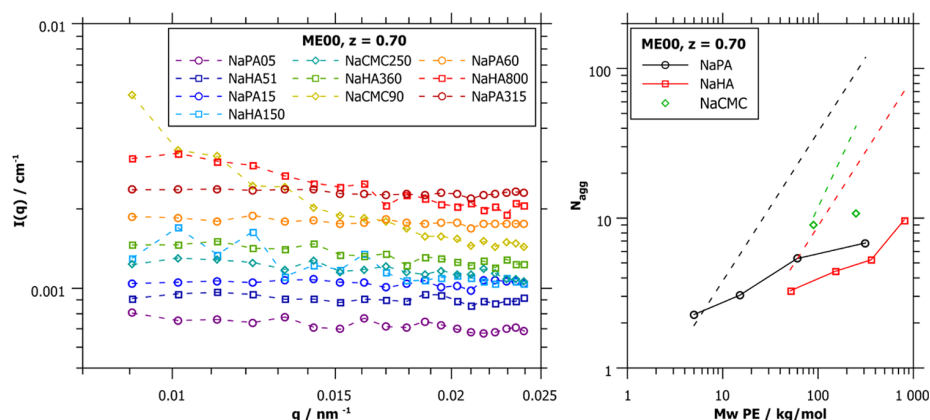


**Figure 7.** Left: SLS data of ME00 (small droplets,  $R = 3.1$  nm) mixed with different polyelectrolytes at  $z = 0.7$ . Right: aggregation numbers,  $N_{agg}$  (droplets per complex), as obtained from SLS, as a function of the molecular weight  $M_w$  (including the  $\text{Na}^+$  counterion). The dotted lines represent theoretical number of droplets per PE chain according to the number of charges.

are formed close to the phase boundary ( $z \sim 0.6$ ), and the  $q^{-2}$  slope suggests random walk assemblies of microemulsion droplets at this mixing ratio. At  $z = 0.7$ , the slope of the intensity is close to  $q^{-1}$ , which indicates locally linear arrangements of the microemulsion droplets. At high polyelectrolyte excess ( $z = 0.9$ ), only a small intensity increase is still visible. Figure 5 (right) compares the SANS data of complexes of small microemulsion droplets at the same mixing ratio ( $z = 0.7$ , where linear droplet arrangements were found) with different  $M_w$ 's NaHA. Here, only small deviations in the  $q^{-1}$  slope are visible, becoming somewhat steeper with increasing  $M_w$  value of NaHA. The bigger the droplet, the smaller is the visible difference between the NaHAs of different  $M_w$ 's (see Figure S14 for medium and large droplets). Due to the lack of a plateau, no characteristic length of these linear complexes can be determined from SANS. Simulations of SANS curves based on homogeneous cylinders with different lengths show that the linear PEMECs arrangements extend over more than 100 nm (see Figure S15), but cannot be much larger than the values as seen by the plateau in the SLS data.

It is interesting to note that the local arrangement of ME droplets in the PEMECs apparently is rather independent of the droplet size and the  $M_w$  of the NaHA and depends largely

on the mixing ratio. For larger ME droplets, the main difference in the SANS data is simply explained by the higher  $M_w$  values of these droplets. This result is different from previous measurements with NaPA, where we had found higher aggregation numbers for larger droplets.<sup>17</sup>

Knowing that the droplets are arranged in locally linear arrangements while retaining their original size and shape, we can now interpret the (fast) diffusion coefficients measured in DLS as the diffusion of cylinders with a diameter of one droplet. The length of one cylinder was calculated using the established expression for the diffusion coefficient by Ortega et al.<sup>42</sup> (the radius was taken as that of the microemulsion droplets; more details are given in SI D).

$$D_t(L) = \frac{1}{3} \frac{k_B T (\ln p + C_t)}{\pi \eta_0 L} \quad (2)$$

The values given in Figure 6 show that this model predicts the presence of rods in the length range of 50–200 nm, in good agreement with the SANS data (and one should keep in mind that this still corresponds to a value of  $R_g$  smaller than 50 nm).

#### Comparison of PEMECs Formed with Sodium Hyaluronate (NaHA), Sodium Carboxymethyl Cellulose

(NaCMC), and Sodium Polyacrylate (NaPA). After having analyzed the structural information regarding PEMECs formed with NaHA of different  $M_w$ 's, it is now interesting to compare their structural features with those seen previously for sodium polyacrylate (NaPA).<sup>17</sup> This comparison is interesting since NaPA is a much more flexible polyanion than NaHA with its polysaccharide backbone (intrinsic persistence lengths of 1.3 nm compared to 9 nm for NaHA).<sup>25,27</sup> Accordingly, we can elucidate the effect of the polymer persistence length on the mesoscopic structure of the PEMECs. In addition, some experiments were performed with the sodium salt of carboxymethyl cellulose (NaCMC) to see how the location of the charge on the polysaccharide affects the complexation behavior, while the backbone and its stiffness (persistence length of 16 nm<sup>28</sup>) are quite similar to those of NaHA. For NaHA and NaPA, the charge is located close to the backbone, while for NaCMC, it is much more easily accessible, as it is connected to the backbone by a rather flexible spacer (see Figure 1). The charge density of NaCMC depends on the degree of carboxylation, and the two NaCMCs used in this work differ not only in their molecular weight but also in their charge density. The longer NaCMC chain (NaCMC250) also has the higher charge density with 1.2 charges per monomer unit, while the shorter NaCMC90 has a degree of substitution (DS) of 0.7.

Static light scattering was measured for all samples to determine the molecular weight and the aggregation number (Figure 7). The SLS data show the same trend for all polyelectrolytes: the aggregation numbers at a constant charge ratio,  $z$ , increase with increasing  $M_w$  of the PE. NaPA/ME complexes have a higher aggregation number than NaHA complexes at a given  $M_w$  of PE, but the aggregation number is highest for NaCMC complexes. In general,  $N_{\text{agg}}$  is smaller than that calculated theoretically with the assumption of having one polymer chain complexed stoichiometrically with ME droplets according to the number of charges (given as dotted lines in Figure 7, right). Here, it should be noted that the droplets have a rather low charge density, as the average spacing between the charges on the droplet surface is  $\sim 3.5$  nm, while that of NaHA is  $\sim 1$  nm, i.e., a 3.5 times higher value. Under these conditions, it is not possible to fully compensate all PE charges, leading to smaller aggregation numbers. Because of this, the complexes will build up a negative net charge, which is the driving force for their locally elongated form, and which also prevents the complexes from growing very large. This effect is more pronounced with increasing  $M_w$  of the polyelectrolyte, because at the given conditions, the PE concentration is typically above the overlap concentration, which means that the formation of complexes with only one PE chain is unlikely. In addition, only an effective domain size of the structures is visible in light scattering, making it more difficult to give exact aggregation numbers.

The SANS measurements are able to give more information about the shape and composition of the mixed complexes. At first glance, the complexes formed with microemulsion droplets and NaHA, NaCMC, or NaPA look rather similar in SANS. We observe large mixed complexes close to the phase boundary that decrease in size with increasing polyelectrolyte excess (Figures S12 and S17). Figure 8 shows the SANS data for samples of small microemulsion droplets (ME00,  $R = 3.1$  nm) with different polyelectrolytes at a constant charge ratio of  $z = 0.7$  (polyelectrolyte excess, close to the phase boundary for NaPA and NaCMC, not so close for NaHA). All of these

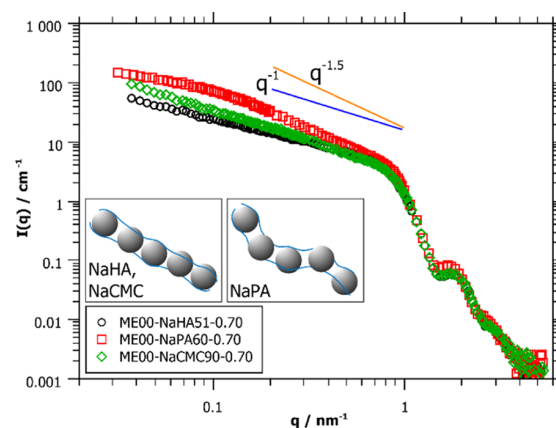


**Figure 8.** Comparison of SANS data for small (ME00,  $R = 3.1$  nm) microemulsion droplets mixed with NaHA ( $M_w = 51$  kDa), NaPA ( $M_w = 60$  kDa), and NaCMC ( $M_w = 90$  kDa) of comparable length, at  $z = 0.7$ , close to the phase boundary.

complexes show a slope between  $q^{-1}$  and  $q^{-1.5}$  in the neutron scattering data, which corresponds to elongated structures. The  $M_w$  values of the polyelectrolytes were chosen so that the stretched chains (contour lengths) are similar in lengths (NaPA60  $\sim 160$  nm, NaHA51  $\sim 130$  nm, NaCMC90  $\sim 200$  nm). However, it should be noted here that being mixed at the same charge ratio implies that the weight fraction of NaHA (NaCMC90/NaCMC250) is about 4 (3/2) times higher than that of NaPA, due to the lower charge density per mass of NaHA (NaCMC). In Figure S16, the same comparison is done for medium-sized droplets (ME50,  $R = 4.1$  nm), and the scattering curves look very similar. Figure S17 shows more SANS data of NaCMC complexes, which resemble those of the NaHA in their general behavior.

The direct comparison for a constant mixing ratio of  $z = 0.7$  shows that the slope for the NaPA samples is generally higher than those for the NaHA or NaCMC ones. While the slopes of the more rigid polysaccharides are very close to a  $q^{-1}$  power law, the slope of the flexible NaPA is  $\sim q^{-1.5}$ . This can be attributed to the different stiffnesses of the polyelectrolytes; NaHA and NaCMC are quite rigid due to their backbones being composed of disaccharide units, while NaPA is rather flexible. The stiffer NaHA and NaCMC are more likely to arrange the droplets in a straight cylindrical geometry leading to a  $q^{-1}$  dependence, while the less rigid NaPA forms curved chains of droplets, i.e., assumes the conformation of a semiflexible polymer. Consequently, the low- $q$  region exhibits a higher slope ( $q^{-1.5}$ ). The two limits generally known to describe SANS data of similar polymeric structures quantitatively are long straight cylinders with a slope of  $q^{-1}$  or flexible Gaussian coils with a slope of  $q^{-2}$ .<sup>43</sup> We can therefore qualitatively conclude that the two polysaccharides employed here form long aggregates with essentially linear arrangements of separate droplets, when interacting with oppositely charged microemulsion droplets. In contrast, the formed aggregates of the flexible NaPA show a semiflexible behavior.

The comparison of the SANS data of NaPA and NaHA samples at  $z = 0.9$  (data shown in Figure S18), i.e., at very high PE excess, points out another difference. At this high PE excess, the NaPA samples resemble those of single microemulsion droplets without interactions. Apparently, the PE excess at this charge ratio is high enough to stabilize each

droplet separately. NaHA and NaCMC complexes at the same mixing ratio still show a small intensity increase at very low  $q$ . Here, the polyelectrolyte network formation becomes visible, which is much more pronounced for NaHA, in agreement with the highly viscous properties that it shows in aqueous solution.<sup>44,45</sup> The small dent visible in these SANS data at  $q \sim 0.2 \text{ nm}^{-1}$  reminds of a correlation hole, which arises from excluded-volume correlations due to the increased amount of polyelectrolyte.<sup>46</sup>

Cryo-TEM images were taken of samples of large ME droplets with NaPA and NaHA at PE excess, but close to the phase boundary ( $z = 0.7$  and  $0.8$ ) to validate the droplet arrangements suggested by SANS measurements (Figure 9).

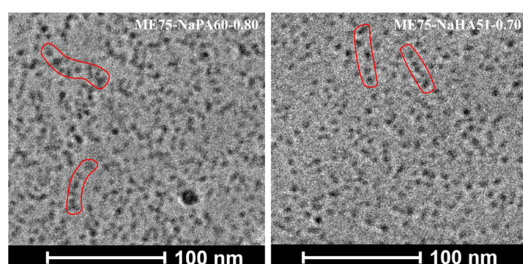


**Figure 9.** Comparison of cryo-TEM micrographs of large ME droplets (ME75,  $R = 6.6 \text{ nm}$ ) mixed with NaPA (left) and NaHA (right) at  $z$ -values in PE excess, close to the phase boundary ( $z = 0.7$  for NaHA and  $0.8$  for NaPA, because a  $z = 0.7$  sample was not stable with large droplets).

While both images show dense packings of droplets that are hard to separate into single aggregates, those images also do not contradict the findings obtained by SANS, which is an important observation. In both images, we can find linear arrangements of droplets. For the NaPA sample, the strands of droplets look more branched and bend than for the NaHA sample, where more extended strings of ME droplets are visible (see indications in red in Figure 9). To be able to interpret the results of two fundamentally different methods in the same way increases the chances that this interpretation represents the real situation substantially.

**Further Analysis of the Scattering Data.** Further information regarding the SANS data can be obtained by plotting and analyzing the data in the so-called “Holtzer

plot,”<sup>47</sup>  $I(q) \cdot q$  vs  $q$ . For flexible polymers, the Holtzer plot shows a maximum in intensity at low  $q$ , which decreases first rapidly and then with a smaller slope. The kink between the two linear parts at  $q_p$  (transition from coiled to linear structure) can be used to calculate the persistence length  $l_p = 1.9/q_p$ .<sup>48</sup> When looking at SANS data of different polyelectrolytes with microemulsion droplets at  $z = 0.7$  in the Holtzer plot, the differences become much more visible than in the simple log–log plot (Figure 10). While NaPA samples follow the classical behavior of polymers, the trend of NaHA samples looks completely different. For the flexible NaPA, a polymer-like behavior is observed with a persistence length  $l_p = 5.81 \text{ nm}$  for ME00–NaPA60–0.70, and  $l_p = 9.05 \text{ nm}$  for the ME50–NaPA60–0.70 complexes. Interestingly, these lengths correspond almost exactly to the respective droplet diameters, which indicates that dimers of droplets are rather loosely joined. Samples with NaHA at this mixing ratio do not follow the classical Holtzer plot behavior for a flexible chain, so no persistence length can be obtained here. Instead, for the NaHA and NaCMC complexes, one observes the behavior of a stiff rod, and obviously, the persistence length is larger than the experimental observation window of  $100 \text{ nm}$ . This confirms the previously made assumption that here the ME droplets arrange to straight cylindrical aggregates of a substantial length. The Holtzer plots for NaHA samples closer to the phase boundary ( $z = 0.6$  and  $0.65$ ) and at high PE excess are shown in Figure S19A,B.

Another way of comparing the complexes formed by ME droplets with different polyelectrolytes is by fitting the slope,  $A$ , of the linear part of the SANS data at small  $q$  with  $I(q) = q^{-A} + B$ , where  $A$  corresponds to the fractal dimension of the formed complexes. Here, a value of  $A = 1$  corresponds to straight cylinders, whereas higher values indicate more bend cylinders. The limit of this model would be a Gaussian coil with  $A = 2$ .<sup>49</sup> The fitted exponents for  $z = 0.7$  samples are plotted in Figure 11 and show a logarithmic trend with the  $M_w$  value of the polyelectrolyte for all systems. The  $A$  value of NaPA samples is generally higher than that of NaHA samples at a given mixing ratio, confirming again that much more flexible aggregates are formed by the flexible polyelectrolyte, while a stiff polyelectrolyte arranges the ME droplets in straight rods. In addition, the slope increases systematically with increasing size of the microemulsion droplets. The NaHA samples closer to the

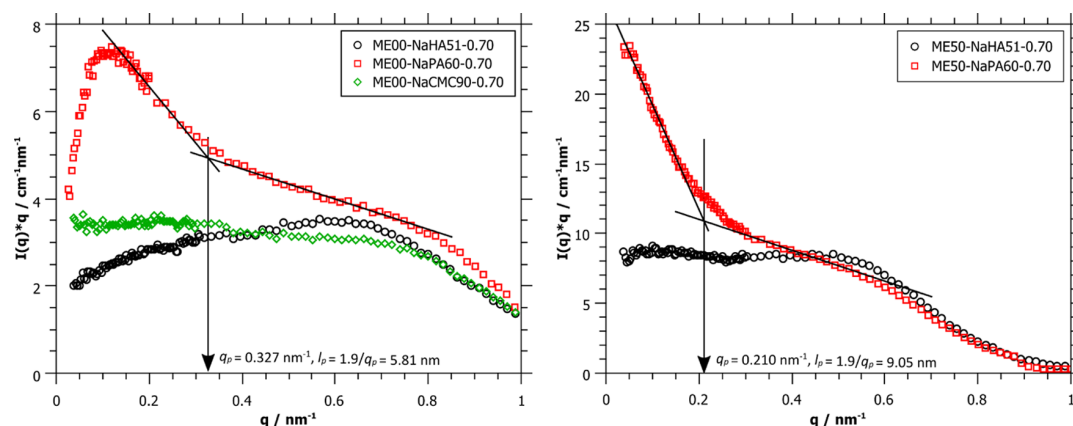


**Figure 10.** Holtzer plots of SANS data of NaHA, NaPA, and NaCMC mixed with small (left) and medium (right)-sized microemulsion droplets. A charge ratio of  $z = 0.7$  was not stable for ME50–NaCMC90 samples.

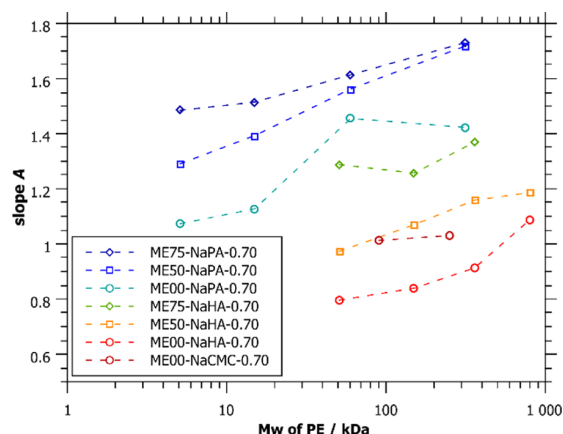


**Figure 11.** Fitted slope low  $q$  SANS data of PEMECs at  $z = 0.7$ . The slope shows a logarithmic dependency on the  $M_w$  of polyelectrolyte for all, NaHA, NaCMC, and NaPA, samples.

phase boundary ( $z = 0.6$ – $0.65$ ) showed slopes between 1.6 and 1.1, but no direct comparison to NaPA can be drawn here because NaPA samples were not stable at these mixing ratios.

More analytical description of the scattering data was also made. As a first step, the data were described with a model of homogeneous cylinders, before a more sophisticated model of linearly arranged spheres<sup>50</sup> was attempted. However, both models showed substantial shortcomings in properly describing the scattering data (see SI F). Due to the lack of an appropriate model to describe SANS data of curved droplet chains, a Monte Carlo model was developed by us for this purpose (a comparison of the fit quality of the different models is given in Figure S20, showing the significant improvement by the new model). The model describes chains of  $N$  homogeneous spheres of average radius  $R$ , which are separated by an average distance  $d$  between the sphere surfaces. Both  $R$  and  $d$  are polydisperse and randomly picked from normal

distributions with standard deviations ( $\sigma$ ) corresponding to the polydispersity parameters. The chains assume the random conformations of semiflexible polymers of a given persistence length. In practice, this was achieved by sampling random conformations while penalizing high angles between the vectors between each sphere and its two neighbors with a harmonic constraint potential of adjustable strength  $V_0$ . In this procedure, nonphysical conformations with overlapping spheres were excluded. To obtain the scattering curves given in Figure 12, at least 5000 conformations were randomly generated in this way. The scattering intensities were then computed by calculating the form factor amplitudes of each sphere, subsequent phase-correct summation based on each set of sphere coordinates using the Debye formula,<sup>51</sup> and averaging over all conformations. The persistence length  $l_p$  was calculated a posteriori from the ensemble-averaged ratio between contour length  $L_C$  and end-to-end distance  $h$ , where  $\langle h^2 \rangle = 2L_C l_p - 2l_p^2(1 - e^{-L_C/l_p})$ <sup>52</sup> (for more details, see SI F).

With this model at hand, it was possible to quantitatively describe the full set of SANS data of samples with  $z = 0.7$  for different polyelectrolytes (Figure 12). To this end, all microemulsion droplet parameters ( $R$ , polydispersity in  $R$ , volume fraction, contrast) were kept constant for all samples. Parameters that depend on the type of polyelectrolyte ( $d$ , polydispersity in  $d$ ,  $V_0$ ) were used as global model parameters for all samples with the same PE type. So, the only parameter changing with the  $M_w$  of PE is the number of droplets per aggregate  $N$ .

The results show that all data of samples close to the phase boundary (where elongated complexes are found) can be described accurately with the new model of cylindrically arranged droplets with a persistence length of the aggregate that depends on the type of polyelectrolyte. The obtained persistence lengths are  $l_p(\text{NaPA}) \sim 17$  nm and  $l_p(\text{NaHA}) \sim 51$  nm, confirming and quantifying the assumptions stated above. Furthermore, the distances between droplet surfaces depend on the type of polyelectrolyte, being  $\sim 2$  nm for NaPA and

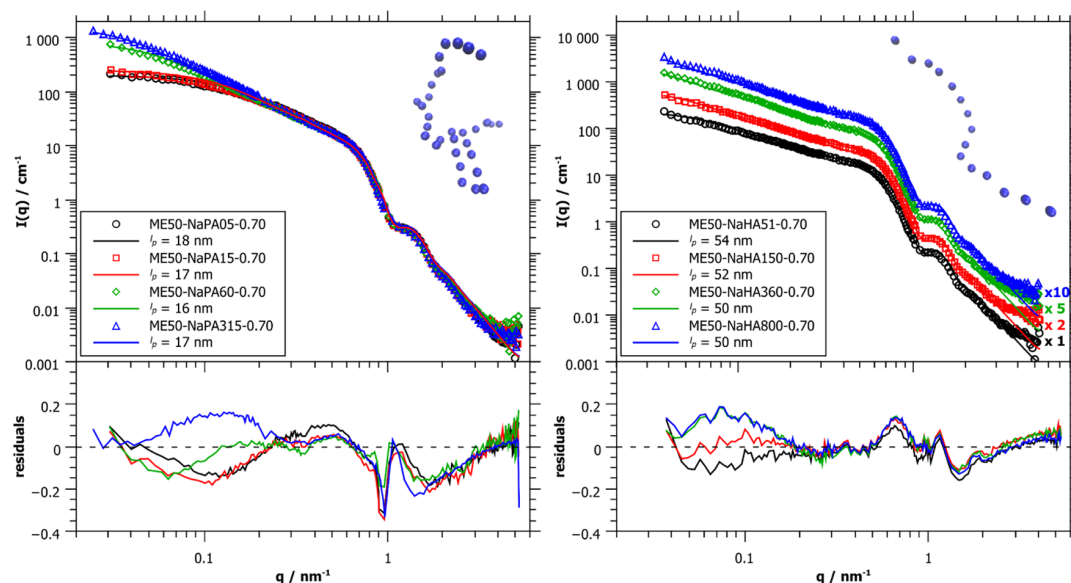


**Figure 12.** Modeled SANS data of NaPA (left) and NaHA (right) samples at  $z = 0.7$ . The persistence length,  $l_p$ , was calculated afterwards from the modeled end-to-end distance and contour length. The angular potential was kept constant for all samples with the same type of PE, resulting in very similar  $l_p$ s. The insets show examples of simulated complexes for the longest chain lengths. More simulations are shown in Figure S21.

$\sim 5.5$  nm for NaHA complexes, which can be explained by the different charge densities of both polyelectrolytes, which are  $4.0\text{ e}_0/\text{nm}$  for NaPA and  $1.0\text{ e}_0/\text{nm}$  for NaHA (Table 1).

**Table 1. Parameters of Modeled SANS Data of ME50 Microemulsion Droplets with NaPA and NaHA at  $z = 0.7^a$**

sample	$R/\text{nm}$ ( $\sigma$ )	$d/\text{nm}$ ( $\sigma$ )	$N$	$V_0/\text{au}$	$L_C/\text{nm}$	$l_p/\text{nm}$
ME50-NaPA05-0.70	4.0 (0.6)	2.0 (1)	4	1.0	30	18
ME50-NaPA15-0.70	4.0 (0.6)	2.0 (1)	5	1.0	40	17
ME50-NaPA60-0.70	4.0 (0.6)	2.0 (1)	17	1.0	160	16
ME50-NaPA315-0.70	4.0 (0.6)	2.0 (1)	32	1.0	310	17
ME50-NaHA51-0.70	4.0 (0.6)	5.5 (3)	6	3.0	68	54
ME50-NaHA150-0.70	4.0 (0.6)	5.5 (3)	9	3.0	108	52
ME50-NaHA360-0.70	4.0 (0.6)	5.5 (3)	13	3.0	162	50
ME50-NaHA800-0.70	4.0 (0.6)	5.5 (3)	15	3.0	190	50

<sup>a</sup> $R$  was kept constant for all ME50 samples.  $d$  and  $V_0$  were used as global fit parameters for each PE type.  $L_C$  and  $l_p$  were calculated from the modeled conformations. Minor variations in  $l_p$  for fixed  $V_0$  reflect the influence of the nonoverlap requirement and the stochastic nature of the model.

## CONCLUSIONS

In summary, we studied the structure of polyelectrolyte/microemulsion complexes (PEMECs) of positively charged microemulsion droplets with different negatively charged polyelectrolytes. Three very different PEs were employed: The biopolymer sodium hyaluronate (NaHA) was the main focus of this study, and sodium polyacrylate (NaPA) and the sodium salt of carboxymethyl cellulose (NaCMC) were studied for a systematic comparison. While the molecular architectures of NaHA and NaCMC and also their persistence lengths in aqueous solution are rather similar, the two PEs exhibit very different phase behaviors when interacting with microemulsion droplets. For NaCMC with its more flexibly attached charge, the strength of the interaction with the oppositely charged microemulsion droplets is much larger, and therefore, a phase separation takes place much more easily, and also the viscosity reduction is more marked. In contrast, NaHA

shows a similar phase behavior to NaPA even though the PE backbone as well as the charge density are very different. In addition, it is interesting to note that for NaHA and NaCMC, a coacervate is formed, while for NaPA, a simple powdery precipitate is observed. Since the charged group, sodium carboxylate, is the same for all employed PEs, we conclude that the main parameter to influence the phase behavior of such systems is the distance between the charged group and the polyelectrolyte backbone. Other parameters, such as  $M_w$  of the PE, nature of the PE backbone, and charge density, play only a secondary role. However, it can be noted that the tendency for precipitation generally increases with increasing droplet size and  $M_w$  of the PE. This can be explained such that with increasing size of the microemulsion droplets, their charge density decreases ( $\sim 1/R$ ), thereby rendering it easier to compensate the excess charge of the PE. In addition, their surface becomes less curved, which should also make it easier for the PE charges to interact with them.

The structural behavior of stable PEMECs for polyelectrolyte excess is similar for all studied PEs. All systems locally form large elongated structures at PE excess close to the phase boundary, which decrease in size when the PE excess is increased, due to the increased local charging in the complexes. The elongated complexes are formed by separate microemulsion droplets arranged in cylindrical geometries. The ME droplets retain their size and shape when interacting with the polyelectrolytes. The number of droplets per complex depends mainly on the  $M_w$  value of the employed polyelectrolyte; it increases proportionally to the latter. The structure of the complexes was studied in detail by small-angle neutron scattering (SANS). It was found that, although though the scattering data of the formed complexes look very similar at first glance, the exact morphology depends strongly on the backbone of the employed polyelectrolyte. For a quantitative analysis, a stochastic model was developed that describes such cylindrically arranged droplets with different persistence lengths of the complexes accurately. The more flexible polyelectrolyte NaPA also forms much more flexible elongated complexes, where the persistence length corresponds to the size of about two microemulsion droplets. Contrarily, stiffer polyelectrolytes like NaHA or NaCMC form much more rigid rodlike aggregates of  $\sim 50$  nm persistence length when interacting with the microemulsion droplets, as shown in Figure 13. The effectively observed length of these cylindrical

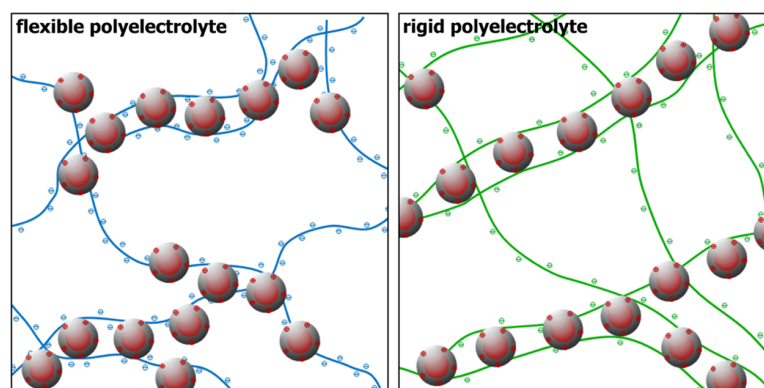


**Figure 13.** Complexes formed by microemulsion droplets with flexible polyelectrolytes (such as NaPA) form flexible droplets chains, approaching random coil-like conformations. In contrast, complexes formed with more rigid polyelectrolytes (such as NaHA and NaCMC) form long linear arrays of droplets.

aggregates then was 100–200 nm, while NaPA on this length scale forms structures similar to Gaussian coils. It should also be noted that these aggregates/complexes are not just containing one polyelectrolyte chain, and especially for longer chains (higher  $M_w$ ), they will be interconnected by such chains, thereby forming a transient network, as depicted in Figure 13.

To conclude, it was found that PEMECs can be formed generically with quite different types of polyelectrolytes, and large complexes are formed at polyelectrolyte excess in the vicinity of the phase boundary. The local structure of the complexes is largely controlled by the stiffness of the polyelectrolyte, where quite flexible complexes with short cylindrical units are formed by the flexible PE NaPA, while much stiffer cylindrical arrangements are present for polysaccharide-based PEs like NaHA. The main finding of our work therefore is that the persistence length of the PE becomes translated and amplified into the persistence length of the PEMEC aggregates in a manner similar to that seen before for complexes of lysozyme and hyaluronan.<sup>25</sup> In this manner, PEMECs with tailor-made structures can be designed, to combine the high loading capacity of a microemulsion with the superstructure arising from the polyelectrolyte.

## ■ ASSOCIATED CONTENT

### Supporting Information

The Supporting Information is available free of charge at <https://pubs.acs.org/doi/10.1021/acs.macromol.0c00236>.

Sample compositions, phase behavior, light scattering data, determination of diffusion coefficient of rods, viscosities, description of SANS models, additional SANS data, and list of abbreviations (PDF)

## ■ AUTHOR INFORMATION

### Corresponding Authors

**Miriam Simon** – Stranski-Laboratorium für Physikalische und Theoretische Chemie, Institut für Chemie, Technische Universität Berlin, 10623 Berlin, Germany; [orcid.org/0000-0003-3065-6230](https://orcid.org/0000-0003-3065-6230); Email: [miriam.simon@tu-berlin.de](mailto:miriam.simon@tu-berlin.de)

**Michael Gradzielski** – Stranski-Laboratorium für Physikalische und Theoretische Chemie, Institut für Chemie, Technische Universität Berlin, 10623 Berlin, Germany; [orcid.org/0000-0002-7262-7115](https://orcid.org/0000-0002-7262-7115); Email: [michael.gradzielski@tu-berlin.de](mailto:michael.gradzielski@tu-berlin.de)

### Authors

**Emanuel Schneck** – Physics Department, Technische Universität Darmstadt, 64289 Darmstadt, Germany; [orcid.org/0000-0001-9769-2194](https://orcid.org/0000-0001-9769-2194)

**Laurence Noirez** – Laboratoire Léon Brillouin (CEA-CNRS), University of Paris-Saclay, 91191 Gif-sur-Yvette, France

**Sofia Rahn** – Stranski-Laboratorium für Physikalische und Theoretische Chemie, Institut für Chemie, Technische Universität Berlin, 10623 Berlin, Germany

**Irina Davidovich** – Department of Chemical Engineering and the Russell Berrie Nanotechnology Institute (RBNI), Technion—Israel Institute of Technology, Haifa 3200003, Israel

**Yeshayahu Talmon** – Department of Chemical Engineering and the Russell Berrie Nanotechnology Institute (RBNI), Technion—Israel Institute of Technology, Haifa 3200003, Israel

Complete contact information is available at: <https://pubs.acs.org/10.1021/acs.macromol.0c00236>

## Notes

The authors declare no competing financial interest.

## ■ ACKNOWLEDGMENTS

The authors thank the Laboratoire Léon Brillouin (LLB) and the Institut Laue-Langevin (ILL) for allocated beamtimes. They also thank Sylvain Prévost for his support during the SANS beamtime at ILL and Sebastian Bayer for providing DLS measurements of the pure NaHA. The cryo-TEM was performed at the Technion Center for Electron Microscopy of Soft Materials, supported by the Technion Russell Berrie Nanotechnology Institute (RBNI). M.S. thanks TU Berlin for funding her Ph.D. project. E.S. thanks Ana Celia Vila Verde for fruitful discussions.

## ■ REFERENCES

- (1) Winsor, P. A. Hydrotropy, solubilisation and related emulsification processes. *Trans. Faraday Soc.* **1948**, *44*, 376–398.
- (2) Kahlweit, M.; Strey, R. Phase Behavior of Ternary Systems of the Type H<sub>2</sub>O–Oil–Nonionic Amphiphile (Microemulsions). *Angew. Chem., Int. Ed.* **1985**, *24*, 654–668.
- (3) Gradzielski, M.; Hoffmann, H.; Langevin, D. Solubilization of Decane into the Ternary System TDMAO/1-Hexanol/Water. *J. Phys. Chem. A* **1995**, *99*, 12612–12623.
- (4) Gradzielski, M. Effect of the cosurfactant structure on the bending elasticity in non-ionic oil-in-water microemulsions. *Langmuir* **1998**, *14*, 6037–6044.
- (5) Lawrence, M. J.; Rees, G. D. Microemulsion-based media as novel drug delivery systems. *Adv. Drug Delivery Rev.* **2012**, *64*, 175–193.
- (6) Boonme, P. Applications of microemulsions in cosmetics. *J. Cosmet. Dermatol.* **2007**, *6*, 223–228.
- (7) Solans, C.; García Domínguez, J.; Friberg, S. E. Evaluation of Textile Detergent Efficiency of Microemulsions in Systems of Water Nonionic Surfactant and Hydrocarbon at Low Temperature. *J. Dispersion Sci. Technol.* **1985**, *6*, 523–537.
- (8) Magno, M.; Tessendorf, R.; Medronho, B.; Miguel, M. G.; Stubenrauch, C. Gelled polymerizable microemulsions. Part 3 rheology. *Soft Matter* **2009**, *5*, 4763–4772.
- (9) Burghardt, W. R.; Krishan, K.; Bates, F. S.; Lodge, T. P. Linear viscoelasticity of a polymeric bicontinuous microemulsion. *Macromolecules* **2002**, *35*, 4210–4215.
- (10) Malo de Molina, P.; Herfurth, C.; Laschewsky, A.; Gradzielski, M. Structure and dynamics of networks in mixtures of hydrophobically modified telechelic multiarm polymers and oil in water microemulsions. *Langmuir* **2012**, *28*, 15994–16006.
- (11) Gradzielski, M.; Hoffmann, I. Polyelectrolyte-surfactant complexes (PESCs) composed of oppositely charged components. *Curr. Opin. Colloid Interface Sci.* **2018**, *35*, 124–141.
- (12) Hoffmann, I.; Heunemann, P.; Prévost, S.; Schweins, R.; Wagner, N. J.; Gradzielski, M. Self-aggregation of mixtures of oppositely charged polyelectrolytes and surfactants studied by rheology, dynamic light scattering and small-angle neutron scattering. *Langmuir* **2011**, *27*, 4386–4396.
- (13) Bronich, T. K.; Nehls, A.; Eisenberg, A.; Kabanov, V. A.; Kabanov, A. V. Novel drug delivery systems based on the complexes of block ionomers and surfactants of opposite charge. *Colloids Surf., B* **1999**, *16*, 243–251.
- (14) Oh, K. T.; Bronich, T. K.; Bromberg, L.; Hatton, T. A.; Kabanov, A. V. Block ionomer complexes as prospective nanocontainers for drug delivery. *J. Controlled Release* **2006**, *115*, 9–17.
- (15) Tam, K. C.; Wyn-Jones, E. Insights on polymer surfactant complex structures during the binding of surfactants to polymers as measured by equilibrium and structural techniques. *Chem. Soc. Rev.* **2006**, *35*, 693–709.

- (16) Hayakawa, K.; Shinohara, S.; Sasawaki, S.; Satake, I.; Kwak, J. C. T. Solubilization of water-insoluble dyes by polyion/surfactant complexes. *Bull. Chem. Soc. Jpn.* **1995**, *68*, 2179–2185.
- (17) Simon, M.; Krause, P.; Chiappisi, C.; Noirez, L.; Gradzielski, G. Structural control of polyelectrolyte/microemulsion droplet complexes (PEMECs) with different polyacrylates. *Chem. Sci.* **2019**, *10*, 385–397.
- (18) Chiappisi, L.; Hoffmann, I.; Gradzielski, M. Complexes of oppositely charged polyelectrolytes and surfactants—recent developments in the field of biologically derived polyelectrolytes. *Soft Matter* **2013**, *9*, 3896–3909.
- (19) Petrak, K. Polyelektrolyte Complexes in Biomedical Applications. *J. Bioact. Compat. Polym.* **1986**, *1*, 202–219.
- (20) Shukla, T.; Upmanyu, N.; Agrawal, M.; Saraf, S.; Saraf, S.; Alexander, A. Biomedical applications of microemulsion through dermal and transdermal route. *Biomed. Pharmacother.* **2018**, *108*, 1477–1494.
- (21) Mitsou, E.; Tavantzis, G.; Sotiroudis, G.; Ladikos, D.; Xenakis, A.; Papadimitriou, V. Food grade water-in-oil microemulsions as replacement of oil phase to help process and stabilization of whipped cream. *Colloids Surf., A* **2016**, *510*, 69–76.
- (22) Chatzidakis, M. D.; Mitsou, E.; Yagmur, A.; Xenakis, A.; Papadimitriou, V. Formulation and characterization of food-grade microemulsions as carriers of natural phenolic antioxidants. *Colloids Surf., A* **2015**, *483*, 130–136.
- (23) Chiappisi, L.; Simon, M.; Gradzielski, M. Toward Bioderived Intelligent Nanocarriers for Controlled Pollutant Recovery and pH-Sensitive Binding. *ACS Appl. Mater. Interfaces* **2015**, *7*, 6139–6145.
- (24) Gorski, N.; Gradzielski, M.; Hoffmann, H. The Influence of Ionic Charges on the Structural and Dynamical Behavior of O/W Microemulsion Droplets. *Ber. Bunsenges. Phys. Chem.* **1996**, *100*, 1109–1117.
- (25) Morfin, I.; Buhler, E.; Cousin, F.; Grillo, I.; Boué, F. Rodlike complexes of a polyelectrolyte (hyaluronan) and a protein (lysozyme) observed by SANS. *Biomacromolecules* **2011**, *12*, 859–870.
- (26) Oelschlaeger, C.; Cota Pinto Coelho, M.; Willenbacher, N. Chain Flexibility and Dynamics of Polysaccharide Hyaluronan in Entangled Solutions: A High Frequency Rheology and Diffusing Wave Spectroscopy Study. *Biomacromolecules* **2013**, *14*, 3689–3696.
- (27) Dong, J.; Ozaki, Y.; Nakashima, K. FTIR studies of conformational energies of poly (acrylic acid) in cast films. *J. Polym. Sci., Part B: Polym. Phys.* **1997**, *35*, 507–515.
- (28) Hoogendam, C. W.; de Keizer, A.; Cohen Stuart, M. A.; Bijsterbosch, B. H.; Smit, J. A. M.; van Dijk, J. A. P. P.; van der Horst, P. M.; Batelaan, J. G. *Macromolecules* **1998**, *31*, 6297.
- (29) Itakura, M.; Shimada, K.; Matsuyama, S.; Saito, T.; Kinugasa, S. A convenient method to determine the Rayleigh ratio with uniform polystyrene oligomers. *J. Appl. Polym. Sci.* **2006**, *99*, 1953–1959.
- (30) Keiderling, U. The new 'BerSANS-PC' software for reduction and treatment of small angle neutron scattering data. *Appl. Phys. A: Mater. Sci. Process.* **2002**, *74*, 1455–1457.
- (31) Chen, S.-H.; Lin, T.-L. Colloidal Solutions. *Methods Exp. Phys.* **1987**, *23*, 489–543.
- (32) Richard, D.; Ferrand, M.; Kearley, G. J. Analysis and visualisation of neutron-scattering data. *J. Neutron Res.* **1996**, *4*, 33–39.
- (33) Breßler, I.; Kohlbrecher, J.; Thünemann, A. SASfit: a tool for small-angle scattering data analysis using a library of analytical expressions. *J. Appl. Crystallogr.* **2015**, *48*, 1587–1598.
- (34) Talmon, Y. The study of nanostructured liquids by cryogenic-temperature electron microscopy - A status report. *J. Mol. Liq.* **2015**, *210*, 2–8.
- (35) Danev, R.; Baumeister, W. Expanding the boundaries of cryo-EM with phase plates. *Curr. Opin. Struct. Biol.* **2017**, *46*, 87–94.
- (36) Thalberg, K.; Lindman, B.; Karlström, G. Phase Diagram of a System of Cationic Surfactant and Anionic Polyelectrolyte: Tetradecyltrimethylammonium Bromide-Hyaluronan-Water. *J. Phys. Chem. B* **1990**, *94*, 4290–4295.
- (37) Förster, S.; Schmidt, M.; Antonietti, M. Static and dynamic light scattering by aqueous polyelectrolyte solutions: effect of molecular weight, charge density and added salt. *Polymer* **1990**, *31*, 781–792.
- (38) Ermi, B. D.; Amis, E. J. Domain Structures in Low Ionic Strength Polyelectrolyte Solutions. *Macromolecules* **1998**, *31*, 7378–7384.
- (39) Li, J.; Ngai, T.; Wu, C. The slow relaxation mode: from solutions to gel networks. *Polym. J.* **2010**, *42*, 609–625.
- (40) Horkay, F.; Falus, P.; Hecht, A.-M.; Geissler, E. Length Scale Dependence of the Dynamic Properties of Hyaluronic Acid Solutions in the Presence of Salt. *J. Phys. Chem. B* **2010**, *114*, 15445–15450.
- (41) Buchhold, P.; Schweins, R.; Di, Z.; Gradzielski, M. Structural behavior of sodium hyaluronate in concentrated oppositely charged surfactant solutions. *Soft Matter* **2017**, *13*, 2253–2263.
- (42) Ortega, A.; García de la Torre, J. Hydrodynamic properties of rodlike and disklike particles in dilute solution. *J. Chem. Phys.* **2003**, *119*, 9914–9919.
- (43) Hammouda, B. Probing Nanoscale Structure - The SANS Toolbox 2016.
- (44) Maleki, A.; Kjoniksen, A.-L.; Nyström, B. Anomalous Viscosity Behavior in Aqueous Solutions of Hyaluronic Acid. *Polym. Bull.* **2007**, *59*, 217–226.
- (45) Von Lospichl, B.; Hemmati-Sadeghi, S.; Dey, P.; Dehne, T.; Haag, R.; Sittinger, M.; Ringe, J.; Gradzielski, M. Injectable hydrogels for treatment of osteoarthritis - A rheological study. *Colloids Surf., B* **2017**, *159*, 477–483.
- (46) Banc, A.; Genix, A. C.; Chirat, M.; Dupas, C.; Caillol, S.; Sztucki, M.; Oberdisse, J. Tuning structure and rheology of silica-latex nanocomposites with the molecular weight of matrix chains: a coupled SAXS-TEM-simulation approach. *Macromolecules* **2014**, *47*, 3219–3230.
- (47) Holtzer, A. Interpretation of the Angular Distribution of the Light Scattered by a Polydisperse System of Rods. *J. Polym. Sci.* **1955**, *19*, 432–434.
- (48) Magid, L. J. The Surfactant-Polyelectrolyte Analogy. *J. Phys. Chem. B* **1998**, *102*, 4064–4074.
- (49) Dreiss, C. A. Wormlike micelles: where do we stand? Recent developments, linear rheology and scattering techniques. *Soft Matter* **2007**, *3*, 956–970.
- (50) Chiappisi, L.; Prévost, S.; Gradzielski, M. Scattering form factor of N linearly aligned particles forming a cylindrical superstructure. *J. Appl. Crystallogr.* **2014**, *47*, 827–834.
- (51) Warren, B. E. X-ray Diffraction. *Courier Corporation*, 1990.
- (52) Hiemenz, P. C.; Lodge, T. P. *Polymer Chemistry*. CRC Press, 2007.



# Dynamics in Polyelectrolyte/Microemulsion Complexes

Miriam Simon\* and Michael Gradzielski†

*Stranski-Laboratorium für Physikalische und Theoretische Chemie,  
Institut für Chemie, Technische Universität Berlin,  
Straße des 17. Juni 124, Sekr. TC 7, D-10623 Berlin, Germany*

Ingo Hoffmann‡

*Institut Max von Laue-Paul Langevin (ILL), 71 avenue des Martyrs, CS 20156, F-38042 Grenoble Cedex 9, France*

(Dated: 2020-03-30)

Oil-in-water (O/W) microemulsion droplets are convenient carriers for hydrophobic molecules in an aqueous phase and are used for a wide range of applications. We studied weakly charged O/W microemulsion droplets complexed with oppositely charged polyacrylates that form long linear arrangements of droplets. All samples showed rather low viscosities, which is in contrast to similar systems of hydrophobically interconnected droplets. Here, we applied small-angle neutron scattering, dynamic light scattering and neutron spin-echo spectroscopy to characterise the dynamic properties of polyacrylate/microemulsion complexes in order to understand the origin of the low-viscous behaviour. We found that the electrostatic interactions lead to very dynamic complexes with high exchange rates of droplets and only a fraction of the droplets is contained within the transient complexes at a given time. These results were only accessible by the combination of different methods as one method alone would have given an incomplete picture.

## INTRODUCTION

Oppositely charged polyelectrolyte/surfactant complexes have been studied intensively in the past and are considered to be very interesting systems for solubilising active agents e.g. in the context of drug delivery [1–4]. However, surfactant micelles are not intrinsically loaded with an active compound and solubilisation might be a problem. In contrast, oil-in-water microemulsion (O/W ME) droplets naturally contain a very high load of hydrophobic molecules. Surprisingly, complexes of microemulsion droplets and oppositely charged polyelectrolytes have received very little attention so far.

Microemulsions have been known since the 1940s [5], they occur as finely dispersed droplets of water in oil (W/O) or oil in water (O/W) but also bicontinuous structures are possible [6]. Microemulsions uniquely combine a number of properties, like thermodynamic stability, transparent appearance, low viscosity and spontaneous formation which makes them very interesting systems whenever it is necessary to disperse hydrophobic molecules in a hydrophilic solvent or vice versa as it is needed for example in drug delivery, nanoparticle synthesis, oil recovery or cosmetics and detergents [7–11]. In order to tailor microemulsion properties to specific needs for applications (like enhanced viscosity), it might be necessary to add additives like polymers.

Complexes formed by microemulsion droplets and polymers [12, 13], including neutral amphiphilic polymers [14, 15], block copolymers [16, 17] or telechelic polymers [18, 19] have already been studied by several groups. In most cases a gelling of the sample due to network formation of the microemulsion droplets with the polymer was found. In contrast, little research has been done on

complexes formed by ionic microemulsion droplets and oppositely charged polyelectrolyte, where the interaction is mainly of electrostatic nature. If charged ME droplets bind to polymers through electrostatic and/or hydrogen bonds, a bridging of the droplets would be possible as well as a decoration of the polymers [20]. For cationic surfactant/anionic polymer complexes it was found that the solubilization capacity of the micelles increases in presence of the polymer, due to the additional ionic strength [21].

In a recent study we have investigated complexes formed by cationic O/W microemulsion droplets with polyacrylates [22]. The structurally most interesting complexes were found in polyelectrolyte excess close to the phase boundary, where Small-Angle Neutrons Scattering (SANS) measurements showed long cylindrical arrangements of droplets on the polyacrylate chains with 3 to 23 droplets per aggregate, depending on the  $M_w$  of polyelectrolyte. When increasing the polyelectrolyte content, thus moving further away from the phase boundary, the complexes become smaller and less extended. Surprisingly, all of these samples showed rather low viscosities (see fig. S1). This is different to previously studied systems of very similar microemulsion droplets that formed highly viscous networks when interacting with telechelic polymers [18, 19]. The telechelic polymers bind to the droplets with 12–18  $k_B T$  per endcap, depending on the length of the alkyl chain, while the interactions due to opposite charges become comparatively weak already at moderate salt concentrations [23]. However, previous static measurements were not able to explain the low-viscous nature of the formed aggregates. For this reason we were now employing a high-resolution dynamic method, namely Neutron Spin-Echo (NSE), to address this question in thorough detail. In that context, it might

be noted that NSE was already successfully employed by Yearley *et al.* [24] to study the relation of cluster formation and solution viscosity.

## MATERIALS AND METHODS

### MATERIALS

Positively charged oil-in-water microemulsion droplets were prepared at a 100 mM surfactant concentration, 95 mol% of the neutral tetradecyldimethylamine oxide (TDMAO, received as a gift from Stepan company, USA, as a 25 wt% TDMAO solution in water named Ammonyx M. The solution was freeze dried before use) and 5 mol% of the cationic tetradecyldimethylammonium bromide (TTAB, 99%, Sigma Aldrich, used without further purification). 50 mM of 1-hexanol (>98%, MERCK-Schuchardt OHG) were added as a cosurfactant and the mixture was then saturated with 80 mM of decane (>98%, Fluka Chemika) as oil. The resulting droplets are about 45 Å in radius (obtained from NSE measurements) and their surface charge is controlled by the TTAB content.

Sodium polyacrylate (NaPA) was employed as polyelectrolyte. It was either purchased directly or prepared by adding a stoichiometric amount of NaOH to the poly(acrylic acid) (PAA). Four different molecular weights ( $M_w$ ) were used in this work: 5.1 kg/mol (sodium salt, used as received from Sigma Aldrich), 15 kg/mol (sodium salt solution from Sigma Aldrich, freeze dried before use), 60 kg/mol (sodium salt, used as received from Fluka Chemika) and 240 kg/mol (PAA; solution from Acros Organics, prepared by adding a stoichiometric amount of NaOH ( $\geq 98\%$ , p.a., ISO, Carl ROTH) to the solution and freeze dried before use, which results in an average molecular weight of 315 kg/mol). These molecular weights correspond to contour lengths (lengths of the stretched polyelectrolyte) of 140, 400, 1600, and 8500 Å respectively, the corresponding overlap concentrations for these polymers (assuming fully stretched chains) are 32, 3.9, 0.25, and 0.007 mM (in monomeric units).

Samples were prepared at a microemulsion concentration of 100 mM surfactant (with 95 mol% TDMAO and 5 mol% TTAB) with 12 mM of added NaPA (monomeric units) to obtain a charge ratio of  $z = [-]/([+] + [-]) = 0.7$ , where  $[+]$  and  $[-]$  are the nominal number of charges of employed TTAB molecules and NaPA monomer units respectively. A charge ratio of  $z = 0.7$  corresponds to samples at polyelectrolyte excess but close to the phase boundary where long-time stable samples containing elongated aggregates were found in previous studies [22]. The respective concentrations of surfactant and NaPA can be used to calculate the number of droplets and total length of PE chain. The ratio of both numbers results in an average length of 14 nm PE per ME droplet

of  $R = 45$  Å, so the space between droplets would be a bit smaller than one droplet diameter. Samples for NSE and SANS measurements were prepared in D<sub>2</sub>O (>99.5% D, Eurisotop), while samples for DLS were prepared in H<sub>2</sub>O from a millipore system.

### Methods

Dynamic Light Scattering (DLS) measurements were performed on an ALV/CGS-3 instrument, with a HeNe laser with a wavelength of  $\lambda = 632.8$  nm. Correlation functions were recorded for detector angles between 40° and 130° and were fitted for each angle with a stretched exponential function to obtain the decay time  $\tau$ . The collective diffusion coefficient  $D$  was calculated from  $\tau$  with the modulus of the scattering vector  $q$ , defined as:  $q = (4\pi n_0 \cdot \sin(\theta/2))/\lambda$  where  $n_0$  is the refractive index of the solution and  $\theta$  the scattering angle.

Neutron Spin Echo (NSE) measurements were performed on the instrument IN15 [25, 26] at Institut Laue Langevin (ILL, Grenoble, France) using wavelengths of 6, 10 and 14 Å reaching fourier times of 42, 194 and 531 ns and covering a  $q$  range from 0.019 to 0.14 1/Å. Standard methods were applied for data reduction.

Small-angle Neutron Scattering (SANS) experiments were carried out on PAXY at Laboratoire Léon Brillouin (LLB, Saclay, France) and on V4 at Helmholtz-Zentrum Berlin (HZB, Germany). Data reduction was done using the software package BerSANS [27].

All measurements were carried out at 25 °C. See Supporting Material for more details.

## RESULTS AND DISCUSSION

In this work we employed TDMAO/TTAB/hexanol/decane O/W microemulsion droplets at a constant surfactant concentration of 100 mM (95 % neutral TDMAO, 5 % cationic TTAB). The ME droplets were mixed with sodium polyacrylates of different  $M_w$  in a charge ratio  $z = 0.7$ , which is close to the phase boundary at the polyelectrolyte charge excess side of the phase diagram. As shown before [22] the static structure of the formed complexes was obtained by small-angle neutron scattering (SANS). The intensity increase in SANS shows that the microemulsion droplets are aggregating to large clusters of separate droplets upon the addition of an oppositely charged polyelectrolyte. Long-time stable samples were obtained in polyelectrolyte excess and especially close to the phase boundary large cylindrically shaped aggregates were observed. This elongation becomes more pronounced the higher the  $M_w$  (= the longer the chain) of the employed polyelectrolytes is (see fig. 1). Previously, the SANS data of these complexes was described reasonably well by a linear arrangement of droplets [28].

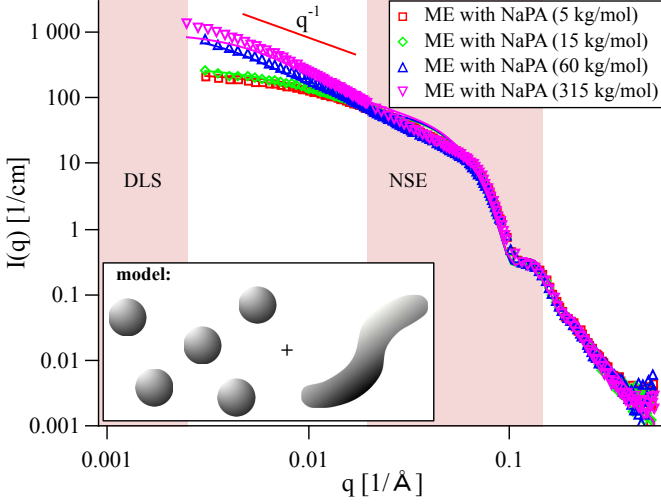


FIG. 1. SANS curves for microemulsion droplets with polyacrylates of different  $M_w$  at  $z = 0.7$ . Solid lines are best fits of a model of coexisting spheres and wormlike chains, see the supporting information for details. The model was chosen after analysis of the NSE data. Pink areas indicate  $q$  regions of DLS and NSE measurements.

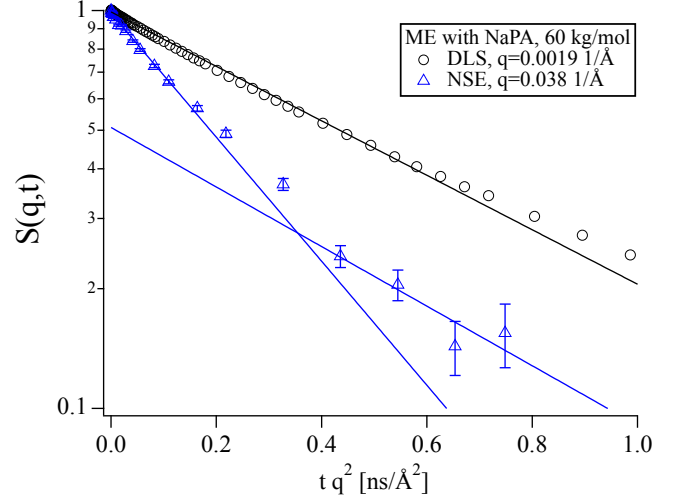


FIG. 3. Normalised intermediate scattering function for the complex using NaPA with  $M_w = 60$  kg/mol, measured by DLS and NSE. While the DLS data can be described with a single exponential, the NSE data clearly shows deviations from single exponential behaviour, indicating the presence of a second slower mode, lines are a guide to the eye.

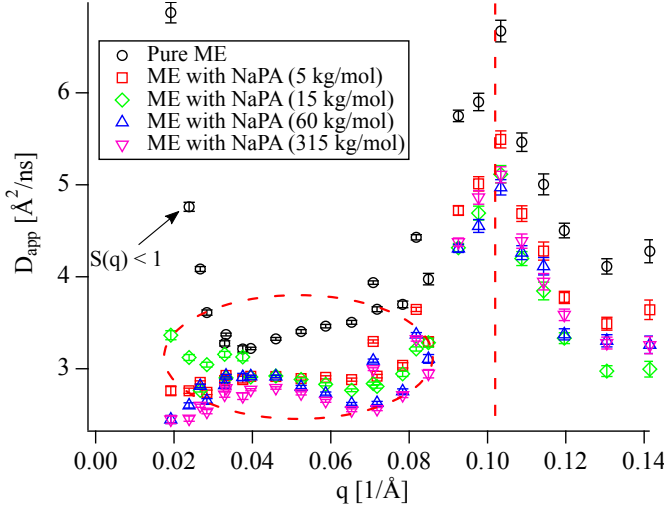


FIG. 2. Apparent diffusion coefficients  $D_{app,NSE}$  for  $z = 0.7$  samples, obtained from NSE measurements as a function of  $q$ , addition of NaPA leads to a decrease in  $D_{app}$  while the values for different NaPA chain lengths are quite similar. The peak at  $0.1$   $1/\text{\AA}$  is due to the undulation motion of the ME droplets

NSE measurements were performed to gain information about the dynamics of the system at nanometer length scales and nanosecond time scales. At first, the measured intermediate scattering functions were fitted with a simple exponential ( $S(q, t)/S(q, 0) = \exp(-D_{app}q^2t)$ , magnitude of the scattering vector  $q$ , Fourier time  $t$ , see figs. S9 to S12) to obtain the apparent diffusion coefficients  $D_{app}$  shown in fig. 2. The peak at  $0.1$   $1/\text{\AA}$  is due to undulation motions of the ME mem-

branes, which are mostly visible at the form factor minimum, located at  $q_{min} R = \tan(q_{min} \cdot R)$ ,  $R \approx 4.5/q_{min}$  for spheres. This means that the ME droplets are about  $45$   $\text{\AA}$  in radius. This peak is in good agreement with the measured SANS data which shows a form factor minimum at the same  $q$  (see fig. 1). The diffusion coefficient corresponding to a sphere with a radius of  $45$   $\text{\AA}$  in a non-interacting sample at our experimental conditions would be  $D = \frac{k_B T}{6\pi\eta R} \approx 4.4$   $\text{\AA}^2/\text{ns}$ , which is significantly more than we observe at  $q < 0.1$   $1/\text{\AA}$  for the pure ME meaning that there are relevant effects from interparticle interactions resulting in a static structure factor  $S(q)$  with a peak at about  $0.04$   $1/\text{\AA}$  (see fig. S13). The  $q$  dependence of  $D_{app}$  is given by  $D_{app} = D_0 \cdot H(q)/S(q)$ , where the hydrodynamic function  $H(q) \approx 1$  in our concentration range,[29] and the strong increase of  $D_{app}$  at the lowest  $q$  values is due to  $S(q) < 1$ .

The characteristic behaviour of ME droplets with a peak in  $D_{app}$  at the form factor minimum is also observed for the complexes but their  $D_{app}$  at lower  $q$  is significantly lower than for the pure ME, showing that the dynamics are slower for the complexes than for the pure ME. The  $D_{app}$  of the different complexes is rather similar regardless of the molecular weight of the NaPA, despite the different structures that are observed using SANS. A closer inspection of the intermediate scattering functions at  $q$  values where only diffusion should be visible reveals that  $S(q, t)$  is not single exponential for the complexes as opposed to the pure ME (see fig. S2). This is in contrast to our findings from DLS where the data of the complexes can be described well as a monomodal

decay (see fig. 3 and figs. S3 to S5).

Having such a bimodal diffusion process as a function of length and time scale can be observed if particles are entrapped within a transient network (and one sees fast movement within the mesh size and slower one across the network) or if some of the droplets are bound within the complex while others are freely moving. Assuming the later scenario to be more likely in our case, this leaves two possible explanations for the monomodality of the DLS data. Either the complexes show much stronger scattering than the free ME droplets at the low  $q$  values of the DLS due to their larger size, rendering the latter virtually invisible. In this case, the diffusion coefficient measured in DLS would be at least as low as the slow diffusion coefficient measured in NSE unless there were strong repulsive interactions between the complexes to which the SANS data do not give any evidence. Alternatively, the complexes could be highly dynamic with a lifetime longer than the nanosecond scale of NSE but shorter than the micro- to millisecond timescale of DLS. For a system where particles change between two different diffusion coefficients  $D_{1,2}$  ( $D_1 < D_2$ ), on a timescale  $\tau$  in the limit of fast exchange ( $\tau \ll 1/(Dq^2)$ ) a single averaged relaxation rate is observed:

$$S(q, t) = \exp(-(xD_1 + (1-x)D_2)q^2t) \quad (1)$$

while in the limit of slow exchange ( $\tau \gg 1/(Dq^2)$ ) the relaxation is bi-exponential [30]:

$$S(q, t) = x \exp(-D_1q^2t) + (1-x) \exp(-D_2q^2t), \quad (2)$$

where  $x$  is the weight of population 1 and in the limit of fast exchange the averaged diffusion coefficient is higher than  $D_1$ .

To address this question in more detail, we proceeded to fit the NSE data from the complexes with a combination of the Milner-Safran model [31, 32] to account for the membrane undulations at high  $q$  and the translational diffusion of the free ME droplets and a second slow diffusive mode with  $q$  independent diffusion coefficient  $D_{slow}$  and  $q$  dependent amplitude  $x_{slow}$ , see eq. (S14). The contribution from the free ME droplets (membrane undulations and translational diffusion) was fixed for all samples according to fits to the data from the pure MEs (see fig. S6), where we obtained a value for the bending rigidity  $\kappa$  of  $4.5 k_B T$ , which is in good agreement with previous results on similar systems [33]. Different approaches to describe the interactions in this system were tried by employing different approximations for the structure factor but it turned out, that different treatments had a rather small effect on the outcome (see figs. S7 and S8 for a comparison). Thus we decided to fit our data treating the PE as simple electrolyte and leaving the volume fraction at its nominal value. The fitting procedure is described in detail in the supporting information and fits are shown in figs. S9 to S12.

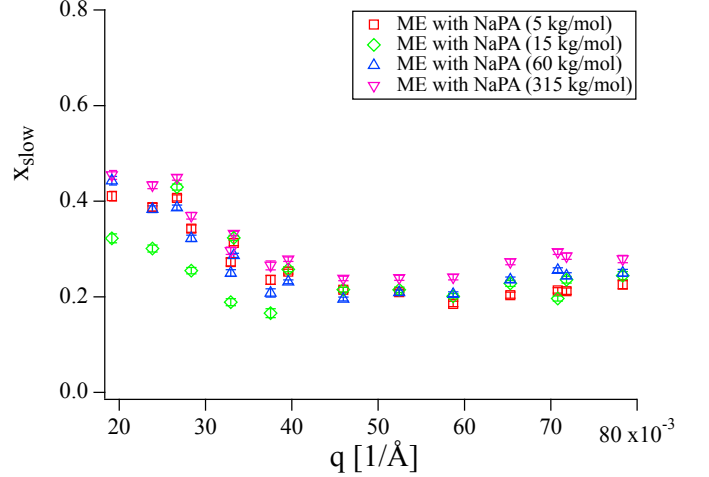


FIG. 4.  $x_{slow}$  obtained from fitting NSE curves with eqs. (S14) and (S15). No significant differences between samples can be seen, while a slight increase with decreasing  $q$  can be observed.

Fit results for  $x_{slow}$  are shown in fig. 4 in a  $q$  range where the influence from the membrane undulations is weak. Even though  $x_{slow}$  is an intensity weight and does not directly correspond to the fraction of ME droplets bound to the complexes, the intensity ratio between a single ME droplet and a single complex using the same droplets as building blocks should be roughly proportional to the volume ratio of the structures in the NSE  $q$  range, as the respective form factors show similar intensity. Therefore,  $x_{slow}$  should be a reasonably good approximation for the fraction of the droplets bound in complexes, which is about 20 to 30 % of the ME droplets for all complexes. The results are quite similar for all samples and do not show a pronounced trend with  $q$ . The small increase of  $x_{slow}$  at low  $q$  can be explained by the intensity of the complexes increasing relative to the intensity of the pure ME droplets towards lower  $q$ .

Alternatively,  $x_{slow}$  could be interpreted as a fraction of ME droplets being affected by the constraints imposed on them by being adsorbed to the NaPA. In this picture all of the ME droplets could be bound in complexes but at short length scales (high  $q$ ) they could still move as if they were not bound. This behaviour could be approximated by the Volino-Dianoux model [34, 35] and would result in a steady increase of  $x_{slow}$  with decreasing  $q$ , quickly approaching 1. While the model strictly describes incoherent scattering, the effect would be even more pronounced in the coherent case where the relative intensity of the larger complexes increases with decreasing  $q$ . As  $x_{slow}$  is rather constant here, this interpretation can be ruled out. Additionally, the diffusion coefficient in the low- $q$  limit, where the amplitude of the internal motion becomes negligible would have to correspond to  $D_{slow}$ .

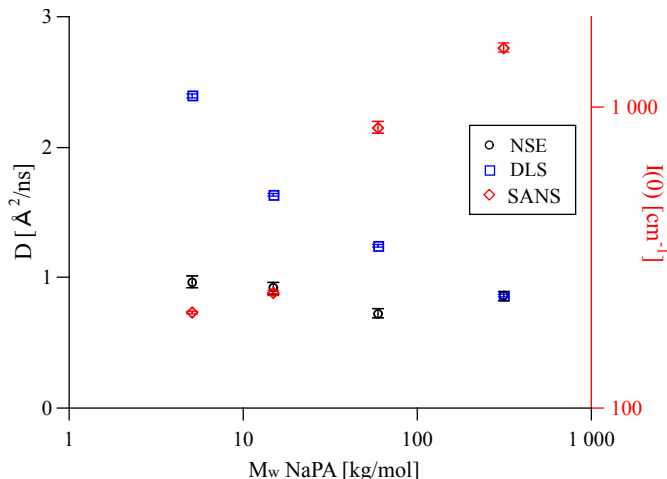


FIG. 5.  $D_{slow}$  obtained from fitting NSE curves with eq. (S14), diffusion coefficients obtained from DLS and  $I(0)$  values obtained from SANS as a function of the molecular weight of the PE. While the observed diffusion coefficient is constant for NSE, it decreases with increasing  $M_w$  for DLS where at high  $M_w$  the scattering signal is dominated by the complexes and the relative contribution of free ME droplets becomes negligible.

The diffusion coefficients obtained from DLS are systematically higher than  $D_{slow}$  obtained from NSE (see fig. 5). While the increased relative intensity of the complexes compared to the free ME droplets at low  $q$  inevitably does affect the comparison between DLS and NSE, the fact that the single diffusion coefficient seen in DLS is faster than the slow diffusion coefficient seen in NSE indicates that the result obtained from DLS is an average from complexes and ME droplets as in eq. (1), meaning that the monomodality of the DLS curves is due to the short life time of the complexes. With increasing  $M_w$ , the complexes become larger, resulting in a higher intensity at low  $q$  (fig. 5, right axis). The relative intensity of the complexes in the DLS  $q$  range increases as well, which explains the decrease of the diffusion coefficient with increasing  $M_w$ . However, the local binding and the binding probability are independent of the length of the NaPA (fig. 4), confirming that the droplet dynamics in these complexes is exclusively governed by the local interaction between droplet and chain fragment.

With this knowledge it was possible to refit the SANS data using a two-component fit, including homogeneous wormlike chains and free spheres with the respective intensity fractions obtained from NSE. The new SANS model is fully consistent with the dynamic NSE results as opposed to the previous descriptions, where it was assumed that all material was contained in the complexes (see fig. S14 for a comparison of the models). The new SANS model is shown as solid lines in fig. 1 and describes the experimental data very accurately. See the supporting information for details on the fit and table S I for the

obtained fit parameters.

The values obtained for  $D_{slow}$  do not show a strong dependence on  $M_w$  (see fig. 5). One likely explanation for this situation would be, that due to the soft and flexible nature of the complexes, the diffusion times  $D_{slow}$  measured in NSE belong to segment motions of the complex, rather than diffusion of large complexes. With a diffusion coefficient of  $1 \text{ \AA}^2/\text{ns}$ , this would correspond to segment lengths of about  $200 \text{ \AA}$ , which is in good agreement with the values of the Kuhn length obtained from the new SANS model (see table S I). The effective segment lengths are similar for PEs of the same nature but different  $M_w$ , consequently  $D_{slow}$  is also similar for all different  $M_w$  measured even though the static picture shows  $M_w$  dependent differences. This explanation could be verified by employing other polyelectrolytes with significantly different persistence lengths which should have a pronounced effect on  $D_{slow}$  and will be done in a consecutive study.

## CONCLUSION

Combining the static and dynamic measurements we can conclude, that polyelectrolyte/microemulsion complexes are highly dynamic systems, with average life times between the nanosecond time scale of NSE and the millisecond time scale of DLS and only about 30 % of ME droplets are bound in complexes at a given time. Our measurements do not allow for a precise determination of the lifetime of the complexes but we can give a reliable estimate to this important property hitherto unknown. The time scale of each experiment is given by  $1/(Dq^2)$ . Using  $q$  values of  $0.02$  and  $0.002 \text{ 1/\AA}$  for NSE and DLS respectively and  $D = 4.4 \text{ \AA}^2/\text{ns}$  we obtain timescales of about  $600 \text{ ns}$  and  $60 \text{ }\mu\text{s}$  as lower and upper limit for the life time of the complexes. Calculating the mean square displacement of a ME droplet, it is seen that it would diffuse a distance of about  $\sqrt{6 \cdot 4.4 \text{ \AA}^2/\text{ns} \cdot 600 \text{ ns}} = 126 \text{ \AA}$ , less than twice its diameter. Therefore, it is not surprising that the life time of the complexes is long compared to the NSE time scale. Even though the structures seen in SANS are significantly different for complexes with PEs of different  $M_w$ , their dynamic behaviour is remarkably similar, due to the transient nature of these complexes. Figure 6 depicts the situation.

Reverting to the initial question concerning the viscosity of polymer/microemulsion complexes, we can now explain the low viscosities observed with the very dynamic situation of these complexes. As even a very high shear modulus  $G_0$ , arising from an interconnection of the droplets, cannot compensate such small relaxation times  $\tau$ , no viscosity ( $\eta$ ) increase can be observed in this system, as  $\eta = \tau \cdot G_0$ . This conclusion could only be drawn from the comparison of different measurement techniques, especially the combination of static and dy-

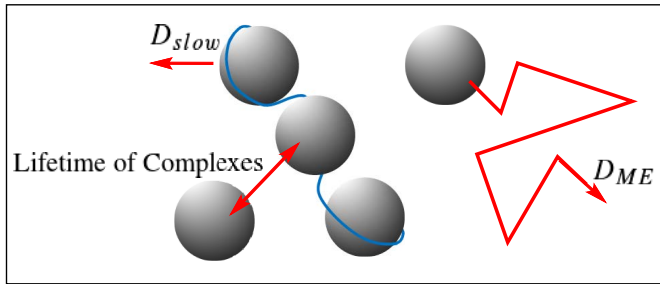


FIG. 6. Schematic illustration of different dynamic processes occurring simultaneously in microemulsion/polyelectrolyte complexes: Diffusion of free microemulsion droplets ( $D_{ME}$ ), Diffusion of larger aggregates ( $D_{slow}$ ) and exchange of droplets within the aggregates (Lifetime).

dynamic methods. One method alone would have given an incomplete picture. This example shows the importance of always studying the static as well as the dynamic behaviour of a system for a thorough characterisation. The observed highly transient nature of the studied polyelectrolyte/microemulsion complexes (PEMECs) should not only be relevant for this particular system, but also be of importance for the understanding of related systems of oppositely charged colloids and polyelectrolytes, systems as they are abundantly occurring in biology, but also in applied formulations in pharmacy, cosmetics, etc.

## CONFLICTS OF INTEREST

There are no conflicts to declare.

## ACKNOWLEDGEMENTS

Financial support from the BMBF project 05K13KT1 is gratefully acknowledged as well as allocation of beamtime by HZB, ILL and LLB. Raw data of the NSE measurements is available under <http://dx.doi.org/10.5291/ILL-DATA.TEST-2591>. M. Simon thanks the TU Berlin for funding her PhD project.

## Associated Content

Electronic Supplementary Information (ESI) available: Viscosity measurements, DLS measurements, examples of NSE and DLS curves, modeling of NSE data and SANS (measurements, fitting models, discussion). See [URL will be inserted by publisher].

\* miriam.simon@tu-berlin.de

- <sup>†</sup> michael.gradzielski@tu-berlin.de  
<sup>‡</sup> hoffmann@ill.fr
- [1] E. Goddard, *Colloids Surf.* **19**, 301 (1986).
  - [2] L. Chiappisi, I. Hoffmann, and M. Gradzielski, *Soft Matter* **9**, 3896 (2013).
  - [3] D. Langevin, *Advances in Colloid and Interface Science* **147-148**, 170 (2009).
  - [4] M. Gradzielski and I. Hoffmann, *Curr. Opin. Colloid Interface Sci.* **35**, 124 (2018).
  - [5] T. P. Hoar and J. H. Schulman, *Nature* **152**, 102 (1943).
  - [6] P. Winsor, *Trans. Faraday Soc.* **44**, 376 (1948).
  - [7] M. J. Lawrence and G. D. Rees, *Adv. Drug Del. Rev.* **64**, 175 (2012).
  - [8] M. J. Schwuger, K. Stickdorn, and R. Schomäcker, *Chem. Rev.* **95**, 849 (1995).
  - [9] V. C. Santanna, F. D. Curbelo, T. N. Castro Dantas, A. A. Dantas Neto, H. S. Albuquerque, and A. I. Garnica, *J. Petroleum Sci. Engineering* **66**, 117 (2009).
  - [10] P. Boonme, *J. Cosmetic Dermatology* **6**, 223 (2007).
  - [11] C. Solans, J. García Dominguez, and S. E. Friberg, *J. Dispersion Sci. Technology* **6**, 523 (1985).
  - [12] B. Kuttich, P. Falus, I. Grillo, and B. Stühn, *J. Chem. Phys.* **141**, 084903 (2014).
  - [13] B. Kuttich, O. Ivanova, I. Grillo, and B. Stühn, *J. Chem. Phys.* **145**, 164904 (2016).
  - [14] A. Holmberg, P. Hansson, L. Piculell, and P. Linse, *J. Phys. Chem. B* **103**, 10807 (1999).
  - [15] A. Kabalnov, B. Lindman, U. Olsson, L. Piculell, K. Thuresson, and H. Wennerström, *Colloid and Polymer Science* **274**, 297 (1996).
  - [16] C. Quellet, H. F. Eicke, G. Xu, and Y. Hauger, *Macromolecules* **23**, 3347 (1990).
  - [17] B. Jakobs, T. Sottmann, R. Strey, J. Allgaier, L. Willner, and D. Richter, *Langmuir* **15**, 6707 (1999).
  - [18] P. Malo De Molina, M. Appavou, and M. Gradzielski, *Soft Matter* **10**, 5072 (2014).
  - [19] P. Malo De Molina, F. S. Ihlefeldt, S. Prévost, C. Herfurth, M. Appavou, A. Laschewsky, and M. Gradzielski, *Langmuir* **31**, 5198 (2015).
  - [20] E. Buhler, J. Appell, and G. Porte, *J. Phys. Chem. B* **110**, 6415 (2006).
  - [21] H. Zhang, L. Deng, P. Sun, F. Que, and J. Weiss, *J. Colloid Interface Sci.* **461**, 88 (2016).
  - [22] M. Simon, P. Krause, L. Chiappisi, L. Noirez, and M. Gradzielski, *Chem. Sci.* **10**, 385 (2019).
  - [23] S. Yu, X. Xu, C. Yigit, M. Van Der Giet, W. Zidek, J. Jankowski, J. Dzubiella, and M. Ballauff, *Soft Matter* **11**, 4630 (2015), arXiv:1507.02938.
  - [24] E. J. Yearley, P. D. Godfrin, T. Perevozchikova, H. Zhang, P. Falus, L. Porcar, M. Nagao, J. E. Curtis, P. Gawande, R. Taing, I. E. Zarraga, N. J. Wagner, and Y. Liu, *Biophys. J.* **106**, 1763 (2014).
  - [25] P. Schleger, B. Alefeld, J. Barthelemy, G. Ehlers, B. Farago, P. Giraud, C. Hayes, A. Kollmar, C. Lartigue, F. Mezei, and D. Richter, *Phys. B* **241-243**, 164 (1997).
  - [26] B. Farago, P. Falus, I. Hoffmann, M. Gradzielski, F. Thomas, and C. Gomez, *Neutron News* **26**, 15 (2015).
  - [27] U. Keiderling, *Appl. Phys. A* **1457**, 1455 (2002).
  - [28] L. Chiappisi, S. Prévost, and M. Gradzielski, *J. Appl. Crystallogr.* **47**, 827 (2014).
  - [29] L. Porcar, P. Falus, W. Chen, A. Faraone, E. Fratini, K. Hong, P. Baglioni, and Y. Liu, *J. Phys. Chem. Lett.* **1**, 126 (2010).

- [30] F. Roosen-Runge, D. J. Bicout, and J. Barrat, J. Chem. Phys. **144**, 204109 (2016).
- [31] S. A. Safran, J. Chem. Phys. **78**, 2073 (1983).
- [32] S. T. Milner and S. A. Safran, Phys. Rev. A **36**, 4371 (1987).
- [33] B. Farago and M. Gradzielski, J. Chem. Phys. **114**, 10105 (2001).
- [34] F. Volino and A. J. Dianoux, Mol. Phys. **41**, 271 (1980).
- [35] I. Hoffmann, P. Malo De Molina, B. Farago, P. Falus, C. Herfurth, A. Laschewsky, and M. Gradzielski, J. Chem. Phys. **140**, 034902 (2014).

